**Università degli Studi di Salerno**

DIPARTIMENTO DI FISICA "E. R. CAIANIELLO"
Corso di Dottorato in Fisica - XIV Ciclo Nuova Serie (2013-2015)
Coordinator: Prof. Canio Noce

DOCTOR OF PHILOSOPHY IN PHYSICS

# Signatures of quantumness: identification, quantification and dynamical preservation

Supervisor:
**Dr. Massimo Blasone**

Co-supervisor:
**Dr. Gerardo Adesso**

Candidate:
**Marco Cianciaruso**
**Matricola 8880800100**

**Anno Accademico 2014–2015**

# Abstract

This Thesis collects results obtained by the candidate via the application of information geometric tools to the quantification and dynamical preservation of quantumness in some of its various manifestations, as well as to the characterisation of quantum phase transitions and the analysis of quantum speed limits. We first develop an experimentally feasible approach to the evaluation of geometric measures of quantumness, according to which the distance from the state of the system to a suitable set of classical states is considered. We then show that all such geometric quantifiers of quantumness exhibit the peculiar freezing phenomenon, i.e. remain completely unaffected by noise when the system undergoes some particular decoherence evolutions. We moreover study the nature of ordered quantum phases and the origin of spontaneous symmetry breaking, by analysing some measures of quantumness for symmetry-breaking and symmetry-preserving quantum ground states. We finally investigate how the non uniqueness of a bona fide geometric measure of distinguishability defined on the quantum state space affects the quantum speed limits and can be exploited in order to derive improved bounds.

# Publications

This Thesis collects some of the results obtained by the candidate as a co-author of the following articles:

1. Frozen Quantum Coherence, *Phys. Rev. Lett.* **114**, 210401 (2015). [1]

2. Universal freezing of quantum correlations within the geometric approach, *Sci. Rep.* **5**, 10177 (2015). [2]

3. Accessible quantification of multiparticle entanglement, *arXiv:1507.01600* (2015). Submitted to Nat. Commun. [3]

4. Robustness of coherence: An operational and observable measure of quantum coherence, *arXiv:1601.03781* (2016). To appear in Phys. Rev. Lett. Editors' Suggestions [4]

5. Robustness of asymmetry and coherence of quantum states, *arXiv:1601.03782* (2016). To appear in Phys. Rev. A [5]

6. Unifying approach to the quantification of bipartite correlations by Bures distance, *J. Phys. A: Math. Theor.* **47**, 405302 (2014). [6]

7. Observation of time-invariant coherence in a room temperature quantum simulator, *arXiv:1511.01971* (2015). Submitted to Phys. Rev. Lett. [7]

8. Entanglement and quantum correlations in many-body systems: a unified approach via local unitary operations, *arXiv:1412.1054v2* (2015). Submitted to Phys. Rev. A [8]

9. Classical nature of ordered phases: origin of spontaneous symmetry breaking, *arXiv:1408.1412* (2014). [9]

10. Generalized Geometric Quantum Speed Limits, *arXiv:1507.05848* (2015). Submitted to Phys. Rev. X [10]

# Acknowledgements

There are a lot of people that have played an important role in my research during these three years. Let me mention them in order of appearance. I am very grateful to my Bachelor's and Master's thesis advisor Prof. Giuseppe Marmo, for having encouraged me to explore other academic environments in order to get acquainted with other approaches and techniques, for his extremely useful advises as well as the enlightening discussions that we have continued to enjoy in many occasions, and finally for his indispensable support through his letters of recommendation. I am also grateful to my Master's thesis co-advisor Dr. Paolo Aniello, for his wise advices and his encouragement. Thanks a lot to my PhD coordinator Prof. Canio Noce, for having been invaluable and constantly available throughout my entire PhD. I warmly thank my supervisor Dr. Massimo Blasone, for his impressive scientific versatility, friendliness and wise advises, as well as for having introduced to me the geometric approach to the quantification of multiparticle entanglement that eventually turned out to be crucial throughout my research, and finally for having massively supported me to extend the network of my collaborations as much as possible. Thanks to Prof. Silvio De Siena, for his massive experience and all the enlightening discussions that we have enjoyed. Many thanks to Prof. Fabrizio Illuminati, for his immense knowledge and amazing sense of humour, as well as for the extremely fruitful collaboration that has arisen, and finally for his crucial support for the realisation of my two-year period abroad at the Quantum Correlations Group at the University of Nottingham. Thanks a lot to Dr. Salvatore Marco Giampaolo, for our fruitful collaboration, his extreme patience and for having introduced to me the wonderful world of condensed matter systems. Many thanks also to the other members and collaborators of the Quantum Theory and Quantum Technologies Group at the University of Salerno, especially Dr. Fabio Dell'Anno, Dr. Wojciech Roga, and Dr. Leonardo Ferro, for all our fruitful collaborations. My immense gratitude to my co-supervisor Dr. Gerardo Adesso, for having hosted me at the Quantum Correlations Group at the University of Nottingham for two years and for having turned out to be the best guide that I could have ever imagined from both a scientific and human perspective. Many thanks to my best colleague Mr. Thomas Bromley, for our outstanding collaboration, whereby I have learnt for the very first time what individualism is not able to achieve, and for having introduced to me the fascinating British culture. Thanks to all the Quantum Correlations Group and the quantum information community at the University of Nottingham, for having been an extremely stimulating and nice environment throughout the last two years of my PhD. I am very grateful to Dr. Rosario Lo Franco, for our very fruitful collaboration and his indispensable support. Thanks to Mr. Diego Paiva

Pires, Dr. Diogo de Oliveira Soares Pinto and Dr. Lucas Celeri, as well as Dr. Marco Piani, Dr. Nathaniel Johnston and Mr. Carmine Napoli for our very fruitful collaboration.

Finally, another kind of gratitude, though impossible to describe or quantify here, goes to my love Elena, my parents and my friends.

# Contents

# Introduction

Quantum coherence and quantum correlations stand as some of the most basic signatures of quantumness [11–14]. Quantum correlations, in turn, manifest themselves in several forms such as non-locality [15], steering [16–18], entanglement [19], and discord-type correlations [20–22]. Identifying these various manifestations of quantumness has at least two purposes. From a fundamental viewpoint, it is indispensable in the long-lasting quest for the understanding of the classical-quantum boundary and the quantum origins of our familiar classical world [23]. On the other hand, from a pragmatic perspective, all such forms of quantumness represent resources for some operational tasks and allow us to achieve them with an efficiency that is unreachable by any classical means [24].

A paradigmatic instance for which quantum coherence represents a resource is within quantum metrology [25], where it sets the precision of the estimate of the physical parameter under investigation. Furthermore, in quantum optics, the coherent superposition of Glauber displaced states [26, 27] corresponds to the notion of optical non-classicality [28], which is useful for example in quantum interferometry. Quantum coherence is also a resource for work extraction in quantum thermodynamics [29,30], as opposed to the classical case of thermal states with no coherence in the basis of the system's Hamiltonian. Another task for which coherence constitutes the figure of merit is the creation of entanglement. Specifically, the degree of coherence of a single system is equivalent to the maximum degree of entanglement that can be created by incoherent operations acting on that system and an incoherent ancilla [31]. Finally, coherence delocalisation is believed to play a fundamental role even in biological processes such as exciton and electron transport [32–36].

On the other hand, the paradigmatic protocol that made entanglement so popular as a resource is quantum teleportation [37]. Furthermore, entanglement is directly linked to the usefulness of initial states for Grover's search algorithms [38]. Genuine multiparticle entanglement is an essential ingredient for quantum technologies including multiuser quantum cryptography [39], quantum metrology [25], and measurement-based quantum computation [40]. Moreover, partial multiparticle entanglement is relevant in quantum informational tasks such as quantum secret sharing [41] and may play a relevant role in biological phenomena [42, 43].

Finally, discord-type correlations represent a resource for quantum metrology, when the Hamiltonian generating the dynamics that imprints the parameter into the input state is unknown [44]. Quantum correlations beyond entanglement are also the figure of merit in quantum state discrimination [45, 46], quantum state hiding [47], local broadcasting [48], quantum state merging [49], entanglement activation [50, 51] and device-dependent quan-

tum cryptography [52].

The quantification of quantumness is thus necessary to gauge the quantum enhancement when performing the aforementioned operational tasks. However, especially when considering multiparticle entanglement, while considerable progress has been achieved in its detection [53–61], its experimentally accessible quantification remains an open problem [62–69].

In Refs. [1–3] we have introduced an experimentally friendly approach to the quantification of geometric measures of quantumness, according to which the distance from the state of the system to a suitable set of classical states is considered. Our approach provides exact results for particular classes of mixed states of $N$ qubits, and analytical lower bounds to global, partial, and genuine multiparticle entanglement, as well as to quantum coherence, for any general state. For global and partial entanglement, as well as quantum coherence, useful lower bounds have been obtained with minimum effort, requiring local measurements in just three settings for any $N$. For genuine entanglement, a number of measurements scaling linearly with $N$ is instead required. We have also shown that our results provide overall accessible quantitative assessments of global, partial, and genuine multiparticle entanglement in a variety of noisy states produced in recent experiments [70–75], going beyond the mere detection [53–61], yet with no added experimental overhead. Compared with some recent complementary approaches to the quantification of multiparticle entanglement [62–69], we find that our method fares surprisingly well in its efficiency and versatility despite the minimal experimental requirements.

Furthermore, in Ref. [4] we have introduced the robustness of coherence, a bona fide quantifier of quantum coherence that we have proved to have many attractive properties, including efficient numerical computability via semidefinite programming, and an operational interpretation in a channel discrimination context. We have also introduced the notion of coherence witnesses, whose measurement in a laboratory detects the presence of coherence, and proved that properly constrained coherence witnesses provide lower bounds to the robustness of coherence, which is thus shown to be a directly measurable quantity itself. In Ref. [5] we have then discussed the generalisation of these results to the case of asymmetry.

Complex systems are inevitably subject to noise, hence it is natural and technologically crucial to question under what conditions the quantum resources that we can extract from them are not deteriorated during open evolutions [76]. Numerous works have investigated the dynamics of quantum correlations in open quantum systems undergoing various types of Markovian or non-Markovian evolution, as reviewed e.g. in [22, 77, 78]. Although different measures of quantum correlations can exhibit distinct features and impose inequivalent orderings on the set of quantum states, it has emerged as a general trait that discord-type quantum correlations are more robust than entanglement against noise [79–85] and cannot generally vanish at a finite evolution time, due to the fact that zero-discord states are of null measure [82], while entanglement can suffer so-called sudden death [86, 87]. In particular, a fascinating and nontrivial phenomenon of *extreme* robustness to noise exhibited by quantum correlations beyond entanglement deserves special attention. Namely, under local non-dissipative decoherence evolutions, it has been observed that a number of known discord-type measures all remain constant ('frozen') for a finite time interval

in Markovian conditions [88–90], and for multiple intervals [91–93] or forever [94] in non-Markovian conditions, when considering two non-interacting qubits initially in a specific class of Bell-diagonal states. This freezing phenomenon is quite appealing since it implies that every protocol relying on discord-type quantum correlations as a resource will run with a performance unaffected by noise in the specific dynamical conditions. However, since the occurrence of freezing has been investigated by explicitly considering the evaluation of specific discord-type measures on a case by case basis [88, 89, 91], it is natural to ask whether this phenomenon is a mere mathematical accident due to the particular choices of quantum correlations quantifiers, or whether it must manifest independently of the adopted measure, thus having a universal character and promising to bear a deep physical meaning.

In Refs. [1–3, 6] we have shown that all valid geometric quantifiers of quantumness exhibit the paradigmatic freezing phenomenon, i.e. remain constant during the evolution of a particular class of states of an even number of qubits each independently interacting with a non-dissipative decohering environment, in the case of quantum coherence and discord-type correlations, and of two qubits undergoing collective dephasing, in the case of entanglement. Interestingly, our results are not confined to the theory. Indeed, we have recently joined an experiment [7] regarding the observation of time-invariant coherence in a two-qubit room temperature nuclear magnetic resonance quantum simulator. We have thus proved that freezing of geometric quantumness is independent of the adopted distance and therefore universal, thus paving the way to a deeper physical interpretation and future practical exploitation of the phenomenon for noisy quantum technologies.

Quantum correlations are not only fundamental resources for quantum technologies but also quite useful tools for the characterisation of quantum phases in many-body systems [95–97]. For instance, topologically ordered phases cannot be characterised by the Landau-Ginzburg paradigm based on symmetry breaking and local order parameters, but rather by the long-range entanglement properties featured by the ground state of the system [98–101]. Within this generalised framework, quantum correlations in many-body ground states allow for the most fundamental characterisation of complex quantum systems. In fact, even for systems that do not feature exotic phases and nonlocal quantum orders, the investigation of ground-state patterns of entanglement and discord can provide a deeper understanding of locally ordered phases associated to spontaneous symmetry breaking [102–111].

In spite of the ongoing efforts to characterise quantum ground states by analysing their quantum correlations, a systematic comparative study of their behaviour in the ordered phase was still lacking. In Refs. [8, 9] we have performed such comparison and shown that the ground states which realise the maximum breaking of the Hamiltonian symmetries are the only ones that: are always locally convertible, i.e. can be obtained from all other ground states by local operations and classical communication, while the reverse is never possible; and minimise the monogamy inequality for bipartite entanglement. These results are of general validity for all systems that belong to the same universality class of exactly solvable models that are standard prototypes for quantum phase transitions associated to spontaneous symmetry breaking, such as the $XY$ quantum spin models [112]. Overall, this provides quantitative support to the always implicit assumption according to which

the maximally symmetry-breaking quantum ground states are the most classical ones corresponding to an ordered phase.

Another fundamental quantum aspect lies in the impossibility of knowing simultaneously and with certainty two incompatible properties of a quantum system [113–115]. Contrarily to the well understood uncertainty relation between any two non-commuting observables, the time-energy uncertainty relation still represents a controversial issue [116, 117], although the last decades witnessed several attempts towards its explanation [118]. This effort led to the interpretation of the time-energy uncertainty relation as a so-called *quantum speed limit* (QSL), i.e. the ultimate bound imposed by quantum mechanics on the minimal evolution time between two distinguishable states of a system [119]. QSLs have been widely investigated within the quantum information setting, since their understanding offers a route to design faster and optimised information processing devices [120], thus attracting constant interest in quantum optimal control, quantum metrology [25], quantum computation and communication [121]. Interestingly, it has been recently recognised that QSLs play a fundamental role also in quantum thermodynamics [122].

In Ref. [10] we have shown how the non uniqueness of a bona fide measure of distinguishability defined on the quantum state space affects the quantum speed limits and can be exploited in order to derive improved bounds. Specifically, we have constructed an infinite family of quantum speed limits valid for any dynamical evolution, based on an information geometric formalism. These findings unify and generalise existing results on quantum speed limits, and provide instances of novel bounds which are tighter than any established one based on the conventional quantum Fisher information.

Overall, this Thesis represents primarily an application of information geometric tools to the quantification and dynamical preservation of quantumness, as well as to the characterisation of quantum phase transitions and derivation of tighter quantum speed limits. This Thesis is organised as follows. In Chapter 1 we briefly introduce the notions of entanglement, quantum coherence and discord-type correlations within a unifying resource theoretic framework. In Chapter 2 we outline the information geometric machinery that we will exploit throughout this Thesis. In Chapters 3 and 4 we review our results [1–7] on the quantification and dynamical preservation of quantumness. In Chapter 5 we review our results [8, 9] on the application of quantumness to quantum phase transitions. In Chapter 6 we review our results [10] on the application of information geometry to quantum speed limits. We finally draw our conclusions in Chapter 7.

# Chapter 1

# Quantumness as a resource

In the Introduction we have seen that each form of quantumness, be it quantum coherence, entanglement or even quantum correlations beyond entanglement, is an indispensable resource for quantum technologies. In this Chapter we will thus introduce these quantum features within a unifying resource theoretic perspective [123, 124].

## 1.1 Resource theories

The overall objective of any resource theory is understanding a given physical phenomenon in order to exploit it in the most efficient way. Prominent examples of such pragmatic theories are chemistry and thermodynamics, which basically study how to transform raw materials and heat into useful products and work, respectively. In fact, any resource theory studies the interconversion between different resources via a restricted class of transformations. Therefore, to define a resource theory we just need two ingredients: the resources and the restriction on the transformations among the resources. The resource theories that we will hereafter focus on identify resources with particular states of the system being exploited, the so-called *resource states*, and restrict to the transformations that are considered to be freely implementable, the so-called *free operations*, in such a way that no resource state can be prepared through free operations[1]. This is why, within such resource theories, the states which are not resourceful are referred to as *free states*.

The focus of such resource theories is on two main types of interconversion among resource states: the *single-copy interconversion*, whereby one copy of a resource state is transformed via free operations into one copy of another resource state, and the *many-copy interconversion*, whereby $n$ copies of a resource state are transformed via free operations into $m$ copies of another resource state.

Another fundamental question that any resource theory must address is how to quantify the resource. One could naively think that there should be a unique quantifier of the resource, determining a universal ordering of the resource states. However, this should not be the case for the following two reasons. First, the same resource can be exploited for

[1] A resource theory is said to be *maximal* when the free operations are all, and only, the operations that cannot create a resource state out of a free state.

different operational tasks, such that a given resource state can be more successful than another one in order to achieve a given operational task, and viceversa when considering another task. Second, it is desirable to assign an operational meaning to any quantifier of a resource, in the sense that it needs to quantify how much the resource possessed by a given state will be useful for achieving a given operational task. An immediate consequence is that, in general, the various quantifiers disagree on the order of the resource states.

Nevertheless, any *bona fide quantifier* of a resource must be compatible with the sets of free states and free operations in the following sense. First, it must zero for any free state. Second, it must be monotonically non-increasing under free operations in order to have an operational significance. In some cases, further assumptions on the quantifier of a resource are usually assumed, like non-increasing on average under selective free operations and non-increasing under classical mixtures.

Consequently, when considering single-copy interconversions, one resource state can be transformed via free operations only into a less resourceful state, so that a state that can be transformed into any other state within its own equivalence class under free operations is necessarily a *maximally resourceful state* within that class. However, by resorting to many-copy interconversions, one can somehow circumvent such montonicity through a process called *resource distillation*, whereby $n$ copies of an arbitrary resource state are transformed via free operations into $m \leq n$ maximally resourceful states.

The inverse process of resource distillation is called instead *resource formation*, whereby $n$ copies of a maximally resourceful state are transformed via free operations into $m \geq n$ arbitrary resource states. Furthermore, the maximal rate at which arbitrarily many copies of a maximally resourceful state can be obtained from arbitrarily many copies of an arbitrary state $\rho$ is called the *distillable resource* of $\rho$, while the minimal rate at which arbitrarily many copies of an arbitrary state $\rho$ can be obtained from arbitrarily many copies of a maximally resourceful state is called the *resource cost* of $\rho$. A resource state which has equal distillable resource and resource cost is thus said to be *reversible*, while if this happens for any state then the corresponding resource theory is said to be *asymptotically reversible*. Finally, a resource state which has zero distillable resource is called *bound resource* state.

## 1.2 Quantum entanglement

Entanglement theory is a well established example of resource theory, wherein the system being exploited is a quantum system composed of $N$ particles [19]. The term entanglement was coined by Schrödinger to describe the following peculiar situation that happens when considering bipartite pure quantum states which are not factorisable [13]: "*the best possible knowledge of a whole does not necessarily include the best possible knowledge of all its parts, even though they may be entirely separate and therefore virtually capable of being best possibly known*". Indeed, the marginals of any bipartite pure state that cannot be written as a tensor product of states of the two subsystems are necessarily mixed. Such loss of information on the pure state of the whole system when accessing only part of it, as quantified e.g. by the von Neumann entropy of any of the marginal states, captures

exactly the entanglement between the two parties[2]:

$$E_S(|\psi\rangle) = S(\rho_A) = S(\rho_B), \tag{1.1}$$

where $\rho_A = \mathrm{Tr}_B(|\psi\rangle\langle\psi|)$, $\rho_B = \mathrm{Tr}_A(|\psi\rangle\langle\psi|)$ and $S(\rho) = -\mathrm{Tr}(\rho \log \rho)$. The pure state entanglement quantifier $E_S$ is also known as *entropy of entanglement*.

Although Schrödinger introduced entanglement "*as not one but rather* ***the*** *characteristic trait of quantum mechanics, the one that enforces its entire departure from classical line of thought*" already in the thirties [13], the awareness that it could have been a resource for quantum technologies arose only in the nineties, especially after the seminal paper by Bennett *et al.* [37]. Here, the information encoded into a quantum state $|\psi\rangle$ of a one-qubit system is teleported intact from one place to another, by a sender who knows neither the state to be teleported nor the location of the receiver. To do so, sender and receiver prearrange the sharing of a quantum system composed of two qubits and being in the celebrated Einstein-Podolsky-Rosen (EPR) maximally entangled state [12], i.e.

$$|\Psi_-\rangle = \frac{1}{\sqrt{2}}(|01\rangle - |10\rangle). \tag{1.2}$$

Then the sender performs a joint measurement on its EPR qubit and on the unknown quantum system, and finally communicate the result to the receiver via a classical channel. In other words, a maximally entangled state is consumed via the allowed local operations and classical communication in order to simulate with maximal fidelity a single use of a non-local quantum channel. Furthermore, the less the shared two-qubit pure state is entangled, i.e. the less its marginals are mixed, the less will be the fidelity[3] of the teleported state with respect to the original state $|\psi\rangle$. This is exactly the spirit of any resource theory, i.e. consuming the resource in order to circumvent the restriction on the allowed operations in such a way that the more resourceful is the consumed state, the more successful will be such circumvention.

When considering an $N$-particle system, there exist two different definitions of entanglement, and conversely of separability, collapsing onto the same notion when $N = 2$. One refers to a particular partition of the composite system under consideration, while the other considers indiscriminately all the partitions with a set number of parties.

In order to characterise the possible partitions of an $N$-particle system, we will employ the following notation [125]:

- the positive integer $M$, $2 \leq M \leq N$, representing the number of subsystems;
- the set of positive integers $\{K_\alpha\}_{\alpha=1}^{M} = \{K_1, K_2, \cdots, K_M\}$, where a given $K_\alpha$ represents the number of particles belonging to the $\alpha$-th subsystem;

[2]Notice that the reduced states $\rho_A$ and $\rho_B$ of any bipartite pure states have the same eigenvalues and so the same von Neumann entropy, thus making the definition of entropy of entanglement $E_S$ well posed.

[3]The fidelity between two quantum states $\rho$ and $\sigma$ is defined as $F(\rho, \sigma) = \left(\mathrm{Tr}\left[\sqrt{\sqrt{\rho}\sigma\sqrt{\rho}}\right]\right)^2$ and is a measure of distinguishability between such states.

- the set of sequences of positive integers $\{Q_\alpha\}_{\alpha=1}^M$, with $Q_\alpha = \left\{i_1^{(\alpha)}, i_2^{(\alpha)}, \cdots, i_{K_\alpha}^{(\alpha)}\right\}$, $i_j^{(\alpha)} \in \{1, \cdots, N\}$ and $Q_\alpha \cap Q_{\alpha'} = \varnothing$ for $\alpha \neq \alpha'$, where a given sequence $Q_\alpha$ represents precisely the particles belonging to the $\alpha$-th subsystem.

In the following, $\{Q_\alpha\}_{\alpha=1}^M$ will denote a generic $M$-partition of an $N$-particle system.

Within the partition dependent setting, the set of free states consists of the *separable states* $\mathcal{S}_{\{Q_\alpha\}_{\alpha=1}^M}$ with respect to the given $M$-partition $\{Q_\alpha\}_{\alpha=1}^M$ , i.e. the set of all, and only, states $\varsigma$ of the form

$$\varsigma = \sum_i p_i \ \tau_i^{(1)} \otimes \tau_i^{(2)} \otimes \ldots \otimes \tau_i^{(M)}, \tag{1.3}$$

where $\{p_i\}$ is a probability distribution and $\tau_i^{(\alpha)}$ are arbitrary states of the $\alpha$-th subsystem. In other words, any $\{Q_\alpha\}_{\alpha=1}^M$-separable state can be written as a convex combination of product states that are all factorised with respect to the same partition $\{Q_\alpha\}_{\alpha=1}^M$. Moreover, the free operations are the so-called *local operations and classical communication* (LOCC) with respect to the given $\{Q_\alpha\}_{\alpha=1}^M$-partition, whereby each of the $M$ parties can perform quantum operations only locally on its own subsystem and is allowed to communicate with the other parties only via classical means [126].

Within the partition independent setting, there exists a hierarchy of free states, also referred to as *$M$-separable states* with $2 \leq M \leq N$, which are states that can be written as convex combinations of product states, each of which is factorised with respect to an $M$-partition that need not be the same. The hierarchy stands as follows: $M$-separability implies $M'$-separability for any $M' < M$, whereas $M$-inseparability implies $M'$-inseparability for any $M' > M$. For example, when considering the two extremes of this hierarchy, we get that: $N$-separability implies any other form of $M$-separability, and is thus called *full separability*, whereas 2-inseparability implies any other form of $M$-inseparability, and is thus called *genuine multiparticle entanglement* or *full inseparability*. One can also easily see that the set $\mathcal{S}_M$ of $M$-separable states is the convex hull[4] of the union of all the sets of $\{Q_\alpha\}_{\alpha=1}^M$-separable states obtained by considering all the possible $M$-partitions $\{Q_\alpha\}_{\alpha=1}^M$. Therefore, quite counterintuitively, a 2-separable state could very well be inseparable with respect to any 2-partition and a state which is separable with respect to any bipartition need not be $N$-separable. Finally, in the partition independent setting the free operations are only LOCC with respect to all of the $M$-partitions, which are given simply by the single-particle LOCC. In the following we will mostly focus on the partition independent perspective, being it the one that really captures all the shades of multiparticle entanglement.

A particular type of single-particle LOCC, which will be quite relevant in the following, is a convex combination of single-particle local unitaries, whose action on a state $\rho$ is given by

$$\sum_i p_i \ U_i^{(1)} \otimes U_i^{(2)} \otimes \ldots \otimes U_i^{(N)} \rho \ U_i^{(1)\dagger} \otimes U_i^{(2)\dagger} \otimes \ldots \otimes U_i^{(N)\dagger}. \tag{1.4}$$

[4]The convex hull of a given set $S$ is defined as the set of all the convex combinations of points in $S$.

It requires only one-way communication and can be physically achieved by allowing one of the parties, e.g. the $\alpha$-th one, to randomly select a local unitary $U_i^{(\alpha)}$ by using the probability distribution $\{p_i\}$ and then to communicate the result to all the other parties.

Having introduced the free states and free operations of the resource theory of multiparticle entanglement, we can now list the axioms that a real and non-negative function $E_M$ on the set of states $\rho$ has to satisfy in order to be a fully bona fide measure $E_M$ of $M$-inseparable multiparticle entanglement[5] [19, 127, 128]:

- (E1) $E_M(\varsigma) = 0$ if $\varsigma \in \mathcal{S}_M$;
- (E2) $E_M(\Phi_{LOCC}(\rho)) \leq E_M(\rho)$ for any single-qubit LOCC $\Phi_{LOCC}$;
- (E3) $\sum_i p_i E_M(\rho_i) \leq E_M(\rho)$, with $p_i = \mathrm{Tr}(K_i \rho K_i^\dagger)$ and $\rho_i = K_i \rho K_i^\dagger / p_i$, for any $\{K_i\}$ such that $\sum_i K_i^\dagger K_i = \mathbb{I}$ and $K_i$ is a single-qubit local operator for any $i$;
- (E4) $E_M(\sum_i p_i \rho_i) \leq \sum_i p_i E_M(\rho_i)$ for any probability distribution $\{p_i\}$ and any set of states $\{\rho_i\}$.

Condition (E1) entails that the separable states have zero resource. Condition (E2) ensures that entanglement cannot increase under the corresponding free operations, i.e. LOCC, and implies that it is invariant under local unitaries, i.e. any local change of basis. Condition (E3) states that entanglement cannot even increase on average under selective LOCC, i.e. non-entangling quantum operations for which the information about the measurement outcomes $\{\rho_i\}$ is retained. This stronger monotonicity requirement is quite important as it allows for sub-selection based on measurement outcomes, a process available in well controlled quantum experiments. Finally, (E4) implies that entanglement cannot increase by classical mixture. Notice, however, that while convexity (E4) is physically desirable as it would mean that entanglement cannot increase by classically mixing states, it is not essential, since there are meaningful entanglement monotones that do not share such property [129].

Finally, although there is no general closed expression of the distillable entanglement and entanglement cost of an arbitrary state, it is known that the resource theory of entanglement is not asymptotically reversible and also there are instances of bound entangled states, i.e. entangled states that cannot be distilled into a maximally entangled state [19, 130]. However, when restricting to the class of maximally correlated states of two identical particles defined as [131, 132]:

$$\rho = \sum_{ij} \alpha_{ij} |ii\rangle\langle jj|, \tag{1.5}$$

where $\{|i\rangle\}$ is any local basis and $\alpha_{ij}$ is any $d \times d$ trace one Hermitian matrix, we have that the distillable entanglement $E_d$ and the entanglement cost $E_c$ are given by, respectively,

$$E_d(\rho) = E_{RE}(\rho), \tag{1.6}$$

$$E_c(\rho) = E_f(\rho), \tag{1.7}$$

[5] Analogous axioms hold when defining a fully bona fide measure $E_{\{Q_\alpha\}_{\alpha=1}^M}$ of multiparticle entanglement with respect to the partition $\{Q_\alpha\}_{\alpha=1}^M$, with the only difference that $M$-separable states and single-qubit LOCC are replaced by, respectively, $\{Q_\alpha\}_{\alpha=1}^M$-separable states and $\{Q_\alpha\}_{\alpha=1}^M$-LOCC.

where $E_{RE}(\rho) := \inf_{\sigma\in\mathcal{S}} S(\rho||\sigma)$, with $S(\rho||\sigma) := \mathrm{Tr}[\rho(\log\rho - \log\sigma)]$, is the so-called *relative entropy of entanglement* of $\rho$ and $E_f(\rho)$ is the so-called *entanglement of formation* of $\rho$ and is defined as the convex roof extension of the entropy of entanglement $E_S$, i.e.

$$E_f(\rho) := \inf_{\{p_i,\psi_i\}} \sum_i p_i E_S(|\psi_i\rangle), \tag{1.8}$$

where the optimisation is performed over all decompositions of $\rho$ into pure states, $\rho = \sum_i p_i|\psi_i\rangle\langle\psi_i|$.

## 1.3 Quantum coherence

Although quantum coherence stands as the most fundamental signature of quantumness, its resource theory is still under debate [36, 133–141].

According to [134, 137] the resource theory of quantum coherence is believed to lie within the resource theory of asymmetry, wherein the free states and free operations are those that satisfy a given symmetry. More precisely, in the special case where the symmetry group is the set of translations generated by a given observable, and thus the free states and operations are the so-called *translational invariant* ones, asymmetry can be interpreted as coherence with respect to the eigenbasis of such observable. Within this paradigm, the concept of quantum coherence as a resource can be easily understood for example in the context of quantum estimation theory [142], wherein a paradigmatic protocol consists of estimating the parameter $\phi$ embedded in a unitary $U_\phi = e^{-i\phi H}$ which is generated by the Hamiltonian $H$ and applied to a probe quantum state $\rho$. It turns out that the figure of merit in the precision of the estimation of the parameter $\phi$ is just the coherence of the probe state $\rho$, as measured by its quantum Fisher information, with respect to the eigenbasis of the Hamiltonian $H$ generating the unitary dynamics. Specifically, the more the probe state $\rho$ is far from being diagonal in the eigenbasis of $H$, as measured by its quantum Fisher information, the more precise is the estimation of the parameter $\phi$, provided that a number $\nu \gg 1$ of independent and identically distributed trials of the most informative measurement is performed on the output state $\rho_\phi = U_\phi \rho U_\phi^\dagger$.

This fundamental example clarifies why quantum coherence, contrary to entanglement, features a basis dependence. On the one hand, the choice of a particular basis is due to the physical scenario in consideration. Indeed, as we have seen for example in quantum metrology, the basis is set by the generator of the transformation that imprints the parameter onto the initial probe state. Moreover, in transport processes, including quantum biology [33], the reference basis is given by the eigenbasis of the Hamiltonian of the system.

On the other hand, in the chosen working reference basis $\{|e_i\rangle\}$, we can decompose any state $\rho$ as follows:

$$\rho = \rho_{diag} + \sum_{i\neq j} \rho_{ij} \left|e_i\right\rangle \left\langle e_j\right|, \tag{1.9}$$

where $\rho_{diag} = \sum_i \rho_{ii} \left|e_i\right\rangle \left\langle e_i\right|$ is a classical mixture of the states $\{|e_i\rangle\}$. Now it is the term $\sum_{i\neq j} \rho_{ij} \left|e_i\right\rangle \left\langle e_j\right|$ that marks the difference between the general state $\rho$ and the classical mixture $\rho_{diag}$, and gives rise to purely quantum phenomena, such as quantum interference,

when working in the basis $\{|e_i\rangle\}$, that we attribute to the quantum coherence of $\rho$ with respect to such basis [143]. Of course, we could instead choose to work in another basis, and there will always exist a basis in which $\rho$ is itself a classical mixture and therefore would manifest no quantum interference in this alternate working physical scenario, i.e. its quantum coherence with respect to this other basis must be zero. As a consequence, we can see that the quantum coherence of $\rho$ is dependent upon the chosen working basis, and this is why we naturally expect and require any ingredient of the resource theory of quantum coherence to show such basis dependence.

In the resource theory of quantum coherence, the exploited system is thus any $d$-dimensional quantum system, while the free states form the set $\mathcal{I}$ of states which are diagonal in the given reference basis $\{|i\rangle\}_{i=1}^{d}$, i.e. states of the form $\delta = \sum_{i=1}^{d} \delta_i |i\rangle\langle i|$, also called *incoherent states*. The resource states, i.e. all the states which are not diagonal in the given reference basis, will be instead referred to as *coherent states*.

According to [135, 136], the free operations of the resource theory of coherence correspond instead to another subclass of the physical operations that cannot create a coherent superposition of the states of the given reference basis, which strictly contains the translational invariant operations. More precisely, it is known that physical operations are represented by the completely positive trace preserving (CPTP) maps, i.e. the maps $\Phi$ that can be expressed in Kraus decomposition[6] as follows:

$$\Phi(\rho) = \sum_i K_i \rho K_i^\dagger, \tag{1.10}$$

with $\sum_i K_i^\dagger K_i = \mathbb{I}$, when applied to an input state $\rho$. Any physical operation $\Phi$ is thus a classical mixture of single processes, each one occurring with probability $p_i = \mathrm{Tr}(K_i \rho K_i^\dagger)$ and producing the outcome state $\rho_i = K_i \rho K_i^\dagger / p_i$. A physical map $\Phi$ represents a free operation, within the framework of the resource theory of coherence introduced in [135], if it is a classical mixture of single processes that do not create coherent superpositions of the states of the given reference basis, i.e. such that $K_i \mathcal{I} K_i^\dagger \subseteq \mathcal{I}$ for any $i$. Such operations are referred to as *incoherent operations* and denoted by $\Phi_{\mathcal{I}}$.

Since the translational invariant operations are strictly contained within the set of incoherent operations, the asymmetry-based resource theory of quantum coherence is more restrictive than the resource theory of coherence introduced in [135]. The latter resource theory, in turn, is not maximal, in that the incoherent operations do not cover all the *incoherence preserving operations*, i.e. the operations that leave the set of incoherent states invariant. A maximal resource theory of quantum coherence has been instead considered in [133].

Furthermore, it is important to clarify that the incoherent operations admit *at least* one Kraus decomposition with all Kraus operators being not able to create coherence superpositions. However, there can very well be Kraus decompositions of an incoherent operation whose Kraus operators do create coherent superpositions. An even more restricted resource theory of coherence involves so-called *genuinely incoherent operations* which are operations such that all Kraus representations only involve operations that do

[6] Note that the Kraus decomposition of a CPTP map need not be unique.

not create any coherent superposition [138]. Interestingly, such free operations are entirely contained within the set of translational invariant operations [138]. Finally, another alternative of free operations is given by the *strictly incoherent operations* [36, 139], which are a subset of incoherent operations whose incoherence preserving Kraus operators $\{K_i\}$ further obey $\langle j|K_i\rho K_i^\dagger|j\rangle = \langle j|K_i\rho_{diag}K_i^\dagger|j\rangle \ \forall i,j$, where $\rho_{diag} := \sum_{i=1}^d \langle i|\rho|i\rangle|i\rangle\langle i|$ is the diagonal part of $\rho$ in the reference basis. This means that strictly incoherent operations can neither create nor use coherence.

In summary, the following are the existing alternative choices of free operations in the resource theory of coherence, in order of inclusion: incoherence preserving operations [133] $\supset$ incoherent operations [135] $\supset$ strictly incoherent operations [139] $\supset$ translationally invariant operations [137] $\supset$ genuinely incoherent operations [138].

The paradigmatic noise sources in quantum information processing [135, 144] all embody instances of incoherent operations with respect to the basis of eigenstates of $\sigma_k$, $k \in \{1,2,3\}$, such as the computational basis. They act on a single qubit as follows, in terms of a parameter $q \in [0,1]$ which encodes the strength of the noise and in dynamical terms can be expressed as $q(t) = 1 - \exp(-\gamma t)$ with $t$ representing time and $\gamma$ being the decoherence rate. The bit flip, bit-phase flip and phase flip channels are represented in Kraus form by

$$K_0^{F_k} = \sqrt{1-q/2}\ \mathbb{I}, \ \ K_{i,j\neq k}^{F_k} = 0, \ \ K_k^{F_k} = \sqrt{q/2}\ \sigma_k, \tag{1.11}$$

with $k=1$, $k=2$ and $k=3$, respectively, $\mathbb{I}$ being the $2\times 2$ identity, and $\sigma_j$ the $j$-th Pauli matrix. The depolarising channel is represented by

$$K_0^D = \sqrt{1-3q/4}\ \mathbb{I}, \ K_j^D = \sqrt{q/4}\ \sigma_j, \tag{1.12}$$

with $j \in \{1,2,3\}$, and finally the amplitude damping channel is represented by

$$K_0^A = \begin{pmatrix} 1 & 0 \\ 0 & \sqrt{1-q} \end{pmatrix}, \ K_1^A = \begin{pmatrix} 0 & \sqrt{q} \\ 0 & 0 \end{pmatrix}. \tag{1.13}$$

On the other hand, when considering a multiparticle quantum system such as an $N$-qubit system, a natural choice of reference basis turns out to be a fully factorisable basis. If we consider for example the basis consisting of tensor products of eigenstates of $\sigma_k$, hereafter denoted by $\{|i_k\rangle\}_{i=1}^{2^N}$, with $k \in \{1,2,3\}$, one can immediately see that instances of incoherent operations are the independent and identical local noisy channels on each qubit, that map the system state $\rho$ into the evolved state

$$\Lambda_q^{\Xi\otimes N}(\rho) = \sum_{j_1,\cdots,j_N} \left(K_{j_1}^\Xi \otimes \cdots \otimes K_{j_N}^\Xi\right) \rho \left(K_{j_1}^{\Xi\,\dagger} \otimes \cdots \otimes K_{j_N}^{\Xi\,\dagger}\right), \tag{1.14}$$

where $\Xi = \{F_k, D, A\}$ represents the particular type of one-qubit noise.

Analogously to entanglement theory, once the free states and free operations pertaining to the resource theory of quantum coherence have been identified, the following requirements for any real and non-negative function $C$ on the set of states $\rho$ to be a fully bona fide measure of quantum coherence according to [135] immediately arise[7]:

[7] Analogous axioms hold when defining a bona fide measure of coherence within the other resource theoretic frameworks.

- (C1) $C(\delta) = 0$ if $\delta \in \mathcal{I}$;
- (C2) $C(\Phi_{\mathcal{I}}(\rho)) \leq C(\rho)$ for any incoherent operation $\Phi_{\mathcal{I}}$;
- (C3) $\sum_i p_i C(\rho_i) \leq C(\rho)$, with $p_i = \mathrm{Tr}(K_i \rho K_i^\dagger)$ and $\rho_i = K_i \rho K_i^\dagger / p_i$, for any $\{K_i\}$ such that $\sum_i K_i^\dagger K_i = \mathbb{I}$ and $K_i \mathcal{I} K_i^\dagger \subseteq \mathcal{I}$ for any $i$;
- (C4) $C(\sum_i p_i \rho_i) \leq \sum_i p_i C(\rho_i)$ for any probability distribution $\{p_i\}$ and any set of states $\{\rho_i\}$.

Condition (C1) says that the incoherent states have zero resource, being them the free states. Condition (C2) ensures that coherence cannot increase under incoherent channels, being them the free operations. Condition (C3) states that coherence cannot even increase on average under selective incoherent operations. Finally, (C4) implies that coherence cannot increase by classical mixture.

Two remarks are now in order. The above four conditions are not independent, but rather it can be easily seen that conditions (C3) and (C4) together imply condition (C2). However, it is worthwhile listing all of these properties since there could be operationally meaningful quantifiers of coherence satisfying only conditions (C1), (C2) and (C4), or even only conditions (C1) and (C2). Furthermore, being all the aforementioned non-maximal alternatives of free operations contained in the set of incoherent operations, any bona fide measure of coherence according to [135] is also a bona fide measure according to any other proposal of non-maximal resource theory of coherence existing in the literature, while the opposite is not necessarily true [137]. From now on, if not explicitly stated, we will restrict to quantum coherence within the resource theoretic framework of [135].

The $l_1$-norm of coherence $C_{l_1}$ of a state $\rho$ with respect to a given basis $\{|i\rangle\}_{i=1}^d$ is defined as

$$C_{l_1}(\rho) = \sum_{i \neq j = 1}^{d} |\rho_{ij}|, \tag{1.15}$$

where $\rho_{ij}$ is the representation of $\rho$ in such basis, and stands as the paradigmatic and most intuitive example of fully bona fide quantifier of quantum coherence which complies with all the aforementioned resource theories [135]. Interestingly, it enjoys a nice geometric interpretation, being it equivalent up to a constant factor to the trace distance between the state $\rho$ and its diagonal part $\rho_{diag}$, i.e.

$$C_{l_1}(\rho) = 2 D_{\mathrm{Tr}}(\rho, \rho_{diag}). \tag{1.16}$$

A maximally coherent state within the resource theory of quantum coherence of [135] is of the following form

$$|\Phi_d\rangle = \frac{1}{\sqrt{d}} \sum_{i=1}^{d} |i\rangle, \tag{1.17}$$

since any state can be obtained from the state $|\Phi_d\rangle$ via an incoherent operation [135]. Moreover, as it has been shown in [136], when considering again incoherent operations

as free operations, the distillable coherence $C_d$ and the coherence cost $C_c$ of an arbitrary state $\rho$ are given by, respectively,

$$C_d(\rho) = C_{RE}(\rho), \tag{1.18}$$
$$C_c(\rho) = C_f(\rho), \tag{1.19}$$

where

$$C_{\mathrm{RE}}(\rho) := S(\rho_{diag}) - S(\rho) \tag{1.20}$$

is the so-called *relative entropy of coherence* of $\rho$ and $C_f(\rho)$ is the so-called *coherence of formation* of $\rho$ and is defined as the convex roof extension of the relative entropy of coherence, i.e.

$$C_f(\rho) := \inf_{\{p_i,\psi_i\}} \sum_i p_i C_{RE}(|\psi_i\rangle), \tag{1.21}$$

where the optimisation is performed over all decompositions of $\rho$ into pure states, $\rho = \sum_i p_i |\psi_i\rangle\langle\psi_i|$. Consequently, being in general $C_c(\rho) \leq C_d(\rho)$, such resource theory of coherence is not asymptotically reversible.

Interestingly, it has been recently conjectured that the resource theories of quantum coherence and entanglement are equivalent when restricting the latter to maximally correlated states [136,138]. However, a physical interpretation of this conjecture is still lacking.

Finally, contrary to entanglement, there exists no bound coherent state within the resource theory of [135], since any coherent state can be distilled to the maximally coherent one through incoherent operations, as it can be easily seen from Eq. (1.18).

## 1.4 Quantum correlations beyond entanglement

Quantum correlations beyond entanglement, also known as discord-type correlations, give rise to the inevitable disturbance on a multiparticle quantum system after a local measurement [20–22]. In the bipartite case, such inevitable disturbance can arise via local measurements performed either on a subsystem only, due to one-way discord-type correlations, or on both subsystems, due to two-way discord-type correlations.

The resource theory of quantum correlations beyond entanglement has not been established yet, even though it has been shown that they represent a resource for many operational tasks, as already outlined in the Introduction. We will therefore introduce also this quantum feature by adopting a resource theoretic perspective.

Within the one-way setting, when considering local measurements on subsystem $A$ only[8], the free states are the so-called *classical-quantum* (CQ) *states*, i.e. particular instances of biseparable states than can be written as follows

$$\chi = \sum_i p_i \, |i\rangle \, \langle i|^A \otimes \tau_i^B \,, \tag{1.22}$$

[8] Analogously, when considering local measurements on subsystem $B$ only, the free states are the so-called *quantum-classical* (QC) *states*, which are of the form $\chi = \sum_i p_i \tau_i^A \otimes |i\rangle \, \langle i|^B$, where $\{p_i\}$ is a probability distribution, $\{|i\rangle^B\}$ denotes an orthonormal basis for subsystem $B$, and $\{\tau_i^A\}$ are arbitrary states for subsystem $A$.

where $\{p_i\}$ is a probability distribution, $\{|i\rangle^A\}$ denotes an orthonormal basis for subsystem $A$, and $\{\tau_i^B\}$ are arbitrary states for subsystem $B$. CQ states represent all, and only, the states whose disturbance after a local measurement on subsystem $A$ is not inevitable. Indeed, by measuring any local observable on $A$ whose eigenstates are given by the orthonormal basis $\{|i\rangle^A\}$, the classical-quantum states in Eq. (1.22) are left unperturbed.

Within the two-way setting, i.e. when considering local measurements on both subsystems $A$ and $B$, the free states are the so-called *classical-classical* (CC) *states* that can be written in the following form

$$\chi = \sum_{i,j} p_{ij} \left|i\right\rangle \left\langle i\right|^A \otimes \left|j\right\rangle \left\langle j\right|^B , \tag{1.23}$$

where $p_{ij}$ is a joint probability distribution, while $\{|i\rangle^A\}$ and $\{|j\rangle^B\}$ denote orthonormal bases for subsystem $A$ and $B$, respectively. The set $\mathcal{C}$ of CC states contains all, and only, the states whose disturbance after a local measurement on both subsystems $A$ and $B$ is not inevitable, and is clearly contained in the set of CQ states. Moreover, CC states are diagonal in a product orthonormal basis and thus merely correspond to the embedding of a classical bipartite probability distribution $\{p_{ij}\}$ into the quantum formalism. This is why, in general, by *classical states* we hereafter mean CC states.

It is worth noticing that, contrary to quantum coherence and entanglement, the set of free states associated with the resource theory of discord-type correlations is not convex.

While the free states of the resource theory of discord-type correlations are well identified, the corresponding free operations are still under debate. However, in [145] it has been shown that all, and only, the *local* operations that leave the set of classical states invariant are the *local commutativity preserving operations* $\Phi_{LCPO} := \Lambda_A \otimes \Lambda_B$, where $\Lambda_{A(B)}$ acts on subsystem $A(B)$ is such a way that $[\Lambda_{A(B)}(\rho_{A(B)}), \Lambda_{A(B)}(\sigma_{A(B)})] = 0$ when $[\rho_{A(B)}, \sigma_{A(B)}] = 0$ for arbitrary marginal states $\rho_{A(B)}$ and $\sigma_{A(B)}$. Consequently, due to the fact that free operations cannot create a resource state out of a free state, the free operations of the resource theory of quantum correlations beyond entanglement must be within the set of local commutativity preserving quantum channels if one imposes a priori the locality of such free operations.

In the case of a qubit, the commutative preserving operations are constituted by unital and semi-classical channels [79]. Unital channels are defined as those maps that leave the maximally mixed state alone, whereas semi-classical channels transform the set of all states into a subset of states which are all diagonal in the same basis. More generally, for higher dimensional quantum systems, the commutative preserving operations are either isotropic or completely decohering channels [146].

By assuming that the resource theory of discord-type correlations is the maximal one corresponding to the restriction to local free operations, and taking into account that the corresponding set of free states is not convex, and the fact that, in pure bipartite states, there is a unique kind of quantum correlations arising in all but tensor product states[9], we define any real and non-negative function $Q$ on the set of states $\rho$ satisfying

[9]Even correlations stronger than entanglement, such as steering and non-locality, just collapse back to non-separability in the case of pure states.

the following requirements to be a bona fide quantifier of two-way quantum correlations beyond entanglement:

- (Q1) $Q(\rho) = 0$ if $\rho \in \mathcal{C}$;
- (Q2) $Q(\Phi_{LCPO}(\rho)) \leq Q(\rho)$ for any local commutativity preserving operation $\Phi_{LCPO}$;
- (Q3) $Q$ reduces to an entanglement measure for pure states, i.e. $Q(|\psi^{AB}\rangle) = E(|\psi^{AB}\rangle)$ for any pure state $|\psi^{AB}\rangle$.

The above requirements need to be slightly modified if a one-way discord-type measure $Q_{\rightarrow}$, say with local measurements on $A$, is considered[10]. Specifically, property (Q1) becomes: $Q_{\rightarrow}(\rho) = 0$ if $\rho$ is a CQ state as defined in Eq. (1.22). Furthermore, a stricter monotonicity requirement supplements (Q2) for all valid one-way discord-type measures [51, 88, 147], namely

- (Q2.bis) $Q_{\rightarrow}$ is monotonically non-increasing under arbitrary local quantum channels on the unmeasured subsystem $B$, that is, $Q_{\rightarrow}\big((\mathbb{I}_A \otimes \Lambda_B)(\rho)\big) \leq Q_{\rightarrow}(\rho)$ for any state $\rho$ and any CPTP map $\Lambda_B$ on subsystem $B$.

On the other hand, property (Q3) applies equally to two-way and one-way discord-type measures. We further specify that, for states which are symmetric with respect to permutations of the two subsystems, the two notions of discord are completely equivalent. We also note that concepts such as distillable discord or discord cost have not been investigated yet.

We conclude this section by briefly reviewing one of the most recent operational interpretations of one-way discord-type correlations [44]. Here, an input bipartite quantum state $\rho_{AB}$ enters a two-arm channel, in which subsystem $B$ is left alone while subsystem $A$ undergoes a local unitary evolution generated by the Hamiltonian $H_A$. Overall, the evolved state is thus given by $\rho^{\phi}_{AB} = (U_A \otimes I_B)\rho_{AB}(U^{\dagger}_A \otimes I_B)$, with $U_A = e^{-i\phi H_A}$ and $I_B$ being the identity on $B$. The task of the protocol is to estimate the phase $\phi$ encoded into the evolved state, even though only the spectrum of the Hamiltonian $H_A$ is known. As we have already mentioned, the bigger is the quantum Fisher Information of the evolved state $\rho^{\phi}_{AB}$, the better will be the precision of the estimation of the parameter $\phi$. However, since we know only the spectrum of the Hamiltonian, the only precision that we can guarantee is the one corresponding to the worst case scenario Hamiltonian, i.e. the one that minimises the quantum Fisher information of the evolved state, given the known spectrum. Now it turns out that such minimum is a bona fide quantifier of one-way discord-type correlations of the input probe state $\rho_{AB}$ with respect to subsystem $A$. In other words, quantum correlations beyond entanglement are the power behind quantum metrology when only the spectrum of the Hamiltonian generating the evolution is known, being it the precision of the estimation in the worst case scenario.

[10] Analogously, when one-way discord-type measures $Q_{\leftarrow}$ with local measurements on $B$ are considered, (Q1) becomes $Q_{\leftarrow}(\rho) = 0$ if $\rho$ is a QC state and (Q2) must be integrated with monotonicity under arbitrary local quantum operations on the unmeasured subsystem $A$.

We note in passing that this result also highlights an interesting connection between quantum correlations beyond entanglement and quantum coherence for bipartite systems, whereby the former can be considered as the minimum over all product bases of the latter.

## 1.5 Interplay between the various facets of quantumness

Having introduced these three signatures of quantumness, an obvious question arises. Is it possible to interconvert them between each other? For example, is it possible to convert coherence or discord-type correlations into entanglement? The answer to this question is affirmative and we now briefly mention two protocols allowing for the interconversion between, respectively, discord-type correlations and entanglement [79], and coherence and entanglement [31].

In the first protocol [79] a von Neumann measurement, which consists of a unitary followed by a controlled-NOT gate with a measurement apparatus $M$, is performed on subsystem $B$ of a bipartite quantum system $AB$. Quite remarkably, it turns out that the output state $\tilde{\rho}_{AB:M}$ of the overall system composed by $AB$ and the apparatus $M$ becomes bipartite entangled for all choices of the local unitary $U_B$ applied to $B$ if, and only if, the input state $\rho_{AB}$ of the bipartite system $AB$ has non-vanishing one-way discord-type correlations with respect to subsystem $B$. Even more, the connection between entanglement and discord can be made quantitative, in the sense that the minimal entanglement between the system $AB$ and the measurement apparatus $M$ generated after a local von Neumann measurement on subsystem $B$, i.e.

$$Q_{\leftarrow}(\rho_{AB}) := \inf_{U_B} E(\tilde{\rho}_{AB:M}), \tag{1.24}$$

qualifies as a bona fide quantifier of the one-way discord of the input state $\rho_{AB}$ with respect to subsystem $B$. In other words, one-way discord-type correlations represent the resource behind the activation of bipartite entanglement through local von Neumann measurements.

In the second protocol [31] an incoherent operation is globally applied to a quantum system $S$ and an initially incoherent ancilla $A$. It turns out that the output state of the overall system composed by $S$ and $A$ is entangled if, and only if, the initial state of system $S$ has non-vanishing quantum coherence. Again, quite remarkably, also the connection between quantum coherence and entanglement can be made quantitative in the following sense. The maximal entanglement between the system $S$ and the initially incoherent ancilla $A$ generated after incoherent operations quantifies faithfully the initial coherence of the system $S$. Consequently, quantum coherence constitutes the unexpendable resource to optimally activate bipartite entanglement through incoherent operations.

# Chapter 2

# Information geometry

In this Chapter we will introduce the information geometric framework adopted throughout this Thesis, wherein appropriate distances defined on the set of quantum states are considered. Such geometric machinery has in fact proven to be invaluable in order to obtain all the results that will be presented in the next Chapters, be them related to the quantification, dynamical preservation, and applications to quantum phase transitions of quantumness, or even to the analysis of quantum speed limits.

## 2.1 Metric structures

The main mathematical players will be without doubt the metric structures that can be defined on the set of quantum states. A metric structure on a set $S$ is supposed to quantify how far any two points of $S$ are from each other. This is done via the notion of distance, which is any real function $D$ on the set $S \times S$ satisfying the following properties for any elements $x, y, z$ in $S$:

- (D1) semi-positivity, i.e. $D(x, y) \geqslant 0$, and non-degeneracy, i.e. $D(x, y) = 0 \Leftrightarrow x = y$;
- (D2) symmetry, i.e. $D(x, y) = D(y, x)$;
- (D3) triangle inequality, i.e. $D(x, z) \leq D(x, y) + D(y, z)$.

When considering the most intuitive example of space, that is any Euclidean linear space $V$, such a distance naturally arises from the notion of scalar product $\mathbf{g}$ between any two vectors $\mathbf{x}$ and $\mathbf{y}$ in $V$, also known as metric tensor, which is any sesquilinear function on $V \times V$ satisfying the following properties for any vectors $\mathbf{x}, \mathbf{y}$ in $V$:

- (M1) semi-positivity, i.e. $\mathbf{g}(\mathbf{x}, \mathbf{x}) \geqslant 0$;
- (M2) non-degeneracy, i.e. $\mathbf{g}(\mathbf{x}, \mathbf{y}) = 0 \ \forall \mathbf{y} \Rightarrow \mathbf{x} = \mathbf{0}$;
- (M3) symmetry, i.e. $\mathbf{g}(\mathbf{x}, \mathbf{y}) = \mathbf{g}(\mathbf{y}, \mathbf{x})$.

In particular, the Euclidean distance between any two vectors $\mathbf{x}$ and $\mathbf{y}$ is certainly the most familiar example of metric structure and arises from the underlying metric tensor as follows:

$$D^2_{\mathrm{Eu}}(\mathbf{x},\mathbf{y}) := \mathbf{g}(\mathbf{x}-\mathbf{y},\mathbf{x}-\mathbf{y}). \tag{2.1}$$

To make this expression more explicit, we just need to consider an orthonormal basis $\{\mathbf{e}_i\}$ of $V$ with respect to the given metric tensor, i.e. such that $\mathbf{g}(\mathbf{e}_i,\mathbf{e}_j)=\delta_{ij}$, in such a way that Eq. (2.1) becomes

$$D^2_{\mathrm{Eu}}(\mathbf{x},\mathbf{y}) = \sum_i \left|x^i - y^i\right|^2, \tag{2.2}$$

where $x^i$ and $y^i$ are, respectively, the components of $\mathbf{x}$ and $\mathbf{y}$ in such basis, i.e. $\mathbf{x}=\sum_i x^i\mathbf{e}_i$ and $\mathbf{y}=\sum_i y^i\mathbf{e}_i$.

However, the set of quantum states is not a linear space, but rather a non-linear Riemannian manifold, which is basically a space that only in close proximity to each of its points resembles a Euclidean linear space, i.e. the tangent space at that point. Each of these local tangent spaces, say the one at the point $p$ of the manifold, is endowed with its own metric tensor $\mathbf{g}_p$. Another fundamental property of a Riemannian manifold is that the local metric tensor $\mathbf{g}_p$ varies smoothly with the point $p$. Such smooth function, associating with any point $p$ of the Riemannian manifold a local metric tensor $\mathbf{g}_p$, is called a Riemannian metric. We can thus adopt the local metric tensor $\mathbf{g}_p$ only infinitesimally close to the point $p$ and approximate the squared infinitesimal distance $ds^2$ between such point and another neighbouring one with the squared infinitesimal distance between the corresponding points in the local tangent space, $\mathbf{x}$ and $\mathbf{x}+d\mathbf{x}$, respectively, where $\mathbf{x}$ represents the coordinates of the point $p$, i.e.

$$ds^2 := \mathbf{g}_p(d\mathbf{x},d\mathbf{x}). \tag{2.3}$$

Then, a natural way to quantify the distance between two non-neighbouring points $p$ and $q$ immediately arises. Indeed, one can just consider the length $\mathcal{L}$ of the shortest curve connecting such points, also called a geodesic, where the length of a curve is simply obtained by integrating the differential $ds$ in Eq. (2.3) over the curve itself, i.e.

$$\mathcal{L}(p,q) := \min_\gamma \int_\gamma ds, \tag{2.4}$$

where $\gamma$ is any curve connecting the points $p$ and $q$ and $\int_\gamma$ is the line integral over the curve $\gamma$.

A prominent example of Riemannian metric is the Fisher information metric defined on the manifold of classical probability distributions $\{p^i\}$ as follows

$$ds^2 = \frac{1}{4}\sum_i \frac{(dp^i)^2}{p^i}, \tag{2.5}$$

and whose geodesic distance is the so-called Bures angle

$$\mathcal{L}_{\mathrm{F}}(\mathbf{p},\mathbf{q}) = \arccos\left[\sqrt{F(\mathbf{p},\mathbf{q})}\right], \tag{2.6}$$

where $F(\mathbf{p},\mathbf{q}) = \left(\sum_i \sqrt{p^i q^i}\right)^2$ is the classical fidelity between the probability distributions $\mathbf{p}$ and $\mathbf{q}$.

Two remarks are now in order. First, a distance need not be Riemannian, in the sense that we do not need a Riemannian metric in order to define a distance. A notable example is the trace distance, which is defined as follows:

$$D_{\mathrm{Tr}}(\mathbf{x},\mathbf{y}) := \frac{1}{2}\sum_i \left|x^i - y^i\right|. \tag{2.7}$$

Second, while the symmetry property (D2) is rather intuitive, it is not essential whatsoever. This can be easily understood within the statistical setting, wherein distances are adopted in order to distinguish between two probability distributions $\mathbf{p}$ and $\mathbf{q}$. Let us assume that the latter correspond to the states of two coins, so that each of them is given by an ordered pair representing the probabilities of getting heads and tails, respectively. Moreover, one of the coins is fully biased, say it will always be heads and so $\mathbf{p} = \{1, 0\}$, and the other one is not biased at all, i.e. it can be heads or tails with equal probabilities and so $\mathbf{q} = \{1/2, 1/2\}$. Now, if one is allowed to measure only one coin in order to understand which one is which, an inevitable asymmetry arises. By measuring the fully biased coin, one will always get heads and can never be certain of which coin is being tossed, since the same phenomenon could very well happen by tossing the non-biased one. Instead, by measuring the non-biased coin, whenever one gets tails it can be sure to be tossing the non-biased coin. Overall, the distinguishability among the states of the above two coins depends on which one is measured. This operational asymmetric feature is nicely described e.g. by the so-called relative entropy distance:

$$D_{\mathrm{RE}}(\mathbf{p},\mathbf{q}) := \sum_i p_i(\log p_i - \log q_i). \tag{2.8}$$

## 2.2 Geometric quantum state distinguishability

Distinguishing between two states of a system admitting a probabilistic interpretation is a fundamental task of information theory, whose achievement by adopting differential geometric techniques represents the main job of information geometry [148].

According to statistical mechanics, the set of states of both classical and quantum systems is described by a Riemannian manifold, that is the set of probability distributions over the system phase space and the set of density operators over the system Hilbert space, respectively. A natural way to quantify the distinguishability between two states could be then to consider their geodesic distance with respect to any of the Riemannian metrics defined on the set of states. However, not all distances are appropriate for this purpose. Indeed, a natural requirement for a distance to quantify in a statistically relevant way the distinguishability between two states is that it must contract under stochastic maps. This is due to the fact that stochastic maps represent the mathematical counterpart of noise, thus causing a loss of information that is incompatible with the increasing of distinguishability.

Quite remarkably, Čencov's theorem ensures that the Fisher information metric is the only Riemannian metric on the set of probability distributions that is contractive under classical stochastic maps [149], thus leaving us with only one choice of bona fide Riemannian geometric measure of distinguishability within the classical setting. On the other hand, within the quantum setting, it turns out that the quantum Fisher information metric [150, 151] is not the only contractive Riemannian metric on the set of density operators, but rather there exists an infinite family of such metrics, as characterised by the Morozova, Čencov and Petz (MCP) theorem [152, 153].

We now restrict to the quantum setting and review the vast variety of choices that we have at our disposal to reliably distinguish among quantum states, as provided by the MCP theorem. Let $\mathcal{H}$ be the Hilbert space associated with a given quantum system and $\mathcal{D}(\mathcal{H})$ the corresponding set of states, that is the Riemannian manifold of positive semi-definite and trace one operators over the carrier Hilbert space. A Riemannian metric over $\mathcal{D}(\mathcal{H})$ is said to be contractive if the corresponding geodesic distance $\mathcal{L}$ contracts under quantum stochastic maps, i.e. satisfies the following inequality

$$\mathcal{L}(\Lambda(\rho), \Lambda(\sigma)) \leq \mathcal{L}(\rho, \sigma), \tag{2.9}$$

for any completely positive trace preserving map $\Lambda$ and any $\rho, \sigma \in \mathcal{D}(\mathcal{H})$. The MCP theorem provides us with a characterisation of such metrics in the finite-dimensional case, by establishing a one to one correspondence between them and the Morozova-Čencov (MC) functions, i.e. any function $f(t) : \mathbb{R}_+ \to \mathbb{R}_+$ that is

- $(i)$ operator monotone, i.e. for any semi-positive definite operators $A$ and $B$ such that $A \leq B$, then $f(A) \leq f(B)$;
- $(ii)$ self-inversive, i.e. $f(t) = tf(1/t)$;
- $(iii)$ normalised, i.e. $f(1) = 1$.

Specifically, the MCP theorem states that every contractive Riemannian metric $\mathbf{g}$ assigns, up to a constant factor, the following squared infinitesimal length between two neighbouring density operators $\rho$ and $\rho + d\rho$ [153]

$$ds^2 := \mathbf{g}^f_\rho(d\rho, d\rho), \tag{2.10}$$

with

$$\mathbf{g}^f_\rho(A, B) = \frac{1}{4}\mathrm{Tr}[A\, c^f(\mathbf{L}_\rho, \mathbf{R}_\rho)\, B] \ , \tag{2.11}$$

where $A$ and $B$ are any two traceless hermitian operators, and

$$c^f(x, y) := \frac{1}{yf(x/y)} \tag{2.12}$$

is a family of functions that are symmetric, i.e. $c^f(x, y) = c^f(y, x)$, homogeneous of degree $-1$, i.e. $c^f(\alpha x, \alpha y) = \alpha^{-1} c^f(x, y)$, and are parameterised by the MC functions $f$. Finally, $\mathbf{L}_\rho, \mathbf{R}_\rho : \mathcal{B}(\mathcal{H}) \to \mathcal{B}(\mathcal{H})$ are two linear superoperators defined on the set $\mathcal{B}(\mathcal{H})$ of linear

operators over $\mathcal{H}$ as follows: $\mathbf{L}_\rho A = \rho A$ and $\mathbf{R}_\rho A = A\rho$. In accordance with Ref. [154], in Eq. (2.11) we have chosen the factor $1/4$ in order to make the entire family of contractive Riemannian metrics collapse onto the classical Fisher information metric when $\rho$ and $d\rho$ commute.

To make Eq. (2.10) more explicit, we can write the density operator $\rho$ in its spectral decomposition, i.e. $\rho = \sum_j p_j |j\rangle\langle j\,|$, with $0 < p_j \leq 1$ and $\sum_j p_j = 1$, and get [154]

$$ds^2 = \frac{1}{4}\left[\sum_j \frac{(d\rho_{jj})^2}{p_j} + 2\sum_{j<l} c^f(p_j, p_l)|d\rho_{jl}|^2\right] , \tag{2.13}$$

where $d\rho_{jl} := \langle j|d\rho|l\rangle$ and the summation is over all indices $j$ such that $p_j > 0$. Equation (2.13) clearly discerns among two separate contributions to any contractive Riemannian metric. The first term, which is common to all the family, depends only on the populations $p_j$ of $\rho$ and can be seen as the classical Fisher information metric at the probability distribution $\{p_j\}$. The second term, which is responsible for the non-uniqueness of a contractive Riemmanian metric on the quantum state space, is instead simply due to the coherences of $d\rho$ with respect to the eigenbasis of $\rho$ and is a purely quantum contribution expressing the non-commutativity between the operators $\rho$ and $\rho + d\rho$.

Interestingly, for all the contractive Riemannian metrics that can be naturally extended to the boundary of pure states, i.e. such that $f(0) \neq 0$, the Fubini-Study metric appears always to be such extension up to a constant factor, so that the non uniqueness of a contractive Riemannian geometry can be only witnessed when considering quantum mixed states.

Furthermore, the MC functions satisfy a strict hierarchy. Indeed there exists a minimal MC function, $f_{\min}(t) = 2t/(1+t)$, and a maximal one, $f_{\max}(t) = (1+t)/2$, such that a generic MC function $f(t)$ must satisfy $f_{\min}(t) \leq f(t) \leq f_{\max}(t)$ [155]. Remarkably, the maximal MC function is the one corresponding to the celebrated quantum Fisher information metric, whereas the Wigner-Yanase information metric corresponds to an intermediate MC function, $f_{\mathrm{WY}} = (1/4)(\sqrt{t}+1)^2$, as illustrated in Fig. 2.1.

These metrics play a fundamental role in quantum information theory since the corresponding geodesic lengths $\mathcal{L}$, being by construction contractive under quantum stochastic maps, all stand as bona fide measures of distinguishability over the quantum state space. However, finding such geodesic distances is unfortunately a hard task. In fact, analytic expressions are known only for the geodesic distance related to the quantum Fisher information metric,

$$\mathcal{L}^{\mathrm{QF}}(\rho,\sigma) = \arccos\left[\sqrt{F(\rho,\sigma)}\right], \tag{2.14}$$

where $F(\rho,\sigma)$ is the quantum fidelity, and the Wigner-Yanase information metric [156],

$$\mathcal{L}^{\mathrm{WY}}(\rho,\sigma) = \arccos\left[A(\rho,\sigma)\right], \tag{2.15}$$

where $A(\rho,\sigma) = \mathrm{Tr}\,(\sqrt{\rho}\sqrt{\sigma})$ is called quantum affinity. It is worthwhile to note that such geodesic distances are equivalent to, respectively, the Bures distance,

$$D_{\mathrm{B}}(\rho,\sigma) := \sqrt{2\left(1-\sqrt{F(\rho,\sigma)}\right)}, \tag{2.16}$$

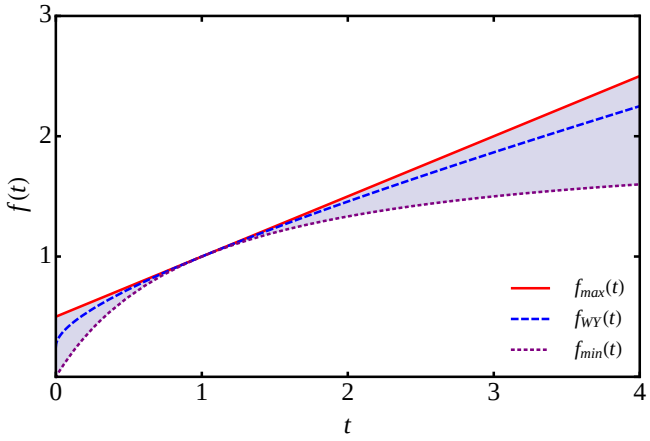


Figure 2.1: The hierarchy of Morozova-Čencov functions. Every MC function $f(t)$ is upper bounded by a maximal one, $f_{\max}(t) = (1+t)/2$, corresponding to the quantum Fisher information metric (red solid line), and lower bounded by a minimal one, $f_{\min}(t) = 2t/(1+t)$ (purple dotted line), in such a way that $f_{\min}(t) \leq f(t) \leq f_{\max}(t)$ and its graph falls into the shaded area. This is shown in the particular case of the MC function $f_{\rm WY} = (1/4)(\sqrt{t}+1)^2$, corresponding to the Wigner-Yanase information metric (blue dashed line). All the MC functions collapse to 1 in $t = 1$, due to the fact that the corresponding Riemannian metrics are regular at the maximally mixed state.

and the Hellinger distance,

$$D_{\rm H}(\rho,\sigma) := \sqrt{2\,(1 - A(\rho,\sigma))}. \tag{2.17}$$

However, while contractivity under stochastic maps is a crucial physical requirement, a distance need not be Riemannian in order to be a bona fide quantifier of distinguishability. Notable examples of such distances are the trace distance and the relative entropy distance, that in the quantum setting are defined as follows:

$$D_{\rm Tr}(\rho,\sigma) := \frac{1}{2} Tr|\rho - \sigma|, \tag{2.18}$$

$$D_{\rm RE}(\rho,\sigma) := Tr[\rho(\log\rho - \log\sigma)]. \tag{2.19}$$

Remarkably, the Euclidean distance, also known as Hilbert-Schmidt distance, as defined as follows:

$$D_{\rm HS}(\rho,\sigma) := \sqrt{Tr[(\rho-\sigma)^2]}, \tag{2.20}$$

is not contractive and thus does not represent a bona fide quantifier of distinguishability and will not be relevant in the following analysis.

## 2.3 Geometric quantification of quantumness

Information geometry allows us for a unifying and intuitive approach to the quantification of any resource whose corresponding set of free states is closed[1], as it happens for example in the resource theories of entanglement, quantum coherence and discord-type correlations. According to this approach, the more a state is distinguishable from the set of free states, the more resourceful this state is. More precisely, the resource of a given state $\rho$ is quantified by considering the distance from $\rho$ to the set of free states $\mathcal{F}$, i.e.

$$R^D(\rho) := \inf_{\sigma\in\mathcal{F}} D(\rho,\sigma), \tag{2.21}$$

where $D$ is a contractive distance.

Clearly this resource quantifier is zero for all, and only, the free states. Moreover, it is also monotonically non-increasing under any CPTP map that leaves the set of free states invariant and so under any possible free operation. Indeed, if $\Phi_{\mathcal{F}}$ is any physical operation that leaves the set of free states $\mathcal{F}$ invariant, then we have

$$R(\Phi_{\mathcal{F}}(\rho)) := \inf_{\sigma\in\mathcal{F}} D(\Phi_{\mathcal{F}}(\rho),\sigma) \leq \inf_{\sigma\in\mathcal{F}} D(\Phi_{\mathcal{F}}(\rho),\Phi_{\mathcal{F}}(\sigma)) \leq \inf_{\sigma\in\mathcal{F}} D(\rho,\sigma) =: R(\rho), \tag{2.22}$$

where in the first inequality we have used the fact that $\Phi_{\mathcal{F}}(\mathcal{F}) \subseteq \mathcal{F}$ and in the second inequality we have used the contractivity of the distance $D$ under any CPTP map.

In the case of any resource theory whose set of free states is convex, by assuming joint convexity of the distance $D$, i.e.

$$D\left(\sum_i p_i\rho_i, \sum_i p_i\sigma_i\right) \leq \sum_i p_i D(\rho_i,\sigma_i), \tag{2.23}$$

for any probability distribution $\{p_i\}$ and any states $\rho_i$ and $\sigma_i$, one can see in a similar way that we get also the convexity of the corresponding resource quantifier $R^D$.

Therefore, by restricting to the resource theories of entanglement, quantum coherence and discord-type correlations, we get that the following real and non-negative functions defined on the set of quantum states $\rho$:

$$E_M^D(\rho) := \inf_{\varsigma\in\mathcal{S}_M} D(\rho,\varsigma), \tag{2.24}$$

$$C^D(\rho) := \inf_{\delta\in\mathcal{I}} D(\rho,\delta), \tag{2.25}$$

$$Q^D(\rho) := \inf_{\chi\in\mathcal{C}} D(\rho,\chi), \tag{2.26}$$

$$Q_{\rightarrow}^D(\rho) := \inf_{\chi\in\mathcal{C}\mathcal{Q}} D(\rho,\chi), \tag{2.27}$$

$$Q_{\leftarrow}^D(\rho) := \inf_{\chi\in\mathcal{Q}\mathcal{C}} D(\rho,\chi), \tag{2.28}$$

[1] A set $S$ is said to be closed if it contains all of its limit points.

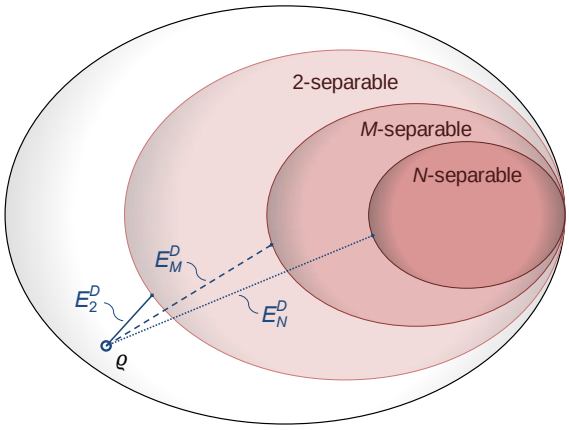


Figure 2.2: Geometric picture of multiparticle entanglement in a quantum system of $N$ particles. Each red-shaded convex set contains $M$-separable states, for $2 \leq M \leq N$. For any $M$, the geometric multiparticle entanglement measure $E_M^D$ of a state $\rho$ is defined as the minimum distance, with respect to a contractive and jointly convex distance $D$, from the set of $M$-separable states. We refer to the case $M = N$ (dotted line) as global geometric entanglement, the case $M = 2$ (solid line) as genuine geometric entanglement, and any intermediate case (dashed line) as partial geometric entanglement.

are bona fide measures of, respectively, $M$-inseparable multiparticle entanglement, quantum coherence, two-way symmetric discord type correlations, and one-way discord-type correlations with local measurements on subsystem $A$ and $B$, in the sense that the axioms (E1), (E2), (E4), (C1), (C2), (C4), (Q1), (Q2) and (Q2.bis) are all automatically satisfied, just by assuming contractivity and joint convexity of the distance $D$. We are only left with the axioms (E3), (C3) and (Q3). (E3) and (C3) refer to a monotonicity under selective LOCC and incoherent operations, respectively, that can be satisfied if the distance $D$ fulfils the following further requirements for any states $\rho$ and $\sigma$ [157]:

- $\sum_i p_i D\left(\frac{\rho_i}{p_i}, \frac{\sigma_i}{q_i}\right) \leq \sum_i D(\rho_i, \sigma_i)$, where $\rho_i = K_i \rho K_i^\dagger$, $\sigma_i = K_i \sigma K_i^\dagger$, $p_i = \mathrm{Tr}(\rho_i)$ and $q_i = \mathrm{Tr}(\sigma_i)$, for any Kraus operators $\{K_i\}$;
- $D(\sum_i P_i \rho P_i, \sum_i P_i \sigma P_i) = \sum_i D(P_i \rho P_i, P_i \sigma P_i)$, where $\{P_i\}$ is any set of orthogonal projectors such that $P_i P_j = \delta_{ij} P_i$;
- $D(\rho \otimes P, \sigma \otimes P) = D(\rho, \sigma)$, where $P$ is any projector.

On the other hand, it is still unknown which properties of a distance $D$ are sufficient for the corresponding geometric measure of discord-type correlations to satisfy (Q3).

In Fig. 2.2 we provide an illustration of such geometric approach to the quantification of $M$-inseparable multiparticle entanglement.

There is yet another unifying geometric approach that is tailored to the quantification of both bipartite entanglement and one-way discord-type correlations, and is based

on the inevitable disturbance caused by quantum correlations when non-degenerate local unitaries are applied on one subsystem only [158–162]. According to this approach, the distinguishability between a given state and its image after a least perturbing non-degenerate local unitary operation on one subsystem only is a bona fide measure of entanglement, the so-called *entanglement of response* [158–160], in the case of pure states. In the case of mixed states, it is a bona fide measure of one-way discord type correlations, the so-called *discord of response* [161, 162].

To be more specific, let us denote by $\rho_\psi \equiv |\psi\rangle\langle\psi|$ and $\Lambda$, respectively, a generic pure state of the bipartite quantum system $AB$ and the set of local unitaries applied only on subsystem $A$, $U_A \equiv U_A \otimes \mathbb{I}_B$, such that $\mathbb{I}_B$ is the identity operator on $\mathcal{H}_B$ and $U_A$ is any unitary operator on $\mathcal{H}_A$ whose spectrum is given by the $d_A$-th complex roots of unity, with $d_A := \dim \mathcal{H}_A$. The *entanglement of response* [158, 159] of $\rho_\psi$, $E(|\psi\rangle)$, is defined by:

$$E(|\psi\rangle) := \min_{U_A \in \Lambda} D^2(\rho_\psi, \tilde{\rho}_\psi) \ , \tag{2.29}$$

where $\tilde{\rho}_\psi \equiv U_A \rho_\psi U_A^\dagger$ and $D$ is any contractive distance.

There are at least two distinct ways to extend the entanglement of response to mixed states: the convex roof extension, which then identifies the entanglement of response of mixed states, and the *discord of response* defined directly as the distance between a given mixed state and the one obtained from it through the action of the least perturbing non-degenerate local unitary operation on subsystem $A$ only [161, 162]. More precisely, the *entanglement of response* of a bipartite mixed state $\rho$, $E(\rho)$, is defined as:

$$E(\rho) := \min_{\{|\psi_i\rangle, p_i\}} \sum_i p_i E(|\psi_i\rangle) \ , \tag{2.30}$$

where the minimisation is performed over all the decompositions of $\rho$ in pure states $\sum_i p_i |\psi_i\rangle\langle\psi_i| = \rho$, $p_i \geq 0$, $\sum_i p_i = 1$. On the other hand, the *discord of response* of a bipartite state $\rho$, $Q_\rightarrow(\rho)$, is defined as [161, 162]:

$$Q_\rightarrow(\rho) := \min_{U_A \in \Lambda} D^2(\rho, \tilde{\rho}) \, , \tag{2.31}$$

where, as in the case of pure states, $\tilde{\rho} \equiv U_A \rho U_A^\dagger$.

Therefore, the entanglement and the discord of response quantify different aspects of bipartite quantum correlations via two different uses of non-degenerate local unitary operations on one subsystem only. The discord of response arises by applying such local unitaries directly to the generally mixed state $\rho$, while the entanglement of response stems from the application of these local unitaries to pure states.

In terms of the trace distance, which will be relevant in the analysis of Chapter 5, the two-qubit entanglement of response is simply given by the squared concurrence [162, 163], whereas the two-qubit discord of response relates nicely to the corresponding geometric discord defined in Eq. (2.27) [164], whose closed formula is known only for a particular class of two-qubit states [165], although it can be computed for a more general class of two-qubit states through a very efficient numerical optimisation.

## 2.4 Operational interpretation of the geometric quantifiers

The quantitative amount of a resource, be it quantum coherence, entanglement or even quantum correlations beyond entanglement, has an intuitive operational meaning when adopting the geometric approach expressed in Eq. (2.21), that is measuring how distinguishable a given state is from the closest free state. We now conclude this chapter by considering some widely adopted distances and seeing that such a distinguishability is directly connected to the usefulness of the given state for quantum information tasks relying on the resource.

As we have seen in the case of entanglement for maximally correlated states and in the case of coherence for any state, but as it actually happens for any maximal and convex resource [124], the relative entropy distance-based measure coincides with the distillable resource, quantifying the ability of a state to be converted into a maximally resourceful state via free operations.

The Bures distance-based measure of one-way discord-type correlations is directly linked to the success in the ambiguous quantum state discrimination protocol [45, 46], which plays a fundamental role both in quantum communication and cryptography [166, 167]. In this protocol, a family of $n$ known states $\{\rho_i\}_{i=1}^n$ encodes a message. A sender randomly selects the states from this family via a probability distribution $\{p_i\}_{i=1}^n$ and gives them one by one to a receiver, whose task is to identify them and thus decode the message. To do this, the receiver performs a generalised measurement with $n$ outcomes[2] $\{M_i\}_{i=1}^n$ on each of the states given to him by the sender and concludes that the received state is $\rho_j$ when the measurement outcome is the $j^{\text{th}}$ one. Since the states $\{\rho_i\}_{i=1}^n$ need not be orthogonal, there is in general no measurement that can perfectly distinguish between them, so that the best the receiver can do is to perform a measurement minimising the probability of equivocation. Such optimal measurement is the one maximising the so-called success probability $P_S = \sum_{i=1}^n p_i P_{i|i}$, where $P_{i|i} = \text{Tr}(M_i\rho_i)$ is the probability of getting the $i^{\text{th}}$ result provided that the given state is the $i^{\text{th}}$ one. It turns out that the maximal fidelity between the state $\rho = \sum_{i=1}^n p_i\rho_i$ and the set of classical-quantum states is exactly the maximal success probability in the ambiguous quantum state discrimination between the states $\{\rho_i\}_{i=1}^n$ with prior probabilities $\{p_i\}_{i=1}^n$, thus providing us with the promised direct link between the corresponding geometric measure of one-way discord-type correlations and such protocol.

Moreover, the Bures distance-based measure of global entanglement directly assesses the usefulness of an input state in order to perform the celebrated Grover's search algorithm [38] and has also a dual interpretation based on the convex roof construction [168], in the sense that it quantifies the minimum average pure-state geometric entanglement required to create a given state by classical statistical mixing [169].

If $D$ denotes instead the trace distance, the distinguishability between the resource state $\rho$ and the corresponding closest free state is operationally related to the minimum probability of error in discriminating between them with a single measurement [154].

[2] A generalised measurement with $n$ outcomes is described by a set of $n$ positive operators $M_i \geq 0$ satisfying $\sum_{i=1}^n M_i = \mathbb{I}$. The probability of getting the $j^{\text{th}}$ outcome, after that such a measurement has been performed on a system in the state $\rho$, is given by $\text{Tr}(\rho M_i)$.

Overall, evaluating geometric measures of resources defined by meaningful distances on practically relevant states is thus a central challenge to benchmark quantum technologies, although this is in principle a formidable mathematical problem. What is more, even if we managed to solve this problem for any state, there would remain major challenges for experimental evaluation, which would in general require a complete reconstruction of the state through full state tomography. For multiparticle states of any reasonable number of qubits, full state tomography places significant demands on experimental resources, and it is thus highly desirable to provide quantitative guarantees on the geometric quantumness present in a state, via non-trivial lower bounds, in an experimentally accessible way. In the following Chapter we will provide substantial advances towards addressing this problem in a general fashion.

# Chapter 3

# Quantification of quantumness

This Chapter collects our results [1–3] on the quantification of geometric measures of quantumness, be it in the form of multiparticle entanglement, quantum coherence, or discord-type correlations, as well as our results [4, 5] specific to the quantification of quantum coherence and based on the newly introduced robustness of coherence.

We start by introducing a family of $N$-qubit mixed states, the so-called $\mathcal{M}_N^3$ states, which are particular instances of states having all maximally mixed marginals and are simply characterised by the three correlation functions $\{c_j = \langle \sigma_j^{\otimes N} \rangle\}_{j=1}^3$, where $\sigma_j$ is the $j$-th Pauli matrix.

These states will prove to be rather appealing since, regardless of the adopted distance $D$, type of quantumness and number $N$ of qubits, the closest free state to any $\mathcal{M}_N^3$ state can always be found within the subset of free $\mathcal{M}_N^3$ states. This feature dramatically simplifies the optimisation in Eq. (2.21) for these states and allows us to analytically compute the corresponding geometric measures of quantumness through a unifying and general technique that adopts simply the information theoretic tools of contractivity and joint convexity introduced in the previous Chapter.

Even more, an arbitrary $N$-qubit state can be transformed into an $\mathcal{M}_N^3$ state via a quantum operation that is both a single-qubit LOCC, which cannot increase any form of multiparticle entanglement, and an incoherent operation with respect to the basis consisting of tensor products of eigenstates of $\sigma_j$, for any $j = 1, 2, 3$, which cannot increase the corresponding quantum coherence. Together with the fact that the $\mathcal{M}_N^3$ states can be $M$-inseparable for any $M > \lceil N/2 \rceil$ and are in general not diagonal in the aforementioned bases, this implies that our exact results immediately provide practical lower bounds to the amount of global and partial multiparticle entanglement, as well as of quantum coherence in such bases, for completely general states.

Most importantly, for any number of qubits $N$, these bounds are obtained by accessing simply to the three easily measurable quantities $\{c_j\}_{j=1}^3$. Moreover, they can be further improved by adjusting the local measurement basis in the case of multiparticle entanglement, while this is not possible in the case of quantum coherence, being it not invariant under local unitaries.

Overall, for both entanglement, coherence and discord-type correlations we analyti-

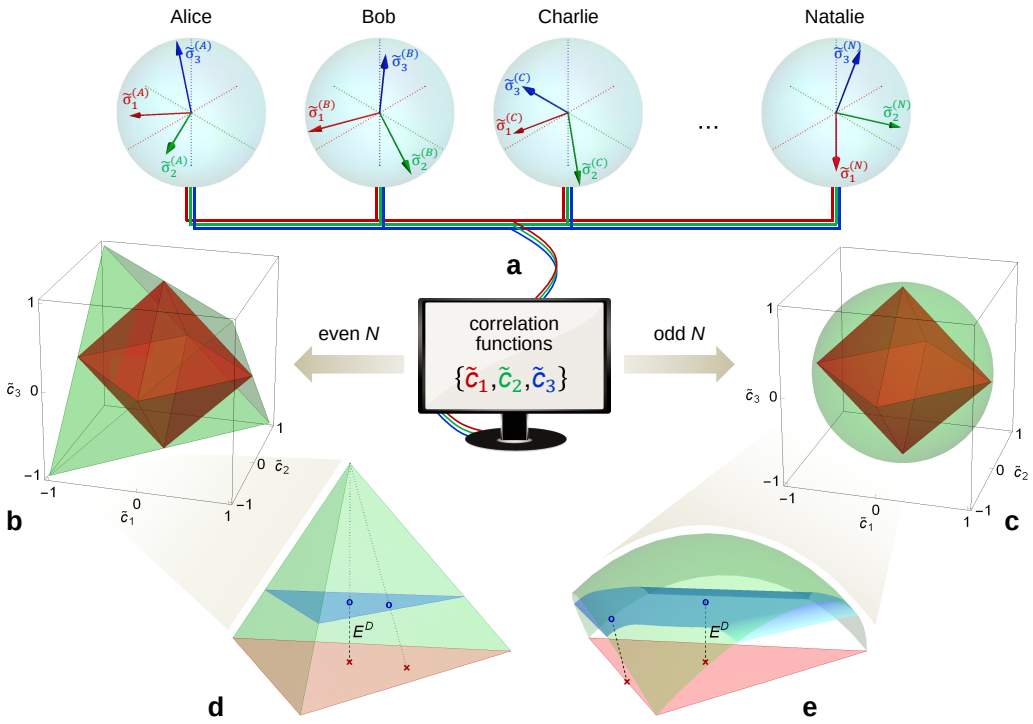


Figure 3.1: Experimentally friendly protocol to quantify global and partial $N$-qubit entanglement.

cally evaluate the corresponding geometric quantifiers on the family of $\mathcal{M}_N^3$ states, while only for entanglement and coherence such analytical results provide a lower bound to the quantumness of a general state and, finally, only for entanglement such lower bound can be ameliorated by resorting to local unitaries. Specifically, Fig. 3.1 provides the schema of our experimentally friendly protocol to quantify global and partial multiparticle entanglement, as detailed in the following:

- *Top row:* (a) An $N$-qubit state $\varrho$ is shared by $N$ parties, named Alice, Bob, Charlie, ..., Natalie. Each party, labelled by $\alpha = A, \ldots, N$, locally measures her or his qubit in three orthogonal directions $\{\tilde{\sigma}_j^{(\alpha)}\}_{j=1}^3$ indicated by the solid arrows. If the shared state $\varrho$ is completely unknown, a standard choice can be to measure the three canonical Pauli operators for all the qubits, corresponding to the directions of the dashed axes. If instead some partial information on $\varrho$ is available, the measurement directions can be optimised a priori. Once all the data are collected, the $N$ parties communicate classically to construct the three correlation functions $\{\tilde{c}_j\}_{j=1}^3$, with $\tilde{c}_j = \langle \bigotimes_\alpha \tilde{\sigma}_j^{(\alpha)} \rangle$.

- *Middle row*: For any $N$, one can define a reference subset of $N$-qubit states with all maximally mixed marginals ($\mathcal{M}_N^3$ states), which are completely specified by a

triple of orthogonal correlation functions $\{c_j\}_{j=1}^3$. These states enjoy a nice geometrical representation in the $\{c_1, c_2, c_3\}$-space. (b) For even $N$, $\mathcal{M}_N^3$ states fill the tetrahedron with vertices $\{1, (-1)^{N/2}, 1\}$, $\{-1, -(-1)^{N/2}, 1\}$, $\{1, -(-1)^{N/2}, -1\}$ and $\{-1, (-1)^{N/2}, -1\}$. (c) For odd $N$, they are instead contained in the unit ball, also known as the Bloch sphere for a single qubit. For any $M > \lceil N/2 \rceil$, $M$-separable $\mathcal{M}_N^3$ states are confined to the octahedron with vertices $\{\pm 1, 0, 0\}$, $\{0, \pm 1, 0\}$ and $\{0, 0, \pm 1\}$, illustrated in red in both panels. Otherwise, for any $M \leq \lceil N/2 \rceil$, all $\mathcal{M}_N^3$ states are $M$-separable.

- *Bottom row*: Geometric analysis of $M$-inseparable multiparticle entanglement for any $M > \lceil N/2 \rceil$. The bottom panels depict zooms of (d) a corner of the tetrahedron for even $N$ and (e) a sector of the unit sphere for odd $N$, opposing a face of the octahedron of $M$-separable $\mathcal{M}_N^3$ states. Instances of inseparable $\mathcal{M}_N^3$ states are indicated by blue circles, and their closest $M$-separable states by red crosses. The cyan surfaces in each of the two bottom panels contain states with equal global and partial multiparticle entanglement $E_M^D$, which we compute exactly. The results are valid for any contractive and jointly convex distance $D$ in the even $N$ case, and for the trace distance in the odd $N$ case. The entanglement of an $\mathcal{M}_N^3$ state with correlation functions $\{\tilde{c}_1, \tilde{c}_2, \tilde{c}_3\}$ provides an analytical lower bound for the entanglement of any $N$-qubit state with the same correlation functions, such as the state $\varrho$ initially shared by the $N$ parties in (a). The bound is effective for the most relevant families of $N$-qubit states in theoretical and experimental investigations of quantum information processing, as we show in Section 3.3.

From our results for $\mathcal{M}_N^3$ states, we identify a general framework for the provision of experimentally friendly quantitative guarantees on the geometric multiparticle entanglement present in a state. This approach consists of:

***(1) Choose a reference family:*** Select a particular family of states, whose characterisation is comparatively simple, such that any state can be transformed to a reference one through some single-qubit LOCC. This family can be chosen on experimental or theoretical considerations. *(See Sections 3.1 and 3.2.)*

***(2) Identify $M$-separable reference states:*** Perform the single-qubit LOCC transformation from step (1) on the general set of $M$-separable states, to identify the subset of $M$-separable states in the reference family. *(See Section 3.3.1.)*

***(3) Calculate $E_M^D$ for the reference family:*** By using the properties of contractivity under quantum operations and joint convexity, which hold for any valid distance $D$, one can show that one of the states achieving the minimum in Eq. (2.21) is within the $M$-separable reference states, and thus analytically find $E_M^D$ for the entire reference family. *(See Sections 3.2 and 3.3.1.)*

***(4) Derive optimised lower bounds for any state:*** For a completely general state, one can vary over local unitaries and find the corresponding reference state with the highest geometric multiparticle entanglement. The latter provides a lower bound to the multiparticle entanglement of the original state under investigation. *(See Section 3.3.2.)*

This process presents a distance-independent approach to obtain lower bounds on geometric multiparticle entanglement according to any distance. While building on some previously utilised methods for steps (1) [62–64] and (4) [62, 64], it introduces a novel reference family in step (1), and novel techniques in steps (2) and most importantly (3), which are crucial for completing the general framework and making it effective in practice.

In particular, we discuss how our approach can be exploited to allow for the quantitative estimation of genuine multiparticle entanglement as well, at the cost of performing extra measurements. Since $\mathcal{M}_N^3$ states are always biseparable, we must consider a different reference family. We focus on the class of $N$-qubit states obtained as mixtures of Greenberger-Horne-Zeilinger (GHZ) states [54, 170], the latter being central resources for quantum communication and estimation; this class of states depends on $2^N - 1$ real parameters. We calculate exactly distance-based measures of genuine multiparticle entanglement $E_2^D$ for these states, for every valid $D$. Once more, these analytical results provide lower bounds to geometric measures of genuine entanglement for any general state of $N$ qubits, obtainable experimentally in this case by performing at least $N + 1$ local measurements [171].

Finally, regarding in particular the quantification of quantum coherence, we will also introduce the robustness of coherence and see that it is: (i) a fully bona fide quantifier according to any resource theory of quantum coherence; (ii) observable, as it can be recast as the expectation value of a coherence witness operator for any quantum state; (iii) computable, as there exists an efficient semidefinite program that computes it on general states; (iv) operationally meaningful, as it quantifies the advantage enabled by a quantum state in a phase discrimination task. We will also briefly discuss the generalisation of these results to the case of asymmetry.

## 3.1 The set of $\mathcal{M}_N^3$ states

We define the $\mathcal{M}_N^3$ states as those $N$-qubit states whose matrix representation in the computational basis $\{|0\rangle, |1\rangle\}^{\otimes N}$ is given by:

$$\varpi = \frac{1}{2^N}\left(\mathbb{I}^{\otimes N} + \sum_{i=1}^{3} c_i \sigma_i^{\otimes N}\right), \tag{3.1}$$

where $\mathbb{I}$ is the $2 \times 2$ identity matrix and $c_i = \mathrm{Tr}\left(\varpi \sigma_i^{\otimes N}\right)$. For $N = 2$ these states form the set of Bell-diagonal (BD) states, which are all the classical mixtures of the maximally entangled Bell states, whereas for any even $N \geq 4$ they include multiparticle bound entangled states such as the so-called Smolin states [71, 172–174]. Moreover, the $\mathcal{M}_N^3$ states have all maximally mixed marginals, are invariant under permutations of any pair of qubits and will be denoted in the following also by the triple $\{c_1, c_2, c_3\}$.

The characterisation of the $\mathcal{M}_N^3$ states is manifestly different between the even and odd $N$ case. For even $N$, the eigenvectors are given by the so-called Greenberger-Horne-

Zeilinger (GHZ) states [170]:

$$|\beta_i^{\pm}\rangle = \frac{1}{\sqrt{2}}\left(\mathbb{I}^{\otimes N} \pm \sigma_1^{\otimes N}\right)|i\rangle, \tag{3.2}$$

whereas the eigenvalues are given by:

$$\lambda_p^{\pm} = \frac{1}{2^N}\left[1 \pm c_1 \pm (-1)^{N/2}(-1)^p c_2 + (-1)^p c_3\right], \tag{3.3}$$

where $i \in \{1, \cdots, 2^{N-1}\}$, $\{|i\rangle\}_{i=1}^{2^N}$ is the binary ordered $N$-qubit computational basis and finally $p$ is the parity of $|\beta_i^{\pm}\rangle$ with respect to the parity operator along the $z$-axis $\Pi_3 = \sigma_3^{\otimes N}$, i.e.

$$\Pi_3|\beta_i^{\pm}\rangle = (-1)^p|\beta_i^{\pm}\rangle. \tag{3.4}$$

In the $\{c_1, c_2, c_3\}$-space, the set of $\mathcal{M}_N^3$ states with even $N$ is represented by the tetrahedron $\mathcal{T}_{(-1)^{N/2}}$ with vertices $\{1, (-1)^{N/2}, 1\}$, $\{-1, -(-1)^{N/2}, 1\}$, $\{1, -(-1)^{N/2}, -1\}$ and $\{-1, (-1)^{N/2}, -1\}$, as illustrated in Fig. 3.1(b) for odd $N/2$. This tetrahedron is constructed simply by imposing the non-negativity of the four eigenvalues (3.3) of such $\mathcal{M}_N^3$ states.

For odd $N$, the eigenvectors and eigenvalues of the $\mathcal{M}_N^3$ states can be easily written in spherical coordinates as

$$\begin{aligned} |\alpha_i^{\pm}\rangle \;=\; & \cos\left[\frac{\theta}{2} + (1 \mp (-1)^p)\frac{\pi}{4}\right]|i\rangle \\ & + (-1)^p e^{i(-1)^p(-1)^{\frac{N-1}{2}}\phi}\sin\left[\frac{\theta}{2} + (1 \mp (-1)^p)\frac{\pi}{4}\right]\sigma_1^{\otimes N}|i\rangle, \end{aligned} \tag{3.5}$$

and

$$\lambda_{\pm} = \frac{1}{2^N}(1 \pm r), \tag{3.6}$$

where $i \in \{1, \cdots, 2^{N-1}\}$, $\{|i\rangle\}_{i=1}^{2^N}$ is again the binary ordered $N$-qubit computational basis, $p$ is the parity of $|i\rangle$ with respect to the parity operator $\Pi_3 = \sigma_3^{\otimes N}$, $c_1 = r\sin\theta\cos\phi$, $c_2 = r\sin\theta\sin\phi$ and $c_3 = r\cos\theta$, with $r = \sqrt{c_1^2 + c_2^2 + c_3^2}$, $\theta \in [0, \pi]$ and $\phi \in [0, 2\pi[$.

Consequently, thanks again to the semi-positivity constraint, the set of $\mathcal{M}_N^3$ states with odd $N$ is represented in the $\{c_1, c_2, c_3\}$-space by the unit ball $\mathcal{B}_1$ centred into the origin, as shown in Fig. 3.1(c).

## 3.2 $\mathcal{M}_N^3$-fication

The following Theorem will turn out to be crucial not only for analytically computing the multiparticle geometric entanglement and the quantum coherence of any $\mathcal{M}_N^3$ state $\varpi$, but also for providing a lower bound to any multiparticle entanglement and quantum coherence monotone of any state $\varrho$.

**Theorem 3.2.1.** *Any $N$-qubit state $\varrho$ can be transformed into a corresponding $\mathcal{M}_N^3$ state $\varrho_{\mathcal{M}_N^3}$ through a fixed operation, $\Theta$, such that*

$$\Theta(\varrho) = \varrho_{\mathcal{M}_N^3} = \frac{1}{2^N}\left(\mathbb{I}^{\otimes N} + \sum_{i=1}^{3} c_i \sigma_i^{\otimes N}\right), \tag{3.7}$$

*where $c_i = \mathrm{Tr}\left(\varrho\sigma_i^{\otimes N}\right)$. Moreover, $\Theta$ is both a single-qubit LOCC and an incoherent operation with respect to the basis consisting of tensor products of eigenstates of $\sigma_j$, for any $j = 1, 2, 3$.*

*Proof*: We will give the form of $\Theta(\varrho)$, show that $\Theta$ is both a single-qubit LOCC and an incoherent operation with respect to the basis consisting of tensor products of eigenstates of $\sigma_j$, for any $j = 1, 2, 3$, and finally prove that it transforms any $N$-qubit state $\varrho$ into $\varrho_{\mathcal{M}_N^3}$.

To define $\Theta(\varrho)$, we begin by setting $2(N-1)$ single-qubit local unitaries

$$\begin{aligned}\{U_j\}_{j=1}^{2(N-1)} = \{&(\sigma_1 \otimes \sigma_1 \otimes I^{\otimes N-2}), (I \otimes \sigma_1 \otimes \sigma_1 \otimes I^{\otimes N-3}),\\ &\ldots (I^{\otimes N-3} \otimes \sigma_1 \otimes \sigma_1 \otimes I), (I^{\otimes N-2} \otimes \sigma_1 \otimes \sigma_1)\\ &, (\sigma_2 \otimes \sigma_2 \otimes I^{\otimes N-2}), (I \otimes \sigma_2 \otimes \sigma_2 \otimes I^{\otimes N-3}),\\ &\ldots (I^{\otimes N-3} \otimes \sigma_2 \otimes \sigma_2 \otimes I), (I^{\otimes N-2} \otimes \sigma_2 \otimes \sigma_2)\}.\end{aligned} \tag{3.8}$$

Then, we fix a sequence of states $\{\varrho_0, \varrho_1, \ldots \varrho_{2(N-1)}\}$ defined by

$$\varrho_j := \frac{1}{2}\left(\varrho_{j-1} + U_j \varrho_{j-1} U_j^\dagger\right), \tag{3.9}$$

for $j \in \{1, 2, \ldots 2(N-1)\}$. By setting $\varrho_0 = \varrho$ and $\varrho_{2(N-1)} = \Theta(\varrho)$, we define the required channel, i.e. $\Theta(\varrho) = \frac{1}{2^{2(N-1)}} \sum_{i=1}^{2^{2(N-1)}} U_i' \varrho U_i'^\dagger$ where $U_i'$ are the following unitaries

$$\{U_i'\}_{i=1}^{2^{2(N-1)}} = \left\{ \begin{array}{c} \mathbb{I}^{\otimes N} \\ \{U_{i_1}\}_{i_1=1}^{2(N-1)} \\ \{U_{i_2} U_{i_1}\}_{i_2 > i_1 = 1}^{2(N-1)} \\ \cdots \\ \{U_{i_{2(N-1)}} \ldots U_{i_2} U_{i_1}\}_{i_{2(N-1)} > \ldots > i_2 > i_1 = 1}^{2(N-1)} \end{array} \right\}. \tag{3.10}$$

It is clear that $\{U_i'\}_{i=1}^{2^{2(N-1)}}$ are unitaries that still act locally on individual qubits. Since $\Theta$ is a convex mixture of such local unitaries, we conclude that $\Theta$ is a single-qubit LOCC.

We now prove that $\Theta$ is an incoherent operation with respect to the basis consisting of tensor products of eigenstates of $\sigma_1$, the so-called plus/minus basis, although analogous proofs hold when considering the other two Pauli matrices. Since the Kraus operators of

the map $\Theta$ are given by $K_j = \frac{1}{2^{N-1}} U'_j$, in order for $\Theta$ to be an incoherent operation in the plus/minus basis we need that $U'_j \delta U'^{\dagger}_j \in \mathcal{I}$ for any $\delta \in \mathcal{I}$ and any $j \in \{1, \cdots, 2^{2(N-1)}\}$, where $\mathcal{I}$ is the set of states diagonal in this basis. This obviously holds for $j = 1$, being $U'_1$ the identity. On the other hand, as it can be seen from Eq. (3.10), all the other single-qubit unitaries $U'_j$ are just products of the single-qubit unitaries $U_j$ listed in Eq. (3.8), so that we just need to prove that $U_j \delta U_j^{\dagger} \in \mathcal{I}$ for any $\delta \in \mathcal{I}$ and for any $j \in \{1, \cdots, 2(N-1)\}$.

If $j \in \{1, \cdots, N-1\}$, $U_j$ just leaves any state which is diagonal in the plus/minus basis invariant, being it a tensor product between two $\sigma_1$'s acting on two neighbouring qubits and the identity acting on the remaining ones.

Otherwise, if $j \in \{N, \cdots, 2(N-1)\}$, $U_j$ is the tensor product between two $\sigma_2$'s acting on two neighbouring qubits and the identity on the rest of the qubits. Consequently, by using $\sigma_2|\pm\rangle\langle\pm|\sigma_2 = |\mp\rangle\langle\mp|$ and the fact that the general form of a state $\delta$ diagonal in the plus/minus basis is $\delta = \sum_{j_1, j_2, \cdots, j_N = \pm} p_{j_1, j_2, \cdots, j_N} |j_1, j_2, \cdots, j_N\rangle\langle j_1, j_2, \cdots, j_N|$, we have that when e.g. $j = N$

$$
\begin{aligned}
& U_N \delta U_N^{\dagger} \qquad (3.11)\\
&= \sum_{j_1, j_2, \cdots, j_N = \pm} p_{j_1, j_2, \cdots, j_N} U_N |j_1, j_2, \cdots, j_N\rangle\langle j_1, j_2, \cdots, j_N| U_N^{\dagger} \\
&= \sum_{j_1, j_2, \cdots, j_N = \pm} p_{j_1, j_2, \cdots, j_N} |\pi(j_1), \pi(j_2), \cdots, j_N\rangle\langle \pi(j_1), \pi(j_2), \cdots, j_N|,
\end{aligned}
$$

where $\pi(\pm) \equiv \mp$, so that $U_N \delta U_N^{\dagger} \in \mathcal{I}$. Analogously, one can see that all the remaining single-qubit local unitaries $U_j$ are such that $U_j \delta U_j \in \mathcal{I}$, thus completing the proof that $\Theta$ is incoherent in the plus/minus basis.

Now we will show that $\Theta(\varrho) = \varrho_{\mathcal{M}_N^3}$. Consider the arbitrary $N$-qubit state $\varrho$ written in the form

$$
\varrho = \frac{1}{2^N} \sum_{i_1 i_2 \ldots i_N = 0}^{3} R^{\varrho}_{i_1 i_2 \ldots i_N} \sigma_{i_1} \otimes \sigma_{i_2} \ldots \otimes \sigma_{i_N}, \qquad (3.12)
$$

where the coefficients $R^{\varrho}_{i_1, i_2, \ldots i_N} = \mathrm{Tr}\left[\varrho \left(\sigma_{i_1} \otimes \sigma_{i_2} \ldots \otimes \sigma_{i_N}\right)\right]$ are the so-called correlation tensor elements of $\varrho$ and $\sigma_0 = \mathbb{I}$. Convex combination of two arbitrary $N$-qubit states $\varrho$ and $\varrho'$ gives

$$
q\varrho + (1-q)\varrho' = \frac{1}{2^N} \sum_{i_1 i_2 \ldots i_N = 0}^{3} R^{q\varrho + (1-q)\varrho'}_{i_1 i_2 \ldots i_N} \sigma_{i_1} \otimes \sigma_{i_2} \ldots \otimes \sigma_{i_N}, \qquad (3.13)
$$

where $R^{q\varrho + (1-q)\varrho'}_{i_1 i_2 \ldots i_N} = q R^{\varrho}_{i_1 i_2 \ldots i_N} + (1-q) R^{\varrho'}_{i_1 i_2 \ldots i_N}$.

We will now understand the evolution of the correlation tensor elements $R^{\varrho_j}_{i_1 i_2 \ldots i_N}$ for each step $j$ in Eq. (3.9). The action of $U_1$ on $\varrho$ is

$$
U_1 \varrho U_1^{\dagger} = \frac{1}{2^N} \sum_{i_1 i_2 \ldots i_N = 0}^{3} R^{\varrho}_{i_1 i_2 \ldots i_N} \sigma_1 \sigma_{i_1} \sigma_1 \otimes \sigma_1 \sigma_{i_2} \sigma_1 \otimes \sigma_{i_3} \ldots \otimes \sigma_{i_N}. \qquad (3.14)
$$

From $\sigma_1\sigma_i\sigma_1 = -(-1)^{\delta_{0i}+\delta_{1i}}\sigma_i$ we have that the correlation tensor elements of $U_1\varrho U_1^\dagger$ are $R^{U_1\varrho U_1^\dagger}_{i_1i_2\ldots i_N} = (-1)^{\delta_{0i_1}+\delta_{1i_1}+\delta_{0i_2}+\delta_{1i_2}} R^{\varrho}_{i_1i_2\ldots i_N}$. By using Eqs. (3.9) and (3.13), it is clear that the correlation tensor elements $R^{\varrho_1}_{i_1i_2\ldots i_N}$ of $\varrho_1$ are equal to the correlation tensor elements $R^{\varrho}_{i_1i_2\ldots i_N}$ of $\varrho$ if $i_1$ and $i_2$ are (i) any combination of only 1 and 0 or (ii) any combination of only 2 and 3, and are equal to zero otherwise.

Generally, for $j \in \{1, \cdots, N-1\}$, the correlation tensor elements $R^{\varrho_j}_{i_1i_2\ldots i_N}$ of $\varrho_j$ are equal to the correlation tensor elements $R^{\varrho_{j-1}}_{i_1i_2\ldots i_N}$ of $\varrho_{j-1}$ if $i_j$ and $i_{j+1}$ are (i) any combination of only 1 and 0 or (ii) any combination of only 2 and 3, and are equal to zero otherwise. For $j \in \{N, \cdots, 2(N-1)\}$ the conditions are analogous, where the correlation tensor elements $R^{\varrho_j}_{i_1i_2\ldots i_N}$ of $\varrho_j$ are equal to the correlation tensor elements $R^{\varrho_{j-1}}_{i_1i_2\ldots i_N}$ of $\varrho_{j-1}$ if $i_j$ and $i_{j+1}$ are (i) any combination of only 2 and 0 or (ii) any combination of only 1 and 3, and are equal to zero otherwise. For the final state $\varrho_{2(N-1)}$, the only nonzero correlation tensor elements $R^{\varrho_{2(N-1)}}_{i_1i_2\ldots i_N}$ are those for which $\{i_1i_2\ldots i_N\}$ consist of only 0, 1, 2, or 3, and for these elements $R^{\varrho_{2(N-1)}}_{i_1i_2\ldots i_N} = R^{\varrho}_{i_1i_2\ldots i_N}$. Therefore

$$\begin{aligned}\Theta(\varrho) = \varrho_{2(N-1)} &= \frac{1}{2^N}\sum_{i=0}^{3} R^{\varrho}_{ii\ldots i}\sigma_i\otimes\sigma_i\ldots\otimes\sigma_i \\ &= \frac{1}{2^N}\left(\mathbb{I}^{\otimes N} + \sum_{i=1}^{3} c_i\sigma_i^{\otimes N}\right) = \varrho_{\mathcal{M}_N^3} \end{aligned} \tag{3.15}$$

where we have used $R^{\varrho}_{ii\ldots i} = \mathrm{Tr}(\varrho\sigma_i^{\otimes N}) = c_i$ for $i \in \{1,2,3\}$ and $R^{\varrho}_{00\ldots0} = \mathrm{Tr}(\varrho) = 1$.

■

Herein, we will refer to $\varrho_{\mathcal{M}_N^3} = \Theta(\varrho)$ as the $\mathcal{M}_N^3$-fication of the state $\varrho$.

Theorem 3.2.1 entails two major results, each one holding for both entanglement and quantum coherence theory. The first result applies on one hand to any multiparticle entanglement monotone and on the other hand to any coherence monotone with respect to the basis $\{|i_k\rangle\}_{i=1}^{2^N}$ consisting of tensor products of eigenstates of $\sigma_k$, for any $k = 1, 2, 3$. When considering entanglement, we have that

$$E_M(\varrho_{\mathcal{M}_N^3}) = E_M(\Theta(\varrho)) \leq E_M(\varrho), \tag{3.16}$$

where in the first equality we use $\varrho_{\mathcal{M}_N^3} = \Theta(\varrho)$, while in the inequality we use the monotonicity under single-qubit LOCC of any measure of multiparticle entanglement and the fact that $\Theta$ is a single-qubit LOCC. Analogously, when considering quantum coherence in the basis $\{|i_k\rangle\}_{i=1}^{2^N}$ we have that

$$C_{\{|i_k\rangle\}}(\varrho_{\mathcal{M}_N^3}) = C_{\{|i_k\rangle\}}(\Theta(\varrho)) \leq C_{\{|i_k\rangle\}}(\varrho), \tag{3.17}$$

where in the inequality we use the fact that no coherence monotone in the basis $\{|i_k\rangle\}_{i=1}^{2^N}$ can increase under operations which are incoherent in this basis, such as $\Theta$.

In other words, the multiparticle entanglement and the quantum coherence in the basis $\{|i_k\rangle\}_{i=1}^{2^N}$ of the $\mathcal{M}_N^3$-fication $\varrho_{\mathcal{M}_N^3}$ of any state $\varrho$ provides us with a lower bound of, respectively, the multiparticle entanglement and corresponding quantum coherence of $\varrho$.

The second result applies specifically to distance-based measures of multiparticle entanglement, and to any distance-based measure of quantum coherence in the basis $\{|i_k\rangle\}_{i=1}^{2^N}$.

When considering entanglement, we have that, for any $\mathcal{M}_N^3$ state $\varpi$ and any $M$-separable state $\varsigma$,

$$D(\varpi, \varsigma_{\mathcal{M}_N^3}) = D(\Theta(\varpi), \Theta(\varsigma)) \leq D(\varpi, \varsigma), \tag{3.18}$$

where in the first equality we use the invariance of any $\mathcal{M}_N^3$ state through $\Theta$ and that $\Theta(\varsigma) =: \varsigma_{\mathcal{M}_N^3}$ is the $\mathcal{M}^3$-fication of $\varsigma$, and in the inequality we use the contractivity of the distance through any completely positive trace-preserving channel. Moreover, the $\mathcal{M}_N^3$-fication $\varsigma_{\mathcal{M}_N^3}$ of any $M$-separable state $\varsigma$ is an $M$-separable $\mathcal{M}_N^3$ state, since $\Theta$ is a single-qubit LOCC.

Therefore, the set $\mathcal{S}_M^{\mathcal{M}_N^3}$ of $M$-separable $\mathcal{M}_N^3$ states will be crucial to identify, since it allows us to use Eq. (3.18) to conclude that for any distance-based measure of multiparticle entanglement of an $\mathcal{M}_N^3$ state $\varpi$,

$$E_M^D(\varpi) := \inf_{\varsigma \in \mathcal{S}_M} D(\varpi, \varsigma) = \inf_{\varsigma_{\mathcal{M}_N^3} \in \mathcal{S}_M^{\mathcal{M}_N^3}} D(\varpi, \varsigma_{\mathcal{M}_N^3}), \tag{3.19}$$

i.e. that one of the closest $M$-separable states $\varsigma_\varpi$ to an $\mathcal{M}_N^3$ state $\varpi$ is itself an $\mathcal{M}_N^3$ state.

Analogously, when considering quantum coherence in the basis $\{|i_k\rangle\}_{i=1}^{2^N}$, we have that

$$D(\varpi, \delta_{\mathcal{M}_N^3}) = D(\Theta(\varpi), \Theta(\delta)) \leq D(\varpi, \delta), \tag{3.20}$$

for any $\mathcal{M}_N^3$ state $\varpi$ and any state $\delta$ which is incoherent in such basis. Moreover, since $\Theta$ is $\{|i_k\rangle\}_{i=1}^{2^N}$-incoherent, we get that $\delta_{\mathcal{M}_N^3} := \Theta(\delta) \in \mathcal{I}$ and so

$$C_{\{|i_k\rangle\}}^D(\varpi) := \inf_{\delta \in \mathcal{I}} D(\varpi, \delta) = \inf_{\delta_{\mathcal{M}_N^3} \in \mathcal{I}^{\mathcal{M}_N^3}} D(\varpi, \delta_{\mathcal{M}_N^3}), \tag{3.21}$$

where $\mathcal{I}^{\mathcal{M}_N^3}$ is the set of $\{|i_k\rangle\}_{i=1}^{2^N}$-incoherent $\mathcal{M}_N^3$ states. In other words, one of the closest $\{|i_k\rangle\}_{i=1}^{2^N}$-incoherent states $\delta_\varpi$ to an $\mathcal{M}_N^3$ state $\varpi$ is itself an $\mathcal{M}_N^3$ state.

We now formalise these two results as corollaries.

**Corollary 3.2.1.** *For any $N$-qubit state $\varrho$, the $M$-inseparable multiparticle entanglement of the corresponding $\mathcal{M}_N^3$-fied state $\varrho_{\mathcal{M}_N^3}$ is always less than or equal to the $M$-inseparable multiparticle entanglement of $\varrho$, i.e.*

$$E_M(\varrho_{\mathcal{M}_N^3}) \leq E_M(\varrho), \tag{3.22}$$

*for any $2 \leq M \leq N$.*

**Corollary 3.2.2.** *For any $N$-qubit state $\varrho$, the quantum coherence in the basis $\{|i_k\rangle\}_{i=1}^{2^N}$ of the corresponding $\mathcal{M}_N^3$-fied state $\varrho_{\mathcal{M}_N^3}$ is always less than or equal to the quantum coherence in the same basis of $\varrho$, i.e.*

$$C_{\{|i_k\rangle\}}(\varrho_{\mathcal{M}_N^3}) \leq C_{\{|i_k\rangle\}}(\varrho), \tag{3.23}$$

*for any $k = 1, 2, 3$.*

**Corollary 3.2.3.** *For any contractive distance $D$ and any $\mathcal{M}_N^3$ state $\varpi$, one of the closest $M$-separable states $\varsigma_\varpi$ to $\varpi$ is itself an $\mathcal{M}_N^3$ state, i.e.*

$$\varsigma_\varpi = \frac{1}{2^N}\left(\mathbb{I}^{\otimes N} + \sum_i s_i \sigma_i^{\otimes N}\right), \tag{3.24}$$

*for any $2 \leq M \leq N$.*

**Corollary 3.2.4.** *For any contractive distance $D$ and any $\mathcal{M}_N^3$ state $\varpi$, one of the closest $\{|i_k\rangle\}_{i=1}^{2^N}$-incoherent states $\delta_\varpi$ to $\varpi$ is itself an $\mathcal{M}_N^3$ state, i.e.*

$$\delta_\varpi = \frac{1}{2^N}\left(\mathbb{I}^{\otimes N} + s\sigma_k^{\otimes N}\right), \tag{3.25}$$

*for any $k = 1, 2, 3$.*

## 3.3 Quantification of entanglement

In this Section we will focus in particular on the quantification of geometric measures of $M$-inseparable multiparticle entanglement.

### 3.3.1 Multiparticle entanglement of the $\mathcal{M}_N^3$ states

In the previous Section we have shown that for $\mathcal{M}_N^3$ states it suffices to restrict to the set $\mathcal{S}_M^{\mathcal{M}_N^3}$ of $M$-separable $\mathcal{M}_N^3$ states in order to achieve the optimisation underlying the definition of the geometric measures of $M$-inseparable multiparticle entanglement. This makes the characterisation of $\mathcal{S}_M^{\mathcal{M}_N^3}$ impelling.

To achieve such characterisation, we first need to identify the sets $\mathcal{S}_{\{Q_\alpha\}_{\alpha=1}^M}^{\mathcal{M}_N^3}$ of $\{Q_\alpha\}_{\alpha=1}^M$-separable $\mathcal{M}_N^3$ states obtained by considering all the possible $M$-partitions $\{Q_\alpha\}_{\alpha=1}^M$, being

the convex hull of their union exactly the set $\mathcal{S}_M^{\mathcal{M}_N^3}$, i.e.

$$\mathcal{S}_M^{\mathcal{M}_N^3} = conv\left(\bigcup_{\{Q_\alpha\}_{\alpha=1}^M} \mathcal{S}_{\{Q_\alpha\}_{\alpha=1}^M}^{\mathcal{M}_N^3}\right). \tag{3.26}$$

Theorem 3.2.1 allows for another result which will be useful for this purpose.

**Corollary 3.3.1.** *The set of the triples* $\{c_1, c_2, c_3\}$, *with* $c_i = \mathrm{Tr}(\varrho\sigma_i^{\otimes N})$, *obtained by considering any possible* $N$*-qubit state* $\varrho$ *is*

- *the unit ball* $\mathcal{B}_1$, *when* $N$ *is odd;*
- *the tetrahedron* $\mathcal{T}_{(-1)^{N/2}}$, *when* $N$ *is even.*

This is because the set of $\mathcal{M}_N^3$-fications of all the states coincides exactly with the set of $\mathcal{M}_N^3$ states. Indeed, the $\mathcal{M}_N^3$-fication channel $\Theta$ makes the entire set of states collapse into the set of $\mathcal{M}_N^3$ states, whereas it leaves the set of $\mathcal{M}_N^3$ states invariant. Herein, we shall refer to the triple $\{c_1, c_2, c_3\}$, with $c_i = \mathrm{Tr}(\varrho\sigma_i^{\otimes N})$, as the Pauli correlation vector corresponding to the state $\varrho$.

Another crucial ingredient is to note that $\mathcal{S}_{\{Q_\alpha\}_{\alpha=1}^M}^{\mathcal{M}_N^3}$ coincides exactly with the set $\Theta\left[\mathcal{S}_{\{Q_\alpha\}_{\alpha=1}^M}\right]$ of the $\mathcal{M}_N^3$-fications of any $\{Q_\alpha\}_{\alpha=1}^M$-separable state. Furthermore, we note that since any $\mathcal{M}_N^3$ state is invariant under any permutation of the $N$ qubits, then the set of $\{Q_\alpha\}_{\alpha=1}^M$-separable $\mathcal{M}_N^3$ states $\mathcal{S}_{\{Q_\alpha\}_{\alpha=1}^M}^{\mathcal{M}_N^3}$ does not depend on which qubits belong to each of the subsystems. Therefore we need only to specify the cardinalities $\{K_\alpha\}_{\alpha=1}^M$ to completely characterise $\mathcal{S}_{\{Q_\alpha\}_{\alpha=1}^M}^{\mathcal{M}_N^3}$, and we will herein refer to the latter as the set of $\{K_\alpha\}_{\alpha=1}^M$-separable $\mathcal{M}_N^3$ states $\mathcal{S}_{\{K_\alpha\}_{\alpha=1}^M}^{\mathcal{M}_N^3}$.

**Theorem 3.3.1.** *For any* $N$, *the set of* $\{K_\alpha\}_{\alpha=1}^M$*-separable* $\mathcal{M}_N^3$ *states* $\mathcal{S}_{\{K_\alpha\}_{\alpha=1}^M}^{\mathcal{M}_N^3}$ *is either*

- *the set of all* $\mathcal{M}_N^3$ *states, for any allowed* $\{K_\alpha\}_{\alpha=1}^M$ *partition such that* $K_\alpha$ *is odd for at most one value of* $\alpha$*;*
- *the set of* $\mathcal{M}_N^3$ *states represented in the* $\{c_1, c_2, c_3\}$*-space by the unit octahedron* $\mathcal{O}_1$ *with vertices* $\{\pm 1, 0, 0\}$, $\{0, \pm 1, 0\}$ *and* $\{0, 0, \pm 1\}$, *for any allowed* $\{K_\alpha\}_{\alpha=1}^M$ *partition such that* $K_\alpha$ *is odd for more than one value of* $\alpha$.

*Proof*: In order to characterise the set of $\{K_\alpha\}_{\alpha=1}^M$-separable $\mathcal{M}_N^3$ states, $\mathcal{S}_{\{K_\alpha\}_{\alpha=1}^M}^{\mathcal{M}_N^3}$, we simply need to identify its representation in the $\{c_1, c_2, c_3\}$-space. Since $\mathcal{S}_{\{K_\alpha\}_{\alpha=1}^M}^{\mathcal{M}_N^3} = \Theta\left[\mathcal{S}_{\{Q_\alpha\}_{\alpha=1}^M}\right]$, we know that such a representation is the set of Pauli correlation vectors corresponding to all the elements of $\mathcal{S}_{\{Q_\alpha\}_{\alpha=1}^M}$.

Due to Eq. (1.3), the Pauli correlation vector of any $\varsigma \in \mathcal{S}_{\{Q_\alpha\}_{\alpha=1}^M}$ is given by

$$\begin{aligned} s_j &= \mathrm{Tr}\left(\varsigma \sigma_j^{\otimes N}\right) = \mathrm{Tr}\left[\left(\sum_i p_i \tau_i^{(1)} \otimes \tau_i^{(2)} \otimes \ldots \otimes \tau_i^{(M)}\right) \sigma_j^{\otimes N}\right] \\ &= \sum_i p_i \mathrm{Tr}\left[\tau_i^{(1)} \sigma_j^{\otimes K_1} \otimes \tau_i^{(2)} \sigma_j^{\otimes K_2} \otimes \ldots \otimes \tau_i^{(M)} \sigma_j^{\otimes K_M}\right] \\ &= \sum_i p_i \prod_{\alpha=1}^M \mathrm{Tr}\left(\tau_i^{(\alpha)} \sigma_j^{\otimes K_\alpha}\right) = \sum_i p_i \prod_{\alpha=1}^M c_{i,j}^{(\alpha)} \end{aligned} \tag{3.27}$$

where in the final equality we denote $c_{i,j}^{(\alpha)} = \mathrm{Tr}\left(\tau_i^{(\alpha)} \sigma_j^{\otimes K_\alpha}\right)$ as the $j$-th component of the Pauli correlation vector $\vec{c}_i^{(\alpha)} = \{c_{i,1}^{(\alpha)}, c_{i,2}^{(\alpha)}, c_{i,3}^{(\alpha)}\}$ corresponding to the arbitrary state $\tau_i^{(\alpha)}$ of subsystem $\alpha$. Eq. (3.27) can be simplified further by introducing the Hadamard product as the componentwise multiplication of vectors, i.e. for $\vec{u} = \{u_1, u_2, u_3\}$ and $\vec{v} = \{v_1, v_2, v_3\}$ the Hadamard product is $\vec{u} \circ \vec{v} = \{u_1 v_1, u_2 v_2, u_3 v_3\}$. Using the Hadamard product gives Eq. (3.27) as

$$\vec{s} = \sum_i p_i \vec{c}_i^{(1)} \circ \vec{c}_i^{(2)} \circ \ldots \circ \vec{c}_i^{(M)}, \tag{3.28}$$

i.e., that the Pauli correlation vector of any $\{Q_\alpha\}_{\alpha=1}^M$-separable state is a convex combination of Hadamard products of Pauli correlation vectors corresponding to subsystem states. Due to Corollary 3.3.1, we know that $\vec{c}_i^{(\alpha)} \in \mathcal{B}_1$ when $K_\alpha$ is odd and $\vec{c}_i^{(\alpha)} \in \mathcal{T}_{(-1)^{K_\alpha/2}}$ when $K_\alpha$ is even, and so $\mathcal{S}^{\mathcal{M}_N^3}_{\{K_\alpha\}_{\alpha=1}^M}$ is represented by the following set

$$\mathcal{S}^{\mathcal{M}_N^3}_{\{K_\alpha\}_{\alpha=1}^M} = conv\left(A^{(1)} \circ A^{(2)} \circ \ldots \circ A^{(M)}\right), \tag{3.29}$$

with

$$A^{(\alpha)} = \begin{cases} \mathcal{B}_1 & \text{if } K_\alpha \text{ is odd,} \\ \mathcal{T}_{(-1)^{K_\alpha/2}} & \text{if } K_\alpha \text{ is even,} \end{cases} \tag{3.30}$$

where we define the Hadamard product between any two sets $A$ and $B$ as

$$A \circ B = \{\vec{a} \circ \vec{b} \,|\, \vec{a} \in A\,,\, \vec{b} \in B\}. \tag{3.31}$$

The commutativity and associativity of the Hadamard product allow us to rearrange the ordering in Eq. (3.29) in the following way

$$\mathcal{S}^{\mathcal{M}_N^3}_{\{K_\alpha\}_{\alpha=1}^M} = conv\left[\left(\bigcirc_{\mu:K_\mu even} \mathcal{T}_{(-1)^{K_\mu/2}}\right) \circ \left(\bigcirc_{\nu:K_\nu odd} \mathcal{B}_1\right)\right], \tag{3.32}$$

where $\bigcirc_{\alpha=1}^n A^{(\alpha)} = A^{(1)} \circ A^{(2)} \circ \ldots \circ A^{(n)}$.

By writing any vector in $\mathcal{T}_{\pm 1}$ as a convex combination of the vertices of $\mathcal{T}_{\pm 1}$, one can easily show that

$$\begin{aligned} \mathcal{T}_{-1} \circ \mathcal{T}_{-1} &= \mathcal{T}_1, \\ \mathcal{T}_1 \circ \mathcal{T}_1 &= \mathcal{T}_1, \\ \mathcal{T}_1 \circ \mathcal{T}_{-1} &= \mathcal{T}_{-1}, \end{aligned} \tag{3.33}$$

so that

$$\bigcirc_{\mu:K_\mu even} \mathcal{T}_{(-1)^{K_\mu/2}} = \mathcal{T}_{(-1)^{\mathcal{M}_-}}, \tag{3.34}$$

where $\mathcal{M}_-$ is the number of $K_\mu$ with odd $K_\mu/2$. Similarly, one can see that

$$\mathcal{T}_{\pm 1} \circ \mathcal{B}_1 = \mathcal{B}_1. \tag{3.35}$$

Finally, we have that

$$conv\left(\bigcirc_{i=1}^n \mathcal{B}_1\right) = \mathcal{O}_1 \quad \forall n \geq 2. \tag{3.36}$$

Indeed, since

$$\{\{\pm 1, 0, 0\}, \{0, \pm 1, 0\}, \{0, 0, \pm 1\}\} \subset \bigcirc_{i=1}^n \mathcal{B}_1 \tag{3.37}$$

and

$$conv\{\{\pm 1, 0, 0\}, \{0, \pm 1, 0\}, \{0, 0, \pm 1\}\} = \mathcal{O}_1, \tag{3.38}$$

we have that $\mathcal{O}_1 \subseteq conv\left(\bigcirc_{i=1}^n \mathcal{B}_1\right)$. Now we will show that $\mathcal{O}_1 \supseteq conv\left(\bigcirc_{i=1}^n \mathcal{B}_1\right)$. To do so, it is sufficient to see that

$$\vec{b} \circ \vec{b}' \in \mathcal{O}_1 \tag{3.39}$$

for any $\vec{b}, \vec{b}' \in \mathcal{B}_1$, which trivially implies that $\bigcirc_{i=1}^n \mathcal{B}_1 \subseteq \mathcal{O}_1$, and so $conv\left(\bigcirc_{i=1}^n \mathcal{B}_1\right) \subseteq conv\left(\mathcal{O}_1\right) = \mathcal{O}_1$. Equation (3.39) holds since

$$\begin{aligned} \left|b_1 b_1'\right| + \left|b_2 b_2'\right| + \left|b_3 b_3'\right| &= |b_1|\left|b_1'\right| + |b_2|\left|b_2'\right| + |b_3|\left|b_3'\right| \\ &= \vec{n} \cdot \vec{n}' = ||\vec{n}||\,\left|\left|\vec{n}'\right|\right| \cos\theta \leq 1, \end{aligned} \tag{3.40}$$

where we define $\vec{n} = \{|b_1|, |b_2|, |b_3|\}$ and $\vec{n}' = \{|b_1'|, |b_2'|, |b_3'|\}$, respectively, as the vectors corresponding to $\vec{b}$ and $\vec{b}'$ in the positive octant of the unit ball, and $\theta$ as the angle between these vectors.

Now, due to Eqs. (3.32), (3.34), (3.35) and (3.36), and the fact that $conv(A) = A$ for any convex set $A$, we identify four cases:

1. if $K_\alpha$ is even for any $\alpha$ then

$$\begin{aligned} \mathcal{S}^{\mathcal{M}_N^3}_{\{K_\alpha\}_{\alpha=1}^M} &= conv\left(\bigcirc_{\mu:K_\mu even} \mathcal{T}_{(-1)^{K_\mu/2}}\right) \\ &= conv\left(\mathcal{T}_{(-1)^{\mathcal{M}_-}}\right) \\ &= \mathcal{T}_{(-1)^{\mathcal{M}_-}}, \end{aligned} \tag{3.41}$$

   where $\mathcal{M}_-$ is the number of $K_\mu$ with odd $K_\mu/2$;

2. if $K_\alpha$ is odd for just one value of $\alpha$ then

$$\begin{aligned} \mathcal{S}^{\mathcal{M}_N^3}_{\{K_\alpha\}_{\alpha=1}^M} &= conv\left[\left(\bigcirc_{\mu:K_\mu even} \mathcal{T}_{(-1)^{K_\mu/2}}\right) \circ \mathcal{B}_1\right] \\ &= conv\left(\mathcal{T}_{\pm 1} \circ \mathcal{B}_1\right) \\ &= \mathcal{B}_1; \end{aligned} \tag{3.42}$$

3. if $K_\alpha$ is odd for all values of $\alpha$ then

$$\begin{aligned} \mathcal{S}^{\mathcal{M}_N^3}_{\{K_\alpha\}_{\alpha=1}^M} &= conv\left(\bigcirc_{\nu:K_\nu odd} \mathcal{B}_1\right) \\ &= \mathcal{O}_1; \end{aligned} \tag{3.43}$$

4. otherwise,

$$\begin{aligned} \mathcal{S}^{\mathcal{M}_N^3}_{\{K_\alpha\}_{\alpha=1}^M} &= conv\left[\left(\bigcirc_{\mu:K_\mu even} \mathcal{T}_{(-1)^{K_\mu/2}}\right) \circ \left(\bigcirc_{\nu:K_\nu odd} \mathcal{B}_1\right)\right] \\ &= conv\left[\mathcal{T}_{\pm 1} \circ \left(\bigcirc_{\nu:K_\nu odd} \mathcal{B}_1\right)\right] \\ &= conv\left[\mathcal{T}_{\pm 1} \circ \mathcal{B}_1 \circ \ldots \circ \mathcal{B}_1\right] \\ &= conv\left(\bigcirc_{\nu:K_\nu odd} \mathcal{B}_1\right) \\ &= \mathcal{O}_1. \end{aligned} \tag{3.44}$$

For any even $N$-qubit system, only a $\{K_\alpha\}_{\alpha=1}^M$ partitioning within cases 1, 3 and 4 may be realised. In case 1, i.e. when $K_\alpha$ is even for any $\alpha$, we have $\mathcal{S}^{\mathcal{M}_N^3}_{\{K_\alpha\}_{\alpha=1}^M} = \mathcal{T}_{(-1)^{\mathcal{M}_-}}$, where $\mathcal{M}_-$ is the number of $K_\alpha$ with odd $K_\alpha/2$. However, one can simply see that $(-1)^{\mathcal{M}_-} = (-1)^{N/2}$, and thus $\mathcal{S}^{\mathcal{M}_N^3}_{\{K_\alpha\}_{\alpha=1}^M}$ is the set $\mathcal{T}_{(-1)^{N/2}}$ of all $\mathcal{M}_N^3$ states. Otherwise, in cases 3 and 4, we have $\mathcal{S}^{\mathcal{M}_N^3}_{\{K_\alpha\}_{\alpha=1}^M} = \mathcal{O}_1$.

For any odd $N$-qubit system, only a $\{K_\alpha\}_{\alpha=1}^M$ partitioning within cases 2, 3 and 4 may be realised. In case 2, i.e. when $K_\alpha$ is odd for only one $\alpha$, we have $\mathcal{S}^{\mathcal{M}_N^3}_{\{K_\alpha\}_{\alpha=1}^M} = \mathcal{B}_1$, and thus $\mathcal{S}^{\mathcal{M}_N^3}_{\{K_\alpha\}_{\alpha=1}^M}$ is the set $\mathcal{B}_1$ of all $\mathcal{M}_N^3$ states. Otherwise, in cases 3 and 4, we have $\mathcal{S}^{\mathcal{M}_N^3}_{\{K_\alpha\}_{\alpha=1}^M} = \mathcal{O}_1$.

■

Now we are ready to characterise also the set of $M$-separable $\mathcal{M}_N^3$ states $\mathcal{S}_M^{\mathcal{M}_N^3}$ by using Eq. (3.26). One can easily see that for any $M \leq \lceil N/2 \rceil$ one can always find an $M$-partition $\{Q_\alpha\}_{\alpha=1}^M$ such that $K_\alpha$ is odd for at most one value of $\alpha$ and thus $\mathcal{S}^{\mathcal{M}_N^3}_{\{Q_\alpha\}_{\alpha=1}^M} = \mathcal{M}_N^3$, whereas for any $M > \lceil N/2 \rceil$ this is impossible and thus $\mathcal{S}^{\mathcal{M}_N^3}_{\{Q_\alpha\}_{\alpha=1}^M} = \mathcal{O}_1$ for any $M$-partition $\{Q_\alpha\}_{\alpha=1}^M$. This immediately implies the following two Corollaries.

**Corollary 3.3.2.** *For any $N$, the set of $M$-separable $\mathcal{M}_N^3$ states $\mathcal{S}_M^{\mathcal{M}_N^3}$ is either*

- *the set of all $\mathcal{M}_N^3$ states, for any $M \leq \lceil N/2 \rceil$;*
- *the set of $\mathcal{M}_N^3$ states represented in the $\{c_1, c_2, c_3\}$-space by the unit octahedron $\mathcal{O}_1$ with vertices $\{\pm 1, 0, 0\}$, $\{0, \pm 1, 0\}$ and $\{0, 0, \pm 1\}$, for any $M > \lceil N/2 \rceil$.*

**Corollary 3.3.3.** *For any multiparticle entanglement monotone $E_M$ and any $\mathcal{M}_N^3$ state $\varpi$, $E_M(\varpi) = 0$ if*

1. *$M \leq \lceil N/2 \rceil$;*
2. *$M > \lceil N/2 \rceil$ and $|c_1| + |c_2| + |c_3| \leq 1$ for $c_i = \mathrm{Tr}(\varpi \sigma_i^{\otimes N})$.*

We now provide analytical expressions for the geometric measures of $M$-inseparable multiparticle entanglement $E_M^D(\varpi)$ of any $\mathcal{M}_N^3$ state $\varpi$. We will restrict to any non trivial number of parties $M'$, i.e. such that $M' > \lceil N/2 \rceil$.

As we have already seen, we simply need to find the minimal distance from $\varpi$ to the set of $\mathcal{M}_N^3$ states inside the unit octahedron $\mathcal{O}_1$. In the even $N$ case, we will reveal an intuitive geometric picture common to all convex and contractive distances $D$. On the other hand, for odd $N$, the results will turn out to be distance-dependent; we will show nonetheless that $E_M^D(\varpi)$ can still be evaluated exactly if D denotes the trace distance.

### Even $N$ case

For even $N$, the $M'$-inseparable $\mathcal{M}_N^3$ states belong to the four corners obtained by removing the unit octahedron $\mathcal{O}_1$ from the whole tetrahedron $\mathcal{T}_{(-1)^{N/2}}$ of $\mathcal{M}_N^3$ states (see Fig. 3.1(b)). In the following we will focus only on the corner containing the vertex $\{-1, (-1)^{N/2}, -1\}$ (see Fig. 3.1(d)), since all the $\mathcal{M}_N^3$ states belonging to the other three corners can be obtained from this by simply applying a single-qubit local unitary $\sigma_i \otimes \mathbb{I}^{\otimes N-1}$, $i \in \{1, 2, 3\}$, under which any sort of multiparticle entanglement is invariant.

In order to characterise all the $\mathcal{M}_N^3$ states with even $N$ belonging to the $\{-1, (-1)^{N/2}, -1\}$-corner, it will be convenient to move from the coordinate system $\{c_1, c_2, c_3\}$ to a new coordinate system $(p, q, h)$, where we assign the coordinates $\left(\frac{1}{3}, \frac{1}{3}, 1\right)$ to the vertex $\{-1, (-1)^{N/2}, -1\}$ and the coordinates

$$p = \frac{1 + c_1 - (-1)^{N/2} c_2 - c_3}{3 + c_1 - (-1)^{N/2} c_2 + c_3}, \tag{3.45}$$

$$q = \frac{1 + c_1 + (-1)^{N/2} c_2 + c_3}{3 + c_1 - (-1)^{N/2} c_2 + c_3}, \tag{3.46}$$

$$h = (-1 - (c_1 - (-1)^{N/2} c_2 + c_3))/2, \tag{3.47}$$

to any other point in the corner. In order to avoid confusion between the above two coordinate systems, we will denote an $\mathcal{M}_N^3$ state $\varpi$ with curly brackets when representing

it in the $\{c_1, c_2, c_3\}$ coordinate system, whereas we will denote $\varpi$ with round brackets when representing it in the $(p, q, h)$ coordinate system. Specifically, the $\mathcal{M}_N^3$ states represented by the triples $(p, q, h)$, with a fixed value of $h \in [0, 1[$, correspond in the $\{c_1, c_2, c_3\}$-space to all, and only, the $\mathcal{M}_N^3$ states belonging to the triangle with the following vertices (see cyan triangle in Fig. 3.1(d)):

$$\begin{aligned} V_1(h) &= \left\{-h, (-1)^{N/2}h, -1\right\}, \\ V_2(h) &= \left\{-h, (-1)^{N/2}, -h\right\}, \\ V_3(h) &= \left\{-1, (-1)^{N/2}h, -h\right\}, \end{aligned} \tag{3.48}$$

in such a way that

$$(p, q, h) = pV_1(h) + qV_2(h) + (1 - p - q)V_3(h). \tag{3.49}$$

These triangles corresponding to constant values of $h$ will play a crucial role, as they represent the sets of $\mathcal{M}_N^3$ states with constant $M'$-inseparable multiparticle entanglement for even $N$. In particular, for $h = 0$ we get one of the faces of the octahedron of $M'$-separable states (see red triangle in Fig. 3.1(d)), whereas with increasing $h$, we will prove that the $M'$-inseparable multiparticle entanglement of the $\mathcal{M}_N^3$ states belonging to the corresponding triangle will increase monotonically.

We will now show that, according to any convex and contractive distance, the $M'$-separable state represented by the triple $(p, q, 0)$ is one of the closest $M'$-separable states to the $\mathcal{M}_N^3$ state $(p, q, h)$. More generally, this entails that one of the closest $M'$-separable states $\varsigma_\varpi$ to an $\mathcal{M}_N^3$ state $\varpi$ is on the face of the octahedron bounding the corner of the tetrahedron in which $\varpi$ is located, and is identified by the intersection of such octahedron face with the line connecting $\varpi$ to the vertex of the tetrahedron corner, as depicted in Fig. 3.1(d).

To establish this claim, we first prove two auxiliary results introducing the information theoretic machinery that will be exploited in the rest of this Thesis not only for the quantification but also for the analysis of the dynamical preservation of other forms of quantumness. Specifically, by opportunely modifying Lemma 3.3.1 we will also manage to evaluate exactly all the valid geometric measures of genuine multiparticle entanglement for another family of $N$-qubit states, i.e. the states diagonal in the GHZ basis, for any $N$. On the other hand, via a proper adaptation of Lemma 3.3.2, we will be able to unveil the universal freezing phenomenon of both quantum coherence and discord-type correlations as detailed in the following Chapter.

**Lemma 3.3.1.** *For every even $N$, according to any convex and contractive distance, one of the closest $M'$-separable states $\varsigma_\varpi$ to any $\mathcal{M}_N^3$ state $\varpi$ belonging to the $\{-1, (-1)^{N/2}, -1\}$-corner is always an $\mathcal{M}_N^3$ state of the form $(p', q', 0)$ for some $p', q' \in [0, 1]$, $p' + q' \leq 1$.*

*Proof.* Let $\varpi$ and $\varsigma$ be, respectively, any $\mathcal{M}_N^3$ state belonging to the $\{-1, (-1)^{N/2}, -1\}$-corner and any $M'$-separable $\mathcal{M}_N^3$ state, i.e. any $\mathcal{M}_N^3$ state contained in the unit octahedron $\mathcal{O}_1$. There will always be an $M'$-separable $\mathcal{M}_N^3$ state $\varsigma'$, belonging to the octahedron face whose vertices are $V_1(0)$, $V_2(0)$, and $V_3(0)$ given in Eqs. (3.48), such that

$\varsigma' = \lambda\varpi + (1-\lambda)\varsigma$ for some $\lambda \in [0,1]$. Now, for any convex distance, the following holds

$$\begin{aligned} & D(\varpi, \varsigma') \\ = \; & D(\varpi, \lambda\varpi + (1-\lambda)\varsigma) \\ \leq \; & \lambda D(\varpi, \varpi) + (1-\lambda) D(\varpi, \varsigma) \\ = \; & (1-\lambda) D(\varpi, \varsigma) \\ \leq \; & D(\varpi, \varsigma). \end{aligned} \tag{3.50}$$

As one of the closest $M'$-separable states $\varsigma_\varpi$ to any $\mathcal{M}_N^3$ state $\varpi$ is always an $M'$-separable $\mathcal{M}_N^3$ state, then the above inequality implies that, for any $\mathcal{M}_N^3$ state $\varpi$ belonging to the $\{-1, (-1)^{N/2}, -1\}$-corner, $\varsigma_\varpi$ always belongs to the triangle with vertices $V_1(0)$, $V_2(0)$, and $V_3(0)$ i.e. $\varsigma_\varpi = (p', q', 0)$ for some $p', q' \in [0,1]$, $p' + q' \leq 1$.

■

**Lemma 3.3.2.** *For every even $N$, any contractive distance satisfies the following translational invariance property:*

$$D\left((p,q,h),(p,q,0)\right) = D\left(\left(\frac{1}{3},\frac{1}{3},h\right),\left(\frac{1}{3},\frac{1}{3},0\right)\right), \tag{3.51}$$

*for any $p, q \in [0,1]$ with $p+q \leq 1$ and $h \in [0,1[$.*

*Proof.* First of all, by considering the following single-qubit LOCC,

$$\Lambda_{\{p,q\}}(\varrho) = p\varrho + qU_1\varrho U_1^\dagger + (1-p-q)U_2\varrho U_2^\dagger \tag{3.52}$$

where $p, q \in [0,1]$, $p+q \leq 1$ and

$$U_1 = S_2^{\otimes N} S_1^{\otimes N} F_N, \tag{3.53}$$

$$U_2 = S_1^{\otimes N} F_N S_2^{\otimes N}, \tag{3.54}$$

with $S_i = \frac{1}{\sqrt{2}}\left(\mathbb{I} + i\sigma_i\right)$ and $F_N = \sigma_1^{\otimes(N/2+1)} \otimes \mathbb{I}^{\otimes(N/2-1)}$, we have the following inequality,

$$\begin{aligned} & D\left(\left(\frac{1}{3},\frac{1}{3},h\right),\left(\frac{1}{3},\frac{1}{3},0\right)\right) \\ = \; & D\left(\Lambda_{\{\frac{1}{3},\frac{1}{3}\}}\left(p,q,h\right), \Lambda_{\{\frac{1}{3},\frac{1}{3}\}}(p,q,0)\right) \\ \leq \; & D((p,q,h),(p,q,0)), \end{aligned} \tag{3.55}$$

where the inequality is due to the contractivity of the distance $D$, whereas the equality is due to the fact that

$$\left(\frac{1}{3},\frac{1}{3},h\right) = \Lambda_{\{\frac{1}{3},\frac{1}{3}\}}\left(p,q,h\right), \tag{3.56}$$

which in turn is due to Eqs. (3.48), (3.49), and:

$$U_1\{c_1,c_2,c_3\}U_1^\dagger = \{-(-1)^{N/2}c_2,-(-1)^{N/2}c_3,c_1\}, \tag{3.57}$$
$$U_2\{c_1,c_2,c_3\}U_2^\dagger = \{c_3,-(-1)^{N/2}c_1,-(-1)^{N/2}c_2\}. \tag{3.58}$$

In order to prove the opposite inequality and thus Eq. (3.51), we now introduce a global $N$-qubit channel $\Omega$ with operator-sum representation

$$\Omega(\varrho)=\sum_{i=1}^{2^N} A_i\varrho A_i^\dagger, \tag{3.59}$$

where

$$\{A_i\}_{i=1}^{2^N} = \Big\{\{|\Psi_j^+\rangle\langle\Phi_j^+|\}_{j=1}^{2^{N-2}},\{|\Psi_j^+\rangle\langle\Phi_j^-|\}_{j=1}^{2^{N-2}}, \{|\Psi_j^+\rangle\langle\Psi_j^+|\}_{j=1}^{2^{N-2}},\{|\Psi_j^-\rangle\langle\Psi_j^-|\}_{j=1}^{2^{N-2}}\Big\} \tag{3.60}$$

with the $2^N$ Kraus operators satisfying $\sum_i A_i^\dagger A_i=\mathbb{I}^{\otimes N}$, where $\{|\Phi_j^\pm\rangle\}$ and $\{|\Psi_j^\pm\rangle\}$ constitute the binary ordered $N$-qubit GHZ eigenbasis $\{|\beta_i^\pm\rangle\}$ with even and odd parity, respectively, i.e. they are such that

$$\Pi_3|\Phi_j^\pm\rangle = |\Phi_j^\pm\rangle,$$
$$\Pi_3|\Psi_j^\pm\rangle = -|\Psi_j^\pm\rangle, \tag{3.61}$$

where $j\in\{1,\cdots,2^{N-2}\}$. It will be crucial in the following to see that the effect of $\Omega$ on an $\mathcal{M}_N^3$ state represented by the triple $\left(\frac{1}{3},\frac{1}{3},h\right)$ is given by

$$\Omega\left(\left(\frac{1}{3},\frac{1}{3},h\right)\right)=(1,0,h)\,. \tag{3.62}$$

Thanks to Eqs. (3.3) and (3.61), one gets that the spectral decomposition of an $\mathcal{M}_N^3$ state with even $N$ can be written as follows:

$$\begin{aligned}\{c_1,c_2,c_3\} &= \frac{1}{2^N}\Big[1+c_1+(-1)^{N/2}c_2+c_3\Big]\sum_j|\Phi_j^+\rangle\langle\Phi_j^+| \\ &+ \frac{1}{2^N}\Big[1-c_1-(-1)^{N/2}c_2+c_3\Big]\sum_j|\Phi_j^-\rangle\langle\Phi_j^-| \\ &+ \frac{1}{2^N}\Big[1+c_1-(-1)^{N/2}c_2-c_3\Big]\sum_j|\Psi_j^+\rangle\langle\Psi_j^+| \\ &+ \frac{1}{2^N}\Big[1-c_1+(-1)^{N/2}c_2-c_3\Big]\sum_j|\Psi_j^-\rangle\langle\Psi_j^-|.\end{aligned} \tag{3.63}$$

Consequently, the spectral decompositions of the $\mathcal{M}_N^3$ states represented by the triples $\left(\frac{1}{3},\frac{1}{3},h\right)$ and $(1,0,h)$ are, respectively,

$$\begin{aligned}\left(\frac{1}{3},\frac{1}{3},h\right) &= \left\{-\frac{2h+1}{3},(-1)^{N/2}\frac{2h+1}{3},-\frac{2h+1}{3}\right\}\\ &= \frac{1}{2^{N-1}}\left(\frac{1-h}{3}\right)\sum_j|\Phi_j^+\rangle\langle\Phi_j^+|\\ &+ \frac{1}{2^{N-1}}\left(\frac{1-h}{3}\right)\sum_j|\Phi_j^-\rangle\langle\Phi_j^-|\\ &+ \frac{1}{2^{N-1}}\left(\frac{1-h}{3}\right)\sum_j|\Psi_j^+\rangle\langle\Psi_j^+|\\ &+ \frac{1}{2^{N-1}}(1+h)\sum_j|\Psi_j^-\rangle\langle\Psi_j^-|,\end{aligned} \tag{3.64}$$

and

$$\begin{aligned}(1,0,h) &= \left\{-h,(-1)^{N/2}h,-1\right\}\\ &= \frac{1}{2^{N-1}}(1-h)\sum_j|\Psi_j^+\rangle\langle\Psi_j^+|\\ &+ \frac{1}{2^{N-1}}(1+h)\sum_j|\Psi_j^-\rangle\langle\Psi_j^-|.\end{aligned} \tag{3.65}$$

By exploiting the following equalities

$$\begin{aligned}\Omega(|\Phi_j^+\rangle\langle\Phi_j^+|) &= |\Psi_j^+\rangle\langle\Psi_j^+|,\\ \Omega(|\Phi_j^-\rangle\langle\Phi_j^-|) &= |\Psi_j^+\rangle\langle\Psi_j^+|,\\ \Omega(|\Psi_j^+\rangle\langle\Psi_j^+|) &= |\Psi_j^+\rangle\langle\Psi_j^+|,\\ \Omega(|\Psi_j^-\rangle\langle\Psi_j^-|) &= |\Psi_j^-\rangle\langle\Psi_j^-|,\end{aligned} \tag{3.66}$$

and the linearity of the channel $\Omega$, we immediately get Eq. (3.62). We then have the inequality

$$\begin{aligned}& D((p,q,h),(p,q,0))\\ =\ & D\left(\Lambda_{\{p,q\}}\left(\Omega\left(\frac{1}{3},\frac{1}{3},h\right)\right),\Lambda_{\{p,q\}}\left(\Omega\left(\frac{1}{3},\frac{1}{3},0\right)\right)\right)\\ \leq\ & D\left(\left(\frac{1}{3},\frac{1}{3},h\right),\left(\frac{1}{3},\frac{1}{3},0\right)\right),\end{aligned} \tag{3.67}$$

where the inequality is again due to the contractivity of the distance $D$, whereas the equality is due to the fact that

$$(p,q,h) \;=\; \Lambda_{\{p,q\}}\left(\Omega\left(\frac{1}{3},\frac{1}{3},h\right)\right),$$

which in turn is due to Eqs. (3.62), (3.52), (3.49) and (3.48) . By putting together the two opposite inequalities (3.55) and (3.67), we immediately get the invariance of Eq. (3.51) for any contractive distance.

■

Now we are ready to find out the analytical expression of one of the closest $M'$-separable states $\varsigma_{\varpi}$ to any $\mathcal{M}_N^3$ state $\varpi$ belonging to the $\{-1,(-1)^{N/2},-1\}$-corner according to any convex and contractive distance.

**Theorem 3.3.2.** *For any even $N$, according to any convex and contractive distance, the $\mathcal{M}_N^3$ state $(p,q,0)$ is one of the closest $M'$-separable states to the $\mathcal{M}_N^3$ state $(p,q,h)$.*

*Proof.* Thanks to Lemma 3.3.1, which holds for any convex and contractive distance and any even $N$, we just need to prove that for any $p',q' \in [0,1]$, $p'+q' \leq 1$,

$$D((p,q,h),(p,q,0)) \leq D((p,q,h),(p',q',0)).$$

In fact

$$\begin{aligned}
& D((p,q,h),(p,q,0)) \\
=\;& D\left(\left(\frac{1}{3},\frac{1}{3},h\right),\left(\frac{1}{3},\frac{1}{3},0\right)\right) \\
=\;& D\left(\Lambda_{\left\{\frac{1}{3},\frac{1}{3}\right\}}(p,q,h),\Lambda_{\left\{\frac{1}{3},\frac{1}{3}\right\}}(p',q',0)\right) \\
\leq\;& D((p,q,h),(p',q',0)),
\end{aligned}$$

where the first equality is due to Lemma 3.3.2, which holds for any contractive distance and any even $N$, the second equality is due to the fact that

$$\left(\frac{1}{3},\frac{1}{3},h\right) \;=\; \Lambda_{\left\{\frac{1}{3},\frac{1}{3}\right\}}(p,q,h), \tag{3.68}$$

$$\left(\frac{1}{3},\frac{1}{3},0\right) \;=\; \Lambda_{\left\{\frac{1}{3},\frac{1}{3}\right\}}(p',q',0), \tag{3.69}$$

with $\Lambda_{\left\{\frac{1}{3},\frac{1}{3}\right\}}$ representing the LOCC expressed by Eq. (3.52), and finally the inequality is due to the contractivity of the distance $D$.

■

Now that we know the analytical expression of one of the closest $M'$-separable states to any $\mathcal{M}_N^3$ state with even $N$ according to any convex and contractive distance, we can unveil the general hierarchy of $M'$-inseparable multiparticle entanglement of these $\mathcal{M}_N^3$ states with respect to any geometric entanglement monotone $E_{M'}^D$.

**Corollary 3.3.4.** *For every even $N$ and according to any valid geometric measure of $M'$-inseparable multiparticle entanglement $E_{M'}^D$, the following holds:*

$$E_{M'}^D((p,q,h)) = E_{M'}^D((p',q',h)) \tag{3.70}$$
$$E_{M'}^D((p,q,h)) \leq E_{M'}^D((p',q',h')), \tag{3.71}$$

*for any $h \leq h'$.*

*Proof.* Let us start by proving Eq. (3.70). By using Theorem 3.3.2 and Lemma 3.3.2, we obtain

$$\begin{aligned} E_{M'}^D((p,q,h)) &= D((p,q,h),(p,q,0)) \\ &= D\left(\left(\frac{1}{3},\frac{1}{3},h\right),\left(\frac{1}{3},\frac{1}{3},0\right)\right) \\ &= D((p',q',h),(p',q',0)) \\ &= E_{M'}^D((p',q',h)), \end{aligned} \tag{3.72}$$

for any $p,q,p',q' \in [0,1]$, $p+q \leq 1$, $p'+q' \leq 1$ and $h \in [0,1[$.

In order to prove Eq. (3.71), let us consider the $\mathcal{M}_N^3$ states $\varpi = (p,q,h)$, $\varpi' = (p,q,h')$ such that $h \leq h'$, and $\varsigma = \varsigma_\varpi = \varsigma_{\varpi'} = (p,q,0)$, which is one of the closest $M'$-separable states to both $\varpi$ and $\varpi'$ according to Theorem 3.3.2. We can write $\varpi = \lambda\varpi' + (1-\lambda)\varsigma$, for some $\lambda \in [0,1]$. Now, by using the convexity of the distance and Eq. (3.70), we get

$$\begin{aligned} E_{M'}^D((p,q,h)) &= D(\varpi,\varsigma) \\ &= D(\lambda\varpi' + (1-\lambda)\varsigma,\varsigma) \\ &\leq \lambda D(\varpi',\varsigma) + (1-\lambda)D(\varsigma,\varsigma) \\ &= \lambda D(\varpi',\varsigma) \\ &\leq D(\varpi',\varsigma). \\ &= E_{M'}^D((p,q,h')) \\ &= E_{M'}^D((p',q',h')). \end{aligned} \tag{3.73}$$

■

We are now ready to apply the above general results to calculate the geometric $M$-inseparable multiparticle entanglement $E_M^D(\varpi)$ of any $\mathcal{M}_N^3$ state $\varpi$ with even $N$ for particular instances of $D$. As we have already pointed out in the proof of Corollary 3.3.4, for $\mathcal{M}_N^3$ states in the $\{-1,(-1)^{N/2},-1\}$-corner,

$$E_{M'}^D(\varpi) = D\left(\left(\frac{1}{3},\frac{1}{3},h\right),\left(\frac{1}{3},\frac{1}{3},0\right)\right) = f_D(h), \tag{3.74}$$

where $f_D(h)$ is some monotonically increasing function of $h$ only, which depends on the chosen distance $D$. By local unitary equivalence, this is true indeed for any $\mathcal{M}_N^3$ state in any of the four corners if we define the generalised $h$ to be $h_\varpi = \frac{1}{2}\left(\sum_{j=1}^3 |c_j| - 1\right)$. We have then

$$E_M^D(\varpi) = \begin{cases} 0\,, & h_\varpi \leq 0 \text{ or } M \leq N/2; \\ f_D(h_\varpi)\,, & \text{otherwise.} \end{cases} \tag{3.75}$$

Table 3.1 shows $f_D(h_\varpi)$ for the relative entropy, trace, infidelity, squared Bures, and squared Hellinger distance.

| Distance $D$ | $D(\varrho,\varsigma)$ | $f_D(h_\varpi)$ |
|---|---|---|
| Relative entropy $D_{\mathrm{RE}}$ | $\mathrm{Tr}\left[\varrho\left(\log_2\varrho - \log_2\varsigma\right)\right]$ | $\frac{1}{2}\big[(1-h_\varpi)\log_2(1-h_\varpi) + (1+h_\varpi)\log_2(1+h_\varpi)\big]$ |
| Trace $D_{\mathrm{Tr}}$ | $\frac{1}{2}\mathrm{Tr}\left\lvert\varrho-\varsigma\right\rvert$ | $\frac{1}{2}h_\varpi$ |
| Infidelity $D_{\mathrm{F}}$ | $1-\left[\mathrm{Tr}\left(\sqrt{\sqrt{\varsigma}\varrho\sqrt{\varsigma}}\right)\right]^2$ | $\frac{1}{2}\left(1-\sqrt{1-h_\varpi^2}\right)$ |
| Squared Bures $D_{\mathrm{B}}$ | $2\left[1-\mathrm{Tr}\left(\sqrt{\sqrt{\varsigma}\varrho\sqrt{\varsigma}}\right)\right]$ | $2-\sqrt{1-h_\varpi}-\sqrt{1+h_\varpi}$ |
| Squared Hellinger $D_{\mathrm{H}}$ | $2\left[1-\mathrm{Tr}\left(\sqrt{\varrho}\sqrt{\varsigma}\right)\right]$ | $2-\sqrt{1-h_\varpi}-\sqrt{1+h_\varpi}$ |

Table 3.1: Analytical expression of $M$-inseparable multiparticle entanglement $E_M^D$ for $\mathcal{M}_N^3$ states of an even number $N$ of qubits as defined by Eq. (3.75), for representative choices of the distance $D$.

Here we show the derivation of the given expressions for $f_D(h)$. Since the two $\mathcal{M}_N^3$ states $\left(\frac{1}{3},\frac{1}{3},h\right)$ and $\left(\frac{1}{3},\frac{1}{3},0\right)$ are diagonal in the same basis, we have that their distance reduces to the corresponding classical distance between the probability distributions formed by their eigenvalues, denoted by $P_h$ and $P_0$ respectively. We recall that the classical relative entropy, trace, infidelity, squared Bures, and squared Hellinger distance between two probability distributions $P=\{p_i\}$ and $Q=\{q_i\}$ are given by, respectively

$$\begin{aligned} D_{\mathrm{RE}}(P,Q) &= \sum_i p_i \log_2(p_i/q_i), \\ D_{\mathrm{Tr}}(P,Q) &= \sum_i |p_i - q_i|/2, \\ D_{\mathrm{F}}(P,Q) &= 1-\left(\sum_i \sqrt{p_i q_i}\right)^2, \\ D_{\mathrm{B}}^2(P,Q) &= D_{\mathrm{H}}^2(P,Q) = 2\left(1-\sum_i \sqrt{p_i q_i}\right). \end{aligned} \tag{3.76}$$

Consequently, by using Eq. (3.64) to get both $P_h$ and $P_0$, we obtain the desired expressions for $f_D(h)$.

**Odd $N$ case**

Let us now turn our attention to the evaluation of the geometric $M$-inseparable multiparticle entanglement $E_M^D(\varpi)$ of an $\mathcal{M}_N^3$ state $\varpi$ in the case of odd $N$. Unlike the even $N$ case, where all the convex and contractive distances $D$ concur on what is one of the closest separable states to an $\mathcal{M}_N^3$ state, there is unfortunately no such agreement in the odd $N$ case.

In the following we will focus in particular on the important but notoriously hard-to-evaluate case of the trace distance-based geometric measures of multiparticle entanglement $E_{M'}^{D_{\mathrm{Tr}}}(\varpi)$ of any $\mathcal{M}_N^3$ state with odd $N$, when considering as before a non trivial number of parties $M'$, i.e. such that $M' > \lceil N/2 \rceil$.

We know that the trace distance-based $M'$-inseparable multiparticle entanglement of an $\mathcal{M}_N^3$ state $\varpi$ with odd $N$ is the minimal distance from $\varpi$ to the unit octahedron $\mathcal{O}_1$ (see Fig. 3.1(c)). Due to convexity of the trace distance and of the unit octahedron $\mathcal{O}_1$, we get that one of the closest $M'$-separable $\mathcal{M}_N^3$ states to an entangled $\mathcal{M}_N^3$ state $\varpi$ must belong necessarily to the boundary of the octahedron, i.e. either to one of its faces or edges. We can easily see that the trace distance between two arbitrary odd $N$ $\mathcal{M}_N^3$ states $\varpi_1 = \left\{c_1^{(1)}, c_2^{(1)}, c_3^{(1)}\right\}$ and $\varpi_2 = \left\{c_1^{(2)}, c_2^{(2)}, c_3^{(2)}\right\}$ is nothing but one half of the Euclidean distance between their representing triples, i.e.

$$D_{\mathrm{Tr}}(\varpi_1, \varpi_2) = \frac{1}{2}\sqrt{\sum_{i=1}^{3}\left(c_i^{(1)} - c_i^{(2)}\right)^2}. \tag{3.77}$$

This is proven as follows. In order to evaluate the trace distance between any two $\mathcal{M}_N^3$ states with odd $N$, we just need to calculate the eigenvalues of their difference, because

$$D_{\mathrm{Tr}}(\varpi_1, \varpi_2) = \frac{1}{2}\mathrm{Tr}(|\varpi_1 - \varpi_2|) = \frac{1}{2}\sum_i |\lambda_i|, \tag{3.78}$$

where $\{\lambda_i\}$ are just the eigenvalues of $\varpi_1 - \varpi_2$. Since $\varpi_1 - \varpi_2 = \frac{1}{2^N}\sum_i d_i \sigma_i^{\otimes N}$, with $d_i = c_i^{(1)} - c_i^{(2)}$, one can easily see that its eigenvectors are exactly the ones expressed in Eq. (3.5), with $d_1 = r\sin\theta\cos\phi$, $d_2 = r\sin\theta\sin\phi$ and $d_3 = r\cos\theta$ while its eigenvalues are given by either $\frac{1}{2^N}r$ or $-\frac{1}{2^N}r$, with $r = \sqrt{d_1^2 + d_2^2 + d_3^2}$. By putting these eigenvalues into Eq. (3.78) one immediately gets Eq. (3.77).

An immediate consequence of Eq. (3.77) is that the closest $M'$-separable $\mathcal{M}_N^3$ state $\varsigma_\varpi = \{s_1, s_2, s_3\}$ to an entangled $\mathcal{M}_N^3$ state $\varpi = \{c_1, c_2, c_3\}$ is just its Euclidean orthogonal projection onto the boundary of the unit octahedron $\mathcal{O}_1$, as depicted in Fig. 3.1(e). We can thus distinguish between the following two cases:

1. the Euclidean projection of $\{c_1, c_2, c_3\}$ onto the boundary of the unit octahedron $\mathcal{O}_1$ falls onto one of its faces. This case happens if, and only if, $0 \leq \mathrm{sign}(c_i)s_i \leq 1$

for any $i$, where $\{s_i = \mathrm{sign}(c_i)(1 - |c_1| - |c_2| - |c_3| + 3|c_i|)/3\}$ is exactly the triple representing such Euclidean projection;

2. the Euclidean projection of $\{c_1, c_2, c_3\}$ onto the boundary of the unit octahedron $\mathcal{O}_1$ falls onto one of its edges. This case happens when any of the conditions listed in case 1 do not hold. Moreover, the triple $\{s_1, s_2, s_3\}$ representing such Euclidean projection is given by $s_k = 0$ and $s_i = \mathrm{sign}(c_i)(1 - \sum_{j\neq k} |c_j| + 2|c_i|)/2$, where $k$ is set by $f_k = \min\{f_1, f_2, f_3\}$ with $f_i = \sqrt{c_i^2 + (1 - \sum_{j\neq i} |c_j|)^2/2}$.

This provides the following explicit expressions for the trace distance-based measure of $M$-inseparable multiparticle entanglement on an arbitrary $\mathcal{M}_N^3$ state $\varpi$ with odd $N$:

$$E_M^{D_{\mathrm{Tr}}}(\varpi) = \begin{cases} 0\,, & h_\varpi \leq 0 \text{ or } M \leq \lceil N/2 \rceil; \\ \frac{h_\varpi}{\sqrt{3}}\,, & 0 < h_\varpi \leq 3|c_j|/2 \;\forall j; \\ \min\limits_j \frac{1}{2}\sqrt{|c_j|^2 + \frac{1}{2}(2h_\varpi - |c_j|)^2}\,, & \text{otherwise.} \end{cases} \tag{3.79}$$

### 3.3.2 Global and partial multiparticle entanglement bounds for arbitrary $N$-qubit states

The usefulness of the above analytical results for the quantification of multiparticle entanglement is not limited to the $\mathcal{M}_N^3$ states. Indeed, Corollary 3.2.1 can be rephrased as follows: the $\mathcal{M}_N^3$ state $\varpi^{\{c_j\}}$ with given correlation functions $\{c_j\}$ is extremal among all quantum states with the same correlation functions, in the sense that

$$E_M^D(\varpi^{\{c_j\}}) \leq E_M^D(\varrho)\,, \;\forall\, \varrho : \mathrm{Tr}\big(\varrho\, \sigma_j^{\otimes N}\big) = c_j \;(j = 1, 2, 3). \tag{3.80}$$

This immediately implies that for any $M > \lceil N/2 \rceil$ the $M$-inseparable multiparticle entanglement $E_M^D$ of $\varrho$ can have a nontrivial exact lower bound given by the corresponding multiparticle entanglement of the $\mathcal{M}_N^3$ state $\varpi$ with the same $\{c_j\}$.

From a practical point of view, one needs only to measure the three correlation functions $\{c_j\}$, as routinely done in optical, atomic, and spin systems [53, 70, 71, 73], to obtain an estimate of the global or partial multiparticle entanglement content of an unknown state $\varrho$ with no need for a full state reconstruction.

Furthermore, the lower bound can be improved if a partial knowledge of the state $\varrho$ is assumed, as is usually the case for experiments aiming to produce specific families of states for applications in quantum information processing [70, 71, 173]. In those realisations, one typically aims to detect entanglement by constructing optimised entanglement witnesses tailored on the target states [53]. By exploiting similar ideas, we can optimise the quantitative lower bound in Eq. (3.80) over all possible single-qubit local unitaries applied to the state $\varrho$ before the $\mathcal{M}_N^3$-fication,

$$\sup_{U_\otimes} E_M^D(\varpi^{\{\tilde{c}_j\}}) \leq E_M^D(\tilde{U}_\otimes \varrho \tilde{U}_\otimes^\dagger) = E_M^D(\varrho)\,, \tag{3.81}$$

where $\mathrm{Tr}\big(U_\otimes \varrho U_\otimes^\dagger\, \sigma_j^{\otimes N}\big) = \tilde{c}_j$, $U_\otimes = \bigotimes_{\alpha=1}^N U^{(\alpha)}$ denotes any single-qubit local unitary operation, and $\tilde{U}_\otimes$ denotes the singe-qubit unitary achieving the above optimisation.

Experimentally, the optimised bound can then be still accessed by measuring a triple of correlations functions $\{\tilde{c}_j\}$ given by the expectation values of correspondingly rotated Pauli operators on each qubit, $\tilde{c}_j = \langle U_\otimes^\dagger \sigma_j^{\otimes N} U_\otimes \rangle$, as illustrated in Figure 3.1(a), and is non-zero whenever $M > \lceil N/2 \rceil$ and $\sum_{j=1}^3 |\tilde{c}_j| > 1$.

Optimality in Eq. (3.81) can be achieved by the choice of $U_\otimes$ such that the quantity $\tilde{h}_\varpi = \frac{1}{2}\left(\sum_{j=1}^3 |\tilde{c}_j| - 1\right)$ is maximum. By using the well known correspondence between the special unitary group $\mathsf{SU}(2)$ and special orthogonal group $\mathsf{SO}(3)$, we have that to any one-qubit unitary $U^{(\alpha)}$ corresponds the orthogonal $3 \times 3$ matrix $O^{(\alpha)}$ such that

$$U^{(\alpha)} \vec{n} \cdot \vec{\sigma} U^{(\alpha)\dagger} = (O^{(\alpha)} \vec{n}) \cdot \vec{\sigma}, \tag{3.82}$$

where $\vec{n} = \{n_1, n_2, n_3\} \in \mathbb{R}^3$ and $\vec{\sigma} = \{\sigma_1, \sigma_2, \sigma_3\}$ is the vector of Pauli matrices. We have then that

$$\sup_{\{U^{(\alpha)}\}} (|\tilde{c}_1| + |\tilde{c}_2| + |\tilde{c}_3|) = \sup_{\{O^{(\alpha)}\}} (|\tilde{T}_{11\cdots1}| + |\tilde{T}_{22\cdots2}| + |\tilde{T}_{33\cdots3}|), \tag{3.83}$$

where

$$\tilde{T}_{i_1 i_2 \cdots i_N} = \sum_{j_1 j_2 \cdots j_N} T_{j_1 j_2 \cdots j_N} O^{(1)}_{i_1 j_1} O^{(2)}_{i_2 j_2} \cdots O^{(N)}_{i_N j_N} \tag{3.84}$$

and

$$T_{i_1 i_2 \cdots i_N} = \mathrm{Tr}\left[\varrho\, (\sigma_{i_1} \otimes \sigma_{i_2} \otimes \cdots \otimes \sigma_{i_N})\right]. \tag{3.85}$$

In the case of permutationally invariant states $\varrho$, the $3 \times 3 \times \cdots \times 3$ tensor $T_{i_1 i_2 \cdots i_N}$ is fully symmetric, i.e. $T_{i_1 i_2 \cdots i_N} = T_{\vartheta(i_1 i_2 \cdots i_N)}$ for any permutation $\vartheta$ of the indices, so that the optimisation can be achieved when $O^{(1)} = O^{(2)} = \cdots = O^{(N)}$ [175]. In this case we then need to perform the maximisation over just the three angles $\{\theta, \psi, \phi\}$ which determine the orthogonal matrix $O^{(\alpha)}$ corresponding to an arbitrary single-qubit unitary

$$U^{(\alpha)} = \begin{pmatrix} \cos\frac{\theta}{2} e^{-i\frac{\psi+\phi}{2}} & -i\sin\frac{\theta}{2} e^{-i\frac{\phi-\psi}{2}} \\ -i\sin\frac{\theta}{2} e^{i\frac{\phi-\psi}{2}} & \cos\frac{\theta}{2} e^{i\frac{\psi+\phi}{2}} \end{pmatrix}.$$

As a special case, for a two-qubit state ($N = 2$) the optimal local operation is the one which diagonalises the correlation matrix $(T_{i_1 i_2})$.

We now see how useful our results are on concrete examples. Table 3.2 presents a compendium of optimised analytical lower bounds on the global and partial multiparticle entanglement of the following relevant families of $N$-qubit states [74,75,170,174,176–183], up to $N = 8$:

- $N$-qubit GHZ states [170]

$$|\mathrm{GHZ}^{(N)}\rangle = \frac{1}{\sqrt{2}}\left(|00\cdots00\rangle + |11\cdots11\rangle\right), \tag{3.86}$$

with $N \geq 3$;

- $N$-qubit W states [176]

$$|\mathrm{W}^{(N)}\rangle = \frac{1}{\sqrt{N}}\left(|00\cdots01\rangle + |00\cdots10\rangle + \cdots + |10\cdots00\rangle\right), \tag{3.87}$$

with $N \geq 3$;

- $N$-qubit Wei states [182, 183]

$$\varrho_{\mathrm{Wei}}^{(N)}(x) = x|\mathrm{GHZ}^{(N)}\rangle\langle\mathrm{GHZ}^{(N)}| + \frac{(1-x)}{2N}\sum_{k=1}^{N}\left(P_k + \overline{P}_k\right), \tag{3.88}$$

where $N \geq 4$, $x \in [0,1]$ and $P_k$ is the projector onto the binary $N$-qubit representation of $2^{k-1}$ whereas $\bar{P}_i = \sigma_1^{\otimes N} P_i \sigma_1^{\otimes N}$;

- $N$-qubit linear cluster states $|\mathrm{C}_1^{(N)}\rangle$ corresponding to the $N$-vertex linear graph [40, 63];

- $N$-qubit rectangular cluster states $|\mathrm{C}_2^{(N)}\rangle$ corresponding to the $N$-vertex ladder-type graph [40, 178];

- $N$-qubit Dicke states

$$|\mathrm{D}_k^{(N)}\rangle = \frac{1}{\sqrt{Z}}\sum_i \Pi_i(|0\rangle^{\otimes N-k} \otimes |1\rangle^{\otimes k}), \tag{3.89}$$

which are superpositions of all states with $k$ qubits in the excited state $|1\rangle$ and $N-k$ qubits in the ground state $|0\rangle$, with the symbol $\{\Pi_i(|0\rangle^{\otimes N-k} \otimes |1\rangle^{\otimes k})\}_{i=1}^{Z}$ denoting the $Z \equiv \binom{N}{k}$ states obtained by all the possible combinations of the $k$ qubits in the excited state $|1\rangle$ and the $N-k$ qubits in the ground state $|0\rangle$. We focus in particular on half-excited Dicke states, given by $k = N/2$ for any even $N$ [74, 75, 180, 184];

- 4-qubit singlet state [185]

$$|\Psi^{(4)}\rangle = \frac{1}{\sqrt{3}}\left[|0011\rangle + |1100\rangle - \frac{1}{2}(|0101\rangle + |0110\rangle + |1001\rangle + |1010\rangle)\right]; \tag{3.90}$$

- $N$-qubit generalised Smolin states [172, 174, 186] $\varrho_{\mathrm{S}}^{(N)}$ for even $N \geq 4$, which are instances of $\mathcal{M}_N^3$ states with correlation triple $\{(-1)^{N/2}, (-1)^{N/2}, (-1)^{N/2}\}$, hence their entanglement quantification is exact.

| $N$ | State | $\{\tilde{c}_1, \tilde{c}_2, \tilde{c}_3\}$ | $\sum_{j=1}^{3} \lvert\tilde{c}_j\rvert$ | $\{\theta, \psi, \phi\}$ |
|---|---|---|---|---|
| $N=3$ | $\lvert\mathrm{GHZ}^{(3)}\rangle$ | $\left\{-\sqrt{\frac{8}{27}}, \sqrt{\frac{8}{27}}, -\sqrt{\frac{8}{27}}\right\}$ | $2\sqrt{\frac{2}{3}}$ | $\left\{\cos^{-1}(\frac{1}{\sqrt{3}}), \frac{5\pi}{30}, \frac{\pi}{4}\right\}$ |
| | $\lvert\mathrm{W}^{(3)}\rangle$ | $\left\{\frac{1}{\sqrt{3}}, -\frac{1}{\sqrt{3}}, \frac{1}{\sqrt{3}}\right\}$ | $\sqrt{3}$ | $\left\{\cos^{-1}(\frac{1}{\sqrt{3}}), 0, \frac{\pi}{4}\right\}$ |
| $N=4$ | $\lvert\mathrm{GHZ}^{(4)}\rangle$ | $\{1,1,1\}$ | 3 | $\{0,0,0\}$ |
| | $\lvert\mathrm{W}^{(4)}\rangle$ | $\left\{\frac{5}{9}, \frac{5}{9}, \frac{5}{9}\right\}$ | $\frac{5}{3}$ | $\left\{\cos^{-1}(\frac{1}{\sqrt{3}}), 0, \frac{\pi}{4}\right\}$ |
| | $\varrho_{\mathrm{Wei}}^{(4)}(x)$ | $\{x, x, 2x-1\}$ | $2x + \lvert 2x-1\rvert$ | $\{0,0,0\}$ |
| | $\lvert\mathrm{C}_1^{(4)}\rangle$ | $\{1,1,1\}$ | 3 | * |
| | $\lvert\mathrm{C}_2^{(4)}\rangle$ | $\{1,1,1\}$ | 3 | $\left\{\frac{\pi}{4}, 0, 0\right\}$ |
| | $\lvert\mathrm{D}_2^{(4)}\rangle$ | $\{1,1,1\}$ | 3 | $\{0,0,0\}$ |
| | $\lvert\Psi^{(4)}\rangle$ | $\{1,1,1\}$ | 3 | $\{0,0,0\}$ |
| | $\varrho_{\mathrm{S}}^{(4)}$ | $\{1,1,1\}$ | 3 | $\{0,0,0\}$ |
| $N=5$ | $\lvert\mathrm{GHZ}^{(5)}\rangle$ | $\left\{\frac{1}{\sqrt{2}}, \frac{1}{\sqrt{2}}, 0\right\}$ | $\sqrt{2}$ | $\left\{0, \frac{\pi}{40}, \frac{\pi}{40}\right\}$ |
| | $\lvert\mathrm{W}^{(5)}\rangle$ | $\left\{\frac{7}{9\sqrt{3}}, -\frac{7}{9\sqrt{3}}, \frac{7}{9\sqrt{3}}\right\}$ | $\frac{7}{3\sqrt{3}}$ | $\left\{\cos^{-1}(\frac{1}{\sqrt{3}}), 0, \frac{\pi}{4}\right\}$ |
| | $\varrho_{\mathrm{Wei}}^{(5)}(x)$ | $\left\{\frac{x}{\sqrt{2}}, \frac{x}{\sqrt{2}}, 0\right\}$ | $\sqrt{2}x$ | $\left\{0, \frac{\pi}{40}, \frac{\pi}{40}\right\}$ |
| | $\lvert\mathrm{C}_1^{(5)}\rangle$ | $\left\{\frac{1}{2}, \frac{1}{2}, \frac{1}{2}\right\}$ | $\frac{3}{2}$ | * |
| $N=6$ | $\lvert\mathrm{GHZ}^{(6)}\rangle$ | $\{1,-1,1\}$ | 3 | $\{0,0,0\}$ |
| | $\varrho_{\mathrm{Wei}}^{(6)}(x)$ | $\{x, -x, 2x-1\}$ | $2x + \lvert 2x-1\rvert$ | $\{0,0,0\}$ |
| | $\lvert\mathrm{C}_1^{(6)}\rangle$ | $\{1,-1,1\}$ | 3 | * |
| | $\lvert\mathrm{C}_2^{(6)}\rangle$ | $\{1,-1,1\}$ | 3 | * |
| | $\lvert\mathrm{D}_3^{(6)}\rangle$ | $\{1,1,-1\}$ | 3 | $\{0,0,0\}$ |
| | $\varrho_{\mathrm{S}}^{(6)}$ | $\{-1,-1,-1\}$ | 3 | $\{0,0,0\}$ |
| $N=7$ | $\lvert\mathrm{GHZ}^{(7)}\rangle$ | $\left\{\frac{1}{\sqrt{2}}, -\frac{1}{\sqrt{2}}, 0\right\}$ | $\sqrt{2}$ | $\left\{0, \frac{\pi}{56}, \frac{\pi}{56}\right\}$ |
| | $\varrho_{\mathrm{Wei}}^{(7)}(x)$ | $\left\{\frac{x}{\sqrt{2}}, -\frac{x}{\sqrt{2}}, 0\right\}$ | $\sqrt{2}x$ | $\left\{0, \frac{\pi}{56}, \frac{\pi}{56}\right\}$ |
| | $\lvert\mathrm{C}_1^{(7)}\rangle$ | $\left\{\frac{1}{2}, -\frac{1}{2}, \frac{1}{2}\right\}$ | $\frac{3}{2}$ | * |
| $N=8$ | $\lvert\mathrm{GHZ}^{(8)}\rangle$ | $\{1,1,1\}$ | 3 | $\{0,0,0\}$ |
| | $\varrho_{\mathrm{Wei}}^{(8)}(x)$ | $\{x, x, 2x-1\}$ | $2x + \lvert 2x-1\rvert$ | $\{0,0,0\}$ |
| | $\lvert\mathrm{C}_1^{(8)}\rangle$ | $\{1,1,1\}$ | 3 | * |
| | $\lvert\mathrm{D}_4^{(8)}\rangle$ | $\{1,1,1\}$ | 3 | $\{0,0,0\}$ |
| | $\varrho_{\mathrm{S}}^{(8)}$ | $\{1,1,1\}$ | 3 | $\{0,0,0\}$ |

Table 3.2: Applications of our framework to construct accessible lower bounds on global and partial multiparticle entanglement. The asterisk * indicates non-symmetric states for which the optimisation of the bounds requires different angles for each qubit (not reported here).

Notice that in the table we listed mostly pure states. In general, if the triple $\{\tilde{c}_j\}$ is optimal for a pure $N$-qubit state $|\Phi^{(N)}\rangle$, then for its noisy versions $\varrho_{\Phi}^{(N)}(q)$, obtained by considering classical mixtures of $|\Phi^{(N)}\rangle$ with probability $q$ and the maximally mixed state with probability $(1-q)$,

$$\varrho_{\Phi}^{(N)}(q) = q|\Phi^{(N)}\rangle\langle\Phi^{(N)}| + \frac{1-q}{2^N}\mathbb{I}^{\otimes N}, \tag{3.91}$$

the optimal triple is simply $\{q\tilde{c}_j\}$ so that one still gets nonzero lower bounds to global and partial entanglement for all $q > 1/\sum_{j=1}^{3}|\tilde{c}_j|$, as shown in Figure 3.2(a) for some representative examples.

Let us comment on some cases where our analysis is particularly effective.

For GHZ states, cluster states, and half-excited Dicke states, which constitute primary resources for quantum computation and metrology [25, 40], we get the maximum $h_{\varpi} = 1$ for any even $N$. This means that our bounds remain robust to estimate global and partial entanglement in noisy versions of these states for all $q > 1/3$. Notably, for values of $q$ sufficiently close to 1, our bounds to global entanglement can be tighter than the more experimentally demanding ones derived very recently in Ref. [62], as shown in Figure 3.2(a).

Focusing on noisy GHZ states, we observe however that our scale-invariant threshold $q > 1/3$, obtained by measuring the three canonical Pauli operators for each qubit, is weaker than the well-established inseparability threshold $q > 1/(1+2^{N-1})$ [58]. Nevertheless, we note that our simple quantitative bound given by Eq. (3.80) becomes tight in the paradigmatic limit of pure GHZ states ($q = 1$) of any even number $N$ of qubits, thus returning the *exact* value of their global multiparticle entanglement via Eq. (3.75), despite the fact that such states are not (and are very different from) $\mathcal{M}_N^3$ states.

Eq. (3.80) also provides a useful nonvanishing lower bound to the global and partial $N$-particle entanglement of Wei states in the interval $x \in \left(\frac{1}{2}, 1\right]$, for any even $N$. A comparison between such a bound with $D$ denoting the relative entropy, which requires only three local measurements, and the true value of the relative entropy of global $N$-particle entanglement for these states [183], whose experimental evaluation would conventionally require a complete state tomography, is presented in Figure 3.2(b).

We now benchmark the applicability of our results to *real data* from recent experiments [70, 71, 73–75, 187].

In Refs. [71, 173], the authors used quantum optical setups to prepare an instance of a bound entangled four-qubit state, known as Smolin state [186]. Such a state cannot be written as a convex mixture of product states of the four qubits, yet no entanglement can be distilled out of it, thus incarnating the irreversibility in entanglement manipulation while still representing a useful resource for information locking and quantum secret sharing [19, 174]. It turns out that noisy Smolin states are particular types of $\mathcal{M}_N^3$ states (for any even $N$) [172,174], that in the representation of Figure 3.1(b) are located along the segment connecting the tetrahedron vertex $\{(-1)^{N/2}, (-1)^{N/2}, (-1)^{N/2}\}$ with the origin. Therefore, this work provides exact analytical formulae for all the nontrivial hierarchy of their global and partial entanglement. In the specific experimental implementation of Ref. [71] for $N = 4$, the global entanglement was detected (but not quantified) via a witness constructed

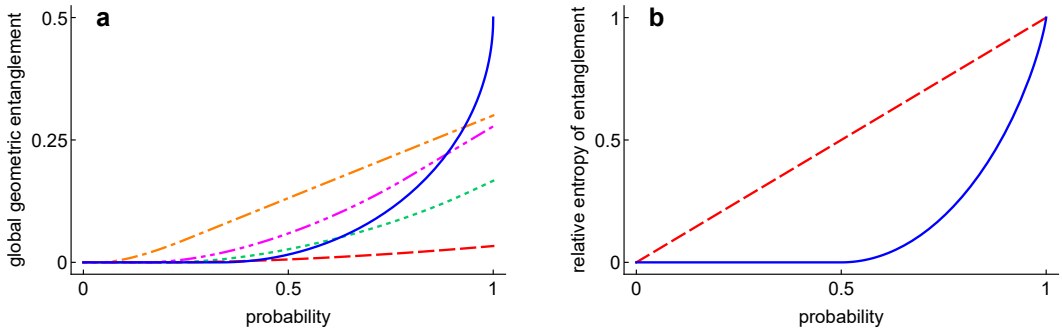


Figure 3.2: (a) Lower bounds to the global geometric entanglement $E_N^{D_{\mathrm{F}}}$ based on infidelity for noisy versions of some $N$-qubit states, as functions of the probability $q$ of obtaining the corresponding pure states. The non-solid lines refer to bounds obtained by the method of Ref. [62] for: 4-qubit noisy linear cluster states (green dotted), 6-qubit noisy rectangular cluster states (red dashed), 6-qubit noisy half-excited Dicke states (orange dot-dashed), 4-qubit noisy singlet states (magenta dot-dot-dashed). The solid blue line corresponds to our bound based on $\mathcal{M}_N^3$-fication for all the considered states, which is accessible by measuring only the three correlation functions $\tilde{c}_j = \langle \bigotimes_\alpha \tilde{\sigma}_j^{(\alpha)} \rangle$. (b) Relative entropy of multiparticle entanglement of $N$-qubit Wei states $\varrho_{\mathrm{Wei}}^{(N)}$, as a function of the probability $x$ of obtaining a GHZ state. The dashed red line $E_N^{D_{\mathrm{RE}}}(\varrho_{\mathrm{Wei}}^{(N)}) = x$ denotes the exact value of the global relative entropy of entanglement as computed in [183]. The solid blue line denotes our accessible lower bound, obtained by combining Eqs. (3.75) and (3.81) with the expressions in Tables 3.1 and 3.2, and given explicitly by $E_{N,\mathrm{low}}^{D_{\mathrm{RE}}}(\varrho_{\mathrm{Wei}}^{(N)}) = \log_2(2-2x) + x\big(\log_2(x) - \log_2(1-x)\big)$ for $\frac{1}{2} < x \leq 1$, while it vanishes for $0 \leq x \leq \frac{1}{2}$. The bound becomes tight for $x = 1$, thus quantifying exactly the global multiparticle entanglement of pure GHZ states. We further show that our lower bound to global entanglement coincides with the exact genuine multiparticle entanglement of Wei states, $E_{N,\mathrm{low}}^{D_{\mathrm{RE}}}(\varrho_{\mathrm{Wei}}^{(N)}) = E_2^{D_{\mathrm{RE}}}(\varrho_{\mathrm{Wei}}^{(N)})$, which is computed in the next Section. The results are scale-invariant and hold for any even $N$.

by measuring precisely the three correlation functions $\{c_j\}$. Based on the existing data alone (and without assuming that the produced state is within the $\mathcal{M}_N^3$ family), we can then provide a quantitative estimate to the multiparticle entanglement of this experimental bound entangled state in terms of any geometric measure $E_M^D$, by using Table 3.1. The results are reported in Table 3.3 for the illustrative case of the trace distance.

Remaining within the domain of quantum optics, recently two laboratories reported the creation of six-photon Dicke states $|\mathrm{D}_3^{(6)}\rangle$ [74, 75]. Dicke states [180] are valuable resources for quantum metrology, computation, and networked communication, and emerge naturally in many-body systems as ground states of the isotropic Lipkin-Meshkov-Glick model [184]. Based on the values of the three correlation functions $\{c_j\}$, which were measured in Refs. [74,75] to construct some entanglement witnesses, we can provide quantitative bounds to their global and partial geometric entanglement $E_M^D$ (for $4 \leq M \leq 6$)

from Eq. (3.80); see Table 3.3.

A series of experiments at Innsbruck [70, 72, 73, 187] has resulted in the generation of a variety of relevant multi-qubit states with trapped ion setups, for explorations of fundamental science and for the implementation of quantum protocols. In those realisations, data acquisition and processing for the purpose of entanglement verification was often a more demanding task than running the experiment itself [70]. Focusing first on global and partial entanglement, we obtained full datasets for experimental density matrices corresponding to particularly noisy GHZ and W states of up to four qubits, produced during laboratory test runs [187]. Despite the relatively low fidelity with their ideal target states, we still obtain meaningful quantitative bounds from Eq. (3.81). The results are compactly presented in Table 3.3.

| Global and partial multiparticle entanglement | | | | | |
|---|---|---|---|---|---|
| State | Ref. | Fidelity (%) | $\{\tilde{c}_1, \tilde{c}_2, \tilde{c}_3\}$ | $\sum_{j=1}^{3} \lvert\tilde{c}_j\rvert$ | $E_M^{D_{\mathrm{Tr}}}$ |
| $\varrho_{\mathrm{S}}^{(4)}$ | [71] | $96.83 \pm 0.05$ | $\{0.401 \pm 0.004, 0.362 \pm 0.004, 0.397 \pm 0.008\}$ | $1.16 \pm 0.01$ | $0.040 \pm 0.002$ |
| $\varrho_{\mathrm{D}_3}^{(6)}$ | [74] | $56 \pm 2$ | $\{0.8 \pm 0.2, 0.5 \pm 0.2, -0.3 \pm 0.1\}$ | $1.6 \pm 0.3$ | $0.15 \pm 0.08$ |
| $\varrho_{\mathrm{D}_3}^{(6)}$ | [75] | $65 \pm 2$ | $\{0.63 \pm 0.02, 0.63 \pm 0.02, -0.42 \pm 0.02\}$ | $1.69 \pm 0.04$ | $0.17 \pm 0.01$ |
| $\varrho_{\mathrm{GHZ}}^{(3)}$ | [187] | 87.9 | $\{-0.497, 0.515, -0.341\}$ | 1.35 | 0.102 |
| $\varrho_{\mathrm{GHZ}}^{(4)}$ | [187] | 80.3 | $\{0.663, 0.683, 0.901\}$ | 2.25 | 0.312 |
| $\varrho_{\mathrm{W}_A}^{(4)}$ | [187] | 19.4 | $\{-0.404, 0.454, -0.378\}$ | 1.24 | 0.0589 |
| $\varrho_{\mathrm{W}_B}^{(4)}$ | [187] | 31.4 | $\{0.472, -0.468, -0.446\}$ | 1.39 | 0.0963 |

Table 3.3: Accessible lower bounds to global and partial multiparticle entanglement of some experimentally prepared states, given by Eq. (3.81) and evaluated in particular for the trace distance of entanglement $E^{D_{\mathrm{Tr}}}$ by using Eq. (3.75) for even $N$ and Eq. (3.79) for odd $N$. Following the theoretical analysis of Table 3.2, data obtained by direct measurements of the canonical correlation functions were used to construct bounds for a noisy Smolin state of 4 photons [71], noisy Dicke states of 6 photons [74, 75], and noisy GHZ states of 4 ions [187]. For noisy GHZ states of 3 ions and noisy W states of 4 ions (two implementations labelled as $A$ and $B$) [187], full datasets were used to extract the optimised correlation functions $\{\tilde{c}_j\}$ required for the bounds. For all the presented experimental states (whose fidelities with the ideal target states are reported for reference), we are able to provide a reliable estimate of the multiparticle entanglement $E_M^D$ for any $M > \lceil N/2 \rceil$.

### 3.3.3 Genuine multiparticle entanglement of GHZ-diagonal states

The results from the previous Sections cannot provide useful bounds for the complete hierarchy of multiparticle entanglement, because $\mathcal{M}_N^3$ states are $M$-separable for all $M \leq \lceil N/2 \rceil$, and thus in particular biseparable for any number of qubits $N > 2$.

In this Section we thus resort to a different reference set of states and show how general analytical results for geometric measures of genuine multiparticle entanglement can be obtained as well within our information theoretic approach.

Specifically, we resort to classical mixtures of GHZ states, which incarnates archetypical representatives of full inseparability [54,170]. Any such state $\xi$, which will be referred to as a GHZ-diagonal (in short, $\mathcal{G}_N$) state, can be written as $\xi = \sum_{i,\pm} p_i^{\pm} |\beta_i^{\pm}\rangle\langle\beta_i^{\pm}|$, in terms of

its eigenvalues $p_i^{\pm}$, with the eigenvectors $|\beta_i^{\pm}\rangle = \frac{1}{\sqrt{2}}\left(\mathbb{I}^{\otimes N} \pm \sigma_1^{\otimes N}\right)|i\rangle$ forming the basis of $N$-qubit GHZ states, where $\{|i\rangle\}_{i=1}^{2^N}$ denotes the binary ordered $N$-qubit computational basis. The $\mathcal{G}_N$ states have been studied in recent years as testbeds for multiparticle entanglement detection [54, 171], and specific algebraic measures of genuine multiparticle entanglement such as the $N$-particle concurrence [66, 67] and negativity [63] have been computed for these states.

We now calculate exactly the whole class of geometric measures of genuine multiparticle entanglement $E_2^D$ defined by Eq. (2.24), with respect to any contractive and jointly convex distance $D$, for $\mathcal{G}_N$ states of an arbitrary number $N$ of qubits.

By applying our general framework, we can prove that, for every valid distance $D$, the closest biseparable state to any $\mathcal{G}_N$ state can be found within the subset of biseparable $\mathcal{G}_N$ states. Indeed, it is known that any $N$-qubit state $\varrho$ can be transformed via a single-qubit LOCC $\Gamma$ into a GHZ-diagonal state $\varrho_{\mathrm{GHZ}} := \Gamma(\varrho)$ with eigenvalues given by $p_i^{\pm} = \langle\beta_i^{\pm}|\varrho|\beta_i^{\pm}\rangle$ [63], a procedure referred to as GHZ-diagonalisation of $\varrho$. Consequently, for any GHZ-diagonal state $\xi$ and any 2-separable state $\varsigma$, we have that

$$D(\xi, \varsigma_{\mathrm{GHZ}}) = D(\Gamma(\xi), \Gamma(\varsigma)) \leq D(\xi, \varsigma), \tag{3.92}$$

where in the first equality we use the invariance of any GHZ-diagonal state through $\Gamma$ and that $\Gamma(\varsigma) := \varsigma_{\mathrm{GHZ}}$ is the GHZ-diagonalisation of $\varsigma$, and in the inequality we use the contractivity of the distance through any completely positive trace-preserving channel. Moreover, the GHZ-diagonalisation $\varsigma_{\mathrm{GHZ}}$ of any 2-separable state $\varsigma$ is a 2-separable GHZ-diagonal state since $\Gamma$ is a single-qubit LOCC.

Therefore, the set $\mathcal{S}_2^{\mathcal{G}}$ of 2-separable GHZ-diagonal states turns out to be the relevant one in order to compute exactly any distance-based measure of genuine multiparticle entanglement of a GHZ-diagonal state $\xi$, thus dramatically simplifying the ensuing optimisation as follows:

$$E_2^D(\xi) := \inf_{\varsigma \in \mathcal{S}_2} D(\xi, \varsigma) = \inf_{\varsigma_{\mathrm{GHZ}} \in \mathcal{S}_2^{\mathcal{G}}} D(\xi, \varsigma_{\mathrm{GHZ}}). \tag{3.93}$$

Now, let us consider an arbitrary GHZ-diagonal state $\xi$ and rearrange its GHZ eigenstates $\{|\beta_i\rangle\}_{i=1}^{2^N}$ in such a way that the corresponding eigenvalues $\{p_i\}_{i=1}^{2^N}$ are in non-increasing order. It is well known that $\xi$ is 2-separable if, and only if, $p_1 \leq 1/2$ [54].

For $p_1 > 1/2$, we now show that one of the closest 2-separable GHZ-diagonal states $\varsigma_\xi$ has eigenvalues $\{q_i\}_{i=1}^{2^N}$ such that $q_1 = 1/2$, with $\{q_i\}_{i=1}^{2^N}$ corresponding again to the ordering of GHZ eigenstates $\{|\beta_i\rangle\}_{i=1}^{2^N}$ set by $\xi$, thus further simplifying the optimisation in Eq. (3.93).

Consider any 2-separable GHZ-diagonal state $\varsigma$, it holds that there will always be a 2-separable GHZ-diagonal state $\varsigma'$ with eigenvalues $\{q_i'\}_{i=1}^{2^N}$ and $q_1' = 1/2$ such that

$\varsigma' = \lambda\xi + (1-\lambda)\varsigma$ for some $\lambda \in [0,1]$. Now, for any convex distance, the following holds

$$\begin{aligned} & D(\xi, \varsigma') \\ = \; & D(\xi, \lambda\xi + (1-\lambda)\varsigma) \\ \leq \; & \lambda D(\xi,\xi) + (1-\lambda) D(\xi,\varsigma) \\ = \; & (1-\lambda) D(\xi,\varsigma) \\ \leq \; & D(\xi,\varsigma). \end{aligned} \tag{3.94}$$

This inequality immediately implies that one of the closest 2-separable GHZ-diagonal states $\varsigma_\xi$ to a 2-inseparable GHZ-diagonal state $\xi$ is of the form $\varsigma'$.

**Theorem 3.3.3.** *For any convex and contractive distance $D$ and any fully inseparable GHZ-diagonal state $\xi$, whose GHZ eigenstates $\{|\beta_i\rangle\}_{i=1}^{2^N}$ are arranged such that the corresponding eigenvalues $\{p_i\}_{i=1}^{2^N}$ are in non-increasing order, one of the closest 2-separable states $\varsigma_\xi$ to $\xi$ is itself a GHZ-diagonal state with eigenvalues $\{q_i\}_{i=1}^{2^N}$ such that $q_1 = 1/2$, with $\{q_i\}_{i=1}^{2^N}$ corresponding again to the ordering of GHZ eigenstates $\{|\beta_i\rangle\}_{i=1}^{2^N}$ set by $\xi$.*

We can now apply this Theorem to calculate the geometric genuine multiparticle entanglement $E_2^D(\xi)$ of any GHZ-diagonal state $\xi$ for particular instances of $D$. Since the closest 2-separable state $\varsigma_\xi$ to a GHZ-diagonal state $\xi$ is also a GHZ-diagonal state, they are diagonal in the same basis and their distance reduces to the corresponding classical distance between the probability distributions formed by their eigenvalues, denoted by $P_\xi$ and $P_{\varsigma_\xi}$ respectively. By using the expressions given in Eqs. (3.76) of the classical relative entropy, trace, infidelity, squared Bures, and squared Hellinger distance between two probability distributions $P_\xi$ and $P_{\varsigma_\xi}$, and minimising it over all probability distributions $P_{\varsigma_\xi}$ such that $q_1 = 1/2$, one easily obtains the desired expressions for $E_2^D(\xi)$ of any $\mathcal{G}_N$ state $\xi$ with maximum eigenvalue $p_1$ expressed in the following:

$$E_2^D(\xi^{\{p_i\}}) = \begin{cases} 0\,, & p_1 \leq 1/2; \\ g_D(p_1)\,, & \text{otherwise}, \end{cases} \tag{3.95}$$

where $g_D$ denotes a monotonically increasing function whose explicit form is specific to each distance $D$, as reported in Table 3.4 for typical instances.

Let us comment on some particular results.

The genuine multiparticle trace distance of entanglement $E_2^{D_{\mathrm{Tr}}}$ is found to coincide with the genuine multiparticle negativity [63] and with half the genuine multiparticle concurrence [66] for all $\mathcal{G}_N$ states, thus providing the latter entanglement measures with an insightful geometrical interpretation on this important set of states.

Examples of $\mathcal{G}_N$ states include several resources for quantum information processing, such as the noisy GHZ states and Wei states introduced in the previous section. In particular, for noisy GHZ states (described by a pure-state probability $q$ as detailed in the

| Distance $D$ | $g_D(p_1)$ |
|---|---|
| Relative entropy $D_{\mathrm{RE}}$ | $1 + p_1 \log_2 p_1 + (1-p_1)\log_2(1-p_1)$ |
| Trace $D_{\mathrm{Tr}}$ | $p_1 - \frac{1}{2}$ |
| Infidelity $D_{\mathrm{F}}$ | $\frac{1}{2} - \sqrt{p_1(1-p_1)}$ |
| Squared Bures $D_{\mathrm{B}}$ | $2 - \sqrt{2}\left(\sqrt{1-p_1} + \sqrt{p_1}\right)$ |
| Squared Hellinger $D_{\mathrm{H}}$ | $2 - \sqrt{2}\left(\sqrt{1-p_1} + \sqrt{p_1}\right)$ |

Table 3.4: Analytical expression of genuine multiparticle entanglement $E_2^D$ for GHZ-diagonal states of any number $N$ of qubits as defined by Eq. (3.95), for representative choices of the distance function $D$ introduced in Table 3.1.

previous Section), we recover that every geometric measure of genuine multiparticle entanglement is nonzero if and only if $q > \left(1 + (1-2^N)^{-1}\right)/2 \xrightarrow[N\gg 1]{} 1/2$ [54] and monotonically increasing with $q$, as expected; for $q = 1$ (pure GHZ states), genuine and global entanglement coincide, i.e. the hierarchy of Figure 2.2 collapses, meaning that all the entanglement of $N$-qubit GHZ states is genuinely shared among all the $N$ particles [125].

On the other hand, the relative entropy of genuine multiparticle entanglement of Wei states [182, 183] can be calculated exactly via Eq. (3.95); interestingly, for even $N$ it is found to coincide with the lower bound to their global entanglement that we had obtained by $\mathcal{M}_N^3$-fication, plotted as a solid line in Figure 3.2(b). This means that for these states also the genuine multiparticle entanglement can be quantified entirely by measuring the three canonical correlation functions $\{c_j\}$, for any $N$.

More generally, for arbitrary $\mathcal{G}_N$ states, all the genuine entanglement measures given by Eq. (3.95) can be obtained by measuring the maximum GHZ overlap $p_1$, which requires $N+1$ local measurement settings given explicitly in Ref. [171]. This is remarkable, since with the same experimental effort needed to detect full inseparability [54] we have now a complete quantitative picture of genuine entanglement in these states based on any geometric measure, agreeing with and extending the findings of [63, 66]. Furthermore, as evident from Eq. (3.95), all the geometric measures are monotonic functions of each other: our analysis thus reveals that there is a unique ordering of genuinely entangled $\mathcal{G}_N$ states within the distance-based approach of Fig. 2.2.

### 3.3.4 Genuine multiparticle entanglement bounds of arbitrary $N$-qubit states

In the same spirit as Section 3.3.2, we note that the exact results obtained for the particular reference family of $\mathcal{G}_N$ states provide quantitative lower bounds to the genuine entanglement of general $N$-qubit states. This follows from the fact that GHZ-diagonalisation, which transforms any $N$-qubit state $\varrho$ into a $\mathcal{G}_N$ state with eigenvalues $p_i^{\pm} = \langle \beta_i^{\pm} | \varrho | \beta_i^{\pm} \rangle$,

| Genuine multiparticle entanglement | | | | | | |
|---|---|---|---|---|---|---|
| State | Ref. | Fidelity (%) | $E_2^{D_{\mathrm{RE}}}$ | $E_2^{D_{\mathrm{Tr}}}$ | $E_2^{D_{\mathrm{F}}}$ | $E_2^{D_{\mathrm{B}}}$ |
| $\varrho_{\mathrm{GHZ}}^{(3)}$ | [73] | $97.0 \pm 0.3$ | $0.81 \pm 0.02$ | $0.470 \pm 0.003$ | $0.329 \pm 0.008$ | $0.36 \pm 0.01$ |
| $\varrho_{\mathrm{GHZ}}^{(4)}$ | [73] | $95.7 \pm 0.3$ | $0.74 \pm 0.01$ | $0.457 \pm 0.003$ | $0.297 \pm 0.007$ | $0.323 \pm 0.008$ |
| $\varrho_{\mathrm{GHZ}}^{(5)}$ | [73] | $94.4 \pm 0.5$ | $0.69 \pm 0.02$ | $0.444 \pm 0.005$ | $0.27 \pm 0.01$ | $0.29 \pm 0.01$ |
| $\varrho_{\mathrm{GHZ}}^{(6)}$ | [73] | $89.2 \pm 0.4$ | $0.51 \pm 0.01$ | $0.392 \pm 0.004$ | $0.190 \pm 0.005$ | $0.200 \pm 0.006$ |
| $\varrho_{\mathrm{GHZ}}^{(8)}$ | [73] | $81.7 \pm 0.4$ | $0.313 \pm 0.009$ | $0.317 \pm 0.004$ | $0.113 \pm 0.003$ | $0.117 \pm 0.003$ |
| $\varrho_{\mathrm{GHZ}}^{(10)}$ | [73] | $62.6 \pm 0.6$ | $0.046 \pm 0.004$ | $0.126 \pm 0.006$ | $0.016 \pm 0.002$ | $0.016 \pm 0.002$ |
| $\varrho_{\mathrm{GHZ}}^{(14)}$ | [73] | $50.8 \pm 0.9$ | $0.0002 \pm 0.0004$ | $0.008 \pm 0.009$ | $0.0001 \pm 0.0001$ | $0.0001 \pm 0.0001$ |

Table 3.5: Lower bounds to genuine multiparticle entanglement of experimental noisy GHZ states of up to 14 ions [73], as quantified in terms of all the distance-based entanglement measures $E_2^D$ reported in Table 3.4, obtained by Eq. (3.95) with $p_1$ given in each case by the measured fidelity with the pure reference GHZ state. All the reported entanglement estimates are obtained from the same data needed to witness full inseparability, which for general $N$-qubit states can be accessed by $N+1$ local measurements without the need for a full tomography.

corresponds to local operations and classical comunication [63]. Therefore, given a completely general state $\varrho$, one only needs to measure its overlap with a suitable reference GHZ state; if this overlap is found larger than $1/2$, then by using Eq. (3.95) with $p_1$ equal to the measured overlap one obtains analytical lower bounds to the genuine multiparticle entanglement $E_2^D$ of $\varrho$ with respect to any desired distance $D$. As before, the bounds can be optimised in situations of partial prior knowledge, e.g. by applying local unitaries on each qubit before the GHZ-diagonalisation, which has the effect of maximising the overlap with a chosen particular GHZ vector in the basis $\{|\beta_i^{\pm}\rangle\}$. The bounds then remain accessible for any state $\varrho$ by $N+1$ local measurements [171], with exactly the same demand as for just witnessing entanglement [54].

For instance, for the singlet state $|\Psi^{(4)}\rangle$ [185], which is a relevant resource in a number of quantum protocols including multiuser secret sharing [188–190], one has $p_1 = \langle\beta_3^+|\Psi^{(4)}\rangle\langle\Psi^{(4)}|\beta_3^+\rangle = 2/3 > 1/2$, obtainable by measuring the overlap with the GHZ basis state $|\beta_3^+\rangle = (|0011\rangle + |1100\rangle)/\sqrt{2}$.

Optimised bounds to the genuine multiparticle entanglement of half-excited Dicke states $|\mathrm{D}_{N/2}^{(N)}\rangle$ [180,184], for even $N \geq 4$, can be found as well based on GHZ-diagonalisation, and are expressed by $p_1^{(N)} = \binom{N}{N/2} 2^{1-N}$, meaning that they become looser with increasing $N$ and stay nonzero only up to $N = 8$. In this respect, we note that alternative methods to detect full inseparability of Dicke states for any $N$ are available [53, 74, 75], but quantitative results are lacking in general. Nevertheless, applying our general approach to an alternative reference family more tailored to the Dicke states could yield tighter lower bounds that do not vanish beyond $N = 8$.

Finally, notice that a lower bound to a distance-based measure of genuine multiparticle entanglement, as derived in this section, is automatically also a lower bound to corresponding measures of global and any form of partial entanglement, as evident by looking at the

geometric picture in Figure 2.2. However, for states which are entangled yet not genuinely entangled, the simple bound from the previous section remains instrumental to assess their inseparability with minimum effort. $\mathcal{M}_N^3$ states are themselves instances of such states. In fact, for even $N$, $\mathcal{M}_N^3$ states are also $\mathcal{G}_N$ states, but with $p_1 \leq 1/2$ for $N > 2$.

Regarding now applications to experimental states, the authors of Ref. [73] reported the creation of (noisy) GHZ states of up to $N = 14$ trapped ions. In each of these states, full inseparability was witnessed by measuring precisely the maximum overlap $p_1$ with a reference pure GHZ state, without the need for complete state tomography. Thanks to Eq. (3.95), we can now use the same data to obtain a full quantification of the genuine $N$-particle entanglement of these realistic states, according to any measure $E_2^D$, at no extra cost in terms of experimental or computational resources. The results are in Table 3.5, for all the representative choices of distances enumerated in Table 3.4. Notice that we do not need to assume that the experimentally produced states are in the $\mathcal{G}_N$ set: the obtained results can be still safely regarded as lower bounds.

## 3.4 Quantification of quantum coherence

We will now focus on the quantification of quantum coherence in $N$-qubit systems. For the sake of simplicity, we will hereafter consider the computational basis $\{|0\rangle, |1\rangle\}^{\otimes N}$ as the reference basis.

### 3.4.1 Geometric quantum coherence

In analogy with the previous Section we now exploit Corollary 3.2.4, i.e. the fact that one of the closest incoherent states to any $\mathcal{M}_N^3$ state is itself an $\mathcal{M}_N^3$ state according to any convex and contractive distance, in order to easily evaluate the trace distance-based geometric quantum coherence for any $\mathcal{M}_N^3$ state and any number of qubits $N$.

Specifically, we will prove that, for any $N$ and for any $\mathcal{M}_N^3$ state, the trace distance-based measure of coherence $C^{D_{\mathrm{Tr}}}$ is equivalent up to a constant factor to the $l_1$-norm of coherence $C_{l_1}$. Due to Eq. (1.16), to this aim we just need to show that, according to the trace distance $D_{\mathrm{Tr}}$, one of the closest incoherent states $\delta_\varpi$ to an $\mathcal{M}_N^3$ state $\varpi$ is always its diagonal part $\varpi_{\mathrm{diag}}$.

The trace distance between an $\mathcal{M}_N^3$ state $\varpi$ with correlation functions $\{c_1, c_2, c_3\}$ and one of its closest incoherent states $\delta_\varpi$ in the computational basis, which is itself an $\mathcal{M}_N^3$ state of the form (3.25) with $k = 3$ according to Corollary 3.2.4, is given by

$$D_{\mathrm{Tr}}(\varpi, \delta_\varpi) = \frac{1}{8}(|s+c_1-c_2-c_3|+|s-c_1+c_2-c_3|+|s+c_1+c_2-c_3|+|-s+c_1+c_2+c_3|), \quad (3.96)$$

for any even $N$ and by

$$D_{\mathrm{Tr}}(\varpi, \delta_\varpi) = \frac{1}{2}\sqrt{c_1^2 + c_2^2 + (c_3 - s)^2}, \quad (3.97)$$

for any odd $N$. It is immediate to see that the minimum over $\delta_\varpi$ is attained by $s = c_3$ in both the even and odd $N$ case, i.e. by $\delta_\varpi = \varpi_{\mathrm{diag}}$ as claimed, so that

$$C^{D_{\mathrm{Tr}}}(\varpi) = \frac{1}{2} C_{l_1}(\varpi) = \frac{1}{2} \begin{cases} \max\{|c_1|, |c_2|\}, & N \text{ even}; \\ \sqrt{c_1^2 + c_2^2}, & N \text{ odd}. \end{cases} \tag{3.98}$$

Notice, however, that the equivalence between $C_{l_1}$ and $C^{D_{\mathrm{Tr}}}$ does not extend to general $N$-qubit states [135].

Interestingly, and again in analogy with the previous Section, the above analytical result is useful not only for $\mathcal{M}_N^3$ states but also for general $N$-qubit states. Corollary 3.2.2 indeed tells us that the $\mathcal{M}_N^3$ state $\varpi^{\{c_j\}}$ with given correlation functions $\{c_j\}$ is extremal among all quantum states with the same correlation functions, in the sense that

$$C^D(\varpi^{\{c_j\}}) \leq C^D(\varrho)\,, \ \forall\, \varrho : \mathrm{Tr}\big(\varrho\, \sigma_j^{\otimes N}\big) = c_j \ (j = 1, 2, 3). \tag{3.99}$$

This immediately implies that the quantum coherence $C^D$ of $\varrho$ has an exact lower bound provided by the quantum coherence of the $\mathcal{M}_N^3$ state $\varpi$ with the same $\{c_j\}$. Moreover, when considering in particular the trace distance-based quantifier, this exact lower bound can be accessed by measuring just two local settings, i.e. $c_1 = \langle \sigma_1^{\otimes N} \rangle$ and $c_2 = \langle \sigma_2^{\otimes N} \rangle$. However, as we have already pointed out, contrary to the entanglement case, such lower bound cannot be ameliorated by adjusting the local measurement basis, since quantum coherence is not invariant under local unitaries.

Quite remarkably, when restricting to a particular subset of $N$-even $\mathcal{M}_N^3$ states $\varpi$, which is defined by the following constraint[1]

$$c_2 = (-1)^{N/2} c_1 c_3, \tag{3.100}$$

it happens that one of the closest incoherent states is always the diagonal part $\varpi_{diag}$ according to any contractive and convex distance $D$. To prove this claim we adopt our usual information theoretic tools, as detailed in the following two results.

**Theorem 3.4.1.** *For all even $N$, any contractive distance satisfies the following translational invariance properties within the space of $N$-qubit $\mathcal{M}_N^3$ states:*

$$D(\{c_1, (-1)^{N/2} c_1 c_3, c_3\}, \{c_1, 0, 0\}) = D(\{0, 0, c_3\}, \{0, 0, 0\}) \tag{3.101}$$

*and*

$$D(\{c_1, (-1)^{N/2} c_1 c_3, c_3\}, \{0, 0, c_3\}) = D(\{c_1, 0, 0\}, \{0, 0, 0\}) \tag{3.102}$$

*for all $c_1$ and $c_3$, where $\{c_1, (-1)^{N/2} c_1 c_3, c_3\}$ denotes an $\mathcal{M}_N^3$ state in Eq. (3.1) with $c_2 = (-1)^{N/2} c_1 c_3$.*

*Proof.* Let us start by proving Eq. (3.101). First of all, by considering the channel $\Lambda_1^{F_3 \otimes N}$ representing the local independent phase flip noise expressed by Eq. (1.14), when $\Xi = F_3$

[1] Analogous results can be obtained by restricting to the other two subsets of $N$-even $\mathcal{M}_N^3$ states defined by, respectively, $c_1 = (-1)^{N/2} c_2 c_3$ and $c_3 = (-1)^{N/2} c_1 c_2$.

and $q = 1$ (i.e. $t \to \infty$), we have the following inequality

$$\begin{aligned} & D(\{0,0,c_3\},\{0,0,0\}) \\ = \; & D(\Lambda_1^{F_3\otimes N}(\{c_1,(-1)^{N/2}c_1c_3,c_3\}),\Lambda_1^{F_3\otimes N}(\{c_1,0,0\})) \\ \leq \; & D(\{c_1,(-1)^{N/2}c_1c_3,c_3\},\{c_1,0,0\}), \end{aligned} \tag{3.103}$$

where the inequality is due to the contractivity of the distance $D$, while the equality is due to the fact that:

$$\{0,0,c_3\} = \Lambda_1^{F_3\otimes N}(\{c_1,(-1)^{N/2}c_1c_3,c_3\}), \tag{3.104}$$

$$\{0,0,0\} = \Lambda_1^{F_3\otimes N}(\{c_1,0,0\}). \tag{3.105}$$

In order to prove the opposite inequality and thus Eq. (3.101), we now introduce an $N$-qubit global *rephasing* channel $\Lambda_r^{R_3}$ which is defined in the operator-sum representation as

$$\Lambda_r^{R_3}(\rho) = \sum_{i,\pm} K_{i,\pm}^{R_3}\rho K_{i,\pm}^{R_3\,\dagger}\,, \tag{3.106}$$

with

$$
\begin{aligned}
K^{R_3}_{1,\pm} &= \sqrt{\frac{1\pm r}{2}}|\beta^{\pm}_1\rangle\langle 000\ldots000|, \qquad (3.107)\\
K^{R_3}_{2,\pm} &= \sqrt{\frac{1\pm r}{2}}|\beta^{\pm}_2\rangle\langle 000\ldots001|,\\
K^{R_3}_{3,\pm} &= \sqrt{\frac{1\pm r}{2}}|\beta^{\pm}_3\rangle\langle 000\ldots010|,\\
K^{R_3}_{4,\pm} &= \sqrt{\frac{1\pm r}{2}}|\beta^{\pm}_4\rangle\langle 000\ldots011|,\\
&\cdots\\
K^{R_3}_{2^{N-1}-1,\pm} &= \sqrt{\frac{1\pm r}{2}}|\beta^{\pm}_{2^{N-1}-1}\rangle\langle 011\ldots110|,\\
K^{R_3}_{2^{N-1},\pm} &= \sqrt{\frac{1\pm r}{2}}|\beta^{\pm}_{2^{N-1}}\rangle\langle 011\ldots111|,\\
K^{R_3}_{2^{N-1}+1,\pm} &= \sqrt{\frac{1\pm r}{2}}|\beta^{\pm}_{2^{N-1}}\rangle\langle 100\ldots000|,\\
K^{R_3}_{2^{N-1}+2,\pm} &= \sqrt{\frac{1\pm r}{2}}|\beta^{\pm}_{2^{N-1}-1}\rangle\langle 100\ldots001|,\\
&\cdots\\
K^{R_3}_{2^{N}-3,\pm} &= \sqrt{\frac{1\pm r}{2}}|\beta^{\pm}_4\rangle\langle 111\ldots100|,\\
K^{R_3}_{2^{N}-2,\pm} &= \sqrt{\frac{1\pm r}{2}}|\beta^{\pm}_3\rangle\langle 111\ldots101|,\\
K^{R_3}_{2^{N}-1,\pm} &= \sqrt{\frac{1\pm r}{2}}|\beta^{\pm}_2\rangle\langle 111\ldots110|,\\
K^{R_3}_{2^{N},\pm} &= \sqrt{\frac{1\pm r}{2}}|\beta^{\pm}_1\rangle\langle 111\ldots111|,
\end{aligned}
$$

where $r \in [0,1]$ is a parameter denoting the rephasing strength, $\{|\beta^{\pm}_i\rangle\}$ is the $N$-qubit GHZ basis defined in Eq. (3.2), and the $2^{N+1}$ Kraus operators satisfy $\sum_{i,\pm} {K^{R_3}_{i,\pm}}^{\dagger} K^{R_3}_{i,\pm} = \mathbb{I}^{\otimes N}$, thus ensuring that $\Lambda^{R_3}_r$ is a CPTP map.

It is now essential to see that the effect of $\Lambda^{R_3}_r$ on an $\mathcal{M}^3_N$ state of the form $\{0,0,c_3\}$ is given by

$$\Lambda^{R_3}_r(\{0,0,c_3\}) = \{r, (-1)^{N/2} r\ c_3, c_3\}, \qquad (3.108)$$

for any even $N$. To prove Eq. (3.108), we need Eq.(3.63), implying that

$$\begin{aligned}\{0,0,c_3\} &= \frac{1}{2^N}(1+c_3)\sum_i |\Phi_i^+\rangle\langle\Phi_i^+| \\ &+ \frac{1}{2^N}(1+c_3)\sum_i |\Phi_i^-\rangle\langle\Phi_i^-| \\ &+ \frac{1}{2^N}(1-c_3)\sum_i |\Psi_i^+\rangle\langle\Psi_i^+| \\ &+ \frac{1}{2^N}(1-c_3)\sum_i |\Psi_i^-\rangle\langle\Psi_i^-|,\end{aligned} \tag{3.109}$$

and

$$\begin{aligned}\{r,(-1)^{N/2}r\ c_3,c_3\} &= \frac{1}{2^N}(1+r)(1+c_3)\sum_i |\Phi_i^+\rangle\langle\Phi_i^+| \\ &+ \frac{1}{2^N}(1-r)(1+c_3)\sum_i |\Phi_i^-\rangle\langle\Phi_i^-| \\ &+ \frac{1}{2^N}(1+r)(1-c_3)\sum_i |\Psi_i^+\rangle\langle\Psi_i^+| \\ &+ \frac{1}{2^N}(1-r)(1-c_3)\sum_i |\Psi_i^-\rangle\langle\Psi_i^-|.\end{aligned} \tag{3.110}$$

By exploiting the following equalities

$$\begin{aligned}\Lambda_r^{R_3}(|\Phi_i^+\rangle\langle\Phi_i^+|) &= \frac{1+r}{2}|\Phi_i^+\rangle\langle\Phi_i^+| + \frac{1-r}{2}|\Phi_i^-\rangle\langle\Phi_i^-|, \\ \Lambda_r^{R_3}(|\Phi_i^-\rangle\langle\Phi_i^-|) &= \frac{1+r}{2}|\Phi_i^+\rangle\langle\Phi_i^+| + \frac{1-r}{2}|\Phi_i^-\rangle\langle\Phi_i^-|, \\ \Lambda_r^{R_3}(|\Psi_i^+\rangle\langle\Psi_i^+|) &= \frac{1+r}{2}|\Psi_i^+\rangle\langle\Psi_i^+| + \frac{1-r}{2}|\Psi_i^-\rangle\langle\Psi_i^-|, \\ \Lambda_r^{R_3}(|\Psi_i^-\rangle\langle\Psi_i^-|) &= \frac{1+r}{2}|\Psi_i^+\rangle\langle\Psi_i^+| + \frac{1-r}{2}|\Psi_i^-\rangle\langle\Psi_i^-|,\end{aligned} \tag{3.111}$$

and the linearity of the global rephasing channel, we get

$$\begin{aligned}\Lambda_r^{R_3}(\{0,0,c_3\}) &= \frac{1}{2^N}(1+c_3)\sum_i \Lambda_r^{R_3}(|\Phi_i^+\rangle\langle\Phi_i^+|) \\ &+ \frac{1}{2^N}(1+c_3)\sum_i \Lambda_r^{R_3}(|\Phi_i^-\rangle\langle\Phi_i^-|) \\ &+ \frac{1}{2^N}(1-c_3)\sum_i \Lambda_r^{R_3}(|\Psi_i^+\rangle\langle\Psi_i^+|) \\ &+ \frac{1}{2^N}(1-c_3)\sum_i \Lambda_r^{R_3}(|\Psi_i^-\rangle\langle\Psi_i^-|) \\ &= \{r,(-1)^{N/2}r\ c_3,c_3\}. \end{aligned} \tag{3.112}$$

We then have the inequality

$$\begin{aligned} &D(\{c_1,(-1)^{N/2}c_1c_3,c_3\},\{c_1,0,0\}) \\ &= D(\Lambda_{c_1}^{R_3}\{0,0,c_3\},\Lambda_{c_1}^{R_3}\{0,0,0\}) \\ &\leq D(\{0,0,c_3\},\{0,0,0\}), \end{aligned} \tag{3.113}$$

where the inequality is again due to the contractivity of the distance $D$, while the equality is due to the fact that

$$\begin{aligned}\{c_1,(-1)^{N/2}c_1c_3,c_3\} &= \Lambda_{c_1}^{R_3}\{0,0,c_3\}, \\ \{c_1,0,0\} &= \Lambda_{c_1}^{R_3}\{0,0,0\}.\end{aligned}$$

By putting together the two inequalities (3.103) and (3.113), we immediately get the invariance of Eq. (3.101) for any contractive distance.

In order now to prove Eq. (3.102), we introduce the local unitary $V^{\otimes N}$ with $V = \frac{1}{\sqrt{2}}(\mathbb{I}+i\sigma_2)$. The effect of $V^{\otimes N}$ on a general $\mathcal{M}_N^3$ state is given by

$$V^{\otimes N}\{c_1,c_2,c_3\}V^{\otimes N\dagger} = \{c_3,c_2,c_1\}, \tag{3.114}$$

where this can be easily seen by utilising the fact that $N$ is even and the following single-qubit identities:

$$\begin{aligned}V\sigma_1V^\dagger &= \sigma_3, \\ V\sigma_2V^\dagger &= \sigma_2, \\ V\sigma_3V^\dagger &= -\sigma_1.\end{aligned}$$

Thanks to the invariance under unitaries of any contractive distance $D$, the effect of the unitary $V^{\otimes N}$ expressed by Eq. (3.114), and the just proven invariance expressed by

Eq. (3.101), we eventually have

$$\begin{aligned} & D(\{c_1,(-1)^{N/2}c_1c_3,c_3\},\{0,0,c_3\}) \\ = \; & D(V^{\otimes N}\{c_1,(-1)^{N/2}c_1c_3,c_3\}V^{\otimes N\dagger},V^{\otimes N}\{0,0,c_3\}V^{\otimes N\dagger}) \\ = \; & D(\{c_3,(-1)^{N/2}c_1c_3,c_1\},\{c_3,0,0\}) \\ = \; & D(\{0,0,c_1\},\{0,0,0\}) \\ = \; & D(V^{\otimes N}\{0,0,c_1\}V^{\otimes N\dagger},V^{\otimes N}\{0,0,0\}V^{\otimes N\dagger}) \\ = \; & D(\{c_1,0,0\},\{0,0,0\}), \end{aligned} \tag{3.115}$$

that is Eq. (3.102).

■

**Theorem 3.4.2.** *For all even $N$, according to any contractive distance $D$, it holds that one of the closest incoherent $\mathcal{M}_N^3$ states $\delta$ with triple $\{0,0,s\}$ to an $\mathcal{M}_N^3$ state $\varpi$ with triple $\{c_1,(-1)^{N/2}c_1c_3,c_3\}$ is specified by $s=c_3$.*

*Proof.* We need to prove that, for any $z$, it holds that

$$\begin{aligned} & D(\{c_1,(-1)^{N/2}c_1c_3,c_3\},\{0,0,c_3\}) \\ \leq \; & D(\{c_1,(-1)^{N/2}c_1c_3,c_3\},\{0,0,c_3+z\}). \end{aligned} \tag{3.116}$$

In fact

$$\begin{aligned} & D(\{c_1,(-1)^{N/2}c_1c_3,c_3\},\{0,0,c_3\}) \\ = \; & D(\{c_1,0,0\},\{0,0,0\}) \\ = \; & D(\Lambda_1^{F_1\otimes N}(\{c_1,(-1)^{N/2}c_1c_3,c_3\}),\Lambda_1^{F_1\otimes N}(\{0,0,c_3+z\})) \\ \leq \; & D(\{c_1,(-1)^{N/2}c_1c_3,c_3\},\{0,0,c_3+z\}), \end{aligned}$$

where the first equality is due to Theorem 3.4.1, which holds for any contractive distance $D$ and any even $N$, the second equality is due to the fact that

$$\{c_1,0,0\} = \Lambda_1^{F_1\otimes N}(\{c_1,(-1)^{N/2}c_1c_3,c_3\}), \tag{3.117}$$

$$\{0,0,0\} = \Lambda_1^{F_1\otimes N}(\{0,0,c_3+z\}), \tag{3.118}$$

with $\Lambda_1^{F_1\otimes N}$ representing the action of $N$ local independent bit flip noisy channels expressed by Eq. (1.14), when $\Xi=F_1$ and $q=1$ (i.e., $t\to\infty$), and finally the inequality is due to contractivity of the distance $D$.

■

This universal behaviour with respect to any convex and contractive distance $D$ on the restricted class of $\mathcal{M}_N^3$ states with $c_2=(-1)^{N/2}c_1c_3$ will turn out to be pivotal in the

analysis of the universal freezing phenomenon of quantum coherence that will be addressed in the following Chapter.

Moreover, it is worthwhile to note that we have introduced an intriguing global rephasing channel, which is able to reverse the effects of decoherence for certain even $N$ $\mathcal{M}_N^3$ states. This physical CPTP channel may be of interest for applications other than proving the universality of the freezing phenomenon, for example quantum error correction [144], where it is desirable to combat the effects of noise, typically manifesting via local bit flip, phase flip, or bit-phase flip channels. For suitable $\mathcal{M}_N^3$ states, all these errors can be corrected by global maps such as the one in Eq. (3.106). The further characterisation and experimental implementation of our global rephasing map for quantum information processing calls for an independent analysis.

### 3.4.2 Robustness of coherence

In this Section we introduce the *robustness of coherence*, which quantifies the minimal mixing required to destroy all the coherence in a quantum state. This definition is inspired by similar concepts previously investigated for entanglement, steering-type correlations, non-locality and other resources [124, 191–194]. Although apparently the robustness of a resource does not arise from an information geometric framework, we see that it plays a crucial role in the quest for experimentally friendly and operationally meaningful quantification of quantum coherence, which is one of the main objectives set by this Thesis.

Indeed, we prove not only that such a measure is a fully bona fide quantifier (computable exactly in relevant cases and numerically in general via a simple semidefinite program) in all possible resource theories of coherence, but also that it is observable, as it can be recast as the expectation value of a witness operator for any quantum state. This makes it very appealing for experimental investigations, e.g. in condensed matter and biological contexts [35, 195, 196]. Even more, we then show that the measure admits a direct operational interpretation: it quantifies the advantage enabled by a quantum state, compared to any incoherent state, in a phase discrimination task. We further mention that it is possible to generalise these results to the case of asymmetry, although details about this generalisation, as well as the proofs of most of the results that we will show in the following, are deferred to Ref. [5].

Let $\mathcal{D}(\mathcal{H})$ be the convex set of density operators acting on a $d$-dimensional Hilbert space $\mathcal{H}$, and let $\mathcal{I} \subset \mathcal{D}(\mathcal{H})$ be the subset of incoherent states. We define the robustness of coherence (RoC) of a quantum state $\rho \in \mathcal{D}(\mathcal{H})$ as

$$C_{\mathcal{R}}(\rho) = \min_{\tau \in \mathcal{D}(\mathcal{H})} \left\{ s \geq 0 \;\middle|\; \frac{\rho + s\,\tau}{1+s} =: \delta \in \mathcal{I} \right\}, \tag{3.119}$$

that is, the minimum weight of another state $\tau$ such that its convex mixture with $\rho$ yields an incoherent state $\delta$. The concept is illustrated in Fig. 3.3 for a qubit ($d = 2$). If we denote by $\tau^\star$ and $\delta^\star$ the states achieving the minimum in (3.119), then

$$\rho = \big(1 + C_{\mathcal{R}}(\rho)\big)\delta^\star - C_{\mathcal{R}}(\rho)\tau^\star, \tag{3.120}$$

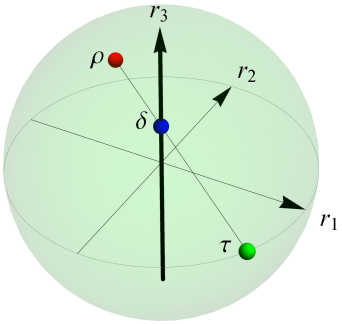


Figure 3.3: Robustness of coherence $C_{\mathcal{R}}(\rho)$ for a single qubit state $\rho = \frac{1}{2}(\mathbb{I} + \vec{r}\cdot\vec{\sigma})$, where $\vec{r}$ is the Bloch vector and $\vec{\sigma}$ is the vector of Pauli matrices. Incoherent states span the thick vertical $r_3$ axis. The optimisation in Eq. (3.119) is fulfilled by an equatorial pure state $\tau^\star$ as depicted, resulting in $C_{\mathcal{R}}(\rho) = (r_1^2 + r_2^2)^{\frac{1}{2}} = 2|\rho_{01}|$.

is said to realise an optimal pseudomixture for $\rho$. Notice that it is necessary in Eq. (3.119) to let $\tau$ be an arbitrary state: if one restricted $\tau$ to be incoherent, then the minimum $s$ would diverge for any state $\rho$ with nonzero coherence, henceforth resulting totally uninformative. This contrasts with the case of entanglement, for which the original robustness was defined in terms of pseudomixtures with separable states [191], and only later extended to pseudomixtures with arbitrary states [192].

We now prove that the RoC is a bona fide measure of coherence. First of all, it is seen by definition that

$$C_{\mathcal{R}}(\rho) \geq 0 \quad \text{and} \quad C_{\mathcal{R}}(\rho) = 0 \iff \rho \in \mathcal{I}\,. \tag{3.121}$$

Second, the RoC is convex. The proof mirrors the one for the robustness of entanglement [191]. Let $\rho_1$ and $\rho_2$ be two states, and write for each the optimal pseudomixture

$$\rho_k = \big(1 + C_{\mathcal{R}}(\rho_k)\big)\delta_k^\star - C_{\mathcal{R}}(\rho_k)\tau_k^\star \qquad (k = 1, 2). \tag{3.122}$$

Taking the convex combination $\rho = p\rho_1 + (1-p)\rho_2$ with $0 \leq p \leq 1$, notice that a pseudomixture $\rho = (1+s)\delta - s\tau$ can be written, with

$$\begin{aligned}
\delta &= \frac{1}{1+s}\big[p\big(1 + C_{\mathcal{R}}(\rho_1)\big)\delta_1^\star + (1-p)\big(1 + C_{\mathcal{R}}(\rho_2)\big)\delta_2^\star\big] \in \mathcal{I}, && (3.123)\\
\tau &= \frac{1}{s}\big[pC_{\mathcal{R}}(\rho_1)\tau_1^\star + (1-p)C_{\mathcal{R}}(\rho_2)\tau_2^\star\big], && (3.124)\\
s &= pC_{\mathcal{R}}(\rho_1) + (1-p)C_{\mathcal{R}}(\rho_2). && (3.125)
\end{aligned}$$

By definition, $C_{\mathcal{R}}(\rho) \leq s$, which proves convexity,

$$C_{\mathcal{R}}\big(p\rho_1 + (1-p)\rho_2\big) \leq pC_{\mathcal{R}}(\rho_1) + (1-p)C_{\mathcal{R}}(\rho_2)\,. \tag{3.126}$$

Third, and most importantly, the RoC is nonincreasing under all the sets of operations used in resource theories of coherence. We prove in fact a general form of monotonicity under incoherence preserving (sub)channels. Let $\{\Gamma_l\}_{l=1}^m$ be an instrument, i.e., a set of

$m$ (sub)channels (completely positive maps whose sum $\sum_{l=1}^{m}\Gamma_l(\rho) =: \Lambda(\rho)$ defines a trace preserving channel $\Lambda$), mapping any incoherent state $\delta \in \mathcal{I}$ into another (un)normalised incoherent state $\Gamma_l(\delta)$. For any $\rho$, we have then

$$C_{\mathcal{R}}(\rho) \geq \sum_{l=1}^{m} p_l \; C_{\mathcal{R}}\left(\rho_l\right) \; , \tag{3.127}$$

where $p_l = \mathrm{Tr}[\Gamma_l(\rho)]$ and $\rho_l = \Gamma_l(\rho)/p_l$. The proof is the following. Take the optimal pseudomixture for $\rho$ given by Eq. (3.120) and apply the (sub)channel $\Gamma_l$ to both sides,

$$\Gamma_l(\rho) = \big(1 + C_{\mathcal{R}}(\rho)\big)\Gamma_l(\delta^\star) - C_{\mathcal{R}}(\rho)\Gamma_l(\tau^\star). \tag{3.128}$$

By defining:

$$\begin{aligned} \sigma_l &= \frac{1}{(1+t)}\frac{1}{p_l}\left(1 + C_{\mathcal{R}}\left(\rho\right)\right)\Gamma_l(\delta^\star) \in \mathcal{I}, \\ \tau_l &= \frac{1}{t}\frac{1}{p_l} C_{\mathcal{R}}\left(\rho\right)\Gamma_l(\tau^\star), \\ t &= \frac{1}{p_l} C_{\mathcal{R}}\left(\rho\right)\mathrm{Tr}\left[\Gamma_l(\tau^\star)\right], \end{aligned} \tag{3.129}$$

we immediately obtain $\rho_l = (1+t)\,\sigma_l - t\tau_l$. Since the latter pseudo-mixture is not necessarily optimal, we readily get $C_{\mathcal{R}}\left(\rho_l\right) \leq t$, i.e.

$$C_{\mathcal{R}}\left(\rho_l\right) \leq C_{\mathcal{R}}(\rho)\frac{1}{p_l}\mathrm{Tr}[\Gamma_l(\tau^\star)]. \tag{3.130}$$

Then,

$$\sum_l p_l C_{\mathcal{R}}\left(\rho_l\right) \leq \sum_l p_l C_{\mathcal{R}}(\rho)\frac{1}{p_l}\mathrm{Tr}[\Gamma_l(\tau^\star)] = C_{\mathcal{R}}(\rho)\sum_l \mathrm{Tr}[\Gamma_l(\tau^\star)] = C_{\mathcal{R}}(\rho), \tag{3.131}$$

concluding the proof.

In the case $m = 1$, Eq. (3.127) proves that the RoC cannot increase, on average, under the maximal set of incoherence preserving operations. For $m \geq 1$, if one identifies each $\Gamma_l$ with a Kraus operator $K_l$ (obeying $\sum_{l=1}^{m} {K_l}^\dagger K_l = \mathbb{I}$), then Eq. (3.127) proves monotonicity of the RoC under selective incoherent operations. Overall, Eq. (3.127) establishes the RoC as a *full monotone* with respect to *all* possible formulations of the theory of coherence.

We now show that the RoC has also desirable properties of computability and accessibility. Inspired by entanglement witnesses [19, 69], which are very useful tools to detect inseparability in laboratory [53], we introduce the notion of *coherence witnesses*. A Hermitian operator $W$ satisfies $W_{diag} \geq 0$ if and only if $\mathrm{Tr}[W\delta] = \mathrm{Tr}[W_{diag}\delta] \geq 0$ for all incoherent states $\delta \in \mathcal{I}$; we call any such observable $W$ a coherence witness, because finding $\mathrm{Tr}[W\rho] < 0$ reveals coherence in the state $\rho$.[2] We find that the expectation value

[2] A coherence witness $W$ could also be defined by $W_{diag} = 0$, but relaxing the latter to $W_{diag} \geq 0$ is experimentally friendlier, and sets the scene for a practical verification of coherence.

of any witness $W$, obeying the further constraint $W \leq \mathbb{I}$, provides a quantitative lower bound to the RoC [5],

$$\max\{0, -\mathrm{Tr}[W\rho]\} \leq C_{\mathcal{R}}(\rho)\,, \qquad \forall\ W \text{ such that} \tag{3.132}$$

$$W_{diag} \geq 0 \text{ and } W \leq \mathbb{I}\,. \tag{3.133}$$

Importantly, given any state $\rho$, there always exists an optimal witness $W^{\star}$, characterised in particular by $W^{\star}_{diag} = 0$, which saturates inequality (3.132). In other words, the RoC is an *observable* quantity, given by the expectation value of a suitable (state-dependent) witness operator for any quantum state $\rho$. Finding such an optimal witness, hence determining $C_{\mathcal{R}}(\rho)$ as defined in (3.119), can be then recast [5] as a simple semidefinite program [197] (significantly more efficient than the convex optimisation one for the robustness of entanglement [198]):

$$\text{maximise} \quad -\mathrm{Tr}[W\rho] \quad \text{subject to} \quad \text{Eq. (3.133)}\,. \tag{3.134}$$

The MATLAB [199] code that makes use of the free CVX package [200, 201] to evaluate the RoC can be found in the Supplemental Material of [4].

These results reveal that one can readily estimate the RoC from below in laboratory, by measuring any observable $W$ obeying the constraints in (3.133), with no need for full tomography of the state $\rho$. This may be particularly valuable for witnessing coherence effects in biological domains, e.g. energy transport phenomena in light-harvesting systems [35, 43, 195, 196].

However, given a state $\rho$, the lower bound of Eq. (3.132) can vanish for non-optimised choices of $W$. Typically, one needs some knowledge on the form of $\rho$ to determine the optimal witness $W^{\star}$; a similar issue is encountered in entanglement detection [53]. Nonetheless Eqs. (3.132) and (3.133) imply that, for any set of observables $\{O_i\}$, $i = 1, \ldots, k$, experimentally measured with expectation values $o_i = \mathrm{Tr}[O_i\rho]$, and not necessarily tailored to the measurement of RoC, one can consider coherence witnesses of the form $W = \sum_{i=1}^{k} c_i O_i + m\mathbb{I}$, for $c_1, \ldots, c_k, m \in \mathbb{R}$, and obtain a lower bound to the RoC by the SDP [5] (code available [4])

$$\begin{aligned} &\text{maximise} \quad -\big(\textstyle\sum_{i=1}^{k} c_i o_i + m\big) \\ &\text{subject to} \quad \big(\textstyle\sum_{i=1}^{k} c_i O_i + m\mathbb{I}\big)_{diag} \geq 0, \quad \textstyle\sum_{i=1}^{k} c_i O_i + m\mathbb{I} \leq \mathbb{I}. \end{aligned}$$

One can even make potentially better use of available experimental data, by exactly estimating the minimal RoC compatible with the data; this can also be cast as an SDP [4, 5].

Accessible *faithful* lower bounds to the RoC can be given too, noting that $W_2 = (\rho_{diag} - \rho)/\|\rho_{diag}\|_{\infty}$ obeys (3.133), so that

$$C_{\mathcal{R}}(\rho) \geq \frac{\|\rho - \rho_{diag}\|_2^2}{\|\rho_{diag}\|_{\infty}} \geq \frac{\|\rho - \rho_{diag}\|_2^2}{\|\rho_{diag}\|_2} \geq \|\rho - \rho_{diag}]\|_2^2, \tag{3.135}$$

since $\mathrm{Tr}[(\rho_{diag} - \rho)\rho] = \mathrm{Tr}[(\rho_{diag})^2] - \mathrm{Tr}[\rho^2] = \|\rho - \rho_{diag}\|_2^2$. Here, $\|\cdot\|_2$ is the 2-norm, and $\|\cdot\|_{\infty}$ is the operator norm. The quantity on the rightmost-hand side of (3.135) is:

(i) nonzero on all but incoherent states; (ii) itself a monotone under genuinely incoherent operations [138], but not under the larger sets of incoherent operations [135]; (iii) accessible via the measurement of the purities $\mathrm{Tr}[\rho^2]$ and $\mathrm{Tr}[(\rho_{diag})^2]$ (notably, the same holds for the tighter second-to-last bound in (3.135)). The latter two quantities can be measured directly on two copies of the state $\rho$ (assumed unknown), as $\mathrm{Tr}[\rho^{\otimes 2}V]$ and $\mathrm{Tr}[\rho^{\otimes 2}V_{diag}]$, respectively, with $V$ being the swap operator [202, 203], defined by its action $V|\psi\rangle|\phi\rangle = |\phi\rangle|\psi\rangle$, for all $|\psi\rangle, |\phi\rangle \in \mathcal{H}$, and $V_{diag}$ being the diagonal part of $V$ in the two-qudit computational basis.

We now show that an *analytical* evaluation of the RoC can be obtained for a relevant class of $d$-dimensional states. Let $\rho \in \mathcal{D}(\mathcal{H})$ be a state for which there exists a unitary $U = \sum_j \mathrm{e}^{\mathrm{i}\phi_j}|j\rangle\langle j|$, belonging to the set of genuinely incoherent operations [138], such that $(U\rho U^\dagger)_{kl} = |\rho_{kl}|$. One has then [5]

$$C_{\mathcal{R}}(\rho) = C_{l_1}(\rho), \tag{3.136}$$

where $C_{l_1}(\rho)$ is the $l_1$-norm of coherence. The class of states for which this equality holds includes, for instance, all one-qubit states ($d = 2$, see Fig. 3.3), all $d$-dimensional states with X-shaped density matrix [66](which contain in particular Bell diagonal states of two qubits), and all pure states $|\psi\rangle \in \mathcal{H}$. For the latter, writing in general $|\psi\rangle = \sum_{j=0}^{d-1}\psi_j|j\rangle$, we get explicitly [135]

$$C_{\mathcal{R}}(|\psi\rangle\langle\psi|) = C_{l_1}(|\psi\rangle\langle\psi|) = \big(\sum_j |\psi_j|\big)^2 - 1. \tag{3.137}$$

In particular, maximally coherent states $|\psi^+\rangle$, characterised by $|\psi_j| = \frac{1}{\sqrt{d}}\ \forall j = 0, \ldots, d-1$, have

$$C_{\mathcal{R}}(|\psi^+\rangle\langle\psi^+|) = C_{l_1}(|\psi^+\rangle\langle\psi^+|) = d - 1, \tag{3.138}$$

that is the maximum possible value for the RoC of any $d$-dimensional state. One can show [5] in fact that these are the only states which can reach maximal RoC, which positively settles another requirement recently advocated for bona fide measures of coherence [204].

The equivalence between RoC and $l_1$-norm of coherence breaks down already in dimension $d = 3$. One can prove however the existence of general upper and lower bounds [5],

$$\frac{1}{d-1}C_{l_1}(\rho) \leq C_{\mathcal{R}}(\rho) \leq C_{l_1}(\rho)\,, \quad \forall\ \rho \in \mathcal{D}(\mathcal{H})\,. \tag{3.139}$$

Both bounds can be tight. Examples of states saturating the upper bound have been provided already (for instance, all pure states). A family of states saturating the lower bound is instead given by

$$\rho_p = (1+p)\mathbb{I}/d - p\,|\psi^+\rangle\langle\psi^+|\,, \quad 0 \leq p \leq \frac{1}{d-1}, \tag{3.140}$$

for which $C_{l_1}(\rho_p) = p(d-1)$ and $C_{\mathcal{R}}(\rho_p) = p$. Nonetheless, the lower bound becomes looser for large values of $C_{l_1}$, and one finds $C_{\mathcal{R}}(\rho) \to d-1$ for all $\rho$ such that $C_{l_1}(\rho) \to d-1$ [5].

We are finally ready to provide a direct operational interpretation for the RoC in a metrology context. Consider the following *phase discrimination* (PD) game. Alice prepares a quantum state $\rho \in \mathcal{D}(\mathcal{H})$, which then enters a black box. The black box encodes a phase on $\rho$ by implementing a unitary $U_\phi = \exp(\mathrm{i}N\phi)$, with $N = \sum_{j=0}^{d-1} j\,|j\rangle\langle j|$ and $\phi \in \mathbb{R}$, so that the output state is determined by the action of the unitary channel $\mathcal{U}_\phi(\rho) := U_\phi \rho U_\phi^\dagger$. We can think of $N$ as a Hamiltonian for the system with equispaced spectrum, assuming unit spacing without loss of generality. In this way, the reference basis $\{|j\rangle\}$, with respect to which coherence is defined and measured, is physically identified by the choice of the Hamiltonian. Suppose one of $m$ phases $\{\phi_k\}_{k=0}^{m-1}$ can be applied, each with a prior probability $p_k$. Any collection of pairs $\{(p_k, \phi_k)\}_{k=0}^{m-1} =: \Theta$ defines a PD game, where Alice's goal is that of guessing correctly the phase that was actually imprinted on the state. To this end, she performs a generalised measurement with elements $\{M_k\}$ (satisfying $M_k \geq 0$, $\sum_k M_k = \mathbb{I}$) on the output state $\mathcal{U}_\phi(\rho)$ after the black box. Optimising over all measurements, the maximal probability of success depends on the game $\Theta$ and the input state $\rho$, and is given by

$$p_\Theta^{\mathrm{succ}}(\rho) = \max_{\{M_k\}} \sum\nolimits_k p_k \mathrm{Tr}[U_{\phi_k} \rho U_{\phi_k}^\dagger M_k]. \tag{3.141}$$

Suppose now Alice's input state is incoherent, $\rho \equiv \delta \in \mathcal{I}$. Since every unitary channel $\mathcal{U}_\phi$ leaves any such state invariant, $\mathcal{U}_\phi(\delta) = \delta$, the best strategy for Alice is always to cast the guess $k^{\max}$ corresponding to the phase with the highest prior probability $p_{k^{\max}} := \max_k p_k$. This results in an optimal probability of success for any incoherent state given by

$$p_\Theta^{\mathrm{succ}}(\mathcal{I}) := p_{k^{\max}}, \tag{3.142}$$

which can be achieved even without actually probing the channel, just by a fixed guess.

It is clear that, by preparing a coherent state $\rho \notin \mathcal{I}$, Alice can expect to do better. What is less obvious yet more remarkable, is that the maximum advantage achievable by using $\rho$ as opposed to any incoherent probe $\delta$, in all possible PD games, is quantified exactly by the RoC of $\rho$. More precisely [5]:

$$\max_\Theta \frac{p_\Theta^{\mathrm{succ}}(\rho)}{p_\Theta^{\mathrm{succ}}(\mathcal{I})} = 1 + C_{\mathcal{R}}(\rho)\,. \tag{3.143}$$

The maximum is achieved for the PD game $\Theta^\star \equiv \left\{\left(\frac{1}{d}, \frac{2\pi k}{d}\right)\right\}_{k=0}^{d-1}$. Therefore $C_{\mathcal{R}}(\rho)$ exactly quantifies, in particular, how useful the state $\rho$ is for reliable decoding and transmission of messages encoded by generalised phase channels $\rho \mapsto Z^k \rho Z^{\dagger k}$, with $Z\,|j\rangle = \exp\left(\mathrm{i}\frac{2\pi}{d} j\right)|j\rangle$. These channels feature in several quantum information tasks such as quantum error correction [205], cloning [206], and dense coding [207, 208]. This suggests a prominent role of coherence, specifically measured by the RoC, in quantum communication.

We notice that one can consider more general channel discrimination (CD) games, where each game is associated with a set of pairs $\{(p_k, \Lambda_k)\}_{k=0}^{m-1} =: \Upsilon$, with $\{\Lambda_k\}$ a set of $m$ (generally nonunitary) channels. For each CD game $\Upsilon$, Alice's goal is still that of discriminating which $\Lambda_k$ gets applied by a black box to an input $\rho$, and she succeeds with

optimal probability

$$p_{\Upsilon}^{\text{succ}}(\rho) = \max_{\{M_k\}} \sum\nolimits_k p_k \text{Tr}[\Lambda_k(\rho) M_k], \tag{3.144}$$

where we optimise over measurements similarly as before. By virtue of Eq. (3.120), for any CD game $\Upsilon$ it holds

$$p_{\Upsilon}^{\text{succ}}(\rho) \leq (1 + C_{\mathcal{R}}(\rho)) p_{\Upsilon}^{\text{succ}}(\mathcal{I}), \tag{3.145}$$

where $p_{\Upsilon}^{\text{succ}}(\mathcal{I})$ is the best probability of success by using as input any incoherent state. In general, $p_{\Upsilon}^{\text{succ}}(\mathcal{I})$ can be higher than $p_{k^{\max}}$, because the channels $\Lambda_k$ may act nontrivially on incoherent states. Nonetheless, if one focuses on a subclass of CD games $\{\Upsilon^\star\} \ni \Theta^\star$ containing the PD game $\Theta^\star$, one gets

$$\max_{\Upsilon \in \{\Upsilon^\star\}} \frac{p_{\Upsilon}^{\text{succ}}(\rho)}{p_{\Upsilon}^{\text{succ}}(\mathcal{I})} = 1 + C_{\mathcal{R}}(\rho). \tag{3.146}$$

The RoC $C_{\mathcal{R}}(\rho)$ thus quantifies the maximum achievable advantage in any CD task in which the phase channels $Z^k$ are some of the possible channels applied to a probe $\rho$.

It will be a worthy development to extend this analysis to the scenario of *assisted* CD games, where the collaboration of a correlated party Bob may further increase Alice's probability of success in the discrimination [209].

We conclude this Section by remarking that the definition (3.119) can be extended to a more abstract notion of *robustness of asymmetry* [5], in which the free states (symmetric states) are those invariant under the action of a group [134]. Specifically, given a symmetry group $\mathsf{G}$ with associated unitary representation $\{U_g\}_{g \in \mathsf{G}}$ on the Hilbert space $\mathcal{H}$, and defining the action of $U_g$ on a state $\rho \in \mathcal{D}(\mathcal{H})$ as $\mathcal{U}_g(\rho) = U_g \rho U_g^\dagger$, a state $\sigma \in \mathcal{D}(\mathcal{H})$ is symmetric with respect to $\mathsf{G}$ if and only if $\mathcal{U}_g(\sigma) = \sigma$ for all $g \in \mathsf{G}$. Denoting by $\mathscr{S}$ the convex set of all symmetric states, the robustness of asymmetry of a state $\rho$ is then defined as

$$A_{\mathcal{R}}(\rho) = \min_{\tau \in \mathcal{D}(\mathcal{H})} \left\{ s \geq 0 \;\middle|\; \frac{\rho + s\,\tau}{1+s} =: \sigma \in \mathscr{S} \right\}, \tag{3.147}$$

i.e., as the minimum weight of another state $\tau$ such that its convex mixture with $\rho$ yields a symmetric state $\sigma$. Then, suitable adaptations of all the properties demonstrated above in Eqs. (3.121)–(3.135) carry over to the robustness of asymmetry, including the SDP evaluation and an operational interpretation in the context of channel discrimination games [5]. Coherence can be recovered as a special case of asymmetry with respect to the $d$-dimensional representation of the compact group $\mathsf{U}(1)$.

The approach based on the generalised notion of robustness appears accordingly quite versatile to define and validate insightful quantifiers of resources in quantum physics [124] and beyond [123, 210], as demonstrated here for the fundamental case of quantum coherence.

## 3.5 Quantification of discord-type correlations

We conclude this Chapter by focusing on the quantification of bipartite discord-type correlations for $\mathcal{M}_N^3$ states.

First of all, any $\mathcal{M}_N^3$ state is either classical-quantum or quantum-classical when considering local measurements on a subsystem composed of an even number of qubits. This is due to the fact that all the $\mathcal{M}_N^3$ states are left invariant after a measurement of the local GHZ basis corresponding to such a subsystem. Consequently, we have one hand that $N$-even $\mathcal{M}_N^3$ states are classical-classical with respect to any bipartition whose subsystems are composed of an even number of qubits, and on the other hand that $N$-odd $\mathcal{M}_N^3$ states are either classical-quantum or quantum-classical with respect to any possible bipartition.

Therefore, the relevant bipartitions to be considered are those relating to even $N$-qubit systems and such that both subsystems are composed of an odd number of qubits. In particular, in the following we will focus on a measured subsystem composed of just one qubit.

In analogy with the previous two Sections, the results that we will obtain are again universal with respect to the considered valid distance, with the only difference that now we will require another constraint on a distance in order to prove our results, that is its invariance under transposition with respect to any basis:

$$D(\rho^T, \sigma^T) = D(\rho, \sigma). \tag{3.148}$$

Let us comment on the physical significance of this property that is not typically discussed in the literature. Transposition of an $N \times N$ hermitian matrix, which amounts to complex conjugation, corresponds to a reflection in a $[N(N+1)/2 - 1]$-dimensional hyperplane. Property (3.148) thus means that a distance $D$ on the set of quantum states is assumed to be invariant under reflections, which appears as a fairly natural requirement [154]. Notice that, together with the invariance under unitary operations of any contractive distance, this property implies invariance of the distance $D$ under antiunitary operations. Indeed, any antiunitary matrix $O$ can be expressed as $O = UC$, where $U$ is a unitary matrix and $C$ denotes complex conjugation in the computational basis and so we have

$$\begin{aligned} D(O\rho O^{-1}, O\sigma O^{-1}) & \\ &= D\big(UC(\rho)U^\dagger, UC(\sigma)U^\dagger\big) \\ &= D\big(C(\rho), C(\sigma)\big) \\ &= D(\rho^T, \sigma^T) \\ &= D(\rho, \sigma) \end{aligned} \tag{3.149}$$

for any pair of states $\rho$, $\sigma$.

**Theorem 3.5.1.** *For any even $N$, and according to any contractive, transposition invariant, and convex distance, one of the closest classical-quantum states $\chi_\varpi$ to an $\mathcal{M}_N^3$ state $\varpi$, when considering local measurements on one qubit only, is always an $\mathcal{M}_N^3$ classical state of the form*

$$\chi_\varpi = \frac{1}{2^N}\left(\mathbb{I}^{\otimes N} + s\sigma_k^{\otimes N}\right), \tag{3.150}$$

*for some index $k \in \{1, 2, 3\}$ and some coefficient $s \in [-1, 1]$.*

*Proof.* Let us consider a bipartition of an $N$-qubit system into a subsystem $A$ composed of one qubit and another subsystem $B$ composed of the remaining $N-1$ qubits. An arbitrary state $\varrho$ of such system can be represented in the computational basis by the following matrix:

$$\varrho = \frac{1}{2^N}\left(\mathbb{I}^A \otimes \mathbb{I}^B + \sum_{i=1}^{3} x_i \sigma_i^A \otimes \mathbb{I}^B + \sum_{j=1}^{d_B^2-1} y_j \mathbb{I}^A \otimes \lambda_j^B + \sum_{i=1}^{3}\sum_{j=1}^{d_B^2-1} T_{ij}\sigma_i^A \otimes \lambda_j^B\right), \quad (3.151)$$

where $\mathbb{I}^A$ is the $2\times 2$ identity on subsystem $A$, $\mathbb{I}^B$ is the $2^{N-1}\times 2^{N-1}$ identity on subsystem $B$, $d_B = 2^{N-1}$ is the dimension of subsystem $B$, the $\lambda_j$'s constitute all the possible tensor products, composed of $N-1$ factors, between the matrices $\{\sigma_\alpha\}_{\alpha=0}^3$, with $\sigma_0$ being the $2\times 2$ identity, and finally

$$x_i = Tr\left[\varrho\left(\sigma_i^A \otimes \mathbb{I}^B\right)\right], \quad (3.152)$$

$$y_j = Tr\left[\varrho\left(\mathbb{I}^A \otimes \lambda_j^B\right)\right], \quad (3.153)$$

$$T_{ij} = Tr\left[\varrho\left(\sigma_i^A \otimes \lambda_j^B\right)\right]. \quad (3.154)$$

In the following, we will denote the above state $\varrho$ by the triple $\{\vec{x}, \vec{y}, \mathbf{T}\}$. The specific triple $\{\vec{x}, \vec{y}, \mathbf{T}\}$ for an $\mathcal{M}_N^3$ state as defined in Eq. (3.1) is $\vec{x} = \vec{y} = \vec{0}$ and $T_{ij} = c_i$ when $\lambda_j = \sigma_i^{\otimes(N-1)}$ while $T_{ij} = 0$ otherwise.

We first prove that for any $N$-qubit state $\varrho$ with triple $\{\vec{x}, \vec{y}, \mathbf{T}\}$ there exists a corresponding $N$-qubit state $\varrho'$ with associated triple $\{\vec{x}, \vec{y}', \mathbf{T}'\}$, whose marginal vector $\vec{y}'$ and correlation tensor $\mathbf{T}'$ are obtained from the ones of $\varrho$ by setting all the $y_j$ and $T_{ij}$ equal to zero, except for, respectively, the three components of $\vec{y}$ and the nine entries of $\mathbf{T}$ for which $j$ is such that $\lambda_j = \sigma_k^{\otimes(N-1)}$, for some $k = 1, 2, 3$. We will also prove that $D(\varpi, \varrho') \leq D(\varpi, \varrho)$ for any $\mathcal{M}_N^3$ state $\varpi$ and $N$-qubit state $\varrho$.

For $N = 2$, this is trivial since $\varrho'$ is just $\varrho$ itself. For $N > 2$, we begin by setting $2(N-2)$ single-qubit local unitaries

$$\begin{aligned}\{U_j\}_{j=1}^{2(N-2)} = \{&(\mathbb{I}\otimes\sigma_1\otimes\sigma_1\otimes\mathbb{I}^{\otimes N-3}), (\mathbb{I}^{\otimes 2}\otimes\sigma_1\otimes\sigma_1\otimes\mathbb{I}^{\otimes N-4}), \ldots, (\mathbb{I}^{\otimes N-2}\otimes\sigma_1\otimes\sigma_1),\\ &(\mathbb{I}\otimes\sigma_2\otimes\sigma_2\otimes\mathbb{I}^{\otimes N-3}), (\mathbb{I}^{\otimes 2}\otimes\sigma_2\otimes\sigma_2\otimes\mathbb{I}^{\otimes N-4}), \ldots, (\mathbb{I}^{\otimes N-2}\otimes\sigma_2\otimes\sigma_2)\}.\end{aligned} \quad (3.155)$$

Then, we fix a sequence of states $\{\varrho_0, \varrho_1, \ldots \varrho_{2(N-2)}\}$ defined by

$$\varrho_j := \frac{1}{2}\left(\varrho_{j-1} + U_j \varrho_{j-1} U_j^\dagger\right), \quad (3.156)$$

for $j \in \{1, 2, \ldots 2(N-2)\}$. By setting $\varrho_0 = \varrho$, one can easily see, by adopting similar arguments to those used in the proof of Theorem 3.2.1, that $\varrho_{2(N-2)} = \varrho'$.

Now, convexity and contractivity of the distance $D$ can be used to establish the following inequality for any $\mathcal{M}_N^3$ state $\varpi$ and any $N$-qubit state $\varrho$:

$$\begin{aligned} D(\varpi, \varrho_j) &= D\left(\varpi, \frac{1}{2}(\varrho_{j-1} + U_j \varrho_{j-1} U_j^\dagger)\right) \\ &\leq \frac{1}{2}\left(D(\varpi, \varrho_{j-1}) + D(\varpi, U_j \varrho_{j-1} U_j^\dagger)\right) \\ &= \frac{1}{2}\left(D(\varpi, \varrho_{j-1}) + D(U_j \varpi U_j^\dagger, U_j \varrho_{j-1} U_j^\dagger)\right) \\ &= D(\varpi, \varrho_{j-1}), \end{aligned} \tag{3.157}$$

where we use, in order, the definition of $\varrho_j$ for $j \in \{1, 2, \ldots 2(N-2)\}$, the convexity of $D$, the invariance of $\varpi$ through any $U_j$, and the invariance of $D$ through unitaries.

This process gives a hierarchy of $2(N-2)$ inequalities $D(\varpi, \varrho_j) \leq D(\varpi, \varrho_{j-1})$, which chained together imply $D(\varpi, \varrho_0) \leq D(\varpi, \varrho_{2(N-2)})$. We know that $\varrho_0 = \varrho$ and $\varrho_{2(N-2)} = \varrho'$, hence we have shown that

$$D(\varpi, \varrho') \leq D(\varpi, \varrho) \quad \forall \varrho. \tag{3.158}$$

For any even number of qubits $N$, we can now go one step further and prove that for any $N$-qubit state $\varrho$ with triple $\{\vec{x}, \vec{y}, \mathbf{T}\}$ there exists a corresponding $N$-qubit state $\varrho_0$ with associated triple $\{\vec{0}, \vec{0}, \mathbf{T}'\}$, where $\mathbf{T}'$ is the correlation tensor of $\varrho'$. We will also prove that $D(\varpi, \varrho_0) \leq D(\varpi, \varrho)$ for any $\mathcal{M}_N^3$ state $\varpi$ and $N$-qubit state $\varrho$.

We first define $\varrho'_- = O\varrho' O^{-1}$, where $O$ is an antiunitary operation defined by $O = \left(\sigma_y^{\otimes 2} \otimes \mathbb{I}^{\otimes N-2}\right) C$ and $C$ denotes complex conjugation in the computational basis, which amounts to transposition for quantum states. Then we note that the triple corresponding to $\varrho'_-$ is given by $\{-\vec{x}, -\vec{y}', \mathbf{T}'\}$, so that for any state $\varrho$ we can define a corresponding state $\varrho_0 = (\varrho' + \varrho'_-)/2$ with the desired triple $\{\vec{0}, \vec{0}, \mathbf{T}'\}$. Now, by using again convexity and invariance under transposition of the distance $D$, plus the inequality in Eq. (3.158), we can easily see that

$$D(\varpi, \varrho_0) \leq D(\varpi, \varrho) \quad \forall \varrho. \tag{3.159}$$

We will now consider the distance from $\varpi$ to the set of even $N$-qubit CQ states with respect to the bipartition of one qubit $A$ versus the other $N-1$ qubits, and show that its minimum can be attained by a classical $\mathcal{M}_N^3$ state of the form (3.150), hence proving the main result of the theorem. Recall that any CQ $N$-qubit state, when considering local measurements on one qubit $A$ only, is of the form

$$\chi = p|\psi_1\rangle\langle\psi_1|^A \otimes \rho_1^B + (1-p)|\psi_2\rangle\langle\psi_2|^A \otimes \rho_2^B, \tag{3.160}$$

where $p \in [0,1]$, $\{|\psi_1\rangle^A, |\psi_2\rangle^A\}$ is an orthonormal basis for qubit $A$ and $\rho_1^B$ and $\rho_2^B$ are arbitrary states of subsystem $B$.

Such a CQ state will have the associated triple $\{(2p-1)\vec{e}, \vec{s}_+, \vec{e}\ \vec{s}_-^T\}$, where

$$e_i = \langle\psi_1|\sigma_i|\psi_1\rangle, \ s_{\pm,i} = \mathrm{Tr}\left\{[p\rho_1 \pm (1-p)\rho_2]\,\lambda_i\right\}. \tag{3.161}$$

For any state in this form, a second state

$$\chi'_0 = p'|\psi'_1\rangle\langle\psi'_1|^A \otimes {\rho'_1}^B + (1-p')|\psi'_2\rangle\langle\psi'_2|^A \otimes {\rho'_2}^B, \tag{3.162}$$

can be derived using the identities

$$\begin{aligned} p' &= \frac{1}{2},\ |\psi_1'\rangle = |\psi_1\rangle,\ |\psi_2'\rangle = |\psi_2\rangle, \\ {\rho_1'}^B &= \frac{1}{2^{N-1}}\left[\mathbb{I}^B + p\tau_1^B - (1-p)\tau_2^B\right], \\ {\rho_2'}^B &= \frac{1}{2^{N-1}}\left[\mathbb{I}^B - p\tau_1^B + (1-p)\tau_2^B\right], \end{aligned} \tag{3.163}$$

where $\tau_1$ and $\tau_2$ are the traceless part of $\rho_1$ and $\rho_2$, respectively. This state is manifestly CQ and it can be easily verified that it will have the associated triple $\{\vec{0}, \vec{0}, \vec{e}\ \vec{s}_-^T\}$. Moreover, by applying the procedure defined in Eq. (3.156) to $\chi_0'$, we get another CQ state $\chi_0$ with triple $\{\vec{0}, \vec{0}, \vec{e}\ \vec{s}_{0,-}^T\}$, where $\vec{s}_{0,-}$ is obtained from $\vec{s}_-$ by setting all the $(s_-)_j$ equal to zero, except for the three components of $\vec{s}_-$ for which $j$ is such that $\lambda_j = \sigma_k^{\otimes(N-1)}$, for some $k = 1, 2, 3$. Hereafter, for the sake of simplicity, we will denote the vector $\vec{s}_{0,-}$ simply by the triple of survived components $\{s_1, s_2, s_3\}$, corresponding to $\sigma_1^{\otimes(N-1)}$, $\sigma_2^{\otimes(N-1)}$ and $\sigma_3^{\otimes(N-1)}$, respectively, by discarding all the other vanishing ones.

From the inequality (3.159), we have in particular that $D(\varpi, \chi_0) \leq D(\varpi, \chi)$ for any $\mathcal{M}_N^3$ state $\varpi$ and any CQ state $\chi$, so that in order to minimise $D(\varpi, \chi)$ it suffices to restrict ourselves to CQ states with associated triple $\{\vec{0}, \vec{0}, \vec{e}\ \vec{s}_{0,-}^T\}$.

Moreover, temporarily, we relax the restriction that $\vec{e}$ is of unit length and consider the distance from the even larger set for which $||\vec{e}|| \leq 1$. This is a convex set and so, due to the convexity of the distance, any local minimum will be a global one. We can now use a trick analogous to the one used for Eq. (3.158), this time between $\chi_0$ with $\vec{e} = (e_1, e_2, e_3)$ and $\vec{s}_{0,-} = (s_1, s_2, 0)$ and $\chi_0^-$ with $\vec{e}' = (e_1, e_2, -e_3)$ and $\vec{s}_{0,-}' = \vec{s}_{0,-}$. We then see that

$$D(\varpi, \chi_0) = D(U_z \varpi U_z^\dagger, U_z \chi_0 U_z^\dagger) = D(\varpi, \chi_0^-), \tag{3.164}$$

where we have introduced the unitary operator $U_z = \sigma_z^{\otimes 2} \otimes \mathbb{I}^{\otimes(N-2)}$ such that $\varpi = U_z \varpi U_z^\dagger$ for any $\mathcal{M}_N^3$ state $\varpi$, $\chi_0^- = U_z \chi_0 U_z^\dagger$, and we have exploited the invariance under unitary of any contractive distance. A similar result holds when considering distances from states with either $s_1 = 0$ or $s_2 = 0$, by using, respectively $U_x = \sigma_x^{\otimes 2} \otimes \mathbb{I}^{\otimes(N-2)}$ and $U_y = \sigma_y^{\otimes 2} \otimes \mathbb{I}^{\otimes(N-2)}$. Also, a similar result holds by switching the vectors we consider, for any $e_i = 0$. From these observations we have that, if $s_i = 0$ for some index $i$, then the minimum distance is attained for $e_i = 0$, and viceversa.

We can then restrict our attention to states of the form of $\chi_0$ with $e_i = e\delta_{ik}$ and $s_i = s\delta_{ik}$, where the index $k$ sets the non-zero vector element. From the previous results, we notice in fact that minimisation only needs to be performed over $e_k$ and $s_k$ as the distance can only decrease under any variation in any other single element. Furthermore, $e_k$ and $s_k$ appear only as a product $e_k s_k$ in the density matrix, never on their own. This means that minimising over both is equivalent to setting $e_k = 1$ and minimising only over $s_k$, thus allowing us to reimpose the restriction that $||\vec{e}|| = 1$, thus coming back to analyse the distance from $\varpi$ to CQ states. The remaining states over which the minimisation in the single parameter $s$ needs to be performed amount exactly to the set of $\mathcal{M}_N^3$ classical states in Eq. (3.150), hence finding the minimum among these will return the global minimum

for the distance $D$ from an arbitrary $\mathcal{M}_N^3$ state $\varpi$ to the set of $N$-qubit classical-quantum states, proving the claim.

■

In analogy with the previous Sections we now exploit Theorem 3.5.1 in order to easily evaluate the trace distance-based bipartite discord-type correlations for any $\mathcal{M}_N^3$ state and any even number of qubits $N$, when considering local measurements on one qubit only.

Specifically, we will prove that, for any even $N$ and for any $\mathcal{M}_N^3$ state, the trace distance-based measure of discord-type correlations $Q^{D_{\mathrm{Tr}}}$ is equivalent up to a constant factor to the minimum of the $l_1$-norm of coherence $C_{l_1}^{\{|i_k\rangle\}}$ with respect to the bases $\{|i_k\rangle\}$ consisting of tensor products of eigenstates of $\sigma_k$, with $k \in \{1,2,3\}$. Due to Eq. (1.16), to this aim we just need to show that, according to the trace distance $D_{\mathrm{Tr}}$, one of the closest classical states $\chi_\varpi$ to an $\mathcal{M}_N^3$ state $\varpi$ is always the closest diagonal part $\varpi_{\mathrm{diag}}^{\{|i_k\rangle\}}$ in the aforementioned bases $\{|i_k\rangle\}$.

The trace distance between an $\mathcal{M}_N^3$ state $\varpi$ with correlation functions $\{c_1, c_2, c_3\}$ and one of its closest classical states $\chi_\varpi$, which is itself an $\mathcal{M}_N^3$ state of the form (3.150), is given by

$$D_{\mathrm{Tr}}(\varpi, \chi_\varpi) = \frac{1}{8}(|s+c_i-c_j-c_k|+|s-c_i+c_j-c_k|+|s+c_i+c_j-c_k|+|-s+c_i+c_j+c_k|), \quad (3.165)$$

for any even $N$, where $\{i,j,k\}$ is any permutation of $\{1,2,3\}$ and $k$ is set by Eq. (3.150). It is immediate to see that the minimum over $\chi_\varpi$ is attained by $s = c_k$, i.e. by $\chi_\varpi = \varpi_{\mathrm{diag}}^{\{|i_k\rangle\}}$ as claimed, so that

$$Q^{D_{\mathrm{Tr}}}(\varpi) = \frac{1}{2}\min_k C_{l_1}^{\{|i_k\rangle\}}(\varpi) = \frac{1}{2}\min_{i,j}\max\{|c_i|,|c_j|\} = \frac{1}{2}|c_{int}|, \quad (3.166)$$

where $c_{int}$ represents the the correlation function $c_i$ with intermediate absolute value.

Again, when restricting to the particular subset of $N$-even $\mathcal{M}_N^3$ states $\varpi$, which is defined by the constraint $c_2 = (-1)^{N/2}c_1c_3$, it happens that one of the closest classical states is always the closest diagonal part $\varpi_{\mathrm{diag}}^{\{|i_k\rangle\}}$ in the bases $\{|i_k\rangle\}$ according to any contractive, transposition invariant and convex distance $D$.

**Theorem 3.5.2.** *According to any convex, transposition invariant and contractive distance, and for any even number of qubits $N$, one of the closest classical-quantum states $\chi_\varpi$ to an $\mathcal{M}_N^3$ state $\varpi$ of the form $\{c_1, (-1)^{N/2}c_1c_3, c_3\}$, when considering local measurements on one qubit only, is*

1. *when $|c_1| \geq |c_3|$, the $\mathcal{M}_N^3$ classical state $\{c_1, 0, 0\}$, i.e. the one with $k = 1$ and $s = c_1$ in Eq. (3.150);*
2. *when $|c_3| \geq |c_1|$, the $\mathcal{M}_N^3$ classical state $\{0, 0, c_3\}$, i.e. the one with $k = 3$ and $s = c_3$ in Eq. (3.150).*

*Proof.* According to Theorem 3.5.1, one of the closest classical-quantum states to any $\mathcal{M}_N^3$ state is a classical $\mathcal{M}_N^3$ state. According to Lemmas 3.5.1 and 3.5.2, the closest classical $\mathcal{M}_N^3$ state $\chi_\varpi$ to an $\mathcal{M}_N^3$ state $\varpi$ of the form $\{c_1, (-1)^{N/2} c_1 c_3, c_3\}$ is either $\{c_1, 0, 0\}$ or $\{0, 0, c_3\}$. Finally, according to Lemmas 3.5.3 and 3.5.4, if $|c_1| \geq |c_3|$ then one of the closest classical $\mathcal{M}_N^3$ states to $\varpi$ is $\{c_1, 0, 0\}$, whereas if $|c_3| \geq |c_1|$ then one of the closest classical $\mathcal{M}_N^3$ states to $\varpi$ is $\{0, 0, c_3\}$.

■

Here we derive some technical results needed for the proof of Theorem 3.5.2.

**Lemma 3.5.1.** *According to any contractive distance $D$ and for any even number of qubits $N$, it holds that:*

1. *among the $\mathcal{M}_N^3$ classical states belonging to the $c_1$-axis, the closest state $\chi_\varpi^{(1)}$ to an $\mathcal{M}_N^3$ state $\varpi$ of the form $\{c_1, (-1)^{N/2} c_1 c_3, c_3\}$ is the orthogonal projection of $\varpi$ onto the $c_1$-axis, i.e. $\chi_\varpi^{(1)} = \{c_1, 0, 0\}$;*

2. *among the $\mathcal{M}_N^3$ classical states belonging to the $c_3$-axis, the closest state $\chi_\varpi^{(3)}$ to an $\mathcal{M}_N^3$ state $\varpi$ of the form $\{c_1, (-1)^{N/2} c_1 c_3, c_3\}$ is the orthogonal projection of $\varpi$ onto the $c_3$-axis, i.e. $\chi_\varpi^{(3)} = \{0, 0, c_3\}$;*

*Proof.* Regarding point (1), we need to prove that for any $x$

$$D(\{c_1, (-1)^{N/2} c_1 c_3, c_3\}, \{c_1, 0, 0\}) \leq D(\{c_1, (-1)^{N/2} c_1 c_3, c_3\}, \{c_1 + x, 0, 0\}). \quad (3.167)$$

In fact

$$\begin{aligned} & D(\{c_1, (-1)^{N/2} c_1 c_3, c_3\}, \{c_1, 0, 0\}) \\ = \; & D(\{0, 0, c_3\}, \{0, 0, 0\}) \\ = \; & D(\Lambda_1^{F_3 \otimes N}(\{c_1, (-1)^{N/2} c_1 c_3, c_3\}), \Lambda_1^{F_3 \otimes N}(\{c_1 + x, 0, 0\})) \\ \leq \; & D(\{c_1, (-1)^{N/2} c_1 c_3, c_3\}, \{c_1 + x, 0, 0\}), \end{aligned}$$

where the first equality is due to Theorem 3.4.1, which holds for any contractive distance, the second equality is due to the fact that

$$\{0, 0, c_3\} = \Lambda_1^{F_3 \otimes N}(\{c_1, (-1)^{N/2} c_1 c_3, c_3\}), \quad (3.168)$$

$$\{0, 0, 0\} = \Lambda_1^{F_3 \otimes N}(\{c_1 + x, 0, 0\}), \quad (3.169)$$

with $\Lambda_1^{F_3 \otimes N}$ representing the local independent phase flip noise expressed by Eq. (1.14), when $\Xi = F_3$ and $q = 1$ (i.e. $t \to \infty$), and finally the inequality is due to contractivity of the distance $D$.

Regarding point (2) we need to prove that for any $z$

$$D(\{c_1, (-1)^{N/2} c_1 c_3, c_3\}, \{0, 0, c_3\}) \leq D(\{c_1, (-1)^{N/2} c_1 c_3, c_3\}, \{0, 0, c_3 + z\}). \quad (3.170)$$

In fact

$$\begin{aligned} & D(\{c_1,(-1)^{N/2}c_1c_3,c_3\},\{0,0,c_3\}) \\ = \;& D(\{c_1,0,0\},\{0,0,0\}) \\ = \;& D(\Lambda_1^{F_1\otimes N}(\{c_1,(-1)^{N/2}c_1c_3,c_3\}),\Lambda_1^{F_1\otimes N}(\{0,0,c_3+z\})) \\ \leq \;& D(\{c_1,(-1)^{N/2}c_1c_3,c_3\},\{0,0,c_3+z\}), \end{aligned}$$

where the first equality is due to Theorem 3.4.1, which holds for any contractive distance, the second equality is due to the fact that

$$\{c_1,0,0\} = \Lambda_1^{F_1\otimes N}(\{c_1,(-1)^{N/2}c_1c_3,c_3\}), \tag{3.171}$$

$$\{0,0,0\} = \Lambda_1^{F_1\otimes N}(\{0,0,c_3+z\}), \tag{3.172}$$

with $\Lambda_1^{F_1\otimes N}$ representing the local independent bit flip noise expressed by Eq. (1.14), when $\Xi = F_1$ and $q = 1$ (i.e. $t \to \infty$), and finally the inequality is due to contractivity of the distance $D$.

■

An analogous result does not hold for the classical $\mathcal{M}_N^3$ states lying on the $c_2$-axis. However, due to the following Lemma 3.5.2, we can discard the classical $\mathcal{M}_N^3$ states on the $c_2$-axis in order to find out the closest classical $\mathcal{M}_N^3$ state to an $\mathcal{M}_N^3$ state satisfying the constraint $c_2 = (-1)^{N/2}c_1c_3$.

**Lemma 3.5.2.** *According to any contractive distance $D$ and for any even number of qubits $N$, it holds that:*

1. *the $\mathcal{M}_N^3$ classical state $\chi_\varpi^{(1)} = \{c_1,0,0\}$ on the $c_1$-axis closest to the $\mathcal{M}_N^3$ state $\varpi = \{c_1,(-1)^{N/2}c_1c_3,c_3\}$ is closer to $\varpi$ than any classical $\mathcal{M}_N^3$ state belonging to the $c_2$-axis;*

2. *the $\mathcal{M}_N^3$ classical state $\chi_\varpi^{(3)} = \{0,0,c_3\}$ on the $c_3$-axis closest to the $\mathcal{M}_N^3$ state $\varpi = \{c_1,(-1)^{N/2}c_1c_3,c_3\}$ is closer to $\varpi$ than any classical $\mathcal{M}_N^3$ state belonging to the $c_2$-axis.*

*Proof.* Regarding point (1), we need to prove that for any $y$

$$D(\{c_1,(-1)^{N/2}c_1c_3,c_3\},\{c_1,0,0\}) \leq D(\{c_1,(-1)^{N/2}c_1c_3,c_3\},\{0,y,0\}). \tag{3.173}$$

In fact

$$\begin{aligned} & D(\{c_1,(-1)^{N/2}c_1c_3,c_3\},\{c_1,0,0\}) \\ = \;& D(\{0,0,c_3\},\{0,0,0\}) \\ = \;& D(\Lambda_1^{F_3\otimes N}(\{c_1,(-1)^{N/2}c_1c_3,c_3\}),\Lambda_1^{F_3\otimes N}(\{0,y,0\})) \\ \leq \;& D(\{c_1,(-1)^{N/2}c_1c_3,c_3\},\{0,y,0\}), \end{aligned}$$

where the first equality is due to Theorem 3.4.1, which holds for any contractive distance, the second equality is due to the fact that

$$\{0,0,c_3\} = \Lambda_1^{F_3\otimes N}(\{c_1,(-1)^{N/2}c_1c_3,c_3\}), \tag{3.174}$$
$$\{0,0,0\} = \Lambda_1^{F_3\otimes N}(\{0,y,0\}), \tag{3.175}$$

with $\Lambda_1^{F_3\otimes N}$ representing the local independent phase flip noise expressed by Eq. (1.14), when $\Xi = F_3$ and $q = 1$ (i.e. $t \to \infty$), and finally the inequality is due to contractivity of the distance $D$.

Regarding point (2), we need to prove that

$$D(\{c_1,(-1)^{N/2}c_1c_3,c_3\},\{0,0,c_3\}) \leq D(\{c_1,(-1)^{N/2}c_1c_3,c_3\},\{0,y,0\}). \tag{3.176}$$

In fact

$$\begin{aligned} & D(\{c_1,(-1)^{N/2}c_1c_3,c_3\},\{0,0,c_3\}) \\ = \; & D(\{c_1,0,0\},\{0,0,0\}) \\ = \; & D(\Lambda_1^{F_1\otimes N}(\{c_1,(-1)^{N/2}c_1c_3,c_3\}),\Lambda_1^{F_1\otimes N}(\{0,y,0\})) \\ \leq \; & D(\{c_1,(-1)^{N/2}c_1c_3,c_3\},\{0,y,0\}), \end{aligned}$$

where the first equality is due to Theorem 3.4.1, the second equality is due to the fact that

$$\{c_1,0,0\} = \Lambda_1^{F_1\otimes N}(\{c_1,(-1)^{N/2}c_1c_3,c_3\}), \tag{3.177}$$
$$\{0,0,0\} = \Lambda_1^{F_1\otimes N}(\{0,y,0\}), \tag{3.178}$$

with $\Lambda_1^{F_1\otimes N}$ representing the local independent bit flip noise expressed by Eq. (1.14), when $\Xi = F_1$ and $q = 1$ (i.e. $t \to \infty$), and finally the inequality is due to contractivity of the distance $D$.

■

**Lemma 3.5.3.** *According to any contractive distance $D$ and for any even number of qubits $N$, if $|c_1| = |c_3|$ then*

$$D(\{c_1,0,0\},\{0,0,0\}) = D(\{0,0,c_3\},\{0,0,0\}). \tag{3.179}$$

*Proof.* Let us suppose that $c_1 = \pm c_3 = h$, then we have

$$\begin{aligned} & D(\{h,0,0\},\{0,0,0\}) \\ = \; & D(U_\pm\{0,0,\pm h\}U_\pm^\dagger, U_\pm\{0,0,0\}U_\pm^\dagger) \\ = \; & D(\{0,0,\pm h\},\{0,0,0\}), \end{aligned}$$

where the first equality is due to the fact that

$$\{h,0,0\} = U_\pm\{0,0,\pm h\}U_\pm^\dagger, \tag{3.180}$$
$$\{0,0,0\} = U_\pm\{0,0,0\}U_\pm^\dagger, \tag{3.181}$$

with $U_+ = S_2^{\otimes N}$, $S_2 = \frac{1}{\sqrt{2}}(\mathbb{I} + i\sigma_y)$ and $U_- = \frac{1}{\sqrt{2}}(\sigma_y + i\mathbb{I}) \otimes S_2^{\otimes(N-1)}$ being unitaries, whereas the second equality is due to unitary invariance of any contractive distance $D$.

■

**Lemma 3.5.4.** *According to any contractive distance $D$, for any even number of qubits $N$ and any $q \in [0,1]$ the following holds:*

$$D(\{qc_1,0,0\},\{0,0,0\}) \leq D(\{c_1,0,0\},\{0,0,0\}), \tag{3.182}$$
$$D(\{0,0,qc_3\},\{0,0,0\}) \leq D(\{0,0,c_3\},\{0,0,0\}). \tag{3.183}$$

*Proof.* Regarding Eq. (3.182), we have

$$\begin{aligned} & D(\{qc_1,0,0\},\{0,0,0\}) \\ & \qquad = D(\Lambda_q^{F_3\otimes N}(\{c_1,0,0\}),\Lambda_q^{F_3\otimes N}(\{0,0,0\})) \\ & \qquad \leq D(\{c_1,0,0\}),\{0,0,0\}), \end{aligned}$$

where the inequality is due to contractivity of the distance $D$ whereas the equality is due to the fact that

$$\{qc_1,0,0\} = \Lambda_q^{F_3\otimes N}(\{c_1,0,0\}) \tag{3.184}$$
$$\{0,0,0\} = \Lambda_q^{F_3\otimes N}(\{0,0,0\}), \tag{3.185}$$

with $\Lambda_1^{F_3\otimes N}$ representing the local independent phase flip noise expressed by Eq. (1.14) when $\Xi = F_3$.

Regarding Eq. (3.183) we have

$$\begin{aligned} & D(\{0,0,qc_3\},\{0,0,0\}) \\ & \qquad = D(\Lambda_q^{F_1\otimes N}(\{0,0,c_3\}),\Lambda_q^{F_1\otimes N}(\{0,0,0\})) \\ & \qquad \leq D(\{0,0,c_3\}),\{0,0,0\}) \end{aligned}$$

where the inequality is due to contractivity of the distance $D$ while the equality is due to the fact that

$$\{0,0,qc_3\} = \Lambda_q^{F_1\otimes N}(\{0,0,c_3\}), \tag{3.186}$$
$$\{0,0,0\} = \Lambda_q^{F_1\otimes N}(\{0,0,0\}), \tag{3.187}$$

with $\Lambda_1^{F_1\otimes N}$ representing the local independent bit flip noise expressed by Eq. (1.14) when $\Xi = F_1$, and finally

■

This universal behaviour with respect to any convex, transposition invariant and contractive distance $D$ on the restricted class of $\mathcal{M}_N^3$ states with $c_2 = (-1)^{N/2}c_1c_3$ will turn out to be crucial in the following Chapter when we will deal with the universal freezing phenomenon of quantum correlations beyond entanglement.

We conclude this Section by noting that all its results, still obtained in collaboration with T. R. Bromley and G. Adesso, actually generalise to any even number $N$ of qubits the results presented in Ref. [2].

## 3.6 Discussion

We have achieved a compendium of exact results on the quantification of general distance-based measures of global, partial, and genuine multiparticle entanglement, as well as of quantum coherence and bipartite discord-type correlations in some pivotal reference families of $N$-qubit mixed states.

In the case of entanglement and quantum coherence, this allowed us to establish faithful lower bounds for general states, accessible by few local measurements and effective on prominent resource states for quantum information processing.

Our approach can be regarded as realising simple yet particularly convenient instances of quantitative entanglement witnesses [68,69], as well as of quantum coherence witnesses, with the crucial advance that our lower bounds are analytical, in contrast to conventional numerical approaches requiring semidefinite programming, and hold for *all* valid geometric measures, which are endowed with meaningful operational interpretations yet have been traditionally hard to evaluate [62, 211].

A key aspect of our analysis lies in fact in the generality of the adopted techniques, which rely on natural information-theoretic requirements of contractivity and joint convexity of any distance $D$ entering Eq. (2.21).

We can expect our methods to be applicable to:

- other reference sets of states, such as states diagonal in a basis of cluster states [63, 211], or more general states with X-shaped density matrices [66], thereby leading to alternative entanglement and coherence bounds for general states, which might be more tailored to different classes, or to specific measurement settings in laboratory;

- other useful forms of multiparticle quantum correlations, such as Einstein-Podolsky-Rosen steering [16, 212], and Bell nonlocality in many-body systems [184]. This can eventually lead to a unifying characterisation, resting on the framework of information geometry, of the whole spectrum of genuine signatures of quantumness in cooperative phenomena.

Another key feature of our framework is its accessibility. Having tested our entanglement bounds on a selection of very different families of theoretical and experimentally produced states with high levels of noise, we can certify their usefulness in realistic scenarios. We recall that, for instance, three canonical local measurements suffice to quantify exactly the global entanglement of GHZ states of any even number $N$ of qubits, while $N+1$ local measurements provide their exact genuine entanglement, according to every geometric measure for any $N$, when such states are realistically mixed with white noise. This can lead to a considerable simplification of future experiments based on these archetypical resources, involving e.g. two quantum bytes (16 qubits) and beyond [73, 187].

Finally, we have also introduced the robustness of coherence, showing it to be a fully bona fide quantifier in all possible resource theories of coherence. We have provided a direct operational interpretation for such measure in the context of phase discrimination, and reported other results useful for practical applications, such as introducing and developing the notion of coherence witnesses. Overall, this represents a notable advance in the rigorous

study and potential exploitation of quantum coherence, a concept central to quantum physics and enjoying applications even beyond the realm of physics, e.g. in biology.

# Chapter 4

# Dynamical preservation of quantumness

In this Chapter we review our results [1–3, 6, 7] about the dynamical preservation of quantumness, be it in the form of discord-type correlations, quantum coherence or even entanglement.

In the previous Chapter, in deriving our results, we have also identified curves or even surfaces of constant quantumness within the set of $\mathcal{M}_N^3$ states. This is noteworthy since some typical decoherence mechanisms, such as local identical flip channels or collective dephasing in spin environments, can induce dynamical evolutions which leave these states confined within such curves or surfaces, for any even number of qubits in the case of discord-type correlations and quantum coherence and for two qubits in the case of entanglement.

Our findings thus entail that quantumness, regardless of which distance is adopted for its evaluation, is exactly preserved (*frozen*) under those noisy evolutions, a fact which can have practical implications for the robust implementation of quantum information processing, and might shed further light on the persistence of quantum coherence and entanglement in biological systems [43].

## 4.1 Frozen discord-type correlations

In this Section we prove that freezing occurs for any geometric measure of quantum correlations beyond entanglement, whenever the distance defining the measure respects a minimal set of physical assumptions, namely dynamical contractivity under quantum channels, invariance under transposition, and convexity. The freezing phenomenon is therefore revealed as *universal* within the geometric approach to quantum correlations. We also prove that the universal freezing of bipartite discord-type correlations, when considering local measurements on one qubit only, can actually occur for any even number of non-interacting qubits being initially in a specific class of $\mathcal{M}_N^3$ states and undergoing local flip channels.

Therefore, in the following, when considering discord-type correlations, we will always refer to geometric one-way discord-type bipartite correlations with respect to one qubit

only, which will be simply denoted by $Q^D_{\rightarrow}$.

Notice that our work differs from other complementary investigations of the freezing phenomenon [90, 213]. In particular, in a recent work [213], the authors provide necessary and sufficient conditions for a general state to exhibit freezing under non-dissipative decoherence, according to some specific measure of discord. Here, on the other hand, we focus on a specific class of initial states, and we identify the minimal set of conditions that *any* general distance-based measure of discord needs to satisfy in order to freeze. On some random family of initial states, it is certainly possible to see freezing according to one discord-type measure but not to another. What we prove here is that, for a specific class of $\mathcal{M}^3_N$ states, all *bona fide* geometric quantifiers of bipartite discord-type correlations respecting the three physical assumptions mentioned above undergo the same dynamics, featuring the freezing phenomenon.

We now present the freezing phenomenon from a geometric perspective, by employing a particular *bona fide* measure of discord-type correlations, that is the Bures distance-based measure $Q^{D_B}_{\rightarrow}$ [6, 45, 46, 88].

We first recall the basic ingredients for the complete description of the phenomenon. The evolution of $N$ non-interacting qubits initially in an $\mathcal{M}^3_N$ state, undergoing local identical flip channels, preserves the $\mathcal{M}^3_N$ structure during the entire dynamics. More precisely, by using Eq. (1.14) with $\Xi = F_k$ and Eq. (3.1), one can easily see that the triple $\{c_1(q), c_2(q), c_3(q)\}$ characterising the $\mathcal{M}^3_N$ evolved state $\varpi(q)$ can be written as follows

$$c_{i,j\neq k}(q) = (1-q)^N c_{i,j\neq k}(0), \quad c_k(q) = c_k(0)\,, \tag{4.1}$$

where the index $k \in \{1, 2, 3\}$ respectively identifies the bit flip ($k = 1$), bit-phase flip ($k = 2$), and phase flip ($k = 3$) channel, $q$ is the strength of the noise that in dynamical terms can be expressed as $q(t) = 1 - \exp(-\gamma t)$ with $t$ representing time and $\gamma$ being the decoherence rate, and $\{c_1(0), c_2(0), c_3(0)\}$ is the triple characterising the initial $\mathcal{M}^3_N$ state $\varpi(0)$.

The freezing phenomenon for discord-type correlations occurs when considering an even number $N$ of non-interacting qubits, initially in an $\mathcal{M}^3_N$ state $\varpi(0)$, undergoing identical local flip channels and satisfying further specific initial state conditions. For convenience and without loss of generality, from now on we focus our analysis on the phase flip channel ($k = 3$)[1], for which these initial conditions consist of the triples $\vec{c}(0)$ such that

$$c_2(0) = (-1)^{N/2} c_1(0) c_3(0), \quad |c_1(0)| > |c_3(0)|. \tag{4.2}$$

The $\mathcal{M}^3_N$ states satisfying the constraint of Eq. (4.2) distribute within a two-dimensional surface inside the tetrahedron of all $\mathcal{M}^3_N$ states, which is shown in the case of odd $N/2$ in Fig. 4.1 and will be referred to herein as (phase flip) freezing surface.

From Eq. (4.1) one can see that the corresponding time evolved state $\varpi(t)$ is an $\mathcal{M}^3_N$ state characterised by the triple $\{c_1(0)e^{-N\gamma t}, (-1)^{N/2} c_1(0) c_3(0) e^{-N\gamma t}, c_3(0)\}$, which means that it remains confined within the freezing surface at any time. An example of

[1] The suitable initial conditions for bit flip ($k = 1$) or bit-phase flip ($k = 2$) channels can be obtained by setting analogous relations among the coefficients $c_1, c_2, c_3$.

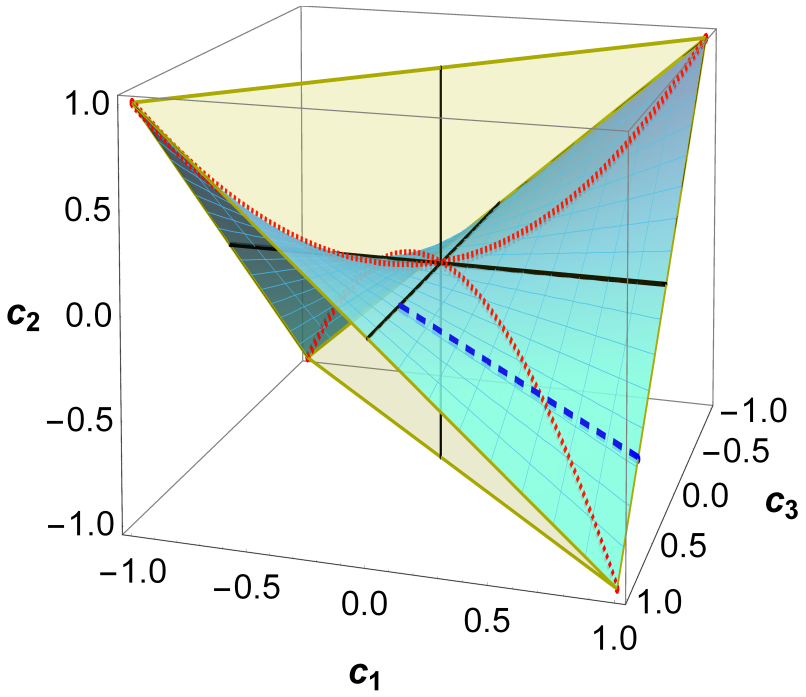


Figure 4.1: The phase flip freezing surface (meshed cyan) within the tetrahedron of all $\mathcal{M}_N^3$ states with even $N$ and odd $N/2$ (light yellow) represented in the $\{c_1, c_2, c_3\}$-space. The surface contains all and only the $\mathcal{M}_N^3$ states with triple $\{c_1, -c_1 c_3, c_3\}$, and thus accommodates all the $\mathcal{M}_N^3$ states respecting Eq. (4.2) when $N/2$ is odd. Solid black lines represent the classical $\mathcal{M}_N^3$ states of the form given in Eq. (3.150), which lie on the axes. The dotted red lines represent the threshold points on the surface when $|c_1| = |c_3|$, which occurs at the time $t = t^*$ defined in Eq. (4.3). For any state obeying the initial conditions of Eq. (4.2), we show that *bona fide* bipartite discord-type quantum correlations, when considering local measurements on one qubit only, are frozen under local phase flip channels up to the time $t^*$. As an example, the dashed blue line represents the dynamical trajectory of the initial $\mathcal{M}_N^3$ state $\{1, -0.6, 0.6\}$, which evolves under local phase flip channels moving towards the $c_3$-axis with increasing time; the aforementioned discord-type correlations are frozen in the initial segment of the trajectory up to the intersection with the red dotted line, and decay exponentially afterwards, as plotted in Fig. 4.2 in the case of $N = 2$.

this dynamical trajectory, in the case of odd $N/2$, is represented in Fig. 4.1 by the dashed blue line.

The above dynamical conditions give rise to a very peculiar evolution of the quantum correlations present in the time evolved state. Namely, defining a threshold time $t^*$ by

$$t^* := -\frac{1}{N\gamma} \ln \frac{|c_3(0)|}{|c_1(0)|}, \tag{4.3}$$

we find that the Bures distance-based measure of discord $Q_{\rightarrow}^{D_B}$ stays constant (freezes) for $0 \leq t < t^*$ and then decays exponentially from $t > t^*$ onwards, as is shown in Fig. 4.2

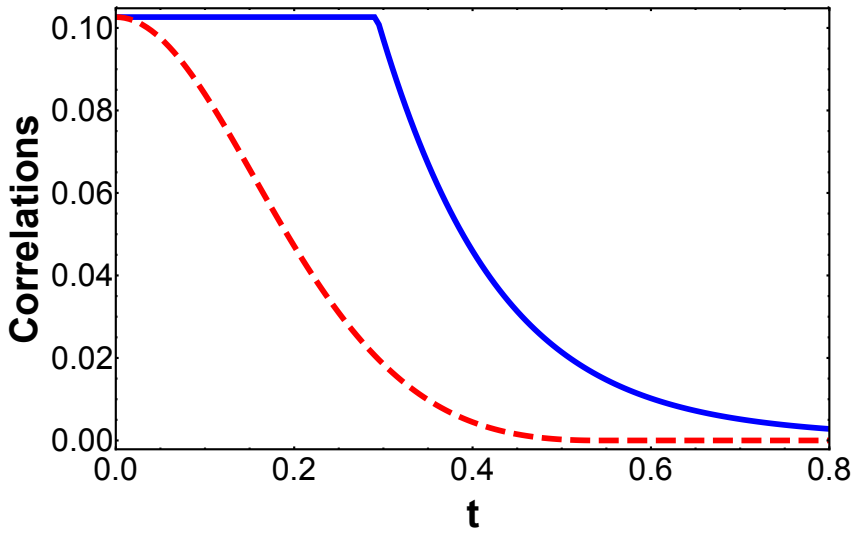


Figure 4.2: The freezing of Bures distance-based bipartite discord-type correlations for an initial $\mathcal{M}_2^3$ state of the form $\vec{c}(0) = \{1, -0.6, 0.6\}$. The solid blue line represents the time evolution of discord-type correlations and the dashed red line represents the time evolution of Bures distance-based entanglement.

in the case of $N = 2$. This can be straightforwardly shown by considering the available closed formula for Bures discord-type correlations of BD states [45,88] and then extending it to any even $N$ $\mathcal{M}_N^3$ state, by using similar arguments to those adopted in Section 3.5 in the case of the trace distance. On the contrary, entanglement measured e.g. by $E^{D_B}$ undergoes a typical sudden death at a finite time [86]. We stress again that this behaviour of quantum correlations, here illustrated for $Q_{\rightarrow}^{D_B}$, has been independently observed (on a case by case basis) in the two-qubit case for several valid discord-type measures in the aforementioned dynamical conditions [88]: our work instead provides a rigorous basis to establish its universality within the *bona fide* geometric approach and its generality for any even $N$.

The freezing phenomenon can be understood in geometric terms by looking at Fig. 4.1, which represents the phase flip freezing surface containing $\mathcal{M}_N^3$ states, with even $N$ and odd $N/2$, of the form $\{c_1, (-1)^{N/2} c_1 c_3, c_3\}$, thus containing all the states with initial conditions identified in Eq. (4.2). The solid black lines represent the axes in the $\{c_1, c_2, c_3\}$ space, which correspond to all the classical $\mathcal{M}_N^3$ states of the form given in Eq. (3.150). The dashed blue line represents a particular state evolution under local phase flip channels, leading to the freezing phenomenon. The intersection between the dotted red line and the dashed blue line represents the time $t^*$ such that $|c_1(t^*)| = |c_3(t^*)|$, i.e., the threshold time (4.3) corresponding to the sudden change from freezing to decaying of quantum correlations.

For $t < t^*$, i.e. when $|c_1(t)| > |c_3(t)|$, one of the closest classical states to the evolved $\mathcal{M}_N^3$ state $\varpi(t) = \{c_1(0)e^{-N\gamma t}, (-1)^{N/2} c_1(0)c_3(0)e^{-N\gamma t}, c_3(0)\}$ is its Euclidean orthogonal

projection onto the $c_1$-axis, i.e. the $\mathcal{M}_N^3$ classical state $\chi_{\varpi(t<t^*)} = \{c_1(0)e^{-N\gamma t}, 0, 0\}$. From Eq. (2.27) we know that the discord-type quantum correlations of $\varpi(t)$ for $t < t^*$ are given exactly by the Bures distance between the evolving state $\varpi(t < t^*)$ and this closest classical state $\chi_{\varpi(t<t^*)}$. Interestingly, one can observe that this distance is constant for any $t < t^*$, which indeed implies that the quantum correlations of $\varpi(t)$ are frozen for any $t < t^*$, given arbitrary initial conditions on the freezing surface defined by (4.2).

For $t > t^*$, i.e. when $|c_3(t)| > |c_1(t)|$, one of the closest classical states to the evolved $\mathcal{M}_N^3$ state $\varpi(t) = \{c_1(0)e^{-N\gamma t}, (-1)^{N/2}c_1(0)c_3(0)e^{-N\gamma t}, c_3(0)\}$ is instead its Euclidean orthogonal projection onto the $c_3$-axis, i.e. the $\mathcal{M}_N^3$ classical state $\chi_{\varpi(t>t^*)} = \{0, 0, c_3(0)\}$, which is independent of time. Therefore the quantum correlations of the evolved state $\varpi(t)$ decrease for any $t > t^*$, as the distance between the evolving state $\varpi(t > t^*)$ and the steady closest classical state $\chi_{\rho(t>t^*)}$ decreases for any $t > t^*$.

For even $N$ $\mathcal{M}_N^3$ states of the form (4.2) undergoing local and independent flip channels, freezing (up to a time $t^*$) of geometric quantum correlations measured by the Bures distance thus relies on the following two properties:

- (F1) (according to the Bures distance) one of the closest classical states to the evolved $\mathcal{M}_N^3$ state $\varpi(t) = \{c_1(t), (-1)^{N/2}c_1(t)c_3(t), c_3(t)\}$ is the classical $\mathcal{M}_N^3$ state $\{c_1(t), 0, 0\}$ when $|c_1(t)| > |c_3(t)|$;
- (F2) the (Bures) distance between the $\mathcal{M}_N^3$ states with triples $\{c_1, (-1)^{N/2}c_1c_2, c_3\}$ and $\{c_1, 0, 0\}$ does not depend on $c_1$, that is

$$D(\{c_1, (-1)^{N/2}c_1c_3, c_3\}, \{c_1, 0, 0\}) = D(\{0, 0, c_3\}, \{0, 0, 0\}), \ \forall c_1, c_3. \tag{4.4}$$

Theorem 3.5.2 and Theorem 3.4.1 tell us exactly that these two properties are satisfied by *any* contractive, transposition invariant, and convex distance, thus implying the freezing phenomenon for any *bona fide* distance-based measure of discord-type quantum correlations as defined above.

Contrarily, we remark that the non-contractive Hilbert-Schmidt distance satisfies only the first property (F1), whereas it does not manifest the kind of translational invariance expressed in Eq. (4.4), due to the fact that the trajectory of the evolved state is not parallel to the $c_1$-axis according to the Euclidean geometry, as is shown in Fig. 4.1 in the case of odd $N/2$. As a result, the Hilbert-Schmidt geometric discord [214], which is not a *bona fide* measure [215], does not manifest freezing in the considered dynamical conditions, as previously observed [88].

## 4.2 Frozen quantum coherence

In this Section we investigate the dynamics of quantum coherence in open $N$-qubit systems under paradigmatic incoherent noisy channels, by considering the computational basis as the reference basis for illustration. While coherence is generally nonincreasing under any incoherent channel [135], our goal is to identify, in analogy with the previous Section, initial states and dynamical conditions such that coherence, regardless of the adopted quantifier, will remain exactly constant (frozen) during the whole evolution.

We start by analysing conditions such that the $l_1$-norm and relative entropy of coherence, defined in Eqs. (1.15) and (1.20) respectively, are invariant during the evolution of a single qubit ($N = 1$), initially in a state $\rho(0)$, under any of the noisy channels $\Lambda_q^{\Xi}$ introduced in Eq. (1.14). This is done by imposing a vanishing differential of the measures on the evolved state, $\partial_q C[\Lambda_q^{\Xi}(\rho(0))] = 0 \ \ \forall q \in [0,1]$, with respect to the noise parameter $q$, which as we have already mentioned can also be interpreted as a dimensionless time. We find that only the bit and bit-phase flip channels allow for nonzero frozen coherence (in the computational basis), while all the other considered incoherent channels leave coherence invariant only trivially when the initial state is already incoherent. We can then ask whether nontrivial common freezing conditions for $C_{l_1}$ and $C_{RE}$ exist.

Writing a single-qubit state in general as $\rho = \frac{1}{2}(\mathbb{I}+\sum_j n_j\sigma_j)$ in terms of its Bloch vector $\vec{n} = \{n_1, n_2, n_3\}$, the bit flip channel $\Lambda_q^{F_1}$ maps an initial Bloch vector $\vec{n}(0)$ to an evolved one $\vec{n}(q) = \{n_1(0), (1-q)n_2(0), (1-q)n_3(0)\}$. As the $l_1$-norm of coherence is independent of $n_3$, while $n_1$ is unaffected by the channel, we get that necessary and sufficient freezing conditions for $C_{l_1}$ under a single-qubit bit flip channel amount to $n_2(0) = 0$ in the initial state. Similar conclusions apply to the bit-phase flip channel $\Lambda_q^{F_2}$ by swapping the roles of $n_1$ and $n_2$.

Conversely, the relative entropy of coherence is also dependent on $n_3$. By analysing the $q$-derivative of $C_{RE}$, we see that such a measure is frozen through the bit flip channel only when either $n_1(0) = 0$ and $n_2(0) = 0$ (trivial because the initial state is incoherent) or $n_2(0) = 0$ and $n_3(0) = 0$ (trivial because the initial state is invariant under the channel). Therefore, there is no nontrivial freezing of the relative entropy of coherence under the bit flip or bit-phase flip channel either.

We conclude that, although the $l_1$-norm of coherence can be frozen for specific initial states under flip channels, nontrivial universal freezing of coherence is impossible for the dynamics of a single qubit under paradigmatic incoherent maps.

This is not true anymore when considering more than one qubit. Indeed, in analogy with the previous Section, we now show that any bona fide distance-based measure of quantum coherence in the computational basis manifests freezing forever when considering an even number of non-interacting qubits undergoing local bit flip channels (expressed by Eq. (1.14) when $\Xi = F_1$) and being initially in an $\mathcal{M}_N^3$ state that satisfies the following constraint[2].

$$c_2(0) = (-1)^{N/2} c_1(0) c_3(0). \tag{4.5}$$

Due to Theorem 3.4.2, we immediately get that any bona fide distance-based measure of quantum coherence $C^D$ of the evolved $\mathcal{M}_N^3$ state $\varpi(q)$, whose triple is given in Eq. (4.1), is equal to the following distance

$$C^D(\varpi(q)) = D(\{c_1, (-1)^{N/2}(1-q)^N c_1 c_3, (1-q)^N c_3\}, \{0, 0, (1-q)^N c_3\}), \tag{4.6}$$

which is frozen for any $q$, or equivalently for any time $t$, thanks to Theorem 3.4.1, Eq. (3.102).

[2]We focus on bit flip channels $\Lambda^{F_1}$ and coherence in the computational basis for illustration; however, analogous results hold for the other $k$-flip channels $\Lambda^{F_k}$ by considering coherence in the basis consisting of tensor products of eigenstates of $\sigma_{j\neq k}$.

Coming back now to the two specific coherence monotones analysed here [135], we know that the relative entropy of coherence $C_{RE}$ is a bona fide distance-based measure, hence it manifests freezing in the conditions of Eq. (4.5). Interestingly, we also know that the $l_1$-norm of coherence $C_{l_1}$ coincides with (twice) the trace distance of coherence $C^{D_{\mathrm{Tr}}}$ for any $\mathcal{M}_N^3$ state, which implies that $C_{l_1}$ also freezes in the same dynamical conditions.

On the other hand, no universal freezing of coherence is instead possible for $\mathcal{M}_N^3$ states with odd $N$, whose dynamical properties are totally analogous to those of one-qubit states.

A remark is now in order. The freezing conditions presented here for coherence are the same dynamical conditions for which also discord-type quantum correlations freeze up to the threshold time $t^*$ defined by the largest value of $q$ such that $|c_3(q)| \geq |c_1(q)|$, for $\mathcal{M}_N^3$ states evolving under local bit flip channels. We note that for $\mathcal{M}_N^3$ states with $|c_3| \geq |c_1|$, and for any bona fide distance $D$, the distance-based measure of coherence $C^D$ *coincides* with the corresponding distance-based measure of discord-type quantum correlations $Q_{\rightarrow}^D$. Hence, the freezing of coherence might provide a deeper insight into the peculiar phenomenon of frozen quantum correlations under local flip channels (see also [216]), as the latter just reduces to coherence for $t \leq t^*$ under the conditions we identified.

More generally, measures of discord-type correlations [22, 44, 217] may be recast as suitable measures of coherence in multiparticle systems, minimised over the reference basis, with minimisation restricted to local product bases. For instance, the minimum $l_1$-norm of coherence [135] yields the negativity of quantumness [50, 164, 218], the minimum relative entropy of coherence [135] yields the relative entropy of discord [50, 79, 219, 220], and the minimum skew information [203] yields the local quantum uncertainty [221]. Our result suggests therefore that the computational basis is the product basis which minimises coherence (according to suitable bona fide measures) for particular even $N$ $\mathcal{M}_N^3$ states undergoing local bit flip noise $\Lambda^{F_1}$ up to $t \leq t^*$, while coherence is afterwards minimised in the basis consisting of tensor products of eigenstates of $\sigma_1$, which is the pointer basis towards which the system eventually converges due to the local decoherence [222]; similar conclusions can be drawn for the other $k$-flip channels.

Last but not least, let us mention that in Ref. [7] we have experimentally observed the paradigmatic freezing phenomenon of quantum coherence, as well as the above described interplay between the latter and discord-type correlations, in a two-qubit room temperature nuclear magnetic resonance quantum simulator. We defer to Ref. [7] for the details of the experiment.

## 4.3 Frozen entanglement

In Ref. [223] it has been shown that the concurrence of two non-interacting qubits, which are initially in a BD state and undergo a collective dephasing dynamics, can remain frozen during the whole evolution. We conclude this Chapter by showing that also this freezing phenomenon turns out to be universal, in the sense that it is a common feature of any bona fide geometric measure of two-qubit entanglement.

We begin with introducing the aforementioned collective dephasing dynamics. Let us

consider $N$ non-interacting two-level atoms with identical energy splitting $\hbar\omega$ and embedded in a fluctuating homogeneous external field. Such fluctuations turn into an effective dephasing process, the so-called collective dephasing, inducing a probability distribution $p(\omega)$ of the energy splitting of each atom. This entails that the evolved state at time $t$, provided that the field fluctuations time scales are longer than $t$, can be described as follows:

$$\rho(t) = \int p(\omega) U_\omega(t)^{\otimes N} \rho(0) U_\omega^\dagger(t)^{\otimes N} d\omega, \tag{4.7}$$

where $U_\omega(t) = e^{-iH_\omega t/\hbar}$ is a single-qubit unitary generated by the time-independent single-qubit Hamiltonian $H_\omega = (\hbar\omega/2)\mathbf{n}\cdot\boldsymbol{\sigma}$, with $\boldsymbol{\sigma} = \{\sigma_1, \sigma_2, \sigma_3\}$ being the vector of Pauli matrices and $\mathbf{n} = \{n_1, n_2, n_3\}$ a vector of real numbers such that $n_1^2 + n_2^2 + n_3^2 = 1$, which represents the orientation of the external field.

In Ref. [223] it has also been shown that if the initial state $\rho(0)$ is a BD state $\varpi$ with triple $\{c_1, c_2, c_3\}$ contained into the $\{-1,-1,-1\}$-corner of the tetrahedron of BD states, then the evolved state under collective dephasing is still a BD state with same value of $h_\varpi = \frac{1}{2}(\sum_{j=1}^3 |c_j| - 1)$ for any time $t$ and for any orientation $\mathbf{n}$ of the external field. According to Eq.(3.75), this immediately entails that the evolved state always lies in the same surface of constant entanglement as the initial state, an example of which is represented by the cyan surface in Fig. 3.1(d), so that any bona fide geometric measure of two-qubit entanglement remains constant for all times under the above dynamical conditions.

Such extreme resilience of entanglement to noise is rather surprising. Indeed, contrary to discord-type correlations, entanglement has in general proved to be quite fragile against noise, usually undergoing the well-known sudden death [86, 87].

## 4.4 Discussion

Summarising, we have first established from first principles the general character of an intriguing dynamical trait of discord-type correlations, namely their *freezing* under given environmental and initial conditions. This phenomenon manifests for an even number of qubits, initialised in a particular class of $\mathcal{M}_N^3$ states, and undergoing local independent and identical flip channels. In particular, we have shown that, within such dynamical conditions, discord-type quantum correlations manifest freezing whenever the distance adopted to measure them is assumed to be invariant under transposition, dynamically contractive and convex. As these physical properties are instrumental to define valid distance-based measures of correlations, our result means that freezing of quantum correlations occurs independently of the adopted distance and is therefore universal within a *bona fide* geometric approach.

Frozen discord-type correlations have been verified both theoretically [81, 88–91, 213, 224] and experimentally [222, 225–229] by using specific measures of quantum correlations [22, 88], but until now it was an open problem whether all suitable discord-type quantifiers, including potentially new ones yet to be defined, would freeze in the same dynamical conditions. Our work rigorously contributes to the settling of this problem and provides elegant evidence strongly supporting the conclusion that freezing of quantum

correlations is a natural physical phenomenon and not merely a mathematical accident. Notice that freezing in $\mathcal{M}_N^3$ states, as described above, has also been observed for some discord-type measures which do not manifestly enjoy a distance-based definition, such as the local quantum uncertainty [88, 221] and the interferometric power [44]. This leaves some room for further research aimed to prove the occurrence of freezing from only the basic axioms of quantum correlations, possibly without the need to invoke a geometric approach as considered in our work. Alternatively, our result might suggest that all measures of discord could possibly be recast into a geometric form via some *bona fide* distance, at least when restricted to $\mathcal{M}_N^3$ states of an even number of qubits. This is the case, for instance, for the conventional entropic measure of discord [20], which becomes equivalent to the relative entropy-based discord [89] for two-qubit BD states. This would also be an interesting direction to explore, in a more mathematical context of information geometry.

We further remark that, although we have explicitly considered Markovian evolutions in our analysis, the freezing of quantum correlations also occurs in the presence of non-Markovian channels which can be described by a master equation with a memory kernel, as in the case of pure dephasing or decoherence under classical random external fields [91–94, 230]. Indeed, in these cases the dynamics of $\mathcal{M}_N^3$ states can be formally written as in Eq. (4.1), but with $N\gamma t$ replaced by a more general time-dependent rate $\Gamma(t)$. This can give rise to a dynamics with multiple intervals of constant discord [91, 92, 230], or discord frozen forever [94] depending on the initial conditions. By our analysis, we conclude that those fascinating features, which might be observable e.g. in the dynamics of impurity atoms in Bose-Einstein condensates [94, 231], are universal too and manifest when probed by any *bona fide* geometric discord-type measure $Q_{\rightarrow}^{D}$.

From a foundational perspective it is important to understand the deeper physical origin of frozen quantum correlations. There are reasons to reckon that the phenomenon is related to the complementary freezing of *classical* correlations. Typically, as observed so far using specific quantifiers, given particular dynamical and initial conditions as studied here, quantum correlations are initially frozen and classical correlations decay but, after a characteristic time $t^*$, classical correlations freeze and quantum correlations decay [6, 89, 232]. This has been linked to the finite-time emergence of the classical pointer basis within the fundamental theory of decoherence [222, 224, 229, 233]. Nevertheless, classical correlations are still inconsistently defined in geometric approaches [6, 234] and it remains unknown whether they exhibit freezing after $t^*$ for any *bona fide* distance. This is certainly an aspect deserving further investigation.

Then we have shown that an even more fundamental property of quantum systems, namely quantum coherence in a reference basis, can also feature the universal freezing under the same class of local nondissipative decoherence channels and initial states as the ones giving rise to the universal freezing of discord-type correlations, thus revealing an intrinsic physical explanation for the freezing of the latter, by exposing and exploiting the intimate link between these two nonclassical signatures.

We have also shown that there is no general agreement on freezing conditions between specific coherence monotones when considering the case of an odd number of qubits. This highlights the prominent role played by the aforementioned universal freezing conditions in ensuring a durable physical exploitation of coherence, regardless of how it is quantified,

for applications such as quantum metrology [142] and nanoscale thermodynamics [29,235].

Even more, we have seen that such coherence invariance phenomenon is observed experimentally in a two-qubit room temperature nuclear magnetic resonance quantum simulator [7].

Finally, we have shown that under some other dynamical conditions, known as collective dephasing dynamics, even the two-qubit entanglement can manifest the universal freezing phenomenon.

Our results have also an impact from an applicative point of view. The fact of leaving quantum resources unaffected for a given period of time makes the above studied noisy dynamical conditions important for emergent quantum technologies. Despite numerous basic experimental investigations, this resilience has yet to be properly exploited for quantum enhanced protocols e.g. in communication, computation, sensing and metrology. The universality of the freezing phenomenon for geometric measures of quantumness, in the dynamical conditions shown here, promises to motivate further research in this context.

# Chapter 5

# Quantumness and quantum phase transitions

This Chapter collects our results [8, 9] about the role played by quantumness in the quest for a deeper understanding of quantum critical phenomena.

In the study of collective quantum phenomena, the understanding of the ordered phases associated to local order parameters relies on the key concept of spontaneous symmetry breaking. The latter is required to explain the existence of locally inequivalent ground states that are not eigenstates of one or more symmetry operators for the corresponding many-body Hamiltonian [112]. In recent years, knowledge of quantum phase transitions has been sharpened by the application of methods and techniques originally developed in the field of quantum information [95, 236]. Various types of quantum phase transitions have been indeed characterised by identifying the singular points in the derivatives of different measures of bipartite [237, 238] and multipartite entanglement [101, 108]. Moreover, different ordered phases have been identified by looking at the factorisation properties of different ground states [105–107] or by studying the behaviour of the ground-state fidelity under local or global variations of the Hamiltonian parameters [239, 240].

Efforts have been devoted to the investigation of the behaviour of the concurrence [241], multipartite entanglement [101, 108, 242] and of the quantum discord [110, 243] for some specific symmetry-breaking ground states. However, on the whole, the complete understanding of the physical mechanism that selects the symmetry-breaking ground states in the thermodynamic limit remains an open problem [244, 245]. In complete analogy with the case of classical phase transitions driven by temperature, the pedagogical explanation of this phenomenon invokes the unavoidable presence of some local, however small, perturbing external field that selects one of the maximally symmetry-breaking ground states (MSBGSs) among all the elements of the quantum ground space. However, the implicit assumption hidden in this type of reasoning is that the MSBGSs are the most classical ones and thus the ones that are selected in real-world situations.

We promote this assumption to an explicit general conjecture on the nature of ordered quantum phases and the origin of spontaneous symmetry breaking, and we test it by comparing various measures of classicality and quantumness for symmetry-breaking

and symmetry-preserving quantum ground states. We first notice how a naive comparison of pairwise quantum correlations might be misleading to this aim, by showing that in symmetry-preserving ground states the two-body entanglement captures only a modest portion of the total two-body quantum correlations, while in maximally symmetry-breaking ground states it is either unchanged or undergoes an enhancement, in such a way that contributes the largest amount to the total two-body quantum correlations. We then make our conjecture quantitatively precise by properly comparing global properties of quantum ground states and showing that, within the quantum ground space corresponding to ordered phases with nonvanishing local order parameters, the MSBGSs are the most classical ones in the sense that they are the only quantum ground states that satisfy the following two quantitatively precise criteria for each set of Hamiltonian parameters consistent with an ordered quantum phase:

- *Local convertibility* – All ground states are locally convertible into MSBGSs via local operations and classical communication (LOCC), while the reverse transformation is impossible;
- *Entanglement distribution* – The MSBGSs are the only ground states that minimise the residual tangle between a dynamical variable and the rest of the system. Stated otherwise, the MSBGSs are the only ground states that satisfy monogamy of entanglement, a quantum constraint on distributed correlations with no classical counterpart, at its minimum among all other possible ground states.

These two features imply that the mechanism of spontaneous symmetry breaking selects the most classical ground states associated to ordered phases of quantum matter.

Our results are of general validity for all systems that belong to the same universality class of exactly solvable models that are standard prototypes for quantum phase transitions associated to spontaneous symmetry breaking, such as the $XY$ quantum spin models [112].

## 5.1 $XY$ models

The one-dimensional spin-1/2 $XY$ Hamiltonian with ferromagnetic nearest-neighbour interactions in a transverse field with periodic boundary conditions reads [246–250]:

$$H = -\sum_{i=1}^{N} \left[ \left( \frac{1+\gamma}{2} \right) \sigma_i^x \sigma_{i+1}^x + \left( \frac{1-\gamma}{2} \right) \sigma_i^y \sigma_{i+1}^y + h\sigma_i^z \right] , \tag{5.1}$$

where $\sigma_i^\mu$, $\mu = x, y, z$, are the Pauli spin-1/2 operators acting on site $i$, $\gamma$ is the anisotropy parameter in the $xy$ plane, $h$ is the transverse magnetic field, and the periodic boundary conditions $\sigma_{N+1}^\mu \equiv \sigma_1^\mu$ ensure the invariance under spatial translations.

For this class of models, the phase diagram can be determined exactly in great detail [246, 248]. In the thermodynamic limit, for any $\gamma \in (0, 1]$, a quantum phase transition occurs at the critical value $h_c = 1$ of the transverse field. For $h < h_c = 1$ the system is ferromagnetically ordered and is characterised by a twofold ground-state degeneracy such that the $\mathbb{Z}_2$ parity symmetry under inversions along the spin-$z$ direction is broken

by some elements of the ground space. Given the two symmetric ground states, the so-called even $|e\rangle$ and odd $|o\rangle$ states belonging to the two orthogonal subspaces associated to the two possible distinct eigenvalues of the parity operator, any symmetry-breaking linear superposition of the form

$$|g(u,v)\rangle = u|e\rangle + v|o\rangle \tag{5.2}$$

is also an admissible ground state, with the complex superposition amplitudes $u$ and $v$ constrained by the normalisation condition $|u|^2+|v|^2=1$. Taking into account that the even and odd ground states are orthogonal, the expectation values of operators that commute with the parity operator are independent of the superposition amplitudes $u$ and $v$. On the other hand, spin operators that do not commute with the parity may have nonvanishing expectation values on such linear combinations and hence break the symmetry of the Hamiltonian (5.1).

Consider observables $O_S$ that are arbitrary products of spin operators and anti-commute with the parity. Their expectation values in the superposition ground states (5.2) are of the form

$$\langle g(u,v)|O_S|g(u,v)\rangle = uv^*\langle o|O_S|e\rangle + vu^*\langle e|O_S|o\rangle \ . \tag{5.3}$$

Both $\langle o|O_S|e\rangle$ and $\langle e|O_S|o\rangle$ are real and independent of $u$ and $v$ and hence the expectation (5.3) is maximum for $u=\pm v=1/\sqrt{2}$ [248]. These are the values of the superposition amplitudes that realise the maximum breaking of the symmetry and identify the order parameter as well as the MSBGSs.

Besides the quantum critical point, there exists another relevant value of the external magnetic field, that is $h_f = \sqrt{1-\gamma^2}$, the *factorising field*. Indeed, at this value of $h$, the system admits a two-fold degenerate, completely factorised ground state [105–107,251,252].

In order to discuss the entanglement and discord-type correlations of quantum ground states, we consider arbitrary bipartitions $(A|B)$ such that subsystem $A = \{i_1, \ldots, i_L\}$ is any subset made of $L$ spins, and subsystem $B$ is the remainder. Given any global ground state of the total system, the reduced density matrix $\rho_A$ ($\rho_B$) of subsystem $A$ ($B$) can be expressed in general in terms of the $n$-point correlation functions [238]:

$$\rho_A(u,v) = \frac{1}{2^L} \sum_{\mu_1,\ldots,\mu_L} \langle g(u,v)|\sigma_{i_1}^{\mu_1}\cdots\sigma_{i_L}^{\mu_L}|g(u,v)\rangle \sigma_{i_1}^{\mu_1}\cdots\sigma_{i_L}^{\mu_L} \ , \tag{5.4}$$

and analogously for $\rho_B$. All expectations in Eq. (5.4) are associated to spin operators that either commute or anti-commute with the parity along the spin-$z$ direction. Therefore the reduced density matrix $\rho_A$ can be expressed as the sum of a symmetric part $\rho_A^{(s)}$, i.e. the reduced density matrix obtained from $|e\rangle$ or $|o\rangle$, and a traceless matrix $\rho_A^{(a)}$ that includes all the terms that are nonvanishing only in the presence of a breaking of the symmetry:

$$\rho_A(u,v) = \rho_A^{(s)} + (uv^* + vu^*)\rho_A^{(a)} \ . \tag{5.5}$$

Both $\rho_A^{(s)}$ and $\rho_A^{(a)}$ are independent of the superposition amplitudes $u$ and $v$, while the reduced density matrix depends on the choice of the ground state. This implies that the elements of the ground space are not locally equivalent. Explicit evaluation of expectations and correlations in symmetry-breaking ground states in the thermodynamic limit is

challenging even when the exact solution for the symmetric elements of the ground space is available.

We will now sketch a method that allows to overcome this difficulty and whose general validity is not in principle restricted to the particular model considered. In order to obtain $\rho_A^{(s)}$ it is sufficient to transform the spin operators in fermionic ones and then apply Wick's theorem. Such algorithm cannot be applied to spin operators $O_A$, acting on subsystem $A$, that anti-commute with the parity. In order to treat this case we first introduce the symmetric operator $O_A O_{A+r}$, for which, by applying the previous procedure, we can evaluate $\langle e|O_A O_{A+r}|e\rangle$. Then, the desired expectation $\langle e|O_A|o\rangle$ can be computed by exploiting the property of asymptotic factorisation of products of local operators at infinite separation [112, 244, 248] that yields $\langle e|O_A|o\rangle = \sqrt{\lim_{r\to\infty}\langle e|O_A O_{A+r}|e\rangle}$, where the root's sign is fixed by imposing positivity of the density matrix $\rho_A(u,v)$. Having obtained the exact reduced density matrix $\rho_A(u,v)$ for all possible subsystems $A$ and superposition amplitudes $u$ and $v$, we are equipped to investigate the nature of quantum ground states with respect to their properties of classicality and quantumness.

## 5.2 Pairwise quantum correlations

In this Section we analyse the behaviour of one-way discord-type correlations and entanglement between any two spins in infinite XY quantum spin chains both in symmetry-preserving and maximally symmetry-breaking ground states.

### 5.2.1 Symmetry-preserving ground states

We first compare the two-body entanglement of response and the two-body discord of response, as defined in Section 2.3, in symmetry-preserving ground states. For two neighbouring spins, these two quantities are plotted in Fig. 5.1 as functions of the external field $h$ and for different values of the anisotropy $\gamma$. For any intermediate value of $\gamma$, the nearest-neighbour entanglement of response $E_1$ exhibits the following behaviour. If $h < h_f$, $E_1$ decreases until it vanishes at the factorising field $h = h_f$. Otherwise, if $h > h_f$, $E_1$ first increases until it reaches a maximum at some value of $h$ higher than the critical point $h_c = 1$, then it decreases again until it vanishes asymptotically for very large values of $h$ in the paramagnetic phase (saturation). Overall, $E_1$ features two maxima at $h = 0$ and $h > h_c$ and two minima at $h = h_f$ (factorisation) and $h \to \infty$ (saturation). For the Ising model ($\gamma = 1$) the point $h = 0$ corresponds instead to a minimum, since it coincides with the factorising field $h_f = \sqrt{1-\gamma^2}$.

On the other hand, regardless of the value of $\gamma$, the nearest-neighbour discord of response $Q_1$ always features a single maximum. Depending on the value of $\gamma$ such maximum can be either in the ordered phase $h < h_c$ or in the disordered (paramagnetic) phase $h > h_c$, moving towards higher values of $h$ with increasing $\gamma$. Remarkably, $Q_1$ never vanishes at the factorising field, except in the extreme case of $\gamma = 1$. Indeed, at the factorising field $h = h_f$ and for any $\gamma \neq 0, 1$, the symmetry-preserving ground state is not completely factorised but rather is a coherent superposition of the two completely factorised symmetry-breaking

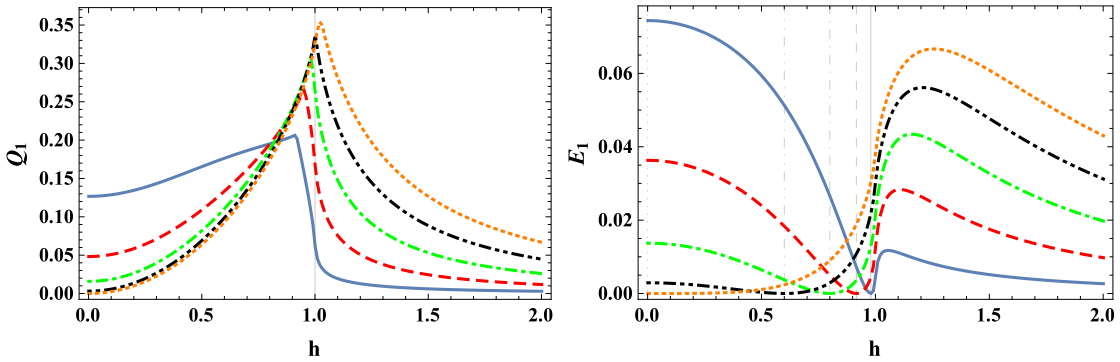


Figure 5.1: Nearest-neighbour trace distance-based discord of response (left panel) and nearest-neighbour trace distance-based entanglement of response (right panel) for symmetry-preserving ground states, in the thermodynamic limit, as functions of the external field $h$, and for different values of the anisotropy $\gamma$. Solid blue curve: $\gamma = 0.2$; dashed red curve: $\gamma = 0.4$; dot-dashed green curve: $\gamma = 0.6$; double-dot-dashed black curve: $\gamma = 0.8$; dotted orange curve: $\gamma = 1$. In the right panel, to each of these curves, there corresponds a vertical line denoting the associated factorising field $h_f$. In the left panel, the solid vertical line denotes the critical field $h_c = 1$.

ground states. Consequently, while the two-body entanglement of response must vanish in accordance with the convex roof extension, the two-body discord of response remains always finite.

When increasing the inter-spin distance $r$, the pairwise entanglement of response $E_r$ and discord of response $Q_r$ behave even more differently (see Fig. 5.2). Due to the monogamy of the squared concurrence [253, 254], $E_r$ dramatically drops to zero as $r$ increases, except in a small region around the factorising field $h = h_f$ that gets smaller and smaller as $r$ increases, in agreement with the findings of Ref. [255]. On the other hand, while in the disordered and critical phases $Q_r$ vanishes as $r$ increases, in the ordered phase $Q_r$ survives even in the limit of infinite $r$. Indeed, in both the disordered and critical phases, and when $r$ goes to infinity, the only non-vanishing one-body and two-body correlation functions in the symmetry-preserving ground states are $\langle \sigma_i^z \rangle$ and $\langle \sigma_i^z \sigma_{i+r}^z \rangle$, so that the two-body reduced state can be written as a classical mixture of eigenvectors of $\sigma_i^z \sigma_{i+r}^z$. On the other hand, in the ordered phase, also the two-body correlation function $\langle \sigma_i^x \sigma_{i+r}^x \rangle$ appears, while $\langle \sigma_i^x \rangle$ vanishes due to symmetry preservation, thus preventing the two-body marginal of the symmetry-preserving ground state from being a mixture of classical states.

### 5.2.2 Maximally symmetry-breaking ground states

Let us move the focus of the comparison between two-body entanglement of response and discord of response from symmetry-preserving to maximally symmetry-breaking ground states. Spontaneous symmetry breaking manifests itself in the thermodynamic limit, in the ordered phase $h < h_c = 1$ and for any non zero anisotropy $\gamma$, so that hereafter we will restrict the region of the phase space under investigation accordingly.

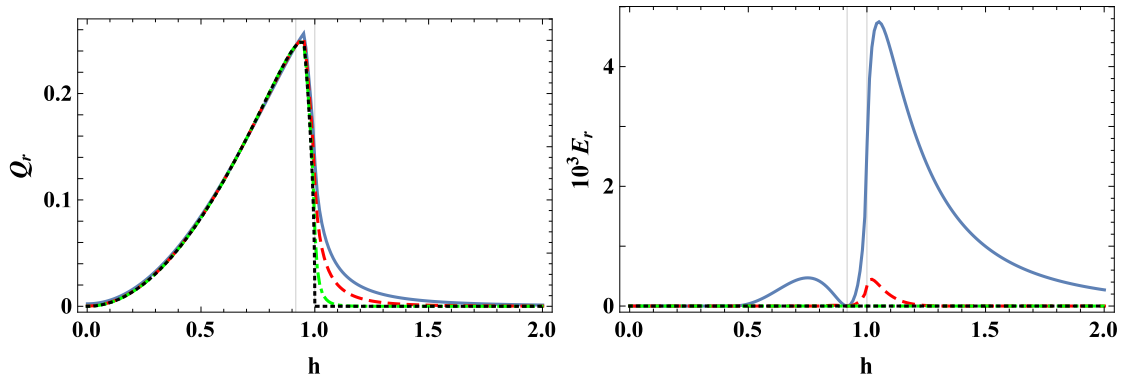


Figure 5.2: Two-body trace distance-based discord of response (left panel) and two-body trace distance-based entanglement of response (right panel) for symmetry-preserving ground states, in the thermodynamic limit, as functions of the external field $h$, in the case of $\gamma = 0.4$, for different inter-spin distances $r$. Solid blue curve: $r = 2$; dashed red curve: $r = 3$; dot-dashed green curve: $r = 8$; dotted black curve: $r = \infty$. In both panels, the two solid vertical lines correspond, respectively, to the factorising field (left) and to the critical field (right).

Fig. 5.3 shows that, as soon as symmetry breaking is taken into account, only the two-body discord of response is affected by symmetry breaking at the critical point $h_c = 1$. In fact, according to Ref. [241], the concurrence and, consequently, the two-body entanglement of response, attain the same value for any $h \geq h_f$ both in the symmetry-preserving and maximally symmetry-breaking ground states. Otherwise, if $h < h_f$, there is a slight enhancement in the pairwise entanglement of response in the maximally symmetry-breaking ground states compared to the corresponding symmetry-preserving ones. Conversely, in general, the pairwise discord of response undergoes a dramatic suppression in the entire ordered phase $h < h_c$ when moving from symmetry-preserving to maximally symmetry-breaking ground states.

Considering the dependence on the inter-spin distance, we observe that the pairwise discord of response loses its long-range nature when moving from symmetry-preserving to maximally symmetry-breaking ground states (see Fig. 5.4). More precisely, both the pairwise entanglement of response and the pairwise discord of response vanish asymptotically with increasing inter-spin distance. In the case of the pairwise entanglement of response, this result is again due to the monogamy of the squared concurrence [253, 254]. In the case of the pairwise discord of response, it is instead due to the fact that not only the correlation function $\langle \sigma_i^x \sigma_{i+r}^x \rangle$ but also $\langle \sigma_i^x \rangle$ and $\langle \sigma_i^x \sigma_{i+r}^z \rangle$ are nonvanishing in the limit of infinite inter-spin distance $r$. This feature allows to write any two-spin reduced density matrix obtained from the symmetry-breaking ground states as a classical mixture of eigenvectors of $O_i O_{i+r}$, where $O_i$ is an Hermitian operator defined on the $i$-th site as $O_i = \cos\beta\sigma_i^z + \sin\beta\sigma_i^x$ with $\tan\beta = \frac{\langle \sigma_i^x \rangle}{\langle \sigma_i^z \rangle}$.

Overall, in symmetry-preserving ground states the two-body entanglement captures

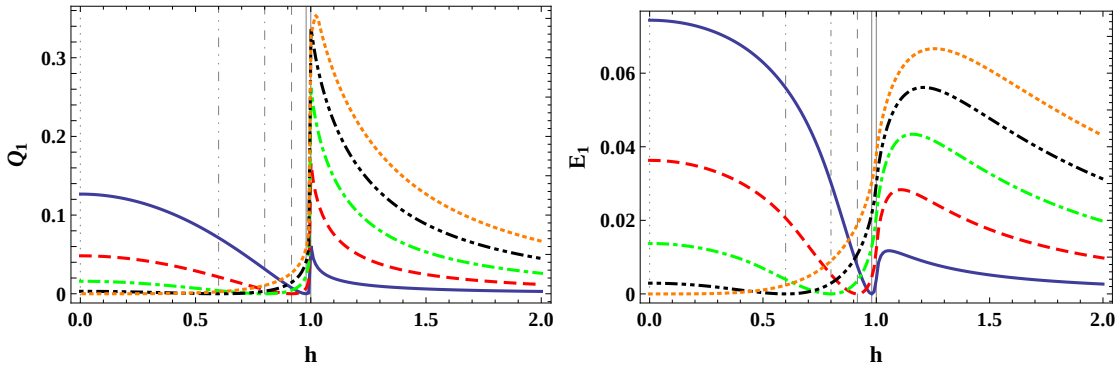


Figure 5.3: Nearest-neighbour trace distance-based discord of response (left panel) and nearest-neighbour trace distance-based entanglement of response (right panel) in maximally symmetry-breaking ground states as functions of the external field $h$, for different values of the anisotropy $\gamma$. Solid blue curve: $\gamma = 0.2$; dashed red curve: $\gamma = 0.4$; dot-dashed green curve: $\gamma = 0.6$; double-dot-dashed black curve: $\gamma = 0.8$; dotted orange curve: $\gamma = 1$. In both panels, to each of these curves, there corresponds a vertical line denoting the associated factorising field $h_f$. The rightmost vertical line denotes the critical point.

only a modest portion of the total two-body quantum correlations, while in maximally symmetry-breaking ground states it is either unchanged or undergoes an enhancement, in such a way that contributes the largest amount to the total two-body quantum correlations. The analysis of pairwise quantum correlations is thus misleading in the quest for a quantitative criterion for the classicality of the MSBGSs among all ground states in the ordered phase.

## 5.3 Global properties of quantum correlations

We now investigate the nature of quantum ground states in the ordered phase with respect to the properties of local convertibility and entanglement distribution.

### 5.3.1 Local convertibility

We begin by studying the property of local convertibility of quantum ground states in an ordered phase. In general, given two pure bipartite quantum states, $|\psi_1\rangle$ and $|\psi_2\rangle$, we say that $|\psi_1\rangle$ is locally convertible into $|\psi_2\rangle$ if $|\psi_1\rangle$ can be transformed into $|\psi_2\rangle$ by using only local quantum operations and classical communication (LOCC), and the aid of an ancillary entangled system [256, 257].

This concept of local convertibility can be formalised in terms of the entire hierarchy of the Rényi entanglement entropies $S_\alpha(\rho_A) = \frac{1}{1-\alpha}\log_2\left[Tr(\rho_A^\alpha)\right]$ of the reduced density operator of subsystem $A$, which provides a complete characterisation of the entanglement spectrum and its scaling behaviour in different quantum phases [258]. The necessary and sufficient conditions for a bipartite state $|\psi_1\rangle$ to be locally convertible to another state

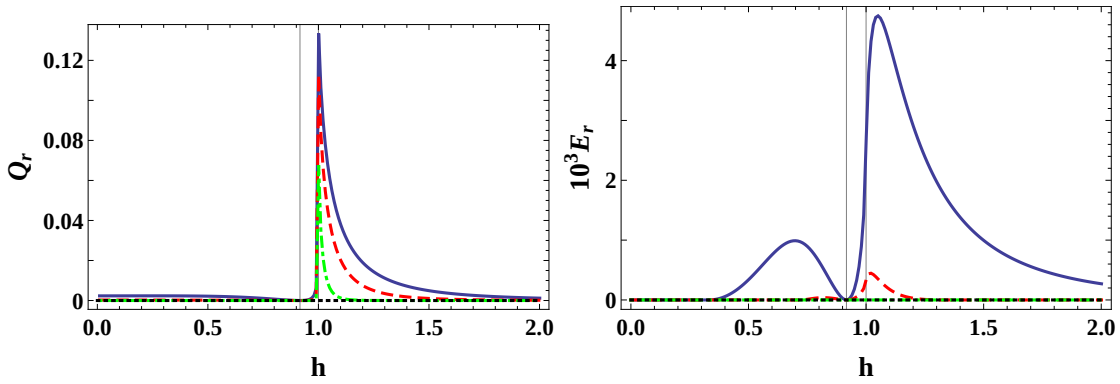


Figure 5.4: Two-body trace distance-based discord of response (left panel) and two-body trace distance-based entanglement of response (right panel) in maximally symmetry-breaking ground states as functions of the external field $h$, at $\gamma = 0.4$, for different inter-spin distances $r$. Solid blue curve: $r = 2$; dashed red curve: $r = 3$; dot-dashed green curve: $r = 8$; dotted black curve: $r = \infty$. In both panels, the two solid vertical lines correspond, respectively, to the factorising field (left) and to the critical field (right).

$|\psi_2\rangle$ is that the inequality $S_\alpha(\psi_1) \geq S_\alpha(\psi_2)$ holds for all bipartitions and all $\alpha > 0$ [259]. Local convertibility has been recently applied to the characterisation of topological order and the computational power of different quantum phases [260–262].

It was previously shown that symmetric ground states are always locally convertible among themselves for $h_f < h < h_c$, and never for $h < h_f < h_c$ [258]. Here, thanks to the general methods developed in Section 5.1, we are able to investigate the local convertibility property of *all* quantum ground states in the ordered phase. In Fig. 5.5 we report the behaviour of the Rényi entropies $S_\alpha$ as functions of the different ground states for a bipartition of the system in which subsystem $A$ is made of $\ell$ contiguous spins, while in Fig. 5.6 we report it for subsystem $A$ made of two spins with various inter-spin distances.

We observe that the MSBGSs are the ground states characterised by the smallest value of all Rényi entropies, independently of the size $\ell$ of the subsystem and of the inter-spin distance $r$. Therefore, all elements in the ground space are always locally convertible to a MSBGS, while the opposite is impossible. This first quantitative criterion for classicality is thus satisfied only by MSBGSs.

### 5.3.2 Entanglement distribution

We now compare symmetry-breaking and symmetry-preserving ground states with respect to entanglement distribution. The monogamy inequality quantifies in a simple and direct way the limits that are imposed on how bipartite entanglement may be distributed among many parties [253, 254]. For a given system of $N$ 1/2-spins it reads:

$$\tau(i|N-1) \geq \sum_{j \neq i} \tau(i|j) \qquad \forall\, i\ . \tag{5.6}$$

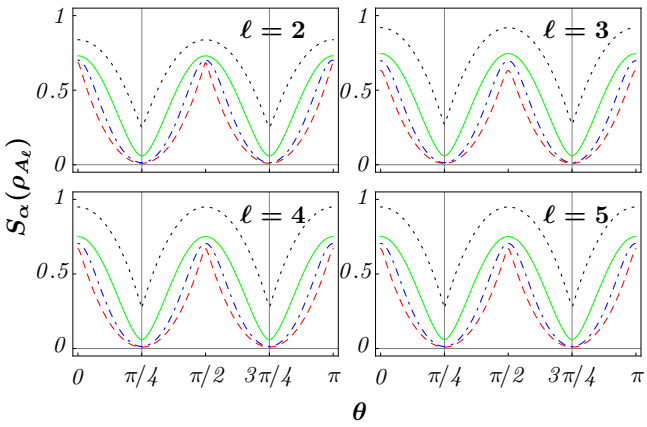


Figure 5.5: Behaviour of the Rényi entropies $S_\alpha(\rho_A)$ as functions of the different ground states in the ordered phase, $h < h_c$, in the case of a subsystem $A_\ell$ made of $\ell$ contiguous spins. Each line stands for a different value of $\alpha$. Black dotted line: $\alpha = 0.5$. Green solid line: $\alpha \to 1^+$ (von Neumann entropy). Blue dot-dashed line: $\alpha = 3$. Red dashed line: $\alpha \to \infty$. The different ground states are parameterised by the superposition amplitudes $u = \cos(\theta)$ and $v = \sin(\theta)$. The two vertical lines correspond to the two MSBGSs, respectively obtained for $\theta = \pi/4$ and $\theta = 3\pi/4$. The Hamiltonian parameters are set at the intermediate values $\gamma = 0.5$ and $h = 0.5$. Analogous behaviours are observed for different values of the anisotropy and external field.

In the above expression, $\tau = C^2$ is known as the tangle, where $C$ is the concurrence [163, 263]; the sum in the r.h.s. runs over all $N-1$ spins excluding spin $i$. The l.h.s. quantifies the bipartite entanglement between one particular, arbitrarily chosen, spin in the collection (reference spin $i$) and all the remaining $N-1$ spins. The r.h.s. is the sum of all the pairwise entanglements between the reference spin and each of the remaining $N-1$ spins. The inequality implies that entanglement cannot be freely distributed among multiple quantum parties $N \geq 3$, a constraint of quantum origin with no classical counterpart.

The residual tangle $\tilde{\tau}$ is the positive semi-definite difference between the l.h.s and the r.h.s in Eq. (5.6). It measures the amount of entanglement not quantifiable as elementary bipartite spin-spin entanglement. Its minimum value compatible with monogamy provides yet another quantitative criterion for classicality.

Specialising, for simplicity but without loss of generality, to translationally-invariant $XY$ spin systems in magnetically ordered phases, since the expectation value of $\sigma_i^y$ vanishes on every element of the ground space, the expressions of the tangle $\tau$ and the residual tangle $\tilde{\tau}$ for any arbitrarily chosen spin in the chain read, respectively,

$$\tau = 1 - m_z^2 - (u^* v + v^* u)^2 m_x^2 \,, \tag{5.7}$$

$$\tilde{\tau} = \tau - 2\sum_{r=1}^{\infty} C_r^2(u,v) \geq 0 \,, \tag{5.8}$$

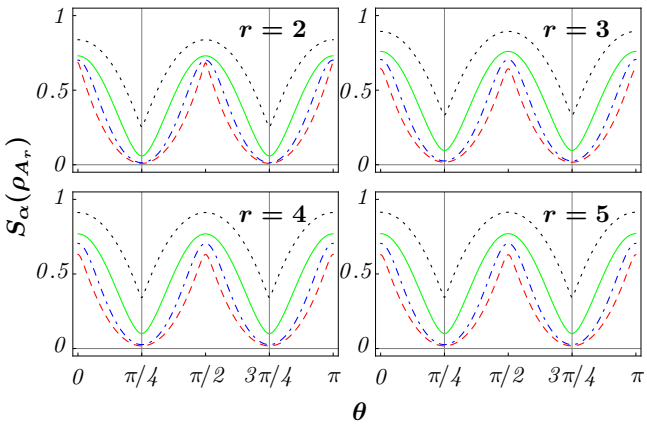


Figure 5.6: Behaviour of the Rényi entropies $S_\alpha(\rho_A)$ as functions of the different ground states in the ordered phase, $h < h_c$, in the case of a subsystem $A_r$ made by two spins, for different inter-spin distances $r$. Each line stands for a different value of $\alpha$. Black dotted line: $\alpha = 0.5$. Green solid line: $\alpha \to 1^+$ (von Neumann entropy). Blue dot-dashed line: $\alpha = 3$. Red dashed line: $\alpha \to \infty$. The different ground states are parameterised by the superposition amplitudes $u = \cos(\theta)$ and $v = \sin(\theta)$. The two vertical lines correspond to the two MSBGSs, respectively obtained for $\theta = \pi/4$ and $\theta = 3\pi/4$. The Hamiltonian parameters are set at the intermediate values $\gamma = 0.5$ and $h = 0.5$. Analogous behaviours are observed for different values of the anisotropy and external field.

where $m_z = \langle e|\sigma_i^z|e\rangle = \langle o|\sigma_i^z|o\rangle$ is the on-site magnetisation along $z$, the order parameter $m_x = \langle e|\sigma_i^x|o\rangle = \sqrt{\lim_{r\to\infty} \langle e|\sigma_i^x \sigma_{i+r}^x|e\rangle}$, and $C_r(u,v)$ stands for the concurrence between two spins at a distance $r$ when the system is in any one of the possible ground states $|g(u,v)\rangle$, Eq. (5.2).

As already mentioned, by comparing the symmetric ground states with the MSBGSs, the spin-spin concurrence is larger in the MSBGSs [241] if $h < h_f < h_c$, where $h_f = \sqrt{1-\gamma^2}$ is the factorising field, while for $h_f < h < h_c$ they are equal. In fact, we have verified that these two results are much more general. We have compared all ground states (symmetric, partially symmetry breaking, and MSBGSs) and we have found that for $h < h_f < h_c$ the spin-spin concurrences are maximum in the MSBGSs for all values of the inter-spin distance $r$, while for $h_f < h < h_c$ and for all values of $r$ they are independent of the superposition amplitudes $u$ and $v$ and thus acquire the same value irrespective of the chosen ground state. Finally, it is immediate to see that the third term in the r.h.s. of Eq. (5.7) is maximised by the two MSBGSs. Collecting all these results, it follows that the residual tangle is minimised by the two MSBGSs and therefore also this second quantitative criterion for classicality is satisfied only by MSBGSs.

## 5.4 Discussion

Summarising, we have investigated the classical nature of quantum ground states associated to ordered phases and spontaneous symmetry breaking. We have introduced two independent quantitative criteria of classicality based on local convertibility between pure quantum states and monogamy of entanglement and entanglement sharing. We have found that maximally symmetry-breaking ground states (MSBGSs) are the most classical among all possible ground states according to these two criteria.

These findings lend a strong quantitative support to the intuitive idea that the physical mechanism which selects the MSBGSs among all possible ground states is due to the unavoidable presence of environmental perturbations, such as local fields, which in real-world experiments necessarily drive the system onto the most classical among the possible ground states. This reasoning is strengthened by the fact that local perturbations may be described by LOCC and for each set of parameters consistent with an ordered phase all ground states are always locally convertible into the MSBGSs.

# Chapter 6

# Generalised geometric quantum speed limits

In this Chapter we review our results obtained in Ref. [10] and regarding quantum speed limits (QSLs). We begin by briefly outlining what is known about QLSs. Then we construct a new fundamental family of geometric QSLs (see Fig. 6.1) which is in one to one correspondence with the family of contractive Riemannian metrics characterised by the Morozova, Čencov and Petz theorem. Finally, we demonstrate how such non uniqueness of a bona fide measure of distinguishability defined on the quantum state space affects the QSLs and can be exploited in order to look for tighter bounds.

Our approach is general enough to provide a unified picture, encompassing both unitary and nonunitary dynamics, and is easy to handle, requiring solely the spectral decomposition of the evolved state. This family of bounds is also naturally tailored to the general case of initial mixed states and clearly separates the contribution of the populations of the evolved state and the coherences of its time variation, thus clarifying their individual role in driving the evolution. Furthermore, we formulate in rigorous terms the problem of identifying the tightest bound within our family for any given dynamics. While such a problem is infeasibly hard to address in general, we establish concrete steps towards its solution in practical scenarios. Specifically, we show explicit instances of QSLs which make use of some particular contractive Riemannian metric such as the Wigner-Yanase skew information and can be provably tighter than the corresponding QSLs obtained with the conventional quantum Fisher information.

## 6.1 Quantum speed limits

The attempt to gain a theoretical understanding of the concept of time in quantum mechanics has triggered significant progress towards the search for faster and more efficient quantum technologies. One of such advances consists in the interpretation of the time-energy uncertainty relations as lower bounds for the minimal evolution time between two distinguishable states of a quantum system, also known as quantum speed limits.

In a seminal work, Mandelstam and Tamm (MT) [264, 265] reported a QSL for a

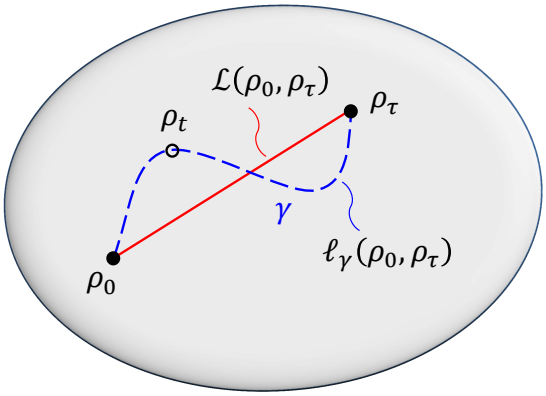


Figure 6.1: Illustration of geometric quantum speed limits. The dashed blue curve is the path $\gamma$ in the quantum state space representing a generic evolution between an initial state $\rho_0$ and a final state $\rho_\tau$, parameterised by time $t \in [0, \tau]$. Given a metric on the quantum state space, the length of this path is denoted by $\ell_\gamma(\rho_0, \rho_\tau)$. The solid red curve denotes the geodesic connecting $\rho_0$ to $\rho_\tau$, whose length is given by $\mathcal{L}(\rho_0, \rho_\tau)$. Quantum speed limits originate from the fact that the geodesic amounts to the path of shortest length among all physical evolutions between the given initial and final states, $\mathcal{L}(\rho_0, \rho_\tau) \leq \ell_\gamma(\rho_0, \rho_\tau)$ $\forall\gamma$. Indeed such inequality can be interpreted as follows. For any given physical evolution $\gamma$ from $\rho_0$ to $\rho_\tau$, and according to any valid metric, the most the final state $\rho_\tau$ can be distant from the initial one $\rho_0$ is the length of the path $\ell_\gamma(\rho_0, \rho_\tau)$ followed by the system. The ensuing minimal time necessary for this distance to reach a chosen value is the time at which the path length reaches this value. This interpretation provides a neat criterion for the saturation of the lower bound on the evolution time, that is when the dynamical evolution coincides with a geodesic of the considered metric. We establish a general family of geometric quantum speed limits with respect to an infinite hierarchy of contractive Riemannian metrics on the space of quantum states, unifying and extending previous results under an information geometric framework.

quantum system that evolves between two distinguishable pure states, $|\psi(0)\rangle$ and $|\psi(\tau)\rangle$, via a unitary dynamics generated by a time independent Hamiltonian $H$. The ensuing lower bound on the evolution time is given by $\tau \geq \hbar \arccos(|\langle\psi(\tau)|\psi(0)\rangle|)/\Delta E$, where $(\Delta E)^2 = \langle H^2\rangle - \langle H\rangle^2$ is the variance of the energy of the system with respect to the initial state. Several years later, Anandan and Aharanov [266] extended the MT bound to time dependent Hamiltonians by using a geometric approach which exploits the Fubini-Study metric defined on the space of quantum pure states. Specifically, they simply used the fact that the geodesic length between two distinguishable pure states according to the Fubini-Study metric, i.e. their Bures angle, is a lower bound to the length of any path connecting the same states. Over half a century after the MT result, Margolus and Levitin (ML) [267] provided a different QSL on the time evolution of a closed system whose Hamiltonian is time independent and evolving between two orthogonal pure states. This bound reads as

$\tau \geq \pi\hbar/(2E)$, where $E = \langle H \rangle$ is the ground state mean energy. Although the ML bound is tight, it does not recover the MT one whatsoever. Therefore, the quantum speed limit for unitary dynamics, when restricting to orthogonal pure states, can be made tighter by combining these two independent results as $\tau \geq \max\{\pi\hbar/(2\Delta E), \pi\hbar/(2E)\}$ [268].

All these results attracted a considerable interest in the subject. Giovannetti *et al.* [269] extended the ML QSL to the case of arbitrary mixed states and also showed that entanglement can speed up the dynamical evolution of a closed composite system. A plethora of other extensions and applications of QSLs for unitary processes has been investigated [119]. For example, in Ref. [270] it has been recently shown that the rate of change of the distinguishability between the initial and the evolved state of a closed quantum system can provide a lower bound for an indicator of quantum coherence based on the Wigner-Yanase information between the evolved state and the Hamiltonian generating the evolution.

Since any information processing device is inevitably subject to environmental noise, QSLs have been also investigated in the nonunitary realm. Taddei *et al.* [271] and del Campo *et al.* [272] were the first to extend the MT bound to any physical process, being it unitary or not. Specifically, Ref. [271] exploits the quantum Fisher information metric on the whole quantum state space and represents a natural extension of the idea used in Ref. [266], whereas Ref. [272] exploits the relative purity. Then, Deffner and Lutz [273] extended the ML bound to open quantum systems by adopting again a geometric approach using the Bures angle. These authors have also introduced a new sort of bound, which is tighter than both the ML and MT ones, and shown that non-Markovianity can speed up the quantum evolution. Some other works have then provided a QSL for open system dynamics by using the relative purity, whose usefulness ranges from thermalisation phenomena [274] to the relativistic effects on the QSL [275]. Further developments include the role of entanglement in QSL for open dynamics [276–278], QSL in the one-dimensional perfect quantum state transfer [121], and the experimental realisability of measuring QSLs through interferometry devices [279]. Finally, a subtle connection was recently highlighted between QSLs and the maximum interaction speed in quantum spin systems [280], with implications for the horizon problem in cosmology.

## 6.2 Generalised Geometric Quantum speed limits

In this Section we derive the aforementioned family of geometric QSLs. The most general dynamical evolution of an initial state $\rho_0$ can be written in the Kraus decomposition as $\rho_\lambda = \mathcal{E}_\lambda[\,\rho_0] = \sum_j K_j^\lambda\, \rho_0 K_j^{\lambda\dagger}$, where $\{K_j^\lambda\}$ are operators satisfying $\sum_j K_j^{\lambda\dagger} K_j^\lambda = \mathbb{I}$ and depending on a set $\lambda = \{\lambda_1, \lambda_2, \ldots, \lambda_r\}$ of $r$ parameters which are encoded into the input state $\rho_0$, in such a way that $\rho_\lambda$ depends analytically on each parameter $\lambda_\mu$ ($\mu = 1, \ldots, r$). In the unitary case, the evolution is given in particular by $\mathcal{E}_\lambda[\,\rho_0] = U_\lambda\, \rho_0 U_\lambda^\dagger$, where $U_\lambda$ is a multiparameter family of unitary operators, fulfilling $U_\lambda U_\lambda^\dagger = U_\lambda^\dagger U_\lambda = \mathbb{I}$. In this case, the observables $H_\mu^\lambda = -i\hbar U_\lambda\, \partial_\mu U_\lambda^\dagger$, with $\partial_\mu \equiv \partial/\partial\lambda_\mu$, are the generators driving the dynamics.

Consider a dynamical evolution $\rho_\lambda$ in which the set of parameters $\lambda$ is changed analytically from the initial configuration $\lambda_I$ to the final one $\lambda_F$. Geometrically, this evolution draws a path $\gamma$ in the quantum state space connecting $\rho_{\lambda_I}$ and $\rho_{\lambda_F}$ whose length is given

by the line integral $\ell_\gamma^f = \int_\gamma ds$ and depends on the chosen contractive Riemannian metric $\mathbf{g}^f$ (see Fig. 6.1). Since $\gamma$ is an arbitrary path between $\rho_{\lambda_I}$ and $\rho_{\lambda_F}$, its length need not be the shortest one, which is instead given by the geodesic length $\mathcal{L}^f(\rho_{\lambda_I}, \rho_{\lambda_F})$ between $\rho_{\lambda_I}$ and $\rho_{\lambda_F}$. Therefore the latter represents a lower bound for the length of the path drawn by the above dynamical evolution. This observation will play a crucial role in the imminent derivation of our family of QSLs, in analogy with Refs. [266] and [271].

Since the density operator $\rho_\lambda$ evolves analytically with respect to the parameters $\lambda$, we can write

$$d\rho_\lambda = \sum_{\mu=1}^{r} \partial_\mu \rho_\lambda \, d\lambda_\mu. \tag{6.1}$$

Let $\rho_\lambda = \sum_j p_j |j\rangle\langle j|$ be the spectral decomposition of $\rho_\lambda$, with $0 < p_j \leq 1$ and $\sum_j p_j = 1$. We note that both the eigenvalues $p_j$ and eigenstates $|j\rangle$ of $\rho_\lambda$ may depend on the set of parameters $\lambda$, i.e. $p_j \equiv p_j(\lambda)$ and $|j\rangle \equiv |j(\lambda)\rangle$, so that

$$\partial_\mu \rho_\lambda = \sum_j \{(\partial_\mu p_j)|j\rangle\langle j| + p_j[(\partial_\mu |j\rangle)\langle j| + |j\rangle(\partial_\mu \langle j|)]\} \ , \tag{6.2}$$

and thus

$$\langle j|\partial_\mu \rho_\lambda|l\rangle = \delta_{jl}\partial_\mu p_j + (p_l - p_j)\langle j|\partial_\mu|l\rangle \ , \tag{6.3}$$

where we used the identity $(\partial_\mu\langle j|)|l\rangle = -\langle j|\partial_\mu|l\rangle$. Combining Eq. (6.1) and Eq. (6.3), we get

$$\langle j|d\rho_\lambda|l\rangle = \sum_{\mu=1}^{r} [\delta_{jl}\partial_\mu p_j + i(p_j - p_l)\mathcal{A}_{jl}^\mu] d\lambda_\mu \ , \tag{6.4}$$

where we define $\mathcal{A}_{jl}^\mu := i\langle j|\partial_\mu|l\rangle$. By using Eq. (6.4), in the case of $j = l$ we get

$$|\langle j|d\rho_\lambda|j\rangle|^2 = \sum_{\mu,\nu=1}^{r} \partial_\mu p_j \partial_\nu p_j \, d\lambda_\mu d\lambda_\nu, \tag{6.5}$$

whereas in the case of $j \neq l$, by using the fact that $d\rho_\lambda$ is hermitian, we obtain

$$|\langle j|d\rho_\lambda|l\rangle|^2 = \sum_{\mu,\nu=1}^{r} (p_j - p_l)^2 \mathcal{A}_{jl}^\mu \mathcal{A}_{lj}^\nu \, d\lambda_\mu d\lambda_\nu \ . \tag{6.6}$$

Finally, by substituting Eq. (6.5) and Eq. (6.6) into Eq. (2.13), the squared infinitesimal length $ds^2$ between $\rho_\lambda$ and $\rho_\lambda + d\rho_\lambda$ according to any contractive Riemannian metric $\mathbf{g}^f$ becomes

$$ds^2 = \sum_{\mu,\nu=1}^{r} g_{\mu\nu}^f d\lambda_\mu d\lambda_\nu \ , \tag{6.7}$$

where

$$g_{\mu\nu}^f = \mathcal{F}_{\mu\nu} + \mathcal{Q}_{\mu\nu}^f \ , \tag{6.8}$$

with

$$\mathcal{F}_{\mu\nu} = \frac{1}{4}\sum_j \frac{\partial_\mu p_j \partial_\nu p_j}{p_j} \ , \tag{6.9}$$

and

$$\mathcal{Q}^f_{\mu\nu} = \frac{1}{2}\sum_{j<l} c^f(p_j, p_l)(p_j - p_l)^2 \mathcal{A}^\mu_{jl}\mathcal{A}^\nu_{lj} \ , \tag{6.10}$$

referring to, respectively, the contribution of the populations of $\rho_\lambda$ and of the coherences of $d\rho_\lambda$ to the contractive Riemannian metric $g^f_{\mu\nu}$. Hereafter we restrict to the case where the parameters $\lambda$ are time-dependent, $\lambda_\mu = \lambda_\mu(t)$, for $\mu = 1, \ldots, r$, and choose the parametrisation $t \in [0, \tau] \to \lambda(t)$ such that $\lambda_I = \lambda(0)$ and $\lambda_F = \lambda(\tau)$, where $\tau$ is the evolution time. Now, being the geodesic distance $\mathcal{L}^f(\rho_0, \rho_\tau)$ between the initial and final state, $\rho_0$ and $\rho_\tau$, a lower bound to the length $\ell^f_\gamma(\rho_0, \rho_\tau) = \int_\gamma ds = \int_0^\tau dt\,(ds/dt)$ of the path $\gamma$ followed by the evolved state $\rho_t$ when going from $\rho_0$ to $\rho_\tau$, we have

$$\mathcal{L}^f(\rho_0, \rho_\tau) \leq \ell^f_\gamma(\rho_0, \rho_\tau) \ , \tag{6.11}$$

where

$$\ell^f_\gamma(\rho_0, \rho_\tau) := \int_0^\tau \left(\frac{ds}{dt}\right) dt = \int_0^\tau dt \sqrt{\sum_{\mu,\nu=1}^r g^f_{\mu\nu} \frac{d\lambda_\mu}{dt}\frac{d\lambda_\nu}{dt}} \ . \tag{6.12}$$

Equation (6.11) represents the anticipated infinite family of generalised geometric QSLs. Any possible contractive Riemannian geometry on the quantum state space, and so any possible bona fide geometric quantifier of distinguishability between quantum states, gives rise to a different QSL. More precisely, we have that both the geodesic distance appearing in the left hand side and the quantity $\ell^f_\gamma(\rho_0, \rho_\tau)$ being in the right hand side of Eq. (6.11) depend on the chosen contractive Riemannian metric, specified by the MC function $f$. In particular, by restricting to the celebrated quantum Fisher information metric we recover exactly the QSL introduced in Ref. [271].

It is intuitively clear that the contractive Riemannian metric whose geodesic is most tailored to the given dynamical evolution is the one that gives rise to the tightest lower bound to the evolution time as expressed in Eq. (6.11). In order to determine how much a certain geometric QSL is saturated, i.e. its *tightness*, we will consider the relative difference

$$\delta^f_\gamma := \frac{\ell^f_\gamma(\rho_0, \rho_\tau) - \mathcal{L}^f(\rho_0, \rho_\tau)}{\mathcal{L}^f(\rho_0, \rho_\tau)}, \tag{6.13}$$

that quantifies how much the dynamical evolution $\gamma$ differs from a geodesic with respect to the considered metric $\mathbf{g}^f$.

By minimising the quantity $\delta^f_\gamma$ over all contractive Riemannian metrics, i.e., over all MC functions $f$, one can in principle identify the tightest geometric QSL, of the form given in Eq. (6.11), for any given dynamics $\gamma$. Formally, labelling by $f^\star_\gamma$ the optimal metric for the dynamics $\gamma$, the tightest possible geometric QSL is therefore defined by

$$\mathcal{L}^{f^\star_\gamma}(\rho_0, \rho_\tau) \leq \ell^{f^\star_\gamma}_\gamma(\rho_0, \rho_\tau) \ , \quad \text{with} \quad f^\star_\gamma \,\big|\, \inf_f \delta^f_\gamma \equiv \delta^{f^\star_\gamma}_\gamma \ , \tag{6.14}$$

where the minimisation is over all MC functions $f$. Finding this minimum is, however, a formidable problem, which is made all the more difficult by the fact that the quantum Fisher information metric and the Wigner-Yanase information metric are the only contractive Riemannian metrics whose geodesic lengths are analytically known for general dynamics.

Nevertheless, in this paper we will move the first steps forward towards addressing such general problem, by restricting the optimisation in Eq. (6.14) over these two paradigmatic and physically significant examples of contractive Riemannian metrics, namely the quantum Fisher information and the Wigner-Yanase skew information. Quite remarkably, this restriction will be enough to reveal how the choice of the quantum Fisher information metric, though ubiquitous in the existing literature, is only a special case which does not always provide the tightest lower bound. On the contrary, we will show how the Wigner-Yanase skew information metric can systematically produce tighter bounds in a number of situations of practical relevance for quantum information and quantum technologies, in particular in open system evolutions.

## 6.3 Examples

In this section we will apply our general formalism to present and analyse QSLs based primarily on the quantum Fisher information and the Wigner-Yanase skew information in a selection of unitary and nonunitary physical processes. This will serve the purpose to illustrate how the choice of a particular bona fide geometric measure of distinguishability on the quantum state space affects the QSLs, therefore providing a guidance to exploit the freedom in this choice to obtain the tightest bounds in practical scenarios.

### 6.3.1 Unitary dynamics

We start by restricting to a closed quantum system, so that our initial state $\rho_0$ undergoes a unitary evolution $\rho_\lambda = U_\lambda \rho_0 U_\lambda^\dagger$. Since the eigenvalues $p_j$ of a unitarily evolving state are constant, $\partial_\mu p_j = 0$, we have that $\mathcal{F}_{\mu\nu} = 0$, and thus $g^f_{\mu\nu} = \mathcal{Q}^f_{\mu\nu}$, along the curve $\gamma$ drawn by the evolved state $\rho_\lambda$. In other words, the coherences of $d\rho_\lambda$ drive the evolution of a closed quantum system. Moreover, one can easily see that $\mathcal{A}^\mu_{jl} = (1/\hbar)\langle j|\Delta H^\lambda_\mu|l\rangle$, where $\Delta H^\lambda_\mu = H^\lambda_\mu - \langle H^\lambda_\mu\rangle$, $\langle H^\lambda_\mu\rangle = \mathrm{Tr}(\rho_\lambda H^\lambda_\mu)$, and $H^\lambda_\mu = -i\hbar U_\lambda\, \partial_\mu U^\dagger_\lambda$ are the generators of the dynamics, so that

$$g^f_{\mu\nu} = \frac{1}{2\hbar^2}\sum_{j<l} c^f(p_j,p_l)(p_j-p_l)^2 \langle j|\Delta H^\lambda_\mu|l\rangle\langle l|\Delta H^\lambda_\nu|j\rangle \ . \tag{6.15}$$

In the following subsections we will focus on, respectively, the quantum Fisher information metric and the Wigner-Yanase information metric.

**Quantum Fisher information metric**

The quantum Fisher information metric corresponds to the MC function $f(t) = 2t/(1+t)$, so that $c^f(x,y) = 2/(x+y)$ and Eq. (6.15) becomes

$$g^{QF}_{\mu\nu} = \frac{1}{2\hbar^2}\sum_{j,l}\frac{(p_j - p_l)^2}{p_j + p_l}\langle j|\Delta H^\lambda_\mu|l\rangle\langle l|\Delta H^\lambda_\nu|j\rangle \ . \tag{6.16}$$

Moreover, by using the following straightforward inequality

$$\frac{(p_j - p_l)^2}{p_j + p_l} \leq p_j + p_l \ , \tag{6.17}$$

we get

$$g^{QF}_{\mu\nu} \leq \frac{1}{2\hbar^2}\sum_{j,l}(p_j + p_l)\langle j|\Delta H^\lambda_\mu|l\rangle\langle l|\Delta H^\lambda_\nu|j\rangle = \hbar^{-2}\mathscr{C}(\Delta H^\lambda_\mu, \Delta H^\lambda_\nu) \ , \tag{6.18}$$

where

$$\mathscr{C}(\Delta H^\lambda_\mu, \Delta H^\lambda_\nu) := \frac{1}{2}\mathrm{Tr}[\rho_\lambda\{\Delta H^\lambda_\mu, \Delta H^\lambda_\nu\}] \tag{6.19}$$

is the symmetrised covariance of $\Delta H^\lambda_\mu$ and $\Delta H^\lambda_\nu$ with respect to the evolved state, which reduces to the squared variance of the operator $H^\lambda_\mu$ when $\mu = \nu$, i.e. $\mathscr{C}(\Delta H^\lambda_\mu, \Delta H^\lambda_\mu) = \mathrm{Tr}[\rho_\lambda(\Delta H^\lambda_\mu)^2] = \langle (H^\lambda_\mu)^2\rangle - \langle H^\lambda_\mu\rangle^2$. By substituting the inequality (6.18) into Eq. (6.11) we get the new bound

$$\mathcal{L}^{\mathrm{QF}}(\rho_0, \rho_\tau) \leq \frac{1}{\hbar}\int_0^\tau dt \sqrt{\sum_{\mu,\nu=1}^{r}\mathscr{C}(\Delta H^\lambda_\mu, \Delta H^\lambda_\nu)\frac{d\lambda_\mu}{dt}\frac{d\lambda_\nu}{dt}} \ , \tag{6.20}$$

where $\mathcal{L}^{\mathrm{QF}}(\rho_0, \rho_\tau)$ is the geodesic distance corresponding to the quantum Fisher information metric and is given in Eq. (2.14).

Although the QSL in Eq. (6.20) applies to the very general $r$-parameter case, let us restrict for simplicity to the one-parameter case where $\lambda = t$. Consequently, we have that $H^\lambda_\mu \to H_t = -i\hbar U_t\,\partial_t U_t^\dagger$ and that the symmetrised covariance just reduces to the variance of the observable $H_t$ generating the dynamics of the system. Therefore, Eq. (6.20) turns into the simpler bound

$$\tau^{-1}\mathcal{L}^{\mathrm{QF}}(\rho_0, \rho_\tau) \leq \frac{1}{\hbar\,\tau}\int_0^\tau dt \sqrt{\langle H_t^2\rangle - \langle H_t\rangle^2} = \hbar^{-1}\overline{\Delta E} \ , \tag{6.21}$$

where $\overline{\Delta E} := \tau^{-1}\int_0^\tau dt \sqrt{\langle H_t^2\rangle - \langle H_t\rangle^2}$ is the mean variance of the generator $H_t$. The following QSL is thus obtained

$$\tau \geq \frac{\hbar}{\overline{\Delta E}}\mathcal{L}^{\mathrm{QF}}(\rho_0, \rho_\tau) \ . \tag{6.22}$$

It is worth emphasising that the bound in Eq. (6.22) applies to arbitrary initial and final mixed states and generic time-dependent generator of the dynamics. Moreover, we can immediately see that it exactly coincides with the one reported in Ref. [281] and reduces to an MT-like bound, when further restricting to the case of a time-independent generator of the dynamics.

**Wigner-Yanase information metric**

The Wigner-Yanase information metric corresponds to the MC function $f(t) = (1/4)(\sqrt{t}+1)^2$, so that $c^f(x,y) = 4/(\sqrt{x}+\sqrt{y})^2$ and Eq. (6.15) becomes

$$\begin{aligned} g^{WY}_{\mu\nu} &= \frac{2}{\hbar^2}\sum_{j<l}\left(\frac{p_j - p_l}{\sqrt{p_j}+\sqrt{p_l}}\right)^2 \langle j|\Delta H^\lambda_\mu|l\rangle\langle l|\Delta H^\lambda_\nu|j\rangle \\ &= \frac{1}{\hbar^2}\sum_{j,l}(\sqrt{p_j}-\sqrt{p_l})^2\langle j|\Delta H^\lambda_\mu|l\rangle\langle l|\Delta H^\lambda_\nu|j\rangle \\ &= -\frac{1}{\hbar^2}\mathrm{Tr}([\sqrt{\rho},\Delta H^\lambda_\mu][\sqrt{\rho},\Delta H^\lambda_\nu]) \\ &= \frac{2}{\hbar^2}\mathcal{C}\left(\Delta H^\lambda_\mu, \Delta H^\lambda_\nu\right) , \end{aligned} \tag{6.23}$$

where

$$\mathcal{C}(\Delta H^\lambda_\mu, \Delta H^\lambda_\nu) := -\frac{1}{2}\mathrm{Tr}([\sqrt{\rho_\lambda},\Delta H^\lambda_\mu][\sqrt{\rho_\lambda},\Delta H^\lambda_\nu]) \tag{6.24}$$

reduces to the skew information between the evolved state and $\Delta H^\lambda_\mu$ when $\mu = \nu$ , $\mathcal{C}(\Delta H^\lambda_\mu, \Delta H^\lambda_\mu) = \mathcal{I}(\rho_\lambda, \Delta H^\lambda_\mu) := -(1/2)\mathrm{Tr}([\sqrt{\rho_\lambda},\Delta H^\lambda_\mu]^2)$ [282]. By putting Eq. (6.23) into the bound in Eq. (6.11), we get

$$\mathcal{L}^{\mathrm{WY}}(\rho_0,\rho_\tau) \leq \frac{\sqrt{2}}{\hbar}\int_0^\tau dt \sqrt{\sum_{\mu,\nu=1}^{r}\mathcal{C}\left(\Delta H^\lambda_\mu, \Delta H^\lambda_\nu\right)\frac{d\lambda_\mu}{dt}\frac{d\lambda_\nu}{dt}} , \tag{6.25}$$

where now $\mathcal{L}^{\mathrm{WY}}(\rho_0,\rho_\tau)$ is the geodesic distance related to the Wigner-Yanase information metric and is given in Eq. (2.15).

For simplicity, let us again analyse the one-parameter case, where $\lambda = t$, $H^\lambda_\mu \to H_t = -i\hbar U_t\,\partial_t U_t^\dagger$ and $\mathcal{C}$ reduces to the skew information $\mathcal{I}(\rho_t, H_t)$ between the evolved state $\rho_t$ and the observable $H_t$ generating the dynamics of the system. Therefore, the bound in Eq. (6.25) turns into

$$\tau^{-1}\mathcal{L}^{\mathrm{WY}}(\rho_0,\rho_\tau) \leq \frac{\sqrt{2}}{\hbar}\frac{1}{\tau}\int_0^\tau dt\,\sqrt{\mathcal{I}(\rho_t,H_t)} = \frac{\sqrt{2}}{\hbar}\overline{\sqrt{\mathcal{I}}} , \tag{6.26}$$

where we define $\overline{\sqrt{\mathcal{I}}} := \tau^{-1}\int_0^\tau dt\,\sqrt{\mathcal{I}(\rho_t,H_t)}$ as the mean skew information between the evolved state and the generator of the evolution. The QSL thus becomes

$$\tau \geq \frac{\hbar}{\sqrt{2}\overline{\sqrt{\mathcal{I}}}}\mathcal{L}^{\mathrm{WY}}(\rho_0,\rho_\tau) . \tag{6.27}$$

As reported by Luo [283], the skew information $\mathcal{I}(\rho_t, H_t)$ is upper bounded by the variance of the observable $H_t$, $\mathcal{I}(\rho_t,H_t) \leq \langle H_t^2\rangle - \langle H_t\rangle^2$, so that $\overline{\sqrt{\mathcal{I}}} \leq \overline{\Delta E}$ and

$$\tau \geq \frac{\hbar}{\sqrt{2}\overline{\sqrt{\mathcal{I}}}}\mathcal{L}^{\mathrm{WY}}(\rho_0,\rho_\tau) \geq \frac{1}{\sqrt{2}}\frac{\hbar}{\overline{\Delta E}}\mathcal{L}^{\mathrm{WY}}(\rho_0,\rho_\tau) . \tag{6.28}$$

The latter QSL strongly resembles the bound expressed in Eq. (6.22) and emerging from the quantum Fisher information metric, with the difference lying in the fact that we are now adopting the Hellinger angle instead of the Bures angle and a $\sqrt{2}$ factor appears in the denominator. However, when the initial and final states commute, we have that the corresponding fidelity and affinity coincide, $F(\rho_0, \rho_\tau) = A(\rho_0, \rho_\tau)$, and so the Bures angle is equal to the Hellinger angle, which implies that in this case the bound emerging from the Wigner-Yanase metric is less tight than the one corresponding to the quantum Fisher information by a factor of $1/\sqrt{2}$.

The above result could be intuitively expected due to the strict hierarchy respected by the MC functions corresponding to the two adopted metrics. To put such an intuition on rigorous grounds, one can prove (see Appendix A of [10]) that the geometric QSL corresponding to the quantum Fisher information metric, as expressed directly by Eq. (6.11), is indeed tighter than the one corresponding to the Wigner-Yanase information metric, when considering *any* single-qubit unitary dynamics. However, we leave it as an open question to assess whether this is still the case when considering higher dimensional quantum systems, or other contractive Riemannian metrics in place of the Wigner-Yanase one.

Quite surprisingly, we will show instead in the next section that, for the realistic and more general case of nonunitary dynamics, the hierarchy of the MC functions does not automatically translate anymore into a hierarchy of tightness for the corresponding QSLs, not even in the case of a single qubit. This will reveal original consequences of our analysis in practically relevant scenarios.

### 6.3.2 Nonunitary dynamics

We will now consider two paradigmatic examples of nonunitary physical processes acting on a single qubit: dephasing and amplitude damping.

#### Parallel and transversal dephasing channels

Let us denote by $\rho = (1/2)(\mathbb{I} + \vec{r} \cdot \vec{\sigma})$ the Bloch sphere representation of an arbitrary single qubit state $\rho$, where $\vec{r} = \{r \sin\theta \cos\phi, r \sin\theta \sin\phi, r \cos\theta\}$ is the Bloch vector, with $r \in [0, 1]$, $\theta \in [0, \pi]$ and $\phi \in [0, 2\pi[$, while $\mathbb{I}$ denotes the $2 \times 2$ identity matrix and $\vec{\sigma} = \{\sigma_1, \sigma_2, \sigma_3\}$ is the vector of Pauli matrices.

Let us now consider a noisy evolution of this state governed by a master equation of Lindblad form

$$\frac{\partial \rho(t)}{\partial t} = \mathscr{H}(\rho) + \mathscr{L}(\rho) \ , \tag{6.29}$$

where $\mathscr{H}(\rho) = -i[H, \rho]$ describes the unitary evolution governed by a Hamiltonian $H$ while $\mathscr{L}(\rho)$ is the Liouvillian that describes the noise. We further consider as Hamiltonian $H = \frac{\omega_0}{2}\sigma_3$, where $\omega_0$ is the unitary frequency, and as Liouvillian

$$\mathscr{L}(\rho) = -\frac{\Gamma}{2}\left(\rho - \sum_{i=1}^{3} \alpha_i \sigma_i \rho \sigma_i\right) \ , \tag{6.30}$$

where $\Gamma$ is the decoherence rate and $\alpha_i \geq 0$ with $\sum_i \alpha_i = 1$.

We can identify two main modalities of dephasing noise. When $\alpha_3 = 1$, the dephasing happens in the same basis as the one specifying the Hamiltonian of our system, a case that can be referred to as 'parallel dephasing'. When instead $\alpha_1 = 1$, the dephasing occurs in a basis orthogonal to the one of the Hamiltonian, leading to the situation typically referred to as 'transversal dephasing' [284, 285]. We will explore these two cases separately.

**Parallel dephasing.** The parallel dephasing noise lets an initial state $\rho_0$ evolve as $\rho_t = \sum_{j=0}^{1} K_j \rho_0 K_j^\dagger$, where

$$K_0 = \sqrt{q_+} \begin{pmatrix} e^{-i\omega_0 t/2} & 0 \\ 0 & e^{i\omega_0 t/2} \end{pmatrix} \ , \ K_1 = \sqrt{q_-} \begin{pmatrix} e^{-i\omega_0 t/2} & 0 \\ 0 & -e^{i\omega_0 t/2} \end{pmatrix} \tag{6.31}$$

are the Kraus operators, and $q_\pm = (1 \pm q_t)/2$ with $q_t = e^{-\Gamma t}$ [144]. Notice that the Kraus operators satisfy not only $\sum_{j=0}^{1} K_j^\dagger K_j = \mathbb{I}$ but also $\sum_{j=0}^{1} K_j K_j^\dagger = \mathbb{I}$, as such a channel is unital. The effect of parallel dephasing is exactly the same as the one of phase flip and consists in shrinking the Bloch sphere onto the $z$-axis of states diagonal in the computational basis, which are instead left invariant. Moreover, $\omega_0$ describes the rotation frequency around the $z$-axis. One can easily see that the evolved state $\rho_t$ has the following spectral decomposition

$$\rho_t = \sum_{j=\pm} p_j |\theta_t, \phi_t\rangle_j \langle \theta_t, \phi_t|_j \ , \tag{6.32}$$

where $p_\pm = (1/2)(1 \pm r_0\, \xi_t)$ and

$$|\theta_t, \phi_t\rangle_\pm = \frac{1}{N_\pm} \left[ (\cos\theta_0 \pm \xi_t)|0\rangle + e^{i(\omega_0 t + \phi_0)} q_t \sin\theta_0 |1\rangle \right] \ , \tag{6.33}$$

with $\xi_t = \sqrt{\cos^2\theta_0 + q_t^2 \sin^2\theta_0}$ and $N_\pm$ a normalisation constant. By putting the above equations into Eqs. (6.9) and (6.10) one obtains, respectively,

$$\mathcal{F} = \frac{r_0^2 q_t^2 \sin^4\theta_0 \, (dq_t/dt)^2}{4\xi_t^2 \, (1 - r_0^2 \xi_t^2)} \tag{6.34}$$

and

$$\mathcal{Q}^f = \frac{1}{8} \left[ \omega_0^2 q_t^2 + \frac{\cos^2\theta_0 \, (dq_t/dt)^2}{\xi_t^2} \right] r_0^2 \sin^2\theta_0 \, c^f(p_+, p_-) \ . \tag{6.35}$$

The contractive Riemannian metric $g^f = \mathcal{F} + \mathcal{Q}^f$ can be interpreted as the speed of evolution of $\rho_t$. Equation (6.34), which corresponds to the contribution to $g^f$ common to all the MC family, is identically zero for all the initial states such that $\theta_0$ is either 0 or $\pi$, that are all the incoherent states lying on the $z$-axis of the Bloch sphere (with density matrices diagonal in the computational basis), which are indeed left unaffected by the parallel dephasing dynamics. Although $\mathcal{F}$ is a function of the initial purity $r_0$ and of time, it does not depend on the initial azimuthal angle $\phi_0$ since the eigenvalues of the evolved state $p_j$ do not depend on $\phi_0$. Equation (6.35), which instead describes the truly

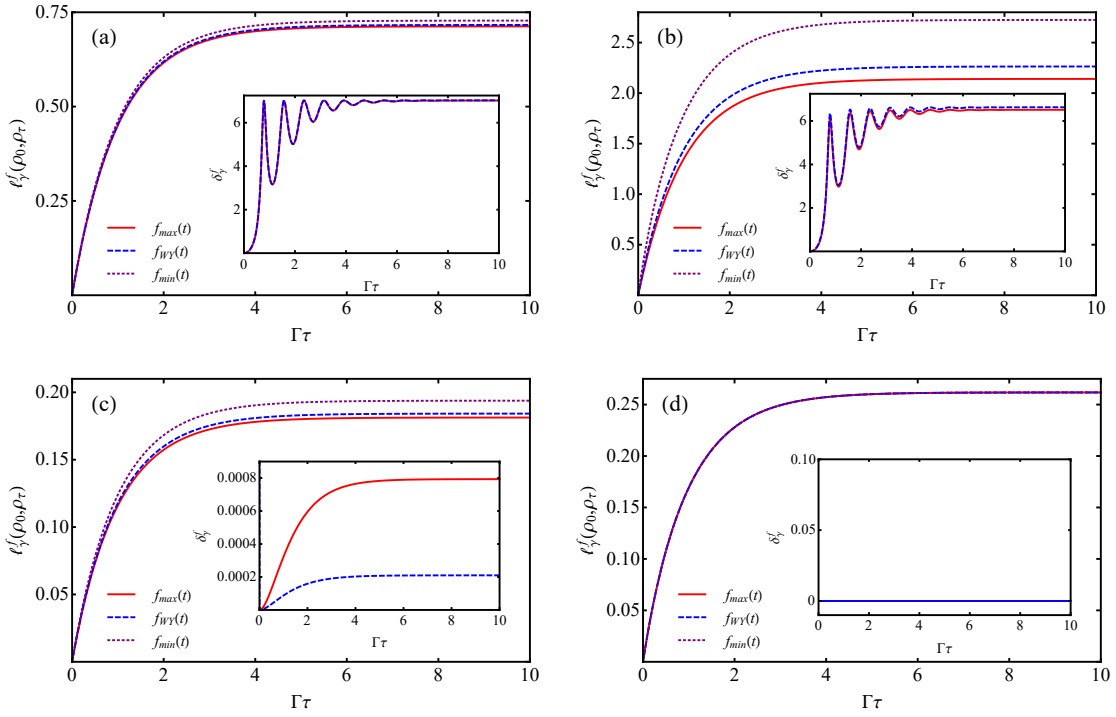


Figure 6.2: Evolution path lengths $\ell^f_\gamma$ for parallel dephasing processes by considering the contractive Riemannian metrics corresponding to the following MC functions: $f_{QF}(t) = f_{max}(t)$ (red solid line), $f_{WY}(t)$ (blue dashed line) and $f_{min}(t)$ (purple dotted line) for (**a**) $r_0 = 1/4$, $\theta_0 = \pi/4$, $\beta = 8$ (**b**) $r_0 = 3/4$, $\theta_0 = \pi/4$, $\beta = 8$ (**c**) $r_0 = 1/2$, $\theta_0 = \pi/4$, $\beta = 0$ and (**d**) $r_0 = 1/2$, $\theta_0 = \pi/2$, $\beta = 0$. The insets in each panel show the relative difference $\delta^f_\gamma$, Eq. (6.13), for parallel dephasing processes by considering the quantum Fisher information metric (red solid line) and the Wigner-Yanase information metric (blue dashed line); such a relative difference can be regarded as an indicator of the tightness of the bounds (the smaller $\delta^f_\gamma$, the tighter the bounds).

quantum contribution to the speed of evolution $g^f$ and depends on the specific choice of the MC function $f$, is identically zero for all the incoherent initial states such that $\theta_0$ is either 0 or $\pi$. Notice that in the case $\theta_0 = \pi/2$, for initial states lying in the equatorial $xy$-plane, $\mathcal{Q}^f$ is nonzero only when the frequency $\omega_0$ is also nonzero. Interestingly, $\mathcal{Q}^f$ does not depend on the initial azimuthal angle $\phi_0$ as well, even though the eigenstates of the evolved state do depend on $\phi_0$. In summary, the speed of evolution is obviously zero for initial states belonging to the $z$-axis, being them invariant under parallel dephasing; it is furthermore symmetric with respect to the initial azimuthal angle $\phi_0$, and it arises only from the populations of the evolving state when starting from the equatorial $xy$-plane with zero frequency $\omega_0$.

In Fig. 6.2 we compare the evolution path lengths appearing in the right hand side of Eq. (6.11) and corresponding to the three paradigmatic examples of contractive Rie-

mannian metrics: the quantum Fisher information metric, the Wigner-Yanase information metric, and the metric corresponding to the minimal MC function. We consider the only initial parameters that play a role in all the above analysis, i.e. the initial purity $r_0$ and polar angle $\theta_0$, and the dynamical parameter $\beta \equiv \omega_0/\Gamma$, while full details on the computation of all the quantities appearing in Eq. (6.11) are deferred to Appendix B of [10]. First, it can be seen that by fixing the initial purity $r_0$ (respectively, polar angle $\theta_0$), the speed of evolution increases as we increase the initial polar angle $\theta_0$ (respectively, purity $r_0$). In other words, the farther the initial state is from the $z$-axis (the larger is its quantum coherence), the faster the corresponding evolution can be. Second, Fig. 6.2(d) in particular unveils the signature of the populations of the evolved state into the speed of evolution. Indeed, according to Eq. (6.35), the purely quantum contribution $\mathcal{Q}^f$ to the metric is equal to zero for $\theta_0 = \pi/2$ and $\omega_0 = 0$ ($\beta = 0$). Thus, the speed of evolution $g^f$ is described solely by the term $\mathcal{F}$ given in Eq. (6.34) and arising only from the populations of the evolved state. In this case, the speed of evolution remains invariant for any contractive Riemannian metric, since $\mathcal{F}$ is common to all of them. However, it is still susceptible to changes depending on the purity and time.

Let us now investigate how the QSLs in Eq. (6.11) behave by considering the quantum Fisher information metric and the Wigner-Yanase information metric, whose geodesic lengths are known analytically. In the insets of Fig. 6.2 we compare the tightness parameter $\delta_\gamma^f$, as defined in Eq. (6.13), when considering these two metrics, for a parallel dephasing dynamical evolution. We can see that for $\beta = 8$ the dynamics does not saturate the bound for any of the two metrics, although the quantum Fisher information metric provides in general a slightly tighter QSL. On the other hand, when $\beta = 0$ and $\theta_0 = \pi/2$, we have that the QSL is saturated for both metrics, whereas for $\beta = 0$ and $\theta_0 = \pi/4$, it is instead the Wigner-Yanase information metric that provides us with a slightly tighter lower bound.

More generally, it is sufficient to compare the difference between the tightness indicators $\delta_\gamma^{QF} - \delta_\gamma^{WI}$ for the two metrics in the whole parameter space of the parallel dephasing model, to identify in which regime each of the two corresponding bounds is the tightest. This analysis is reported in Fig. 6.3, showing that the Wigner-Yanase information metric does lead in general to a tighter QSL when the frequency $\omega_0$ is sufficiently small. This is in stark contrast with the case of unitary evolutions, discussed in the previous section, and constitutes a first demonstration of the usefulness of our generalised approach to speed limits in quantum dynamics.

**Transversal dephasing.** We now focus on the case of transversal dephasing noise, which lets an initial state $\rho_0$ evolve as $\rho_t = (1/2)\sum_{i,j=0}^{3} S_{ij}\sigma_i\rho\sigma_j$, where $S$ is a $4 \times 4$ hermitian matrix whose non-vanishing elements are given by $S_{00} = a + b$, $S_{11} = d + f$,

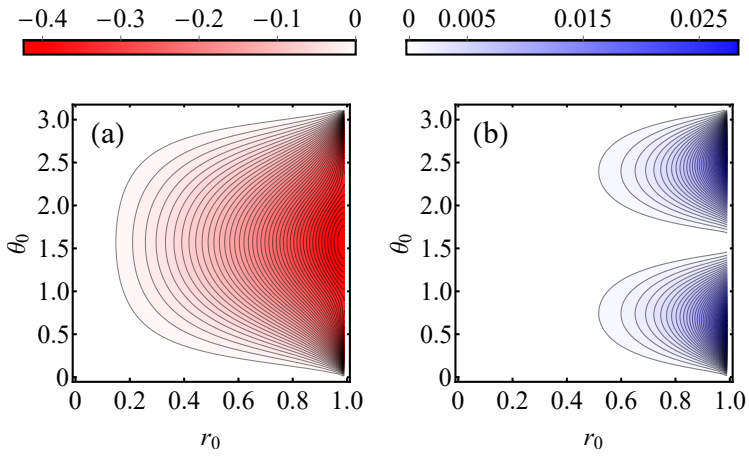


Figure 6.3: Contour plot of the difference $\Delta\delta_\gamma \equiv \delta_\gamma^{QF} - \delta_\gamma^{WY}$ between the tightness parameter corresponding to the quantum Fisher information metric and the one corresponding to the Wigner-Yanase information metric, for the parallel dephasing process as a function of $r_0$ and $\theta_0$, for (**a**) $\Gamma\tau = 10$, $\omega_0 = 10$, and (**b**) $\Gamma\tau = 10$, $\omega_0 = 0.1$. The QSL constructed with the Wigner-Yanase skew information is tighter than (respectively looser than) the one constructed with the quantum Fisher information when $\Delta\delta_\gamma > 0$ (resp. $\Delta\delta_\gamma < 0$), as in panel **b** (resp. **a**).

$S_{22} = d - f$, $S_{33} = a - b$, $S_{03} = ic$ and $S_{30} = -ic$, with

$$a = \frac{1}{2}(1 + e^{-u}) \,, \tag{6.36}$$

$$b = e^{-u/2}\cosh(\Omega u/2) \,, \tag{6.37}$$

$$c = \frac{2\beta\, e^{-u/2}}{\Omega}\sinh(\Omega u/2) \,, \tag{6.38}$$

$$d = \frac{1}{2}(1 - e^{-u}) \,, \tag{6.39}$$

$$f = \frac{e^{-u/2}}{\Omega}\sinh(\Omega u/2) \,, \tag{6.40}$$

where $u = \Gamma t$, $\Omega = \sqrt{1 - 4\beta^2}$ and $\beta = \omega_0/\Gamma$. It is worthwhile noticing that also the transversal dephasing channel is unital, i.e. it leaves the maximally mixed state invariant. This channel has proven to be of fundamental interest within the burgeoning field of noisy quantum metrology, as shown in Chaves *et al.* [284,285]. More precisely, transversal dephasing noise stands as the relevant scenario whereby one can attain a precision in the estimation of the parameter $\omega_0$ that scales superclassically with the number of qubits, even if such noise applies independently to each qubit (while any superclassical advantage is lost in the case of parallel dephasing noise).

By writing the spectral decomposition of the density operator $\rho_t$ we get

$$\rho_t = \sum_{j=\pm} p_j |\theta_t, \phi_t\rangle_j \langle \theta_t, \phi_t|_j \ , \tag{6.41}$$

where $p_\pm = (1/2)(1 + r_0 \tilde{\xi}_t)$ and

$$|\theta_t, \phi_t\rangle_\pm = \frac{1}{N_\pm} \left[ [(2a-1)\cos\theta_0 \pm \tilde{\xi}_t]|0\rangle + [(b+ic)e^{i\phi_0} + fe^{-i\phi_0}]\sin\theta_0 |1\rangle \right] \ , \tag{6.42}$$

with

$$\tilde{\xi}_t = \sqrt{(2a-1)^2 \cos^2\theta_0 + \tilde{\zeta}_t \sin^2\theta_0} \ , \tag{6.43}$$

$$\tilde{\zeta}_t = b^2 + c^2 + f^2 + 2f[b\cos(2\phi_0) - c\sin(2\phi_0)] \ , \tag{6.44}$$

and $N_\pm$ a normalisation constant. By putting the above equations into Eqs. (6.9) and (6.10), one obtains expressions which are too cumbersome to be reported here. However, when restricting to the relevant case of an initial plus state (which is an optimal probe state for frequency estimation), i.e. $\rho_0 = |+\rangle\langle+|$ with $|+\rangle = (|0\rangle + |1\rangle)/\sqrt{2}$, one obtains the following simple expressions:

$$\mathcal{F} = \frac{\beta^4}{\Omega^4} \frac{e^{-u} \sinh^2(\Omega u/2)}{(1 - e^{-u}\mathcal{G})\,\mathcal{G}} \ , \tag{6.45}$$

$$\mathcal{Q}^f = \frac{\beta^2}{8\mathcal{G}} e^{-u} c^f(p_+, p_-) \ , \tag{6.46}$$

where

$$\mathcal{G} = \frac{1}{\Omega^2} \left[ \cosh(\Omega u) + \Omega \sinh(\Omega u) - 4\beta^2 \right] \ . \tag{6.47}$$

Let us now analyse the behaviour of the QSLs in Eq. (6.11) corresponding to the quantum Fisher information metric and the Wigner-Yanase information metric when considering the transversal dephasing dynamics. In Fig. 6.4 we can see that, initialising such dynamics with a plus state, it happens that for small enough $\Gamma$ and $\omega_0$ the Wigner-Yanase information provides a QSL which is tighter (in particular at short times) than the one corresponding to the quantum Fisher information. One might identify more generally the region of parameters in which this behaviour occurs by studying the trade-off between the respective tightness indicators $\delta_\gamma^f$ for an arbitrary initial state, as in the previous case, although such a study does not add any further insight and is not reported here.

Once more, the present analysis shows that our approach applies straightforwardly to obtain novel, tighter bounds in dynamical cases of interest for quantum technologies, as here corroborated in particular for the metrologically relevant case of transversal dephasing noise.

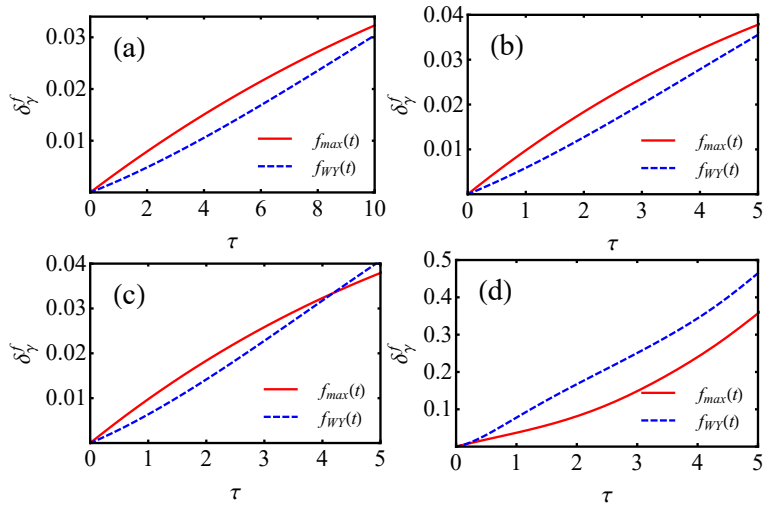


Figure 6.4: Plot of the relative difference $\delta^f_\gamma$, Eq. (6.13), indicating the tightness of the QSLs (the smaller $\delta^f_\gamma$, the tighter the bounds) corresponding respectively to the quantum Fisher information (red solid line) and the Wigner-Yanase skew information (blue dashed line), for a qubit initially in the plus state and undergoing a transversal dephasing process with (**a**) $\Gamma = 0.1$ and $\omega_0 = 0.01$; (**b**) $\Gamma = 0.25$ and $\omega_0 = 0.01$; (**c**) $\Gamma = 0.25$ and $\omega_0 = 0.033$; (**d**) $\Gamma = 1$ and $\omega_0 = 1$.

### Amplitude damping channel

We now consider another canonical model of noise, namely dissipation modelled by an amplitude damping channel acting on a single qubit. For the amplitude damping channel we have the following Kraus operators

$$\tilde{K}_0 = \begin{pmatrix} 1 & 0 \\ 0 & \sqrt{1-\lambda_t} \end{pmatrix} , \quad \tilde{K}_1 = \begin{pmatrix} 0 & \sqrt{\lambda_t} \\ 0 & 0 \end{pmatrix} , \tag{6.48}$$

with $\lambda_t = 1 - e^{-\Gamma t}$ and $1/\Gamma$ is the characteristic time of the process [144], satisfying only $\sum_j \tilde{K}_j^\dagger \tilde{K}_j = \mathbb{I}$ since this channel is not unital. The effect of amplitude damping consists in shrinking the Bloch sphere towards the north pole, or the state $|0\rangle$. In this case, it is easy to verify that the evolved state $\rho_t = \sum_j \tilde{K}_j \rho_0 \tilde{K}_j^\dagger = (1/2)(\mathbb{I} + \vec{r}_t \cdot \vec{\sigma})$ has the following spectral decomposition

$$\rho_t = \sum_{j=\pm} p_j |\theta_t, \phi_t\rangle_j \langle \theta_t, \phi_t|_j , \tag{6.49}$$

where $p_\pm = \frac{1}{2}(1 \pm \vartheta_t)$ and

$$|\theta_t, \phi_t\rangle_\pm = \frac{1}{\sqrt{N_\pm}} \left[ (\varsigma_t \pm \vartheta_t)|0\rangle + e^{i\phi_0} r_0 \sqrt{1-\lambda_t} \sin\theta_0 |1\rangle \right] , \tag{6.50}$$

with

$$\vartheta_t = \sqrt{1-\zeta_t(1-\lambda_t)}\ , \tag{6.51}$$

$$\zeta_t = 1-r_0^2+\lambda_t(1-r_0\cos\theta_0)^2\ , \tag{6.52}$$

$$\varsigma_t = \lambda_t + r_0(1-\lambda_t)\cos\theta_0\ , \tag{6.53}$$

and $N_\pm$ a normalisation constant. By putting the above equations into Eqs. (6.9) and (6.10) one obtains, respectively,

$$\mathcal{F} = \frac{[\zeta_t-(1-\lambda_t)(1-r_0\cos\theta_0)^2]^2}{16\vartheta_t^2\zeta_t(1-\lambda_t)} \tag{6.54}$$

and

$$\mathcal{Q}^f = \frac{r_0^2\sin^2\theta_0\,(2-\varsigma_t)^2\,c^f(p_+,p_-)}{32\vartheta_t^2(1-\lambda_t)}\ . \tag{6.55}$$

As in the case of the parallel dephasing channel, both contributions $\mathcal{F}$ and $\mathcal{Q}^f$ to the speed of evolution $g^f$ do not depend on the initial azimuthal angle $\phi_0$. However, contrarily to the parallel dephasing channel case, here the purely quantum contribution $\mathcal{Q}^f$ vanishes only for $\theta_0 = 0, \pi$, whereas the term $\mathcal{F}$ vanishes in neither of these cases nor for $\theta_0 = \pi/2$, as expected due to the fact that now only the north pole, and not the entire $z$-axis of the Bloch sphere, is left invariant by the dynamics.

In Fig. 6.5 we compare the evolution path lengths appearing in the right hand side of Eq. (6.11) and corresponding to the usual contractive Riemannian metrics, i.e. the quantum Fisher information metric, the Wigner-Yanase information metric and the metric corresponding to the minimal MC function, by changing again the initial purity $r_0$ and polar angle $\theta_0$. First, Fig. 6.5(e) and Fig. 6.5(f) exhibit the following behaviour: fixing the initial polar angle $\theta_0 = 0$, the speed of evolution decreases as we increase the initial purity $r_0$. This feature highlights the fact that the north pole of the Bloch sphere is unaffected by the amplitude damping channel. Moreover, according to Eq. (6.55), the purely quantum contribution $\mathcal{Q}^f$ vanishes identically for $\theta_0 = 0$ and the speed of evolution $g$ and corresponding evolution path length in Eq. (6.11) become independent of the choice of the MC function $f$. The nontrivial contribution to the speed of evolution is in this case exclusively due to the term $\mathcal{F}$ which depends solely on the populations $p_j$ of the evolved state.

Let us now analyse the behaviour of the QSLs in Eq. (6.11) corresponding to the quantum Fisher information metric and the Wigner-Yanase information metric (see Appendix C of [10] for details). In the insets of Fig. 6.5 we compare the tightness indicators $\delta_\gamma^f$, as defined in Eq. (6.13), when considering these two metrics, for the amplitude damping channel. We can see that in this case the Wigner-Yanase information provides a QSL which is almost saturated (in particular at short times) whereas the quantum Fisher information does not, except in the case of $\theta_0 = 0$ where they both realise tight bounds. What is more, in Fig. 6.6 one can see that for almost all initial states, except for a small neighbourhood of the north pole (which is the asymptotic state of the amplitude damping channel), it happens that $\delta^{QF} \geq \delta^{WY}$ and $\delta_{WY} \simeq 0$, i.e. the Wigner-Yanase information

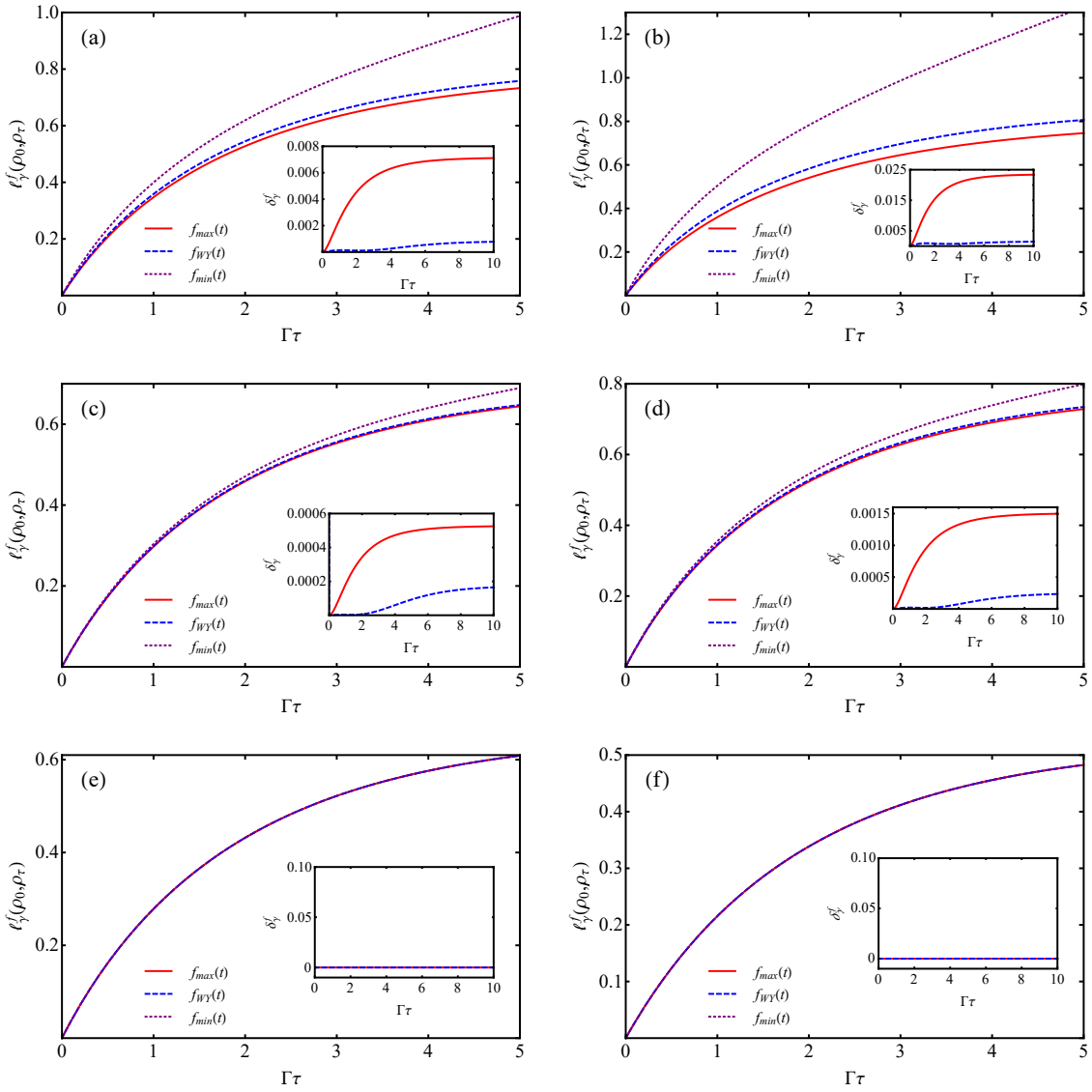


Figure 6.5: Evolution path lengths $\ell_\gamma^f$ for amplitude damping processes related to the contractive Riemannian metrics corresponding to the following MC functions: $f_{QF}(t) = f_{max}(t)$ (red solid line), $f_{WY}(t)$ (blue dashed line) and $f_{min}(t)$ (purple dotted line) for (**a**) $r_0 = 1/2$, $\theta_0 = \pi/2$, (**b**) $r_0 = 3/4$, $\theta_0 = \pi/2$, (**c**) $r_0 = 1/4$, $\theta_0 = \pi/4$, (**d**) $r_0 = 1/4$, $\theta_0 = \pi/2$, (**e**) $r_0 = 1/4$, $\theta_0 = 0$ and (**f**) $r_0 = 1/2$, $\theta_0 = 0$. The insets in each panel show the relative difference $\delta_\gamma^f$, Eq. (6.13), for amplitude damping processes by considering the quantum Fisher information metric (red solid line) and the Wigner-Yanase information metric (blue dashed line); such a relative difference can be regarded as an indicator of the tightness of the bounds (the smaller $\delta_\gamma^f$, the tighter the bounds).

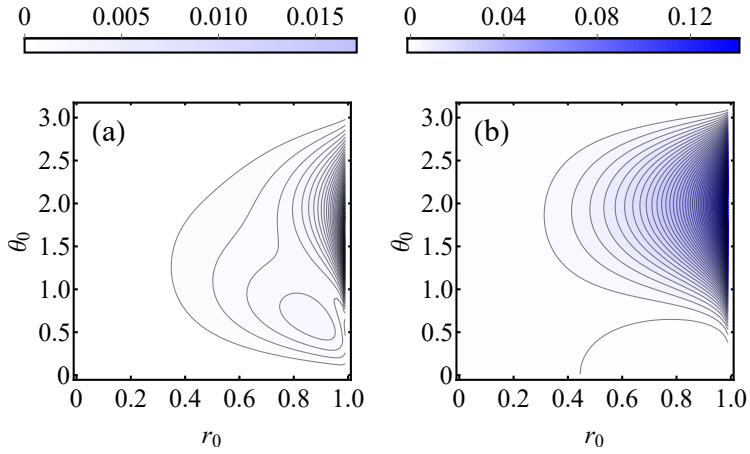


Figure 6.6: Contour plot of (**a**) the tightness indicator $\delta_\gamma^{WY}$ of the bound specified by the Wigner-Yanase information metric, and (**b**) the difference $\Delta\delta_\gamma \equiv \delta_\gamma^{QF} - \delta_\gamma^{WY}$ between the tightness parameter corresponding to the quantum Fisher information metric and the one corresponding to the Wigner-Yanase information metric, for the amplitude damping process as a function of $r_0$ and $\theta_0$, for $\Gamma\tau = 10$. The QSL constructed with the Wigner-Yanase skew information is nearly globally optimal (as $\delta_\gamma^{WY} \simeq 0$) and tighter than the one constructed with the quantum Fisher information (as indicated by $\Delta\delta_\gamma \geq 0$) in almost the whole parameter space, but for a small region in the bottom-right corner (large $r_0$, small $\theta_0$, i.e. around the state $|0\rangle$) in which the quantum Fisher information bound is marginally tighter.

metric provides us with a definitely tighter (and nearly saturated) QSL than the quantum Fisher information metric.

This reveals another important physical mechanism, distinct from dephasing, in which our generalised analysis leads to significantly tighter bounds than those established in previous literature, in this case clearly demonstrated in almost all the parameter space of relevance. This highlights the power of our general approach to reach beyond the state of the art.

## 6.4 Discussion

Based on the fundamental connection between the geometry of quantum states and their statistical distinguishability, we have exploited the fact that more than one privileged Riemannian metric appear in quantum mechanics in order to introduce a new infinite family of geometric quantum speed limits valid for any physical process, be it unitary or not. Specifically, each bona fide geometric measure of distinguishability gives rise to a different quantum speed limit that is particularly tailored to the case of initial mixed states and such that the contributions of the populations of the evolved state and of the coherences of its time variation are clearly separated.

Our work provides a comprehensive general framework which incorporates previous approaches to quantum speed limits and leaves room for novel insights. By investigating paradigmatic examples of unitary and noisy physical processes and of contractive Riemannian metrics, we have seen in fact how the choice of the quantum Fisher information, corresponding to an extremal metric and being ubiquitous in the existing literature, is only a special case which does not always provide the tightest lower bound in the realistic case of open system dynamics. In particular, for parallel and transversal dephasing, as well as amplitude damping dynamics, we defined a tighter quantum speed limit by means of another important but significantly less-studied Riemannian metric, namely the Wigner-Yanase skew information. The bound is useful in practical scenarios of noisy quantum metrology, especially in the case of transversal dephasing [284, 285].

Our unifying approach provides a concrete guidance to select the most informative metric in order to derive the tightest bound for some particular dynamics of interest. We have formulated the problem as an optimisation of a tightness indicator over all the infinite family of contractive quantum Riemannian metrics. The metric giving rise to the tightest bound is identified as the one whose geodesic is most tailored to the evolution under consideration in the sense of Eq. (6.14). While such a problem can only be solved in restricted form at present, due to the fact that the quantum Fisher information and the Wigner-Yanase skew information are the only two metrics admitting known geodesics, further progress will be achievable in case useful advances on the information geometry for other relevant metrics are recorded in the future.

It is important to remark that our family of speed limits is within the class of MT-like bounds. Following [119], it may be possible to implement some adjustments to the adopted unified geometric approach in order to provide a generalised geometric interpretation to ML-like speed limits as well.

Our work readily suggests to explore how the non uniqueness of a contractive Riemannian metric in the quantum state space affects also other scenarios of relevance in quantum information processing. In several of these scenarios, where the quantum Fisher information was adopted and privileged, our approach could lead to a more general investigation based on information geometry.

For example, when considering parameter estimation, one of the paradigmatic tasks of quantum metrology, the inverse of the quantum Fisher information metric sets a lower bound to the mean-square error of any unbiased estimator for the parameters through the quantum Cramér-Rao bound [151, 286]. Our work inspires the quest to provide more general bounds on the sensitivity of quantum states to evolutions encoding unknown parameters, based on the infinite hierarchy of quantum Riemannian contractive geometries. It is useful to recall here that the Fisher information-based quantum Cramér-Rao bound for single parameter estimation can only be achieved asymptotically in the limit of a large number of probes, and upon performing an optimal measurement given by projection into the eigenbasis of the symmetric logarithmic derivative, which is typically hard to implement in the experimental practice [286]. In the realistic case of a finite number of probes, corrections to the bound provide tighter estimates to the attainable estimation precision; these corrections have been first investigated in Ref. [287] for the case of the quantum Fisher information. Motivated by more recent works by Brody [288] and [289], in which

the Wigner-Yanase skew information has been interpreted rather naturally as the speed of mixed quantum state evolution, and by the analysis of the present work, we believe it is a worthy outlook to investigate finite-size corrections to the Cramér-Rao inequality based on the Wigner-Yanase information, in order to determine how tight the bound can be for practical purposes, in particular for the estimation of parameters encoded in open system dynamics.

Furthermore, within the burgeoning field of quantum thermodynamics, our approach could readily provide an infinite class of generalisations of the classical thermodynamical length [290], originally based on the unique classical contractive Riemannian metric, to the quantum setting. Again in the context of quantum thermodynamics, due to the close connections between geometry and entropy, it could be interesting to investigate the role played by the non uniqueness of a contractive Riemannian geometry on the quantum state space in the existence of many second laws of thermodynamics [30, 291].

In the study of quantum criticality, within the condensed matter realm, a geometric approach based on the fidelity, i.e. on the quantum Fisher information metric, proved to be fruitful [240, 292]. Along the lines of this work, one could apply more general tools associated with any quantum Riemanniann contractive metric, in order to seek for further insights and sharper identification of quantum critical phenomena.

Finally, the general approach presented in this paper to pinpoint the tightest speed limits in quantum evolutions is readily useful for applications to quantum engineering and quantum control. Specifically, the present study allows one to certify that, in a particular implementation, quantum states have been driven at the ultimate speed limit [120] and their evolution cannot be sped up further: this occurs whenever saturation of one of our bounds is demonstrated. As our various examples show, this is not possibly verifiable only by considering the standard bound based on quantum Fisher information. For single-qubit evolutions, we showed that the latter is in fact the tightest for the idealised case of unitary dynamics, while our novel bound based on the Wigner-Yanase skew information can instead be significantly tighter in the most common instances of open dynamics, yielding effectively *the* optimal bound (even among all the other unverifiable Riemannian metrics) for amplitude damping dynamics, as certified by a nearly vanishing tightness indicator in such case. Given that the Wigner-Yanase skew information is experimentally accessible [203], one can readily apply our results to current and future demonstrations to benchmark optimality of controlled quantum dynamics in the presence of such ubiquitous noise mechanisms.

In this respect, we would like to point out that an experimental investigation of the main results presented here, for both closed and open system dynamics, can be achieved in particular using a highly controllable Nuclear Magnetic Resonance setup, with no need for a complete quantum state tomography. In fact, dephasing and amplitude damping are naturally occurring sources of decoherence in such an implementation, and our results can be accessed by means of spin ensemble measurements, which constitute the conventional types of detection in such a technique [228, 293]. An experimental investigation as described deserves a study on its own and will be reported elsewhere.

# Chapter 7

# Conclusions

The quantification of quantumness is necessary to assess how much a physical system departs from a classical behaviour and thus gauge the quantum enhancement in operational tasks such as information processing and computation. For arbitrary multiparticle systems, the quantification of quantumness typically involves nontrivial optimisation problems, and may require demanding tomographical techniques. We have developed an experimentally feasible approach to the evaluation of geometric measures of quantumness, according to which the distance from the state of the system to a suitable set of classical states is considered. Our approach provides analytical results for particular classes of mixed states of $N$ qubits, and computable lower bounds to global, partial, and genuine multiparticle entanglement, as well as to quantum coherence, for any general state. For global and partial entanglement, as well as quantum coherence, useful bounds have been obtained with minimum effort, requiring local measurements in just three settings for any $N$. For genuine entanglement, a number of measurements scaling linearly with $N$ is required. We have demonstrated the power of our approach to estimate and quantify different types of multiparticle entanglement in a variety of $N$-qubit states useful for quantum information processing and recently engineered in laboratories with quantum optics and trapped ion setups.

Regarding in particular the quantification of quantum coherence, we have also introduced the robustness of coherence and proved it to be a fully bona fide quantifier in the context of the recently introduced resource theories of quantum coherence. The measure has been shown to be observable, as it can be recast as the expectation value of a coherence witness operator for any quantum state, as well as computable analytically on relevant classes of states, and numerically via an efficient semi-definite program on general states. An operational interpretation has been moreover provided: the robustness of coherence quantifies the advantage enabled by a quantum state in a phase discrimination task.

We have then focused on the open dynamics of quantumness. Those who work on quantum technologies are indeed always looking for ways to manage decoherence, which occurs when a quantum system unavoidably interacts with the surrounding environment. We have shown that all distance functions, which respect natural assumptions of invariance under transposition, convexity, and contractivity under quantum channels, give rise

to geometric quantifiers of quantumness which exhibit the peculiar freezing phenomenon, i.e., remain constant during the evolution of a particular class of states of an even number of qubits each independently interacting with a non-dissipative decohering environment, in the case of quantum coherence and discord-type correlations, and of two qubits undergoing collective dephasing, in the case of entanglement. Even more, in the case of quantum coherence, we have seen that such freezing phenomenon is observed experimentally in a two-qubit room temperature nuclear magnetic resonance quantum simulator. These results demonstrate from first principles that freezing of geometric quantumness is independent of the adopted distance and therefore universal, thus paving the way to a deeper physical interpretation and future practical exploitation of the phenomenon for noisy quantum technologies.

Furthermore, we have investigated the nature of spontaneous symmetry breaking in complex quantum systems by conjecturing that the maximally symmetry-breaking quantum ground states are the most classical ones corresponding to an ordered phase. We have made this argument quantitatively precise by showing that the ground states which realise the maximum breaking of the Hamiltonian symmetries are the only ones that: are always locally convertible, i.e. can be obtained from all other ground states by local operations and classical communication, while the reverse is never possible; and minimise the monogamy inequality for bipartite entanglement.

Finally, we have investigated how the non uniqueness of a bona fide measure of distinguishability defined on the quantum state space affects the quantum speed limits and can be exploited in order to derive improved bounds. Specifically, we have established an infinite family of quantum speed limits valid for unitary and nonunitary evolutions, based on an elegant information geometric formalism. Our work unifies and generalises existing results on quantum speed limits, and provides instances of novel bounds which are tighter than any established one based on the conventional quantum Fisher information. We have illustrated our findings with relevant examples, clarifying the role of classical populations versus quantum coherences in the determination and saturation of the speed limits. These results can find applications in the optimisation and control of quantum technologies such as quantum computation and metrology, and might provide new insights in fundamental investigations of quantum thermodynamics.

# Bibliography


[1] Bromley, T. R., Cianciaruso, M., and Adesso, G. *Phys. Rev. Lett.* **114**, 210401 (2015).

[2] Cianciaruso, M., Bromley, T. R., Roga, W., Lo Franco, R., and Adesso, G. *Sci. Rep.* **5**, 10177 (2015).

[3] Cianciaruso, M., Bromley, T. R., and Adesso, G. *arXiv:1507.01600* (2015).

[4] Napoli, C., Bromley, T. R., Cianciaruso, M., Piani, M., Johnston, N., and Adesso, G. *arXiv:1601.03781* (2016).

[5] Piani, M., Cianciaruso, M., Bromley, T. R., Napoli, C., Johnston, N., and Adesso, G. *arXiv:1601.03782* (2016).

[6] Bromley, T. R., Cianciaruso, M., Lo Franco, R., and Adesso, G. *J. Phys. A: Math. Theor.* **47**, 405302 (2014).

[7] Silva, I., Souza, A. M., Bromley, T. R., Cianciaruso, M., Sarthour, R. S., Oliveira, I. S., Lo Franco, R., deAzevedo, E. R., Soares-Pinto, D. O., and Adesso, G. *arXiv:1511.01971* (2015).

[8] Cianciaruso, M., Giampaolo, S. M., Roga, W., Zonzo, G., Blasone, M., and Illuminati, F. *arXiv:1412.1054v2* (2015).

[9] Cianciaruso, M., Ferro, L., Giampaolo, S. M., Zonzo, G., and Illuminati, F. *arXiv:1408.1412* (2014).

[10] Pires, D. P., Cianciaruso, M., Céleri, L. C., Adesso, G., and Soares-Pinto, D. O. *arXiv:1507.05848* (2015).

[11] Leggett, A. J. *Prog. Theor. Phys. Suppl.* **69**, 80 (1980).

[12] Einstein, A., Podolsky, B., and Rosen, N. *Phys. Rev.* **47**, 777–780 (1935).

[13] Schrödinger, E. *Mathematical Proceedings of the Cambridge Philosophical Society* **31**, 555–563 (1935).

[14] Bell, J. S. *Speakable and unspeakable in quantum mechanics: Collected papers on quantum philosophy.* Cambridge university press, (2004).

[15] Bell, J. S. *Rev. Mod. Phys.* **38**, 447–452 (1966).

[16] Wiseman, H. M., Jones, S. J., and Doherty, A. C. *Phys. Rev. Lett.* **98**, 140402 (2007).

[17] Jones, S. J., Wiseman, H. M., and Doherty, A. C. *Phys. Rev. A* **76**, 052116 (2007).

[18] Saunders, D. J., Jones, S. J., Wiseman, H. M., and Pryde, G. J. *Nature Physics* **6**, 845–849 (2010).

[19] Horodecki, R., Horodecki, P., Horodecki, M., and Horodecki, K. *Rev. Mod. Phys.* **81**, 865 (2009).

[20] Ollivier, H. and Zurek, W. H. *Phys. Rev. Lett.* **88**, 017901 (2001).

[21] Henderson, L. and Vedral, V. *J. Phys. A* **34**, 6899 (2001).

[22] Modi, K., Brodutch, A., Cable, H., Paterek, T., and Vedral, V. *Rev. Mod. Phys.* **84**, 1655 (2012).

[23] Zurek, W. H. *Rev. Mod. Phys.* **75**, 715–775 (2003).

[24] Dowling, J. P. and Milburn, G. J. *Philosophical Transactions of the Royal Society of London A: Mathematical, Physical and Engineering Sciences* **361**, 1655–1674 (2003).

[25] Giovannetti, V., Lloyd, S., and Maccone, L. *Nat. Photon.* **5**, 222 (2011).

[26] Glauber, R. J. *Phys. Rev.* **131**, 2766 (1963).

[27] Sudarshan, E. C. G. *Phys. Rev. Lett.* **10**, 277–279 (1963).

[28] Asbóth, J. K., Calsamiglia, J., and Ritsch, H. *Phys. Rev. Lett.* **94**, 173602 (2005).

[29] Lostaglio, M., Korzekwa, K., Jennings, D., and Rudolph, T. *Phys. Rev. X* **5**, 021001 (2015).

[30] Lostaglio, M., Jennings, D., and Rudolph, T. *Nature communications* **6** (2015).

[31] Streltsov, A., Singh, U., Dhar, H. S., Bera, M. N., and Adesso, G. *Phys. Rev. Lett.* **115**, 020403 (2015).

[32] Plenio, M. B. and Huelga, S. F. *New J. Phys.* **10**, 113019 (2008).

[33] Chin, A. W., Huelga, S. F., and Plenio, M. B. *Phil. Trans. R. Soc. A* **370**, 3638 (2012).

[34] Chin, A. W., Rosenbach, R., Caycedo-Soler, F., Huelga, S. F., and Plenio, M. B. *Nat. Phys.* **9**, 113–118 (2013).

[35] Huelga, S. F. and Plenio, M. B. *Contemp. Phys.* **54**, 181 (2013).

[36] Levi, F. and Mintert, F. *New J. Phys.* **16**, 033007 (2014).

[37] Bennett, C. H., Brassard, G., Crépeau, C., Jozsa, R., Peres, A., and Wootters, W. K. *Phys. Rev. Lett.* **70**, 1895–1899 (1993).

[38] Biham, O., Nielsen, M. A., and Osborne, T. J. *Phys. Rev. A* **65**, 062312 (2002).

[39] Townsend, P. D. *Nature* **385**, 47–49 (1997).

[40] Briegel, H. J., Browne, D. E., Dür, W., Raussendorf, R., and den Nest, M. V. *Nat. Phys.* **5**, 19–26 (2009).

[41] Bell, B. A., Markham, D., Herrera-Martí, D. A., Marin, A., Wadsworth, W. J., Rarity, J. G., and Tame, M. S. *Nat. Commun.* **5**, 5480 (2014).

[42] Tiersch, M., Popescu, S., and Briegel, H. J. *Philosophical Transactions of the Royal Society of London A: Mathematical, Physical and Engineering Sciences* **370**, 3771–3786 (2012).

[43] Sarovar, M., Ishizaki, A., Fleming, G. R., and Whaley, K. B. *Nat. Phys.* **6**, 462–467 (2010).

[44] Girolami, D., Souza, A. M., Giovannetti, V., Tufarelli, T., Filgueiras, J. G., Sarthour, R. S., Soares-Pinto, D. O., Oliveira, I. S., and Adesso, G. *Phys. Rev. Lett.* **112**, 210401 (2014).

[45] Spehner, D. and Orszag, M. *New J. Phys.* **15**, 103001 (2013).

[46] Spehner, D. and Orszag, M. *J. Phys. A: Math.* **47**, 035302 (2014).

[47] Piani, M., Narasimhachar, V., and Calsamiglia, J. *New Journal of Physics* **16**, 113001 (2014).

[48] Piani, M., Horodecki, P., and Horodecki, R. *Phys. Rev. Lett.* **100**, 090502 (2008).

[49] Cavalcanti, D., Aolita, L., Boixo, S., Modi, K., Piani, M., and Winter, A. *Phys. Rev. A* **83**, 032324 (2011).

[50] Piani, M., Gharibian, S., Adesso, G., Calsamiglia, J., Horodecki, P., and Winter, A. *Phys. Rev. Lett.* **106**, 220403 (2011).

[51] Piani, M. and Adesso, G. *Phys. Rev. A* **85**, 040301(R) (2012).

[52] Pirandola, S. *Scientific reports* **4**, 6956 (2014).

[53] Gühne, O. and Tóth, G. *Phys. Rep.* **474**, 1–75 (2009).

[54] Gühne, O. and Seevinck, M. *New Journal of Physics* **12**, 053002 (2010).

[55] Gao, T., Yan, F., and van Enk, S. J. *Phys. Rev. Lett.* **112**, 180501 (2014).

[56] Levi, F. and Mintert, F. *Phys. Rev. Lett.* **110**, 150402 (2013).

[57] Huber, M., Mintert, F., Gabriel, A., and Hiesmayr, B. C. *Phys. Rev. Lett.* **104**, 210501 (2010).

[58] Dür, W. and Cirac, J. I. *Phys. Rev. A* **61**, 042314 (2000).

[59] Gabriel, A., Hiesmayr, B. C., and Huber, M. *Quantum Information and Computation* **10**, 829–836 (2010).

[60] Klöckl, C. and Huber, M. *Phys. Rev. A* **91**, 042339 (2015).

[61] Badziąg, P., Brukner, Č., Laskowski, W., Paterek, T., and Żukowski, M. *Phys. Rev. Lett.* **100**, 140403 (2008).

[62] Buchholz, L. E., Moroder, T., and Gühne, O. *arXiv:1412.7471* (2014).

[63] Hofmann, M., Moroder, T., and Gühne, O. *Journal of Physics A: Mathematical and Theoretical* **47**, 155301 (2014).

[64] Eltschka, C. and Siewert, J. *Sci. Rep.* **2**, 942 (2012).

[65] Wu, J.-Y., Kampermann, H., Bruß, D., Klöckl, C., and Huber, M. *Phys. Rev. A* **86**, 022319 (2012).

[66] Hashemi Rafsanjani, S. M., Huber, M., Broadbent, C. J., and Eberly, J. H. *Phys. Rev. A* **86**, 062303 (2012).

[67] Ma, Z.-H., Chen, Z.-H., Chen, J.-L., Spengler, C., Gabriel, A., and Huber, M. *Phys. Rev. A* **83**, 062325 (2011).

[68] Gühne, O., Reimpell, M., and Werner, R. F. *Phys. Rev. Lett.* **98**, 110502 (2007).

[69] Eisert, J., Brandão, F. G., and Audenaert, K. M. *New J. Phys.* **9**, 46 (2007).

[70] Häffner, H., Hänsel, W., Roos, C., Benhelm, J., Chwalla, M., Körber, T., Rapol, U., Riebe, M., Schmidt, P., Becher, C., Gühne, O., Dür, W., and Blatt, R. *Nature* **438**, 643–646 (2005).

[71] Lavoie, J., Kaltenbaek, R., Piani, M., and Resch, K. J. *Phys. Rev. Lett.* **105**, 130501 (2010).

[72] Barreiro, J. T., Schindler, P., Gühne, O., Monz, T., Chwalla, M., Roos, C. F., Hennrich, M., and Blatt, R. *Nat. Phys.* **6**, 943 (2010).

[73] Monz, T., Schindler, P., Barreiro, J. T., Chwalla, M., Nigg, D., Coish, W. A., Harlander, M., Hänsel, W., Hennrich, M., and Blatt, R. *Phys. Rev. Lett.* **106**, 130506 (2011).

[74] Prevedel, R., Cronenberg, G., Tame, M. S., Paternostro, M., Walther, P., Kim, M. S., and Zeilinger, A. *Phys. Rev. Lett.* **103**, 020503 (2009).

[75] Wieczorek, W., Krischek, R., Kiesel, N., Michelberger, P., Tóth, G., and Weinfurter, H. *Phys. Rev. Lett.* **103**, 020504 (2009).

[76] Buchleitner, A. and Hornberger, K. *Coherent evolution in noisy environments*, volume 611. Springer Science & Business Media, (2002).

[77] Céleri, L. C., Maziero, J., and Serra, R. M. *Int. J. Quant. Inf.* **09**, 1837 (2011).

[78] Lo Franco, R., Bellomo, B., Maniscalco, S., and Compagno, G. *Int. J. Mod. Phys. B* **27**, 1345053 (2013).

[79] Streltsov, A., Kampermann, H., and Bruß, D. *Phys. Rev. Lett.* **107**, 170502 (2011).

[80] Ciccarello, F. and Giovannetti, V. *Phys. Rev. A* **85**, 010102 (2012).

[81] Maziero, J., Céleri, L. C., Serra, R. M., and Vedral, V. *Phys. Rev. A* **80**, 044102 (2009).

[82] Ferraro, A., Aolita, L., Cavalcanti, D., Cucchietti, F. M., and Acín, A. *Phys. Rev. A* **81**, 052318 (2010).

[83] Bellomo, B., Compagno, G., Franco, R. L., Ridolfo, A., and Savasta, S. *Int. J. Quant. Inf.* **9**, 1665 (2011).

[84] Campbell, S. *Quantum Information Processing* **12**, 2623–2636 (2013).

[85] Ma, Z., Chen, Z., and Fanchini, F. F. *New Journal of Physics* **15**, 043023 (2013).

[86] Yu, T. and Eberly, J. H. *Science* **323**, 598 (2009).

[87] Almeida, M. P., de Melo, F., Hor-Meyll, M., Salles, A., Walborn, S. P., Ribeiro, P. H. S., and Davidovich, L. *Science* **316**, 579–582 (2007).

[88] Aaronson, B., Lo Franco, R., and Adesso, G. *Phys. Rev. A* **88**, 012120 (2013).

[89] Mazzola, L., Piilo, J., and Maniscalco, S. *Phys. Rev. Lett.* **104**, 200401 (2010).

[90] You, B. and Cen, L.-X. *Phys. Rev. A* **86**, 012102 (2012).

[91] Mazzola, L., Piilo, J., and Maniscalco, S. *International Journal of Quantum Information* **09**, 981–991 (2011).

[92] Lo Franco, R., Bellomo, B., Andersson, E., and Compagno, G. *Phys. Rev. A* **85**, 032318 (2012).

[93] Mannone, M., Lo Franco, R., and Compagno, G. *Phys. Scr.* **T153**, 014047 (2013).

[94] Haikka, P., Johnson, T. H., and Maniscalco, S. *Phys. Rev. A* **87**, 010103(R) (2013).

[95] Amico, L., Fazio, R., Osterloh, A., and Vedral, V. *Rev. Mod. Phys.* **80**, 517–576 (2008).

[96] Werlang, T., Ribeiro, G. A. P., and Rigolin, G. *International Journal of Modern Physics B* **27**, 1345032 (2013).

[97] Sarandy, M. S., de Oliveira, T. R., and Amico, L. *International Journal of Modern Physics B* **27**, 1345030 (2013).

[98] Jiang, H.-C., Wang, Z., and Balents, L. *Nature Physics* **8**, 902–905 (2012).

[99] Kitaev, A. and Preskill, J. *Phys. Rev. Lett.* **96**, 110404 (2006).

[100] Levin, M. and Wen, X.-G. *Phys. Rev. Lett.* **96**, 110405 (2006).

[101] Giampaolo, S. M. and Hiesmayr, B. C. *New Journal of Physics* **16**, 093033 (2014).

[102] Vidal, G., Latorre, J. I., Rico, E., and Kitaev, A. *Phys. Rev. Lett.* **90**, 227902 (2003).

[103] Latorre, J. I., Rico, E., and Vidal, G. *Quantum Inf. Comp.* **4**, 48 (2004).

[104] Wei, T.-C., Das, D., Mukhopadyay, S., Vishveshwara, S., and Goldbart, P. M. *Phys. Rev. A* **71**, 060305 (2005).

[105] Giampaolo, S. M., Adesso, G., and Illuminati, F. *Phys. Rev. Lett.* **100**, 197201 (2008).

[106] Giampaolo, S. M., Adesso, G., and Illuminati, F. *Phys. Rev. B* **79**, 224434 (2009).

[107] Giampaolo, S. M., Adesso, G., and Illuminati, F. *Phys. Rev. Lett.* **104**, 207202 (2010).

[108] Giampaolo, S. M. and Hiesmayr, B. C. *Phys. Rev. A* **88**, 052305 (2013).

[109] Hofmann, M., Osterloh, A., and Gühne, O. *Phys. Rev. B* **89**, 134101 (2014).

[110] Tomasello, B., Rossini, D., Hamma, A., and Amico, L. *International Journal of Modern Physics B* **26**, 1243002 (2012).

[111] Campbell, S., Richens, J., Gullo, N. L., and Busch, T. *Phys. Rev. A* **88**, 062305 (2013).

[112] Sachdev, S. *Quantum Phase Transitions*. Cambridge University Press, Cambridge, (2000).

[113] Heisenberg, W. *Zeitschrift fur Physik* **43**, 172–198 (1927).

[114] Robertson, H. P. *Phys. Rev.* **34**, 163–164 (1929).

[115] Friedland, S., Gheorghiu, V., and Gour, G. *Phys. Rev. Lett.* **111**, 230401 (2013).

[116] Pauli, W. In *Quanten*, volume 23 of *Handbuch der Physik*, 1–278. Springer Berlin Heidelberg (1926).

[117] Bohr, N. *Nature* **121**, 580 (1928).

[118] Aharonov, Y. and Bohm, D. *Phys. Rev.* **122**, 1649–1658 (1961).

[119] Taddei, M. M. *Quantum speed limits for general physical processes.* PhD thesis, Universitade Federal do Rio de Janeiro, (2014).

[120] Caneva, T., Murphy, M., Calarco, T., Fazio, R., Montangero, S., Giovannetti, V., and Santoro, G. E. *Phys. Rev. Lett.* **103**, 240501 (2009).

[121] Yung, M.-H. *Phys. Rev. A* **74**, 030303 (2006).

[122] Deffner, S. and Lutz, E. *Phys. Rev. Lett.* **105**, 170402 (2010).

[123] Coecke, B., Fritz, T., and Spekkens, R. W. *arXiv:1409.5531v3* (2014).

[124] Brandão, F. G. S. L. and Gour, G. *Phys. Rev. Lett.* **115**, 070503 (2015).

[125] Blasone, M., Dell'Anno, F., De Siena, S., , and Illuminati, F. *Phys. Rev. A* **77**, 062304 (2008).

[126] Chitambar, E., Leung, D., Mancinska, L., Ozols, M., and Winter, A. *Communications in Mathematical Physics* **328**, 303–326 (2014).

[127] Vidal, G. *J. Mod. Opt.* **47**, 355–376 (2000).

[128] Plenio, M. B. and Virmani, S. *Quant. Inf. Comp.* **7**, 1 (2007).

[129] Plenio, M. B. *Phys. Rev. Lett.* **95**, 090503 (2005).

[130] Vidal, G., Dür, W., and Cirac, J. I. *Phys. Rev. Lett.* **89**, 027901 (2002).

[131] Rains, E. M. *Phys. Rev. A* **60**, 179–184 (1999).

[132] Rains, E. M. *IEEE Transactions on Information Theory* **47**, 2921–2933 (2001).

[133] Åberg, J. *arXiv:quant-ph/0612146* (2006).

[134] Marvian, I. and Spekkens, R. W. *New J. Phys.* **15**, 033001 (2013).

[135] Baumgratz, T., Cramer, M., and Plenio, M. B. *Phys. Rev. Lett.* **113**, 140401 (2014).

[136] Winter, A. and Yang, D. *arXiv:1506.07975v2* (2015).

[137] Marvian, I., Spekkens, R. W., and Zanardi, P. *arXiv:1510.06474* (2015).

[138] Streltsov, A. *arXiv:1511.08346* (2015).

[139] Yadin, B., Ma, J., Girolami, D., Gu, M., and Vedral, V. *arXiv:1512.02085* (2015).

[140] Chitambar, E. and Gour, G. *arXiv:1602.06969* (2016).

[141] Marvian, I. and Spekkens, R. *arXiv:1602.08049* (2016).

[142] Giovannetti, V., Lloyd, S., and Maccone, L. *Science* **306**, 1330–1336 (2004).

[143] Walls, D. F. and Milburn, G. J. *Quantum Optics*. Springer–Verlag, Berlin, (1995).

[144] Nielsen, M. and Chuang, I. *Quantum Computation and Quantum Information*. Cambridge University Press, Cambridge, (2000).

[145] Hu, X., Fan, H., Zhou, D. L., and Liu, W.-M. *Phys. Rev. A* **85**, 032102 (2012).

[146] Guo, Y. and Hou, J. *Journal of Physics A: Mathematical and Theoretical* **46**, 155301 (2013).

[147] Streltsov, A., Kampermann, H., and Bruss, D. *Phys. Rev. Lett.* **106**, 160401 (2011).

[148] Amari, S. and Nagaoka, H. *Methods of information geometry*, volume 191. American Mathematical Soc., (2007).

[149] Cencov, N. N. *Statistical decision rules and optimal inference*. Number 53. American Mathematical Soc., (2000).

[150] Wootters, W. K. *Phys. Rev. D* **23**, 357–362 (1981).

[151] Braunstein, S. L. and Caves, C. M. *Phys. Rev. Lett.* **72**, 3439–3443 (1994).

[152] Morozova, E. and Chentsov, N. *Journal of Soviet Mathematics* **56**, 2648–2669 (1991).

[153] Petz, D. *Linear Algebra and its Applications* **244**, 81 – 96 (1996).

[154] Bengtsson, I. and Zyczkowski, K. *Geometry of quantum states: an introduction to quantum entanglement*. Cambridge University Press, (2006).

[155] Kubo, F. and Ando, T. *Mathematische Annalen* **246**, 205–224 (1980).

[156] Gibilisco, P. and Isola, T. *Journal of Mathematical Physics* **44**, 3752–3762 (2003).

[157] Vedral, V. and Plenio, M. B. *Phys. Rev. A* **57**, 1619 (1998).

[158] Giampaolo, S. M. and Illuminati, F. *Phys. Rev. A* **76**, 042301 (2007).

[159] Monras, A., Adesso, G., Giampaolo, S. M., Gualdi, G., Davies, G. B., and Illuminati, F. *Phys. Rev. A* **84**, 012301 (2011).

[160] Gharibian, S. *Phys. Rev. A* **86**, 042106 (2012).

[161] Giampaolo, S. M., Streltsov, A., Roga, W., Bruß, D., and Illuminati, F. *Phys. Rev. A* **87**, 012313 (2013).

[162] Roga, W., Giampaolo, S. M., and Illuminati, F. *Journal of Physics A: Mathematical and Theoretical* **47**, 365301 (2014).

[163] Wootters, W. K. *Phys. Rev. Lett.* **80**, 2245–2248 (1998).

[164] Nakano, T., Piani, M., and Adesso, G. *Phys. Rev. A* **88**, 012117 (2013).

[165] Ciccarello, F., Tufarelli, T., and Giovannetti, V. *New Journal of Physics* **16**, 013038 (2014).

[166] Huttner, B., Muller, A., Gautier, J. D., Zbinden, H., and Gisin, N. *Phys. Rev. A* **54**, 3783 (1996).

[167] Mohseni, M., Steinberg, A. M., and Bergou, J. A. *Phys. Rev. Lett.* **93**, 200403 (2004).

[168] Wei, T.-C. and Goldbart, P. M. *Phys. Rev. A* **68**, 042307 (2003).

[169] Streltsov, A., Kampermann, H., and Bruss, D. *New J. Phys.* **12**, 123004 (2010).

[170] Greenberger, D. M., Horne, M., and Zeilinger, A. *Am. J. Phys.* **58**, 1131 (1990).

[171] Gühne, O., Lu, C.-Y., Gao, W.-B., and Pan, J.-W. *Phys. Rev. A* **76**, 030305 (2007).

[172] Hiesmayr, B. C., Hipp, F., Huber, M., Krammer, P., and Spengler, C. *Phys. Rev. A* **78**, 042327 (2008).

[173] Amselem, E. and Bourennane, M. *Nat. Phys.* **5**, 748 (2009).

[174] Augusiak, R. and Horodecki, P. *Physical Review A* **73**, 012318 (2006).

[175] Comon, P. and Sorensen, M. *Report ISRN I3S-RR-2007-06-FR* (2007).

[176] Dür, W., Vidal, G., and Cirac, J. I. *Phys. Rev. A* **62**, 062314 (2000).

[177] Cabello, A. *Phys. Rev. A* **68**, 012304 (2003).

[178] Raussendorf, R. and Briegel, H. J. *Phys. Rev. Lett.* **86**, 5188–5191 (2001).

[179] Kiesel, N., Schmid, C., Weber, U., Tóth, G., Gühne, O., Ursin, R., and Weinfurter, H. *Phys. Rev. Lett.* **95**, 210502 (2005).

[180] Dicke, R. H. *Phys. Rev.* **93**, 99–110 (1954).

[181] Kiesel, N., Schmid, C., Tóth, G., Solano, E., and Weinfurter, H. *Phys. Rev. Lett.* **98**, 063604 (2007).

[182] Wei, T. C., Altepeter, J. B., Goldbart, P. M., and Munro, W. J. *Phys. Rev. A* **70**, 022322 (2004).

[183] Wei, T.-C. *Phys. Rev. A* **78**, 012327 (2008).

[184] Tura, J., Augusiak, R., Sainz, A., Vértesi, T., Lewenstein, M., and Acín, A. *Science* **344**, 1256–1258 (2014).

[185] Weinfurter, H. and Żukowski, M. *Physical Review A* **64**, 010102 (2001).

[186] Smolin, J. A. *Phys. Rev. A* **63**, 032306 (2001).

[187] Monz, T. *Quantum information processing beyond ten ion-qubits*. PhD thesis, Institute for Experimental Physics, University of Innsbruck, (2011).

[188] Bourennane, M., Eibl, M., Gaertner, S., Kurtsiefer, C., Cabello, A., and Weinfurter, H. *Physical review letters* **92**, 107901 (2004).

[189] Murao, M., Jonathan, D., Plenio, M., and Vedral, V. *Physical Review A* **59**, 156 (1999).

[190] Gaertner, S., Kurtsiefer, C., Bourennane, M., and Weinfurter, H. *Physical Review Letters* **98**, 020503 (2007).

[191] Vidal, G. and Tarrach, R. *Phys. Rev. A* **59**, 141–155 Jan (1999).

[192] Steiner, M. *Phys. Rev. A* **67**, 054305 May (2003).

[193] Piani, M. and Watrous, J. *Phys. Rev. Lett.* **114**, 060404 Feb (2015).

[194] Geller, J. and Piani, M. *J. Phys. A: Math. Theor.* **47** (2014).

[195] Lloyd, S. *J. Phys.: Conf. Ser.* **302**, 012037 (2011).

[196] Li, C.-M., Lambert, N., Chen, Y.-N., Chen, G.-Y., and Nori, F. *Sci. Rep.* **2**, 885 (2012).

[197] Vandenberghe, L. and Boyd, S. *SIAM review* **38**, 49–95 (1996).

[198] Brandão, F. G. S. L. *Phys. Rev. A* **72**, 022310 (2005).

[199] MATLAB. *version 8.5.0 (R2015a)*. The MathWorks Inc., Natick, Massachusetts, (2015).

[200] Grant, M. and Boyd, S. `http://cvxr.com/cvx`, March (2014).

[201] Grant, M. and Boyd, S. In *Recent Advances in Learning and Control,* Blondel, V., Boyd, S., and Kimura, H., editors, Lecture Notes in Control and Information Sciences, 95–110. Springer-Verlag Limited (2008). `http://stanford.edu/~boyd/graph_dcp.html`.

[202] Ekert, A. K., Alves, C. M., Oi, D. K., Horodecki, M., Horodecki, P., and Kwek, L. C. *Phys. Rev. Lett.* **88**, 217901 (2002).

[203] Girolami, D. *Phys. Rev. Lett.* **113**, 170401 (2014).

[204] Peng, Y., Jiang, Y., and Fan, H. *arXiv:1511.02576* (2015).

[205] Gottesman, D. *Chaos, Solitons & Fractals* **10**, 1749 (1999).

[206] Cerf, N. J. *J. Mod. Opt.* **47**, 197 (2000).

[207] Hiroshima, T. *J. Phys. A: Math. Gen.* **34**, 6907 (2001).

[208] Werner, R. F. *J. Phys. A: Math. Gen.* **34**, 7094 (2001).

[209] Chitambar, E., Streltsov, A., Rana, S., Bera, M. N., Adesso, G., and Lewenstein, M. *Phys. Rev. Lett.* **116**, 070402 Feb (2016).

[210] del Rio, L., Krämer, L., and Renner, R. *arXiv:1511.08818* (2015).

[211] Chen, X.-y., Yu, P., Jiang, L.-z., and Tian, M. *Phys. Rev. A* **87**, 012322 (2013).

[212] Armstrong, S., Wang, M., Teh, R. Y., Gong, Q., He, Q., Janousek, J., Bachor, H.-A., Reid, M. D., and Lam, P. K. *Nat. Phys.* **11**, 167 (2015).

[213] Chanda, T., Pal, A. K., Biswas, A., Sen, A., and Sen, U. *Physical Review A* **91**, 062119 (2015).

[214] Dakic, B., Vedral, V., and Brukner, C. *Phys. Rev. Lett.* **105**, 190502 (2010).

[215] Piani, M. *Phys. Rev. A* **86**, 034101 (2012).

[216] Deb, P. and Banik, M. *Journal of Physics A: Mathematical and Theoretical* **48**, 185303 (2015).

[217] Streltsov, A. *Quantum Correlations Beyond Entanglement and their Role in Quantum Information Theory.* SpringerBriefs in Physics, Berlin, (2015).

[218] Adesso, G., D'Ambrosio, V., Nagali, E., Piani, M., and Sciarrino, F. *Phys. Rev. Lett.* **112**, 140501 (2014).

[219] Horodecki, M., Horodecki, P., Horodecki, R., Oppenheim, J., Sen(De), A., Sen, U., and Synak-Radtke, B. *Phys. Rev. A* **71**, 062307 (2005).

[220] Modi, K., Paterek, T., Son, W., Vedral, V., and Williamson, M. *Phys. Rev. Lett.* **104**, 080501 (2010).

[221] Girolami, D., Tufarelli, T., and Adesso, G. *Phys. Rev. Lett.* **110**, 240402 (2013).

[222] Cornelio, M. F. et al. *Phys. Rev. Lett.* **109**, 190402 (2012).

[223] Carnio, E. G., Buchleitner, A., and Gessner, M. *Phys. Rev. Lett.* **115**, 010404 (2015).

[224] Paula, F. M., Montealegre, J. D., Saguia, A., de Oliveira, T. R., and Sarandy, M. S. *Europhys. Lett.* **103**, 50008 (2013).

[225] Xu, J.-S., Xu, X.-Y., Li, C.-F., Zhang, C.-J., Zou, X.-B., and Guo, G.-C. *Nat. Commun.* **1**, 7 (2010).

[226] Auccaise, R., Céleri, L. C., Soares-Pinto, D. O., deAzevedo, E. R., Maziero, J., Souza, A. M., Bonagamba, T. J., Sarthour, R. S., Oliveira, I. S., and Serra, R. M. *Phys. Rev. Lett.* **107**, 140403 (2011).

[227] Xu, J.-S. et al. *Nat. Commun.* **4**, 2851 (2013).

[228] Silva, I. A., Girolami, D., Auccaise, R., Sarthour, R. S., Oliveira, I. S., Bonagamba, T. J., deAzevedo, E. R., Soares-Pinto, D. O., and Adesso, G. *Phys. Rev. Lett.* **110**, 140501 (2013).

[229] Paula, F. M., Silva, I. A., Montealegre, J. D., Souza, A. M., deAzevedo, E. R., Sarthour, R. S., Saguia, A., Oliveira, I. S., Soares-Pinto, D. O., Adesso, G., and Sarandy, M. S. *Phys. Rev. Lett.* **111**, 250401 (2013).

[230] Bellomo, B., Lo Franco, R., and Compagno, G. *Phys. Rev. A* **86**, 012312 (2012).

[231] McEndoo, S., Haikka, P., De Chiara, G., Palma, M., and Maniscalco, S. *Europhys. Lett.* **101**, 60005 (2013).

[232] Aaronson, B., Lo Franco, R., Compagno, G., and Adesso, G. *New J. Phys.* **15**, 093022 (2013).

[233] Zurek, W. H. *Prog. Theor. Phys.* **89**, 281 (1993).

[234] Paula, F. M., Saguia, A., de Oliveira, T. R., and Sarandy, M. S. *Europhys. Lett.* **108**, 10003 (2014).

[235] Åberg, J. *Phys. Rev. Lett.* **113**, 150402 (2014).

[236] Verstraete, F., Murg, V., and Cirac, J. I. *Advances in Physics* **57**, 143–224 (2008).

[237] Osterloh, A., Amico, L., Falci, G., and Fazio, R. *Nature* **416**, 608–610 (2002).

[238] Osborne, T. J. and Nielsen, M. A. *Phys. Rev. A* **66**, 032110 (2002).

[239] Zanardi, P. and Paunković, N. *Phys. Rev. E* **74**, 031123 (2006).

[240] Zanardi, P., Giorda, P., and Cozzini, M. *Phys. Rev. Lett.* **99**, 100603 (2007).

[241] Osterloh, A., Palacios, G., and Montangero, S. *Phys. Rev. Lett.* **97**, 257201 (2006).

[242] de Oliveira, T. R., Rigolin, G., and de Oliveira, M. C. *Phys. Rev. A* **73**, 010305 (2006).

[243] Amico, L., Rossini, D., Hamma, A., and Korepin, V. E. *Phys. Rev. Lett.* **108**, 240503 (2012).

[244] Bratteli, O. and Robinson, D. W. *Operator Algebras and Quantum Statistical Mechanics: Volume 1: C*-and W*-Algebras. Symmetry Groups. Decomposition of States*. Springer Science & Business Media, (2012).

[245] Arodz, H., Dziarmaga, J., and Zurek, W. H. *Patterns of symmetry breaking*, volume 127. Springer Science & Business Media, (2012).

[246] Lieb, E., Schultz, T., and Mattis, D. *Annals of Physics* **16**, 407 – 466 (1961).

[247] Pfeuty, P. *Annals of Physics* **57**, 79 – 90 (1970).

[248] Barouch, E., McCoy, B. M., and Dresden, M. *Phys. Rev. A* **2**, 1075–1092 (1970).

[249] Barouch, E. and McCoy, B. M. *Phys. Rev. A* **3**, 786–804 (1971).

[250] Johnson, J. D. and McCoy, B. M. *Phys. Rev. A* **4**, 2314–2324 (1971).

[251] Kurman, J., Thomas, H., , and Mueller, G. *Physica A* **112**, 235 (1982).

[252] Roscilde, T., Verrucchi, P., Fubini, A., Haas, S., and Tognetti, V. *Phys. Rev. Lett.* **94**, 147208 (2005).

[253] Coffman, V., Kundu, J., and Wootters, W. K. *Phys. Rev. A* **61**, 052306 (2000).

[254] Osborne, T. J. and Verstraete, F. *Phys. Rev. Lett.* **96**, 220503 (2006).

[255] Amico, L., Baroni, F., Fubini, A., Patanè, D., Tognetti, V., and Verrucchi, P. *Phys. Rev. A* **74**, 022322 (2006).

[256] Jonathan, D. and Plenio, M. B. *Phys. Rev. Lett.* **83**, 3566–3569 (1999).

[257] Jonathan, D. and Plenio, M. B. *Phys. Rev. Lett.* **83**, 1455–1458 (1999).

[258] Giampaolo, S. M., Montangero, S., Dell'Anno, F., De Siena, S., and Illuminati, F. *Phys. Rev. B* **88**, 125142 (2013).

[259] Turgut, S. *Journal of Physics A: Mathematical and Theoretical* **40**, 12185 (2007).

[260] Hamma, A., Cincio, L., Santra, S., Zanardi, P., and Amico, L. *Phys. Rev. Lett.* **110**, 210602 (2013).

[261] Cui, J., Gu, M., Kwek, L. C., Santos, M. F., Fan, H., and Vedral, V. *Nature communications* **3**, 812 (2012).

[262] Cui, J., Amico, L., Fan, H., Gu, M., Hamma, A., and Vedral, V. *Phys. Rev. B* **88**, 125117 (2013).

[263] Hill, S. and Wootters, W. K. *Phys. Rev. Lett.* **78**, 5022–5025 (1997).

[264] Mandelstam, L. and Tamm, I. *J. Phys.(USSR)* **9**, 1 (1945).

[265] Mandelstam, L. and Tamm, I. In *Selected Papers,* Bolotovskii, B., Frenkel, V., and Peierls, R., editors, 115–123. Springer Berlin Heidelberg (1991).

[266] Anandan, J. and Aharonov, Y. *Phys. Rev. Lett.* **65**, 1697–1700 (1990).

[267] Margolus, L. and Levitin, L. B. *Physica D* **120**, 188 (1998).

[268] Levitin, L. B. and Toffoli, T. *Phys. Rev. Lett.* **103**, 160502 (2009).

[269] Giovannetti, V., Lloyd, S., and Maccone, L. *Phys. Rev. A* **67**, 052109 (2003).

[270] Pires, D. P., Céleri, L. C., and Soares-Pinto, D. O. *Phys. Rev. A* **91**, 042330 (2015).

[271] Taddei, M. M., Escher, B. M., Davidovich, L., and de Matos Filho, R. L. *Phys. Rev. Lett.* **110**, 050402 (2013).

[272] del Campo, A., Egusquiza, I. L., Plenio, M. B., and Huelga, S. F. *Phys. Rev. Lett.* **110**, 050403 (2013).

[273] Deffner, S. and Lutz, E. *Phys. Rev. Lett.* **111**, 010402 (2013).

[274] Uzdin, R., Lutz, E., and Kosloff, R. *arXiv:1408.1227* (2014).

[275] Zhang, Y.-J., Han, W., Xia, Y.-J., Cao, J.-P., and Fan, H. *Scientific reports* **4**, 4890 (2014).

[276] Liu, C., Xu, Z.-Y., and Zhu, S. *Phys. Rev. A* **91**, 022102 (2015).

[277] Xu, Z.-Y., Luo, S., Yang, W. L., Liu, C., and Zhu, S. *Phys. Rev. A* **89**, 012307 (2014).

[278] Wu, S.-x., Zhang, Y., Yu, C.-s., and Song, H.-s. *Journal of Physics A: Mathematical and Theoretical* **48**, 045301 (2015).

[279] Mondal, D. and Pati, A. K. *arXiv:1403.5182v2* (2015).

[280] Hamma, A., Markopoulou, F., Prémont-Schwarz, I., and Severini, S. *Phys. Rev. Lett.* **102**, 017204 (2009).

[281] Uhlmann, A. *Physics Letters A* **161**, 329 – 331 (1992).

[282] Gibilisco, P. and Isola, T. *Annals of the Institute of Statistical Mathematics* **59**, 147–159 (2007).

[283] Luo, S. *Phys. Rev. A* **73**, 022324 (2006).

[284] Chaves, R., Brask, J. B., Markiewicz, M., Kołodyński, J., and Acín, A. *Phys. Rev. Lett.* **111**, 120401 (2013).

[285] Brask, J. B., Chaves, R., and Kołodyński, J. *Phys. Rev. X* **5**, 031010 (2015).

[286] Paris, M. G. A. *International Journal of Quantum Information* **07**, 125–137 (2009).

[287] Brody, D. C. and Hughston, L. P. *Phys. Rev. Lett.* **77**, 2851–2854 (1996).

[288] Brody, D. C. *Journal of Physics A: Mathematical and Theoretical* **44**, 252002 (2011).

[289] Brody, D. C. and Graefe, E.-M. *Phys. Rev. Lett.* **109**, 230405 (2012).

[290] Crooks, G. E. *Phys. Rev. Lett.* **99**, 100602 (2007).

[291] Brandao, F., Horodecki, M., Ng, N., Oppenheim, J., and Wehner, S. *Proceedings of the National Academy of Sciences* **112**, 3275–3279 (2015).

[292] Zanardi, P., Paris, M. G. A., and Campos Venuti, L. *Phys. Rev. A* **78**, 042105 (2008).

[293] Oliveira, I., Bonagamba, T., Sarthour, R., Freitas, J., and deAzevedo, E. *NMR quantum information processing.* Elsevier, Amsterdam, (2007).